# Process Modeling of Next-Generation Liquid Fuel Production – Commercial Hydrocracking Process and Biodiesel Manufacturing

Ai-Fu Chang

Dissertation submitted to the Faculty of
Virginia Polytechnic Institute and State University
in partial fulfillment of the requirements for the degree of

Doctor of Philosophy
in
Chemical Engineering

Y. A. Liu, Chair
Luke E. K. Achenie
Richey M. Davis
Preston L. Durrill

September 7, 2011
Blacksburg, VA

Keyword: model, hydrocracking, biodiesel, process optimization, product design

# Process Modeling of Next-Generation Liquid Fuel Production – Commercial Hydrocracking Process and Biodiesel Manufacturing

Ai-Fu Chang

## Abstract

This dissertation includes two process modeling studies – (1) predictive modeling of large-scale integrated refinery reaction and fractionation systems from plant data – hydrocracking process; and (2) integrated process modeling and product design of biodiesel manufacturing.

**1. Predictive Modeling of Large-Scale Integrated Refinery Reaction and Fractionation Systems from Plant Data – Hydrocracking Processes**: This work represents a workflow to develop, validate and apply a predictive model for rating and optimization of large-scale integrated refinery reaction and fractionation systems from plant data. We demonstrate the workflow with two commercial processes – medium-pressure hydrocracking unit with a feed capacity of 1 million ton per year and high-pressure hydrocracking unit with a feed capacity of 2 million ton per year in the Asia Pacific. This work represents the detailed procedure for data acquisition to ensure accurate mass balances, and for implementing the workflow using Excel spreadsheets and a commercial software tool, Aspen HYSYS from Aspen Technology, Inc. The workflow includes special tools to facilitate an accurate transition from lumped kinetic components used in reactor modeling to the boiling point based pseudo-components required in the rigorous tray-by-tray distillation simulation. Two to three months of plant data are used to validate models' predictability. The resulting models accurately predict unit performance, product yields, and fuel properties from the corresponding operating conditions.

**2. Integrated Process Modeling and Product Design of Biodiesel Manufacturing:** This work represents first a comprehensive review of published literature pertaining to developing an integrated process modeling and product design of biodiesel manufacturing, and identifies those deficient areas for further development. It also represents new modeling tools and a methodology for the integrated process modeling and product design of an entire biodiesel manufacturing train. We demonstrate the methodology by simulating an integrated process to predict reactor and separator performance, stream conditions, and product qualities with different feedstocks. The results show that the methodology is effective not only for the rating and optimization of an existing biodiesel manufacturing, and but also for the design of a new process to produce biodiesel with specified fuel properties.

# Dedication

I would like to thank my advisor, Dr. Y. A. Liu, for his support and guidance during my tenure as a student at Virginia Tech. He provided me opportunities to work closely with the professionals from SINOPEC and Aspen Tech. I would also like to thank Dr. Luke E. K. Achenie, Dr. Richey M. Davis, and Dr. Preston L. Durrill for serving on my committee, their feedback, times and efforts to help me graduate.

I thank my group member, Kiran Pashikanti, for his friendship and support both in and out of the office. Kiran is a great friend and colleague. We had countless discussions on a wide variety of topics. I gained different perspectives on topics both related and unrelated to academic work. He had many creative ideas which helped me to overcome the difficulties I had in research work. Most importantly, he also served as my English teacher for free by having conversation with me everyday. He turned me from a guy who did not know how to claim baggage in the airport into a person who has no problem with discussing both technical and non-technical conversations in English.

To my parents and my big sister, I can never express enough my sincere love and gratitude to my parents for their unconditional love and encouragement in my life and studies. To my wife, I-Chun Lin, for enduring years as the girlfriend, fiancee, and now wife of a Ph.D. student, for suffering from several lonely summers, Thanksgivings, and birthdays, thank you for your patience.

## Format of Dissertation

This dissertation is written in journal format. Chapter 1 describes the motivations of this research product. Chapters 2 and 3 are self-contained papers that separately describe the literature review, modeling technology, results, and conclusions for commercial hydrocracking process and biodiesel manufacturing, respectively. Chapter 4 summarizes the contributions of this research product.

## Table of Contents

## List of Figures

## List of Tables

# Chapter 1 Introduction and Dissertation Scope.

Nowadays, the disparity between raising demand and decreasing discoveries of fossil fuel sources is increasingly drawing global attention[1]. People are worried that the slow growth of crude oil production will not meet global demand's burst in the near future. Researchers and scientists are seeking for solutions in three areas – (1) improve the exploration technology to exploit more fossil fuel and gas; (2) maximize the usage of fossil fuel and gas; and (3) develop new technology to produce energy from sustainable sources. Chemical engineers are more interested in the second and third areas since they require good understanding of process system engineering and relevant chemistry knowledge. The second area includes many different tasks on improving existing process and/or developing new process to better utilize fossil fuel and gas, such as recovering more gas oil from atmospheric residue (deep-cut operation in vacuum distillation unit), improving the production scenario of hydrocracking process to produce better product distribution and gasifying coal into syngas which can be converted into liquid fuel through Fischer-Tropsch reaction. On the other hand, the third area is concerned with seeking for different sustainable sources and transforming those sustainable sources into usable forms of energy such as bio-ethanol from corns, biodiesel from crops and algae, solar electricity from sunlight and wind power generation.

This dissertation includes two process modeling studies which improve existing simulation technologies in both areas – (1) predictive model of large-scale integrated refinery reaction and fractionation systems from plant data – hydrocracking processes; and (2) integrated process modeling and product design of biodiesel manufacturing.

In **Predictive Model of Large-Scale Integrated Refinery Reaction and Fractionation Systems from Plant Data – Hydrocracking Processes**, the following issues are investigated and addressed:

1. Review of current modeling technologies on plant-wide simulation of hydrocracking process;
2. Identification of the deficiencies in current modeling technologies which are
    a. Lack of plant-wide process model verified with long-term process and production data;
    b. Unable to connect hydrocracking reactor model with the simulation of downstream distillation column;
    c. Most of the published models are either using complex kinetic lumping model or simple boiling point lumping model. The former requires detailed molecular information of feedstock which is not available in daily measurements in a refinery. The latter is only able to provide good predictions of product yields and can not predict unit performance and fuel quality.

In **Integrated Process Modeling and Product Design of Biodiesel Manufacturing**, the following issues are investigated and addressed:

1. Review of current modeling technologies on biodiesel process;
2. Identification of the deficiencies in current modeling technologies which are
    a. Improper representation of feedstock – most models use pure triolein to represent feedstock which is a complex mixture of various triglyceride molecules;
    b. Poor estimation on required physical properties for modeling – none of the published models discuss the estimation of required physical properties for modeling, particularly the thermophysical properties of triglyceride molecules which are major components in feedstock oil;
    c. Simplified reaction kinetics in reactor model – most models utilize simplified reaction kinetics assuming fix reaction conversion regardless of reactor condition;
    d. Lack of biodiesel property prediction – none of the model is able to predict fuel property of biodiesel for product design purpose.

## Literature Cited

1. Strategic Significance of America’s Oil Shale Resource, Office of Naval Petroleum and Oil Shale Reserves, U.S. Department of Energy, **2004**, Washington D.C.

# Chapter 2 Predictive Model of Large-Scale Integrated Refinery Reaction and Fractionation Systems from Plant Data – Hydrocracking Processes.

## Abstract

This paper presents a workflow to develop, validate and apply a predictive model for rating and optimization of large-scale integrated refinery reaction and fractionation systems from plant data. We demonstrate the workflow with two commercial processes – medium-pressure hydrocracking (MP HCR) unit with a feed capacity of 1 million ton per year and high-pressure hydrocracking (HP HCR) unit with a feed capacity of 2 million ton per year in the Asia Pacific. The units include reactors, fractionators, and hydrogen recycle system. With catalyst and hydrogen, the process converts heavy feedstocks, such as vacuum gas oil, into valuable low-boiling products, such as gasoline and diesel. We present the detailed procedure for data acquisition to ensure accurate mass balances, and for implementing the workflow using Excel spreadsheets and a commercial software tool, Aspen HYSYS/Refining from Aspen Technology, Inc. Our procedure is equally applicable to other commercial software tools, such as Petro-SIM from KBC Process Technologies, Inc. The workflow includes special tools to facilitate an accurate transition from lumped kinetic components used in reactor modeling to the pseudo-components based on boiling point ranges required in the rigorous tray-by-tray simulation of fractionators. We validate the two models with two to three months of plant data, and the resulting models accurately predicts unit performance, product yields, and fuel properties from the corresponding operating conditions.

MP HCR model predicts the yields of heavy naphtha, diesel fuel and bottom products with average absolute deviations (AADs) of 3.4 wt%, 2.4 wt% and 2.4 wt%, respectively; it predicts the specific gravities of heavy naphtha, diesel fuel and bottom oil with AADs of 0.0184, 0.0148 and 0.008, respectively; it predicts the flash point and freezing point of diesel fuel with AADs of 3.6℃ and 4.1℃, respectively; and it predicts the outlet temperatures of catalyst beds with AADs

of 1.9℃. HP HCR model predicts the yields of LPG, light naphtha, heavy naphtha, jet fuel, and resid oil with AADs of 0.4 wt%, 0.2 wt%, 0.5 wt%, 0.4 wt%, and 1.7 wt% respectively; it predicts the specific gravities of light naphtha, heavy naphtha, jet fuel, and resid oil with AADs of 0.0049, 0.0062, 0.134, and 0.0045, respectively; it predicts the flash point and freezing point of jet fuel with AADs of 1.6℃ and 2.3℃, respectively; and it predicts the outlet temperatures of catalyst beds of the two hydrocracking reactors with AADs of 1.8 ℃ and 3.2 ℃.

We apply the validated plantwide model to quantify the effect of $H_2$-to-oil ratio on product distribution and catalyst life, and the effect of HCR reactor temperature and feed flow rate on product distribution. The results agree well with experimental observations reported in the literature. We also incorporate the model with linear programming production planning by generating delta-base vector. Our resulting models only require typical operating conditions and routine analysis of feedstock and products, and appears to be the only reported integrated HCR models that can quantitatively simulate all key aspects of reactor operation, fractionator performance, hydrogen consumption, product yield and fuel properties.

## 2.1 Introduction.

Hydrocracking (HCR) is one of the most important process units in modern refinery. It is widely used to upgrade the heavy petroleum fraction such as vacuum gas oil. With catalyst and excess hydrogen, HCR converts heavy oil fractions such as vacuum gas oil (VGO) from crude distillation unit, into broad range of valuable low-boiling products, such as gasoline and diesel. Figure 2.1 represents a typical process flow diagram of a single-stage HCR process with two reactors. The first reactor is usually loaded with hydrotreating catalyst to removes most of the nitrogen and sulfur compounds from feedstock. In addition, small extent of HCR also takes place in the first reactor. The effluent from first reactor passes through the HCR catalyst loaded in the second reactor where most of the HCR is reached.

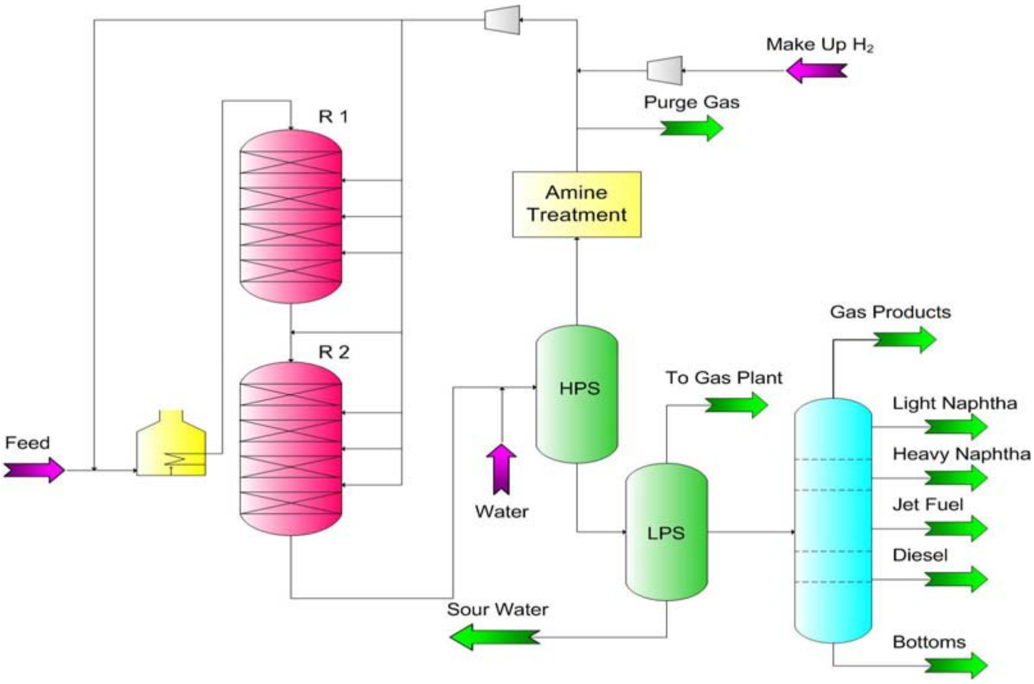

Figure 2.1 Flow diagram of a typical single-stage HCR process.

Petroleum fraction is a complex mixture which contains an enormous number of hydrocarbons. Figure 2.2 illustrates the compositional complexity of petroleum oil, displaying that the number of paraffin isomers rapidly increases with boiling point and carbon number[1]. Therefore, it is difficult to identity the molecules involved in petroleum oil, and study reaction kinetics of HCR process based on the "real compositions" of the feed oil. To overcome this difficulty, refiners apply lumping technique to partition the hydrocarbons into multiple lumps (or model compounds) based on molecular structure or/and boiling point, and assume the hydrocarbons of each lump to have an identical reactivity to build the reaction kinetics of HCR. Since Qader and Hill[2] presented first kinetic model of HCR process by using two lumps approach, kinetic lumping model of HCR has been widely reported in the literature.

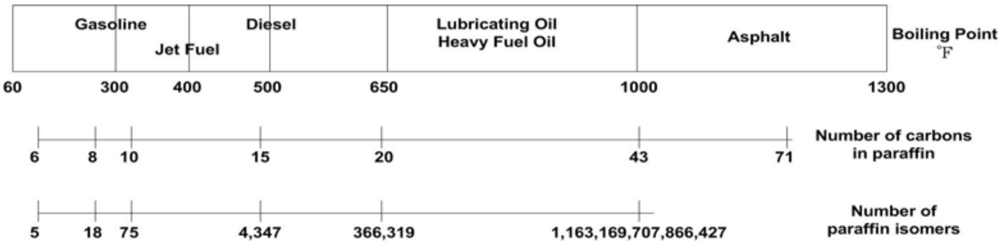

Figure 2.2 Complexity of petroleum oil (redraw from ref. [1]).

Figure 2.3 illustrates the scopes of published HCR models classified according to a three-layer onion. The core of the onion is *kinetic model*, focusing on the micro-kinetic analysis of reaction mechanisms. It allows the study of catalyst selection, feedstock effect and the influence of reaction conditions. *Reactor model* quantifies the reactor performance (e.g. product yield and fuel properties) under different operating conditions, such as flow rate, temperature profile, and hydrogen pressure. It helps the refiner determine the optimal unit operations. A *Process model* aids in the optimization of plantwide operating conditions to maximize the profit, minimize the cost and enhance the safety. However, there is few attention paid on developing a plantwide HCR process model in modeling literature. On the other hand, lumping techniques *of kinetic model,* as the core of HCR modeling work, have been widely reported in the literature. Most of the modeling literature is concerned about developing detail kinetic lumping model to identify the reaction chemistry of HCR process. There are two major classes of lumping techniques: (1) lumping based on non-molecular composition, and (2) lumping based on molecular composition.

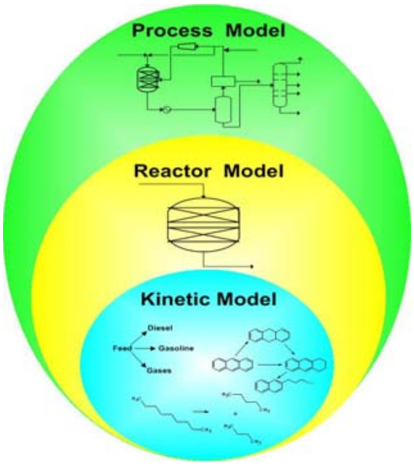

Figure 2.3 A three-layer onion for modeling scope

*Lumping based on molecular composition* defines the kinetic lumps according to structural and reactive characterizations of hydrocarbon species, and tracks interactions among a large number of kinetic lumps and reactions. It selects lumped components to characterize the feed oil, build the reaction network and represent the product composition. By contrast, *lumping based on non-molecular composition* considers molecules of different homologous families. For example, a kinetic lump of boiling point cut assumes the hydrocarbons within certain boiling point range to have the same reactivity and cannot differentiate between the different hydrocarbon types in the same boiling point range. When applying a lumping scheme based on molecular composition, the feed oil composition has small or no effect on the resulting kinetic scheme, and it allows predictions of fuel qualities from molecular composition. The most well-known lumping techniques based on molecular composition are the structure-oriented lumping (SOL) [3, 4, 5] and the single-event model[6]. SOL technique has been applied to plant-wide process models such as hydrodefsufurization[7] and fluid catalytic cracking unit[8]. In addition, there is a report of single-event model of HCR kinetics of oil fraction that includes as many as 1266 kinetic lumps[9]. The lumping based on molecular composition usually requires more computation time and makes it difficult to incorporate equipment simulation such as reactor hydrodynamics. It also requires more data than what the routine chemical analysis in a refinery can provide. This limits its application to kinetics and catalyst studies, and can rarely apply to a plantwide process model. In addition to the SOL and single-event model, however, there are other non-complex lumping techniques based on molecular composition, such as the approach of Aspen HYSYS/Refining hydrocracker model (Aspen Technology, Inc. Burlington, Massachusetts) that we will discuss in Section 2.2. Table 2.1 summarizes the key features of well-known published HCR models based on non-molecular composition lumping. For a review and comparison on HCR reactor models, please see Ancheyta et al.[10]; and for a review of kinetic modeling of large-scale reaction systems through lumping, please refer to Ho[11].

The objective of this work is to develop, validate and apply a methodology for the predictive process model of large-scale integrated refinery reaction and fractionation systems from plant data. In particular, we model two commercial HCR units in the Asia Pacific, These include a medium-pressure HCR (MP HCR) unit that processes 1 million ton feedstock per year with a reactor pressure of 11.5 to 12.5 MPa, and a high-pressure HCR (HP HCR) unit that processes 2 million ton feedstock per year with a reactor pressure of 14.5 to 15.0 MPa.

Table 2.1 Key features of published HCR models built by lumping based on non-molecular composition

| | Nature of the Model | | | | | Model Capability | | | |
|---|---|---|---|---|---|---|---|---|---|
| | Modeling Scope | Lumping Technique | Data Source | Data Requirement (Feed) | Data Requirement** (Product) | Reactor Operation | Product Yield | Colum Simulation | Fuel Quality Estimation |
| Qader and Hill[2] | Kinetic Model | 2 Lumps | Laboratory | None | Yield | N/A | Yes | N/A | N/A |
| Valavarasu et al.[12] | Kinetic Model | 4 Lumps | Laboratory | None | Yield | N/A | Yes | N/A | N/A |
| Sánchez et al.[13] | Kinetic Model | 5 Lumps | Pilot | None | Yield | N/A | Yes | N/A | N/A |
| Verstraete et al.[14] | Kinetic Model | 37 Lumps | Laboratory | TBP Curve / SARA Analysis / Elemental Analysis - C, H, S, N, O, Ni, V | Yield / TBP Curve / SARA Analysis / Elemental Analysis - C, H, S, N, O, Ni, V | N/A | Yes | N/A | N/A |
| Stangeland[15] | Kinetic Model | Discrete Lumps* | Pilot / Commercial | TBP Curve | Yield / TBP Curve | N/A | Yes | N/A | TBP Curve |
| Mohanty et al.[16] | Reactor Model | Discrete Lumps | Commercial | TBP Curve / Density Distribution | Yield / TBP Curve | Temperature Profile / Hydrogen Consumption | Yes | N/A | N/A |
| Pacheco and Dassori[17] | Reactor Model | Discrete Lumps | Commercial | TBP Curve / Density Distribution | Yield / TBP Curve | Temperature Profile / Hydrogen Consumption | Yes | N/A | N/A |
| Bhutani et al.[18] | Reactor Model | Discrete Lumps | Commercial | TBP Curve / Density Distribution | Yield / TBP Curve | Temperature Profile / Hydrogen Consumption | Yes | N/A | N/A |
| Laxminarasimhan et al.[19] | Kinetic Model | Continuous Lumping* | Pilot | TBP Curve | Yield / TBP Curve | N/A | Yes | N/A | N/A |
| Basak et al.[20] | Reactor Model | Continuous Lumping | Commercial | TBP Curve / PNA Distribution along with TBP Curve | TBP Curve / PNA Distribution along with TBP Curve | Temperature Profile / Hydrogen Consumption | Yes | N/A | PNA Composition of Product |
| Fukuyama and Terai[21] | Kinetic Model | 7 Lumps | Laboratory | SARA Analysis | Yield / SARA Analysis | N/A | Yes | N/A | N/A |

*Discrete lump and continuous lump are defined by boiling points.

** TBP = true boiling point; SARA = saturates, aromatics, resins and asphaltenes; PNA = paraffins, naphthalene and aromatics.

## 2.2 Aspen HYSYS/Refining HCR Modeling Tool.

Aspen HYSYS/Refining is an add-on program to Aspen HYSYS, a popular process simulation software tool for refining and chemical businesses. HYSYS/Refining includes several built-in modeling capabilities for refining process modeling, such as hydrocracker (HCR), catalytic reformer (CatRef) and fluid catalytic cracking (FCC). In this work, we use Aspen HYSYS/Refining HCR to model the HCR reactors, and Aspen HYSYS to develop the rigorous plantwide simulation including fractionation units.

Figure 2.4 represents the built-in process flow diagram of Aspen HYSYS/Refining HCR for a single-stage HCR process. It can simulate the feed heater, reactor, high-pressure separator, hydrogen recycle system, amine treatment (optional) and distillation column (optional). To ensure that the simulation agrees with the real process, users have to configure the process type (single-stage or two-stage), number of reactors, number of reactor beds for each reactor, and the operation of each unit. The model of amine treatment is a shortcut component splitter that separates $H_2S$ from the vapor product of high-pressure separator, and the simulation of distillation column is also based on shortcut calculations[22]. In addition, the ammonia ($NH_3$) produced by HDN reactions is split from reactor effluent before its entry into the high-pressure separator that is modeled by rigorous thermodynamics.

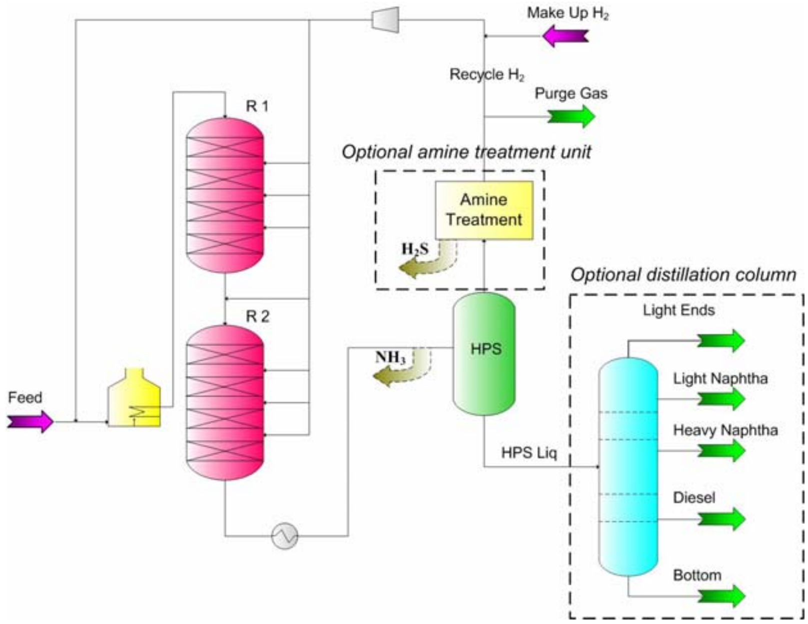

Figure 2.4 Built-in process flow diagram of Aspen HYSYS/Refining HCR.

The reactor model of Aspen HYSYS/Refining HCR utilizes 97-lump reaction kinetics. The selection of 97 model compounds is based on carbon number and structural characteristics and is consistent with previous publications[14, 23, 24, 25, 26]. The 97 model compounds belong to 6 groups – light gases, paraffin, naphthene, aromatics, sulfur compound and nitrogen compound. Furthermore, the sulfur compounds are separated into 8 groups of 13 components – thiophene, sulfide, benzothiophene, naphthabenzothiophene, dibenzothiophene, tetrahyhdro-benzothiophene, tetrahyhdro-dibenzothiophene, and tetrahyhdro- naphthabenzothiophene[22].

In the literature, there are two approaches to develop the kinetic lumping compositions of the feedstock – forward and backward. *The forward approach* requires detailed compositional and structural information by performing comprehensive analysis of the feedstock. However, the refinery can seldom apply the forward approach, because the routine analysis in the refinery does not include the required detailed structural analysis. This leads to *the backward approach*, which requires a reference library and only limited analytical data from routine measurement such as density and sulfur content to estimate kinetic lumping compositions. Brown et al.[27] report a methodology estimating detailed compositional information for SOL-based model and Gomez-Prado et al.[28] develop a molecular-type homologous series (MTHS) representation to characterize heavy petroleum fractions.

In Aspen HYSYS/Refining *the forward approach* requires detailed compositional and structural information by performing comprehensive analysis of the feedstock, including API gravity, ASTM D-2887 distillation, refractive index, viscosity, bromine number, total sulfur, total and basic nitrogen, fluorescent indicator adsorption (FIA, total aromatics in vol%), NMR (carbon in aromatic rings), UV method (wt% of mono-, di-, tri- and tetra- aromatics), HPLC and GC/MS. With the detailed compositional and structural information, Aspen HYSYS/Refining quantifies the so-called “fingerprint” (molecular representation) of the feedstock based on 97 kinetic lumps[29]. On the other hand, *the backward approach* of Aspen HYSYS/Refining requires only the bulk properties (density, ASTM D-2887 distillation curve, and sulfur and nitrogen contents) of the feedstock. Aspen HYSYS/Refining contains a built-in fingerprint databank for various types of feedstock, such as light VGO, heavy VGO, FCC cycle oil, etc. The backward approach assumes that the petroleum feedstock with the same fingerprint type maintains the same generic kinetic lump distribution as the initial composition. Aspen HYSYS/Refining uses a tool called “Feed Adjust”[29] to skew the kinetic lump distribution of the selected fingerprint type in order to minimize the difference between the measured and calculated bulk properties of the feedstock. We use the resulting kinetic lump distribution as the feed condition for the HCR model. If there is specific concern about compositional information, the user can customize the feed finger print to match the measurement. For example, the user can change sulfur lump distribution of selected feed fingerprint manually to ensure the distribution of hindered and non-hindered sulfur compounds match plant measurement.

The 97 lumps construct the reaction pathways of 177 reactions, including[30] : (1) paraffin HCR; (2) ring opening; (3) dealkylation of aromatics, naphthenes, nitrogen lumps and sulfur lumps; (4) saturation of aromatics, non-basic nitrogen lumps and hindered sulfur lumps; (5) hydrodesulfurization (HDS) of unhindered sulfur lumps; and (6) hydrodenitrogenation (HDN) of nitrogen lumps. Figure 2.5 to Figure 2.7 illustrate the reaction network. Rate equation of each reaction is based on Langmuir-Hinshelwood-Hougen-Watson (LHHW) mechanism with both reversible and irreversible reactions. The mechanism includes[30]:

— Adsorption of reactants to the catalyst surface;

— Inhibition of adsorption;

— Reaction of adsorbed molecules;

— Desorption of products;

The kinetic scheme also includes the inhibition resulted from $H_2S$, $NH_3$ and organic nitrogen compounds[30]:

— Inhibition of HDS reactions by $H_2S$;

— Inhibition of paraffin HCR, ring opening and dealkylation reactions by $NH_3$ and organic nitrogen compounds;

Eqs. (1) and (2) represent the LHHW based rate equations for reversible and irreversible reactions respectively[22]:

$$\mathrm{Rate} = \mathrm{K}_{\mathrm{total}} \times \mathrm{k} \times \frac{((\mathrm{K}_{\mathrm{ADS,i}}\mathrm{C}_{\mathrm{i}} \times \mathrm{K}_{\mathrm{ADS,H_2}}(\mathrm{P}_{\mathrm{H_2}})^{x} / \mathrm{K}_{\mathrm{eq}}) - \mathrm{K}_{\mathrm{ADS,j}}\mathrm{C}_{\mathrm{j}})}{\mathrm{ADS}} \tag{1}$$

$$\mathrm{Rate} = \mathrm{K}_{\mathrm{total}} \times \mathrm{k} \times \frac{\mathrm{K}_{\mathrm{ADS,i}}\mathrm{C}_{\mathrm{i}} \times \mathrm{K}_{\mathrm{ADS,H_2}}(\mathrm{P}_{\mathrm{H_2}})^{x}}{\mathrm{ADS}} \tag{2}$$

where $K_{total}$ is overall activity, k is intrinsic rate constant which is assigned by fundamental researches[22], $K_{ADS,\,i}$ and $K_{ADS,\,j}$ are the adsorption constants of hydrocarbon i and j which are assigned by fundamental researches[22], $C_i$ and $C_j$ are the concentrations of hydrocarbon i and j, $P_{H2}$ is the partial pressure of hydrogen, $K_{eq}$ is the equilibrium constant of the reaction which is assigned by fundamental researches[22], and ADS is the LHHW adsorption term which represents competitive adsorption by different inhibitors including aromatic hydrocarbon, $H_2S$, $NH_3$ and organic nitrogen compound. Table 2.2 represents the inhibitors used for each reaction type in Aspen HYSYS/Refining.

In the rate expressions shown in Eq. (1) and Eq. (2), $K_{total}$ is the combination of a series of activity factors to represent apparent reaction rates of different reaction groups. For example, $K_{total}$ of the hydrogenation reaction of a light aromatic hydrocarbon is the product of $K_{global}$, $K_{hdg,\,overall}$ and $K_{hdg,\,light}$. $K_{global}$ is the global activity factor assigned to the each catalyst bed, $K_{hdg,\,overall}$ represents the group activity factor of all hydrogenation reactions and $K_{hdg,\,light}$ indicates the activity factor of the hydrogenation reactions for the compounds belonging to light boiling point cut (below 430°F). Section 2.4.4 includes more details about the idea of reaction group and activity factors. For reactor design and hydrodynamics, Aspen HYSYS/Refining HCR applies the design equations of ideal trickle-bed and the hydrodynamics described by Satterfield[31] and each catalyst bed is modeled as a separate reactor.

Table 2.2 Reaction types and the corresponding inhibitors

| Reaction type | Inhibitors |
|---|---|
| C-C scission*<br>(acid site reaction) | $NH_3$, organic nitrogen compound and aromatic hydrocarbon |
| Aromatic saturation<br>(metal site reaction) | organic nitrogen compound, $H_2S$ and aromatic hydrocarbon |
| HDS<br>(metal site reaction) | organic nitrogen compound, $H_2S$ and aromatic hydrocarbon |
| HDN<br>(metal site reaction) | organic nitrogen compound, $H_2S$ and aromatic hydrocarbon |

* C-C scission includes HCR, ring open and ring dealkylation reactions.

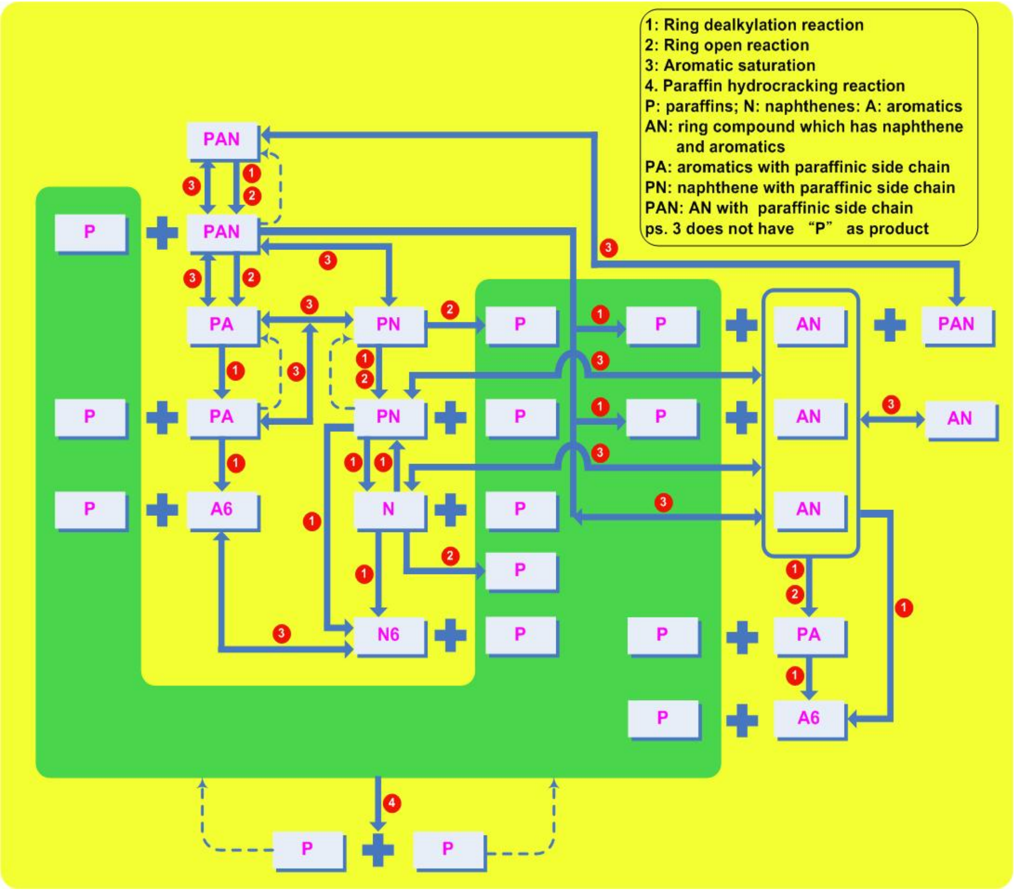

Figure 2.5 Reaction network of Aspen HYSYS/Refining HCR – paraffin HCR (HCR), ring open, ring dealkylation and aromatic saturation.

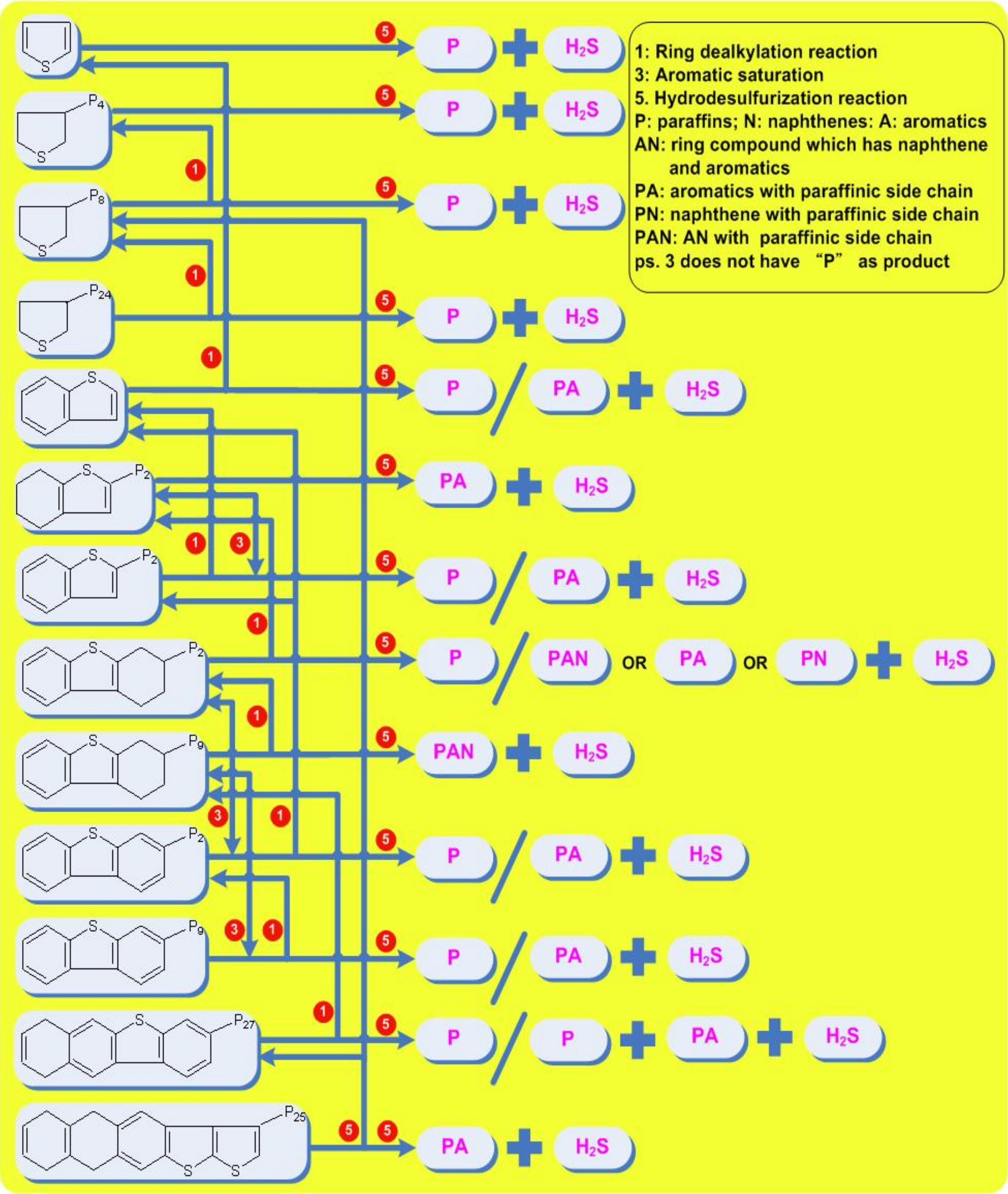

Figure 2.6 Reaction network of Aspen HYSYS/Refining HCR – HDS

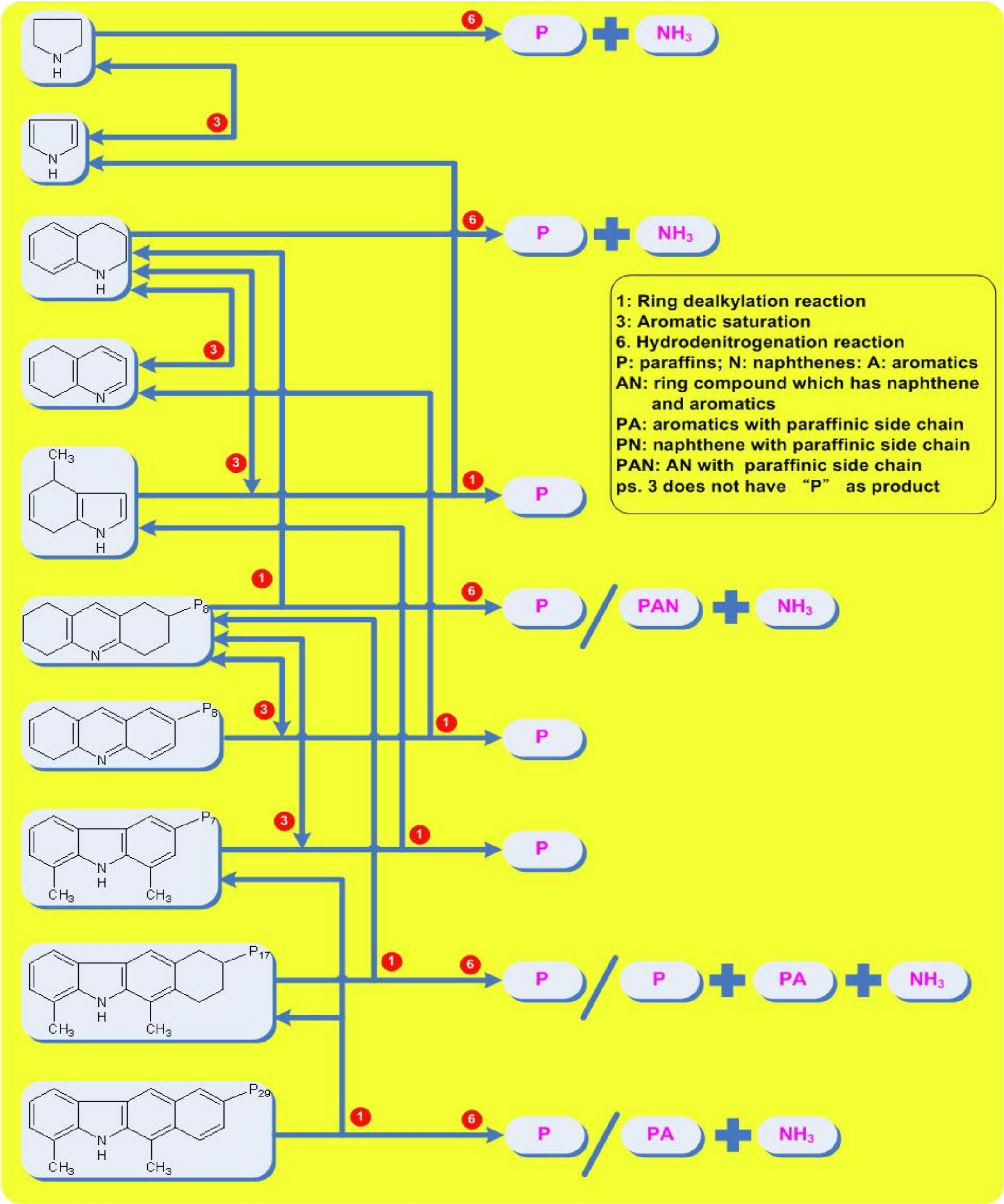

Figure 2.7 Reaction network of Aspen HYSYS/Refining HCR – HDN

## 2.3 Process Description.

### 2.3.1 MP HCR Process.

Figure 2.8 shows the process flow diagram of a MP HCR unit of a large-scale refinery in the

Asia Pacific. The unit upgrades 1 million tons/yr of VGO from the crude distillation unit (CDU) into valuable naphtha, diesel and bottom (the feedstock to ethylene plant) by HCR. The VGO feed from the CDU is mixed with a hydrogen-rich gas and preheated before entering the first reactor. The first reactor uses hydrotreating catalyst to reduce nitrogen and sulfur contents. The second reactor uses HCR catalyst to crack heavy hydrocarbons into lighter oils – naphtha, diesel and bottom. Following the two reactors, a high-pressure separator (HPS) recovers un-reacted hydrogen and a low-pressure separator (LPS) separates the light gases from the liquid outlet of HPS. An amine treatment scrubs sour gases from the vapor product of HPS to concentrate the hydrogen content of the hydrogen recycle stream. To balance the hydrogen in the system, a purge gas stream is removed from amine treatment. In the fractionation part, a $H_2S$ stripper removes the dissolved $H_2S$ from light hydrocarbons and a fractionator with two side strippers produces the major products – light naphtha, heavy naphtha, diesel and bottom.

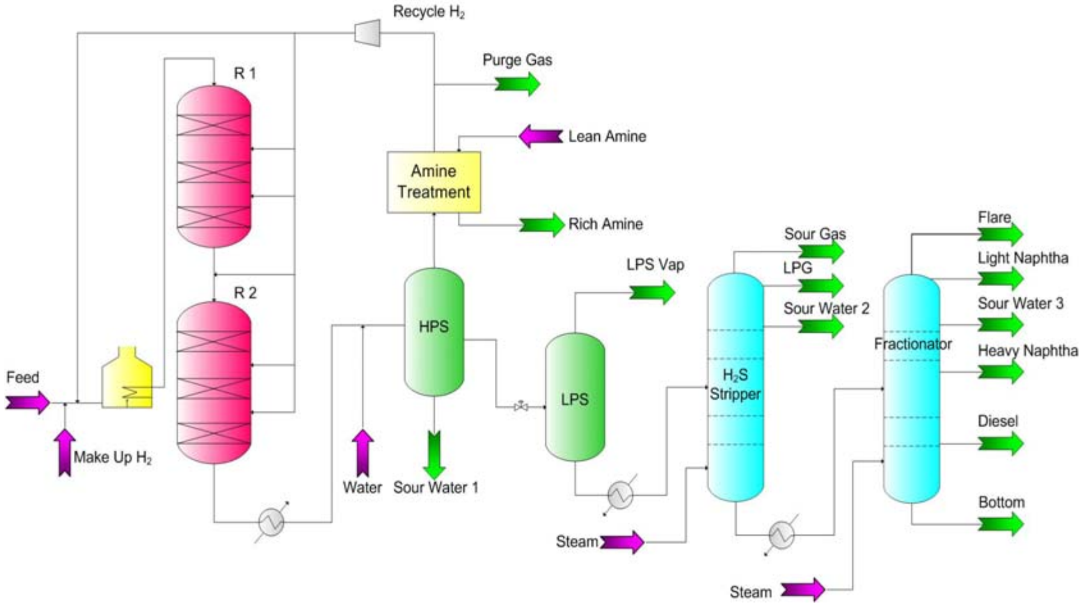

Figure 2.8 The simplified process flow diagram of MP HPR unit

### 2.3.2 HP HCR Process.

Figure 2.9 shows the process flow diagram of a HP HCR unit of a large-scale refinery in the Asia Pacific. The unit upgrades 2 million tons/yr of VGO into valuable naphtha, jet fuel and residue oil by HCR. Unlike a typical HCR unit, this process includes two parallel reactor series and each series contains one hydrotreating reactor and HCR reactor. The VGO feed is mixed with a hydrogen-rich gas and preheated before being fed to the first reactors of both reactor series. The first reactors of both series are loaded with the hydrotreating catalyst to reduce nitrogen and sulfur contents. The second reactor of both series are loaded with the HCR catalyst to crack heavy hydrocarbons into more valuable liquid products – LPG, light naphtha, heavy naphtha, and jet fuel. Following the two reactor series, a HPS recovers un-reacted hydrogen and a LPS separates the light gases from the liquid outlet of HPS. To balance the hydrogen in the system, we remove a purge gas stream from the vapor product of HPS. In the fractionation part, the first fractionator separates light gases and LPG from light hydrocarbons, the second fractionator produces the most valuable products, namely, light naphtha and heavy naphtha, and the third fractionator further produces jet fuel and residue oil.

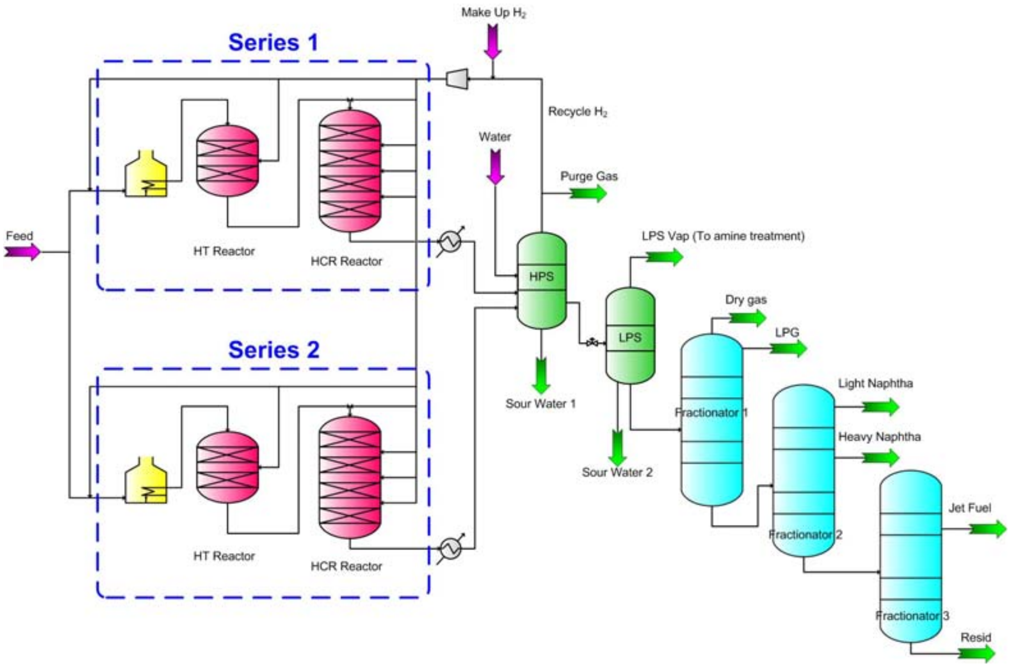

Figure 2.9 The simplified process flow diagram of HP HPR unit

## 2.4 Model Development.

### 2.4.1 Workflow of Developing an Integrated HCR Process Model.

Figure 2.10 shows our workflow of developing an integrated HCR model by using software tools, Aspen HYSYS and Aspen HYSYS/Refining. We recommend that developing all HCR models should follow the same workflow, with only minor changes in the details of each block according to the selection of kinetic model. For example, the different data requirement of feedstock analysis between wide distillation range lumping (distillation curve) and SOL model (FT-IR, API gravity, distillation curve, viscosity etc.) will makes the procedure for data acquisition quite dissimilar. We discuss the details of each block when using Aspen HYSYS and Aspen HYSYS/Refining to build an integrated HCR process model.

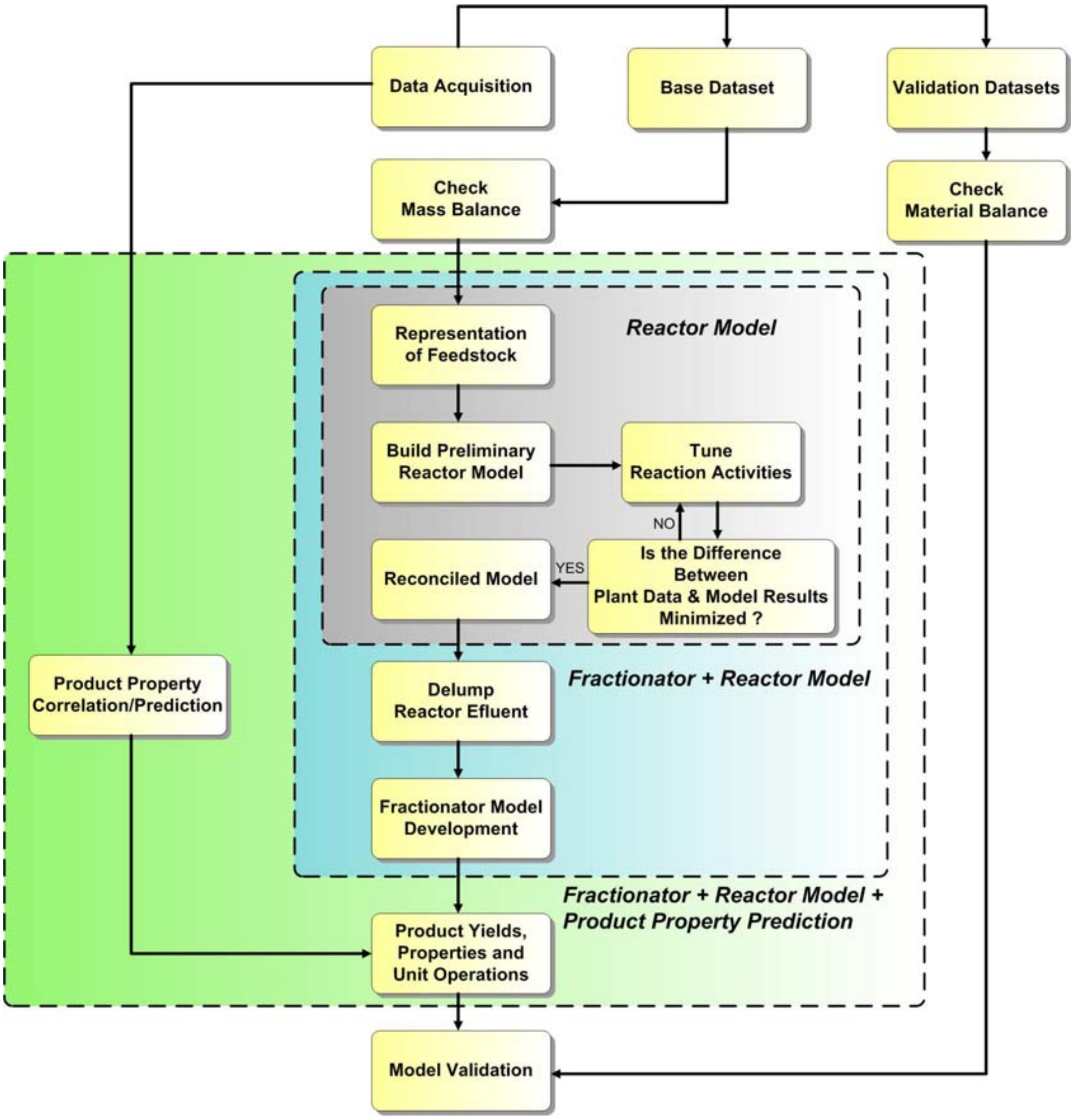

Figure 2.10 The workflow of building an integrated HCR process model.

The first step of model development is data acquisition, i.e., to collect the required data for modeling, and then to organize the gathered data and divide them into base and validation datasets. We use the base dataset to develop the process model, and the validation datasets to test the prediction accuracy of the process model. Before developing the model, it is important to do an accurate mass balance, including the total fresh feed and product streams. If the total mass flow rates of inlets and outlets differs more than 2 or 3%, it is necessary to identify the cause of the imbalance[32].

Following the mass balance is the development of a reactor model. The steps to develop a reactor model also depend on the selection of kinetic model. The procedures shown in Figure 2.10 correspond to the case using Aspen HYSYS/Refining. The development of a fractionator model in a HCR process is similar to a crude distillation unit (CDU). The only difference is the representation of the feed stream to the HCR fractionator, because the HCR reactor effluent is characterized by kinetic lumps instead of the pseudo-components based on boiling point which are widely used in a CDU model. Therefore, we use a step called *delumping* when the chosen kinetic lumps cannot appropriately characterize the feed stream to a HCR fractionator. Delumping is the most important step to build a plantwide model of HCR process, because it needs to capture the key properties of reactor effluent for fractionator simulation during the component transition process. After completing the fractionator model, we incorporate the oil property correlations into the process model to calculate fuel properties such as flash point of diesel fuel. Lastly, we verify the model by comparing the predictions with multiple plant datasets.

### 2.4.2 Data Acquisition.

Regardless of the selection of kinetic model, data acquisition is always the first step of model development. We obtain two months of feedstock/product analysis, production and operation data from plant, and construct multiple datasets to build and validate the model. It is important to consult plant engineers about data consistency to ensure each dataset does not include the data in the period of operation upsets and significant operation changes. Moreover, it is always helpful to revisit the original data for test run, because test run data are usually adjusted to show perfect mass and heat balances[32].

Data required for modeling purpose is quite sensitive to the selection of kinetic model and the modeling scope. This work only requires the operation and analysis data measured daily and Table 2.3 lists the data requirement in this work. We collect the data from March 2009 to June 2009 and organize the data into eight complete datasets for MP HCR process and ten complete datasets for HP HCR process. We only extract small number of complete datasets from months' plant data by considering the following: (1) each product stream has its own analysis period and the analyses of all product streams done in same day is not available; (2) it is necessary to find out the date that includes most analysis data and fill up the missing data from adjacent day; and (3) some of the meters fail to record correct values during the period; (4) some of the datasets fail in mass balance checking (see Section 2.4.3 for the procedure of mass balance calculation). Therefore, it is always useful to collect a long period (1 to 3 months) of data for modeling purpose, particularly for a commercial process. Because it is common to have missing data or failed meters, we take the averages of data a short period (1 to 3 days) of data (an industrial practice recommended also by Kaes[32] ), or make up the missing data by adjacent time period to construct one complete dataset for modeling.

Table 2.3 Data requirement of HCR process model.

Reactor Model
- Flow rate
    - Feed oil
    - Make up $H_2$
    - Wash water
    - All product streams including purge gas and rich amine
    - Recycle $H_2$ (before compressor)
    - Hydrogen quench to each catalyst bed
    - Lean amine
- Pressure
    - Feed oil
    - Inlet and outlet of each catalyst bed
    - Inlet and outlet of recycle $H_2$ compressor
    - High pressure separator
    - Low pressure separator
- Temperature
    - Feed oil

  - Inlet and outlet of each catalyst bed
  - Inlet and outlet of recycle $H_2$ compressor
  - High pressure separator
  - Low pressure separator
- Laboratory Analysis
  - Feed oil (density, distillation curve, total sulfur, total nitrogen and basic nitrogen)
  - All gas products including purge gas (composition analysis)
  - Composition analysis of light naphtha
  - All liquid products from fractionator (density, distillation, element analysis – C, H, S, N)
  - Composition analysis of sour water
  - Composition analysis of lean amine and rich amine
  - Make up $H_2$ (composition analysis)
  - Recycle $H_2$ (composition analysis)
  - Purge gas (composition analysis)
  - Low pressure separator gas (composition analysis)
- Others
  - Bed temperature at SOR (start of run) provided by catalyst vendor
  - Bed temperature at EOR (end of run) provided by catalyst vendor

Fractionator Model

- Flow rate
  - Steams
  - All pumparound streams
- Pressure
  - Feed to the main column
  - Steams
  - Condenser of main column
  - Top tray of main column
  - Bottom tray of main column
  - Feed tray of main column
- Temperature
  - Feed to the main column
  - Steams
  - Inlet and outlet of pumparound
  - Inlet and outlet of sides striper reboiler
  - Condenser
  - Top tray
  - Bottom tray
  - Feed tray
  - Each tray with product draw
  - Each tray with side draw
  - Bottom tray of main column and side strippers

### 2.4.3 Mass Balance.

It is critical to review the collected information to ensure accurate model development, particularly mass balance. The calculation of mass balance should include all of the inlet streams (such as feed oil, make up $H_2$, wash water, lean amine and steam in MP HCR process) and the outlet streams (such as LPS vapor, sour gas, LPG, flare, light naphtha, heavy naphtha, diesel, bottom, purge gas, sour water, rich amine in MP HCR process). However, the streams around amine treatment, wash water and sour water streams are not routinely measured, and it is unlikely to include those streams in the calculation of material balance. Since those streams only affect the mass balance of sulfur and nitrogen, we recommend doing a separate mass balance of sulfur and nitrogen by assuming that all of the removed sulfur and nitrogen atoms are reacted into $H_2S$ and $NH_3$.

We calculate the mass balance as follows: (1) calculate the $H_2S$ and $NH_3$ production by the severity of HDS and HDN reactions; (2) determine the production rates of “sweet” gas products and “sweet” liquid petroleum gas (LPG) which means subtracting any reported $H_2S$ and $NH_3$ from all gas products and LPG; (3) sum up “sweet” gas products, “sweet” LPG, all liquid products, $H_2S$ production and $NH_3$ production to determine the total production rate of the reactor effluent; (4) sum up the flow rates of feed oil and makeup $H_2$ to obtain total feed rate to reactor; and (5) calculate the ratio between total production rate of the reactor effluent and total feed rate;

Figure 2.11 illustrates an Excel spreadsheet we develop to do the mass balance calculations. We have posted all of the Excel spreadsheets mentioned in this article on our group website (www.design.che.vt.edu) for the interested reader to review and download without charge. Although we have developed the spreadsheet and the formulas for a specific HCR process, the reader can generalize the steps described above and apply the spreadsheet to do mass balance of any HCR process with only minor changes.

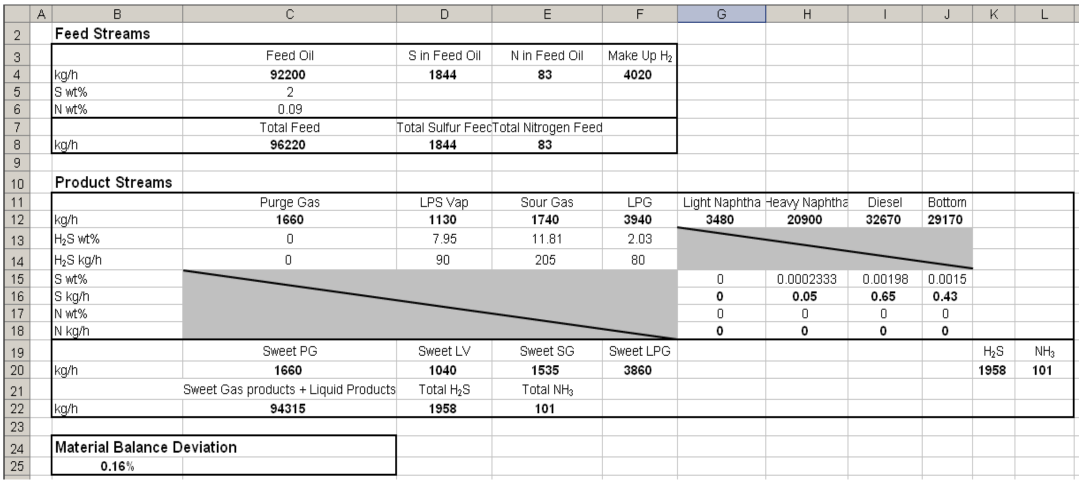

|  | A | B | C | D | E | F | G | H | I | J | K | L |
|---|---|---|---|---|---|---|---|---|---|---|---|---|
| 2 |  | **Feed Streams** |  |  |  |  |  |  |  |  |  |  |
| 3 |  |  | Feed Oil | S in Feed Oil | N in Feed Oil | Make Up $H_2$ |  |  |  |  |  |  |
| 4 |  | kg/h | **92200** | **1844** | **83** | **4020** |  |  |  |  |  |  |
| 5 |  | S wt% | 2 |  |  |  |  |  |  |  |  |  |
| 6 |  | N wt% | 0.09 |  |  |  |  |  |  |  |  |  |
| 7 |  |  | Total Feed | Total Sulfur Feec | Total Nitrogen Feed |  |  |  |  |  |  |  |
| 8 |  | kg/h | **96220** | **1844** | **83** |  |  |  |  |  |  |  |
| 9 |  |  |  |  |  |  |  |  |  |  |  |  |
| 10 |  | **Product Streams** |  |  |  |  |  |  |  |  |  |  |
| 11 |  |  | Purge Gas | LPS Vap | Sour Gas | LPG | Light Naphtha | Heavy Naphtha | Diesel | Bottom |  |  |
| 12 |  | kg/h | **1660** | **1130** | **1740** | **3940** | **3480** | **20900** | **32670** | **29170** |  |  |
| 13 |  | $H_2S$ wt% | 0 | 7.95 | 11.81 | 2.03 |  |  |  |  |  |  |
| 14 |  | $H_2S$ kg/h | 0 | 90 | 205 | 80 |  |  |  |  |  |  |
| 15 |  | S wt% |  |  |  |  | 0 | 0.0002333 | 0.00198 | 0.0015 |  |  |
| 16 |  | S kg/h |  |  |  |  | **0** | **0.05** | **0.65** | **0.43** |  |  |
| 17 |  | N wt% |  |  |  |  | 0 | 0 | 0 | 0 |  |  |
| 18 |  | N kg/h |  |  |  |  | **0** | **0** | **0** | **0** |  |  |
| 19 |  |  | Sweet PG | Sweet LV | Sweet SG | Sweet LPG |  |  |  |  | $H_2S$ | $NH_3$ |
| 20 |  | kg/h | **1660** | **1040** | **1535** | **3860** |  |  |  |  | **1958** | **101** |
| 21 |  |  | Sweet Gas products + Liquid Products | Total $H_2S$ | Total $NH_3$ |  |  |  |  |  |  |  |
| 22 |  | kg/h | **94315** | **1958** | **101** |  |  |  |  |  |  |  |
| 23 |  |  |  |  |  |  |  |  |  |  |  |  |
| 24 |  | **Material Balance Deviation** |  |  |  |  |  |  |  |  |  |  |
| 25 |  | **0.16%** |  |  |  |  |  |  |  |  |  |  |

Figure 2.11 A spreadsheet for the mass balance calculation of a HCR process.

### 2.4.4 Reactor Model Development.

Reactor model development is the core of building a HCR process model. Although the procedure of building a reactor model depends on the selection of kinetic model, we require the following tasks in developing a model for most commercial HCR processes: (1) do the feedstock analysis based on the selected kinetic model; (2) represent the feedstock as a mixture of kinetic lumps which can be modeling compounds or pseudo-components based on boiling point ranges; (3) build the reaction network, define rate equations, and estimate rate constants and heat of reaction; (4) apply the operation data (e.g. reactor temperature, feed rate, etc.) to solve rate equations and reactor design equations simultaneously; (5) and minimize objective functions (user-defined indices to represent the differences between model predictions and plant data) by tuning reaction activity parameters.

#### 2.4.4.1 MP HCR Reactor Model.

We describe in Section 2.2 the concept of the backward approach in representing the feedstock using the Aspen HYSYS/Refining. Since the refinery does not conduct comprehensive analysis of HCR feedstock routinely, this work applies the backward approach to characterize the feedstock. We select “LVGO” fingerprint type for both HCR processes because the feeds to both processes is mainly vacuum gas oil from crude distillation unit and the selected fingerprint type should be as close to the real feeds as possible. This section will demonstrate the last step of building reactor model by using Aspen HYSYS/Refining – to minimize the difference between model predictions and plant data to make the model match plant operation.

Although Aspen HYSYS/Refining assigns the rate constants to the 177 reactions based on fundamental research, it is necessary to identify the activity factor to match plant operation because the reactor configuration, catalyst activity and operating conditions vary for different refineries. The procedure of minimizing the difference between model predictions and plant data in Aspen HYSYS/Refining is called “calibration”, meaning to calibrate the model to agree with plant operation.

Table 2.4 lists the 31 optional objective functions and Table 2.5 shows the 48 reaction activity factors for selection. Aspen HYSYS/Refining combines the input plant product distribution to construct the reactor effluent, and partition the reactor effluent into C1, C2, C3, C4, C5, and four “square cuts”, namely, naphtha (C6 to 430°F cut), diesel (430 to 700°F cut), bottom (700 to 1000°F) cut and resid (1000°F+ cut) which are shown in Table 2.4. All of the objective functions listed in Table 2.4 are either the prediction errors of crucial operations or important product yields for the HCR process. Aspen HYSYS/Refining allows us to select the desired objective functions during calibration. After selecting the objective functions, we choose appropriate activity factors to calibrate the reactor model. Figure 2.12 illustrates the relationships among activity factors, catalyst bed and reactor type and Table 2.5 shows the major effect of each activity factor on the model performance such as global activity ($K_{global}$) on the bed temperature profile to help the selection of activity factors.

The procedure of model calibration depends on the operational mode, product yields and the precision of plant data. For example, a hydrogen-insufficient refinery might pay more attention to hydrogen consumption and makeup hydrogen flow. In addition, it is necessary to have high precision of light-end analysis (C1 to C5) if we desire to have accurate predictions of light gas yields. For MP HCR process, the most important considerations to the plant management are the product yields, flow rate of makeup hydrogen, reactor temperature and properties of liquid fuel products. We note that the reactor model cannot calculate some fuel properties, such as flash point and freezing point of diesel and jet fuel, because the square cuts defined by Aspen HYSYS/Refining have different distillation ranges from plant cuts. Therefore, we develop correlations to estimate such fuel properties (see Section 2.4.6).

Figure 2.13 illustrates the steps to identify activity factors in this work which are divided into two phases. The first phase is applicable to any Aspen HYSYS/Refining HCR model and the second phase depends on the modeling priority of the refinery. Since Aspen HYSYS/Refining assigns small values to $K_{global}$ to ensure the initial convergence, all catalyst beds' performance is almost "dead" initially, meaning that the reaction conversion is small. Thus, the first task is to tune the global activity factor of each catalyst bed to "activate" the reactors. After activating the reactors, the reaction conversion must increase to some extent and we tune the cracking activity factors to minimize the difference between predicted and actual liquid product yields.

Because of heat effects of the reactions, the calculated reactor temperature profiles from previous steps would show deviations from actual plant data. We tune the global activity factors again to ensure the deviations of reactor temperature predictions are within tolerance. We repeat the calibration of “reactor temperature profiles” and “mass yields of liquid products” several times until the errors of model predictions are within the acceptable tolerance. These back-and–forth procedures compose the first phase shown in Figure 2.13 which is a generalized guideline of initial calibration for Aspen HYSYS/Refining HCR model because reactor temperature profiles and major liquid product yields are always crucial considerations for any hydrocracker.

The second phase of Figure 2.13 shows the calibration procedure to reconcile the reactor model’s predictions to agree with the modeling priority of the refinery about process operations and productions. In this case, flow rate of makeup hydrogen, volume yields of liquid products (crucial to density calculation) and light gas yields are important to the MP HCR process. Because of the lack of analysis data of nitrogen and sulfur contents of liquid product streams, the calibration procedure of this case (see Figure 2.13) does not include reconciliation of HDN and HDS activities.

Although the steps involved in second phase depend on the modeling priority of the refinery management, we can give some common guidelines: (1) Always check reactor temperature profiles and mass yields of liquid products; (2) By our experience, the overall model performance is most sensitive to $K_{global}$ and least sensitive to $K_{light}$. The following list is in the order of decreasing sensitivity: $K_{global}$, $K_{crc}$, $K_{hdg}$, $K_{hds}$, $K_{hdn}$, $K_{ro}$, $K_{light}$; (3) $K_{global}$ has the most significant effect on all objective functions; (4) $K_{crc}$ has a significant effect on the product yield, reactor temperature profile, hydrogen consumption and flow rate of makeup hydrogen; (5) $K_{hdg}$ affects the product yield, reactor temperature profile, hydrogen consumption, and flow rate of makeup hydrogen; (6) $K_{hds}$ has a notable effect on the sulfur content, some effect on the hydrogen consumption and flow rate of makeup hydrogen, and small effect on the product yield; (7) $K_{hds}$ has a significant effect on nitrogen content; (8) $K_{light}$ only affects the distribution ratio between light gases; (9) Tuning $K_{light}$ to distribute light gases (C1 to C4) last because the total yields of light gases are determined by cracking reactions. $K_{light}$ only re-distributes the light gases and has little effect on the overall model performance.

The goal of model calibration is to seek an optimal solution for reactor model to match real operation, and there is no single and best solution. It is important to assign reasonable tolerance into the objective functions and loose some of them when necessary.

Table 2.4 Objective Functions in Aspen HYSYS/Refining.

| | Note | Notation in this work |
|---|---|---|
| The predicting error of temperature rise of catalyst bed | One for each catalyst bed | $OBJ_{TR\_i}$<br>$i = 1 – 6$ |
| The predicting error of hydrogen quench of catalyst bed | One for each catalyst bed | $OBJ_{HQ\_i}$<br>$i = 1 – 6$ |
| The predicting error of flow rate of purge gas | | $OBJ_{PGF}$ |
| The predicting error of flow rate of makeup $H_2$ | | $OBJ_{MHF}$ |
| The predicting error of chemical $H_2$ consumption | | $OBJ_{HC}$ |
| The predicting error of C6 to 430°F cut (naphtha) volume flow | | $OBJ_{NVF}$ |
| The predicting error of 430 to 700°F cut (diesel) volume flow | | $OBJ_{DVF}$ |
| The predicting error of 700 to 1000°F cut (bottom) volume flow | | $OBJ_{BVF}$ |
| The predicting error of 1000°F+ cut (resid) volume flow | | $OBJ_{RVF}$ |
| The predicting error of C6 to 430°F cut (naphtha) mass flow | | $OBJ_{NMF}$ |
| The predicting error of 430 to 700°F cut (diesel) mass flow | | $OBJ_{DMF}$ |
| The predicting error of 700 to 1000°F cut (bottom) mass flow | | $OBJ_{BMF}$ |
| The predicting error of 1000°F+ cut (resid) mass flow | | $OBJ_{RMF}$ |
| The predicting error of C1C2 mass yield | | $OBJ_{C1C2}$ |
| The predicting error of C3 mass yield | | $OBJ_{C3}$ |
| The predicting error of C4 mass yield | | $OBJ_{C4}$ |
| The predicting error of sulfur content of 430 to 700°F cut | | $OBJ_{SD}$ |
| The predicting error of sulfur content of 700 to 1000°F cut | | $OBJ_{SB}$ |
| The predicting error of nitrogen content of 430 to 700°F cut | | $OBJ_{ND}$ |
| The predicting error of nitrogen content of 700 to 1000°F cut | | $OBJ_{NB}$ |
| The predicting error of nitrogen content in reactor 1 effluent | | $OBJ_{NR1}$ |

Table 2.5 Reaction activity factors in Aspen HYSYS/Refining

| Notation in this work | Description | Major observation | Number of activity factors | Note |
|---|---|---|---|---|
| $K_{global\_i}$<br>i = 1 – 6 | Global activity for each catalyst bed | Bed temperature profile | 6* | 6 global activity factors for 6 catalyst beds |
| $K_{sul\_i\_j}$<br>i = HT, HCR<br>j = O, L, M, H | HDS Activity | Sulfur content | 8 | 1 factor for overall HDS activity of hydrotreating beds<br>3 factors for 3 wide boiling point cuts** of hydrotreating beds<br>1 factor for overall HDS activity of HCR beds<br>3 factors for 3 wide boiling point cuts of HCR beds |
| $K_{nit\_i\_j}$<br>i = HT, HCR<br>j = O, L, H | HDN Activity | Nitrogen content | 6 | 1 factor for overall HDN activity of hydrotreating beds<br>2 factors for 2 wide boiling point cuts of hydrotreating beds<br>1 factor for overall HDN activity of HCR beds<br>2 factors for 2 wide boiling point cuts of HCR beds |
| $K_{crc\_i\_j}$<br>i = HT, HCR<br>j = O, L, M, H | Activity of HCR and ring dealkylation | Product yield | 8 | 1 factor for overall HCR activity of hydrotreating beds<br>3 factors for 3 wide boiling point cuts of hydrotreating beds<br>1 factor for overall HCR activity of HCR beds<br>3 factors for 3 wide boiling point cuts of HCR beds |
| $K_{hdg\_i\_j}$<br>i = HT, HCR<br>j = O, L, M, H | Activity of hydrogenation (HDG, saturation of aromatic rings) | Hydrogen consumption/ Reactor temperature | 8 | 1 factor for overall HDG activity of hydrotreating beds<br>3 factors for 3 wide boiling point cuts of hydrotreating beds<br>1 factor for overall HDG activity of HCR beds<br>3 factors for 3 wide boiling point cuts of HCR beds |
| $K_{ro\_i\_j}$<br>i = HT, HCR<br>j = O, L, M, H | Activity of ring opening (RO) | Paraffin/naphthene ratio | 8 | 1 factor for overall RO activity of hydrotreating beds<br>3 factors for 3 wide boiling point cuts of hydrotreating beds<br>1 factor for overall RO activity of HCR beds<br>3 factors for 3 wide boiling point cuts of HCR beds |
| $K_{light\_i}$<br>i = 1, 2, 3, 4 | Light gas tuning factor | Distribute C1 to C4 | 4 | 1 factor for each light gas (C1 to C4) |

*number of global activity factors depends on the number of catalyst beds

**the three wide boiling point cuts used to defined activity factors are 430°F- (L). 430 to 950°F (M), and 950°F+ (H)

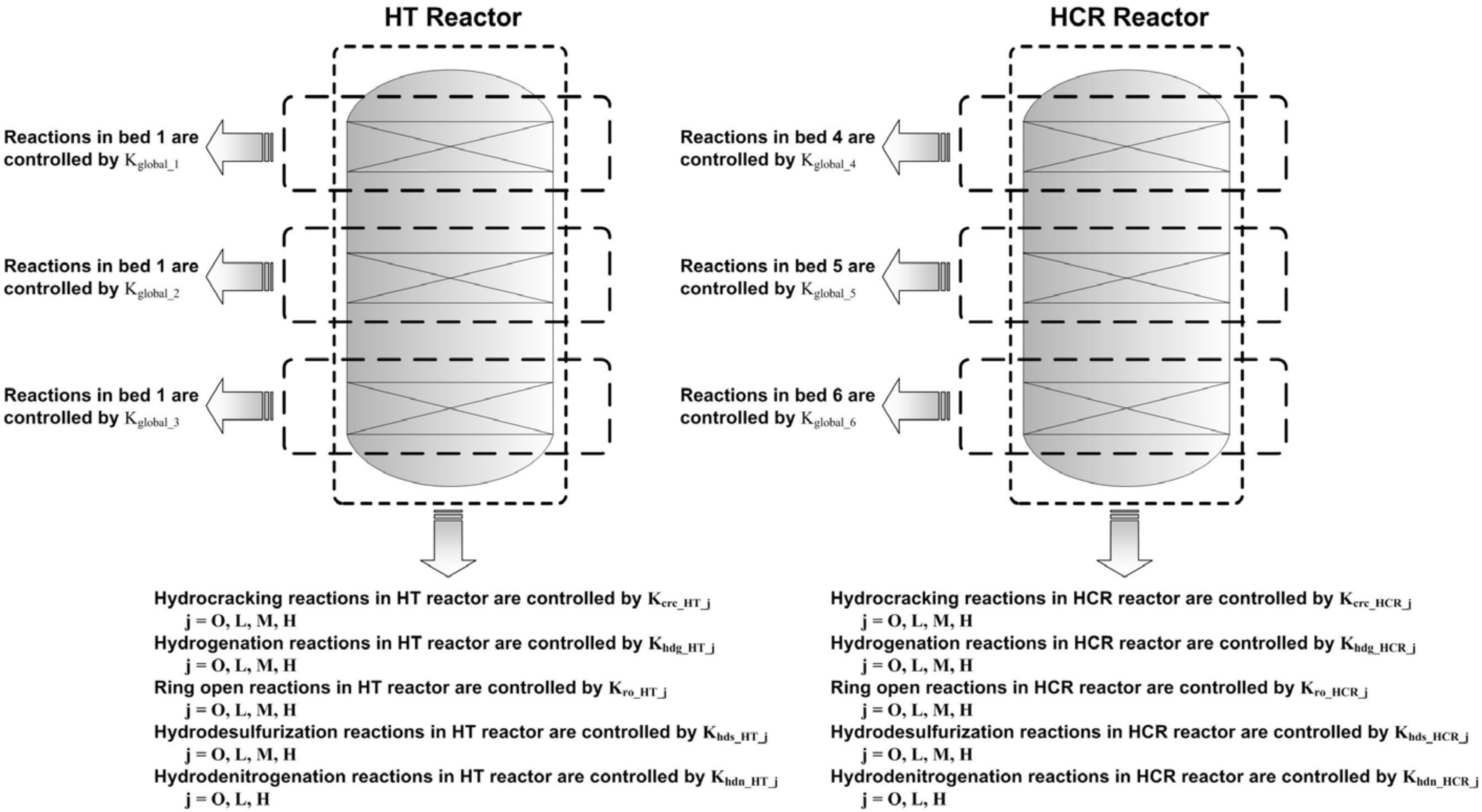

Reactions in bed 1 are controlled by $K_{global\_1}$

Reactions in bed 1 are controlled by $K_{global\_2}$

Reactions in bed 1 are controlled by $K_{global\_3}$

Reactions in bed 4 are controlled by $K_{global\_4}$

Reactions in bed 5 are controlled by $K_{global\_5}$

Reactions in bed 6 are controlled by $K_{global\_6}$

Hydrocracking reactions in HT reactor are controlled by $K_{crc\_HT\_j}$
$j = O, L, M, H$
Hydrogenation reactions in HT reactor are controlled by $K_{hdg\_HT\_j}$
$j = O, L, M, H$
Ring open reactions in HT reactor are controlled by $K_{ro\_HT\_j}$
$j = O, L, M, H$
Hydrodesulfurization reactions in HT reactor are controlled by $K_{hds\_HT\_j}$
$j = O, L, M, H$
Hydrodenitrogenation reactions in HT reactor are controlled by $K_{hdn\_HT\_j}$
$j = O, L, H$

Hydrocracking reactions in HCR reactor are controlled by $K_{crc\_HCR\_j}$
$j = O, L, M, H$
Hydrogenation reactions in HCR reactor are controlled by $K_{hdg\_HCR\_j}$
$j = O, L, M, H$
Ring open reactions in HCR reactor are controlled by $K_{ro\_HCR\_j}$
$j = O, L, M, H$
Hydrodesulfurization reactions in HCR reactor are controlled by $K_{hds\_HCR\_j}$
$j = O, L, M, H$
Hydrodenitrogenation reactions in HCR reactor are controlled by $K_{hdn\_HCR\_j}$
$j = O, L, H$

Figure 2.12 Relationships among activity factor, catalyst bed and reactor type for hydrotreating (HT) and hydrocracking (HCR).

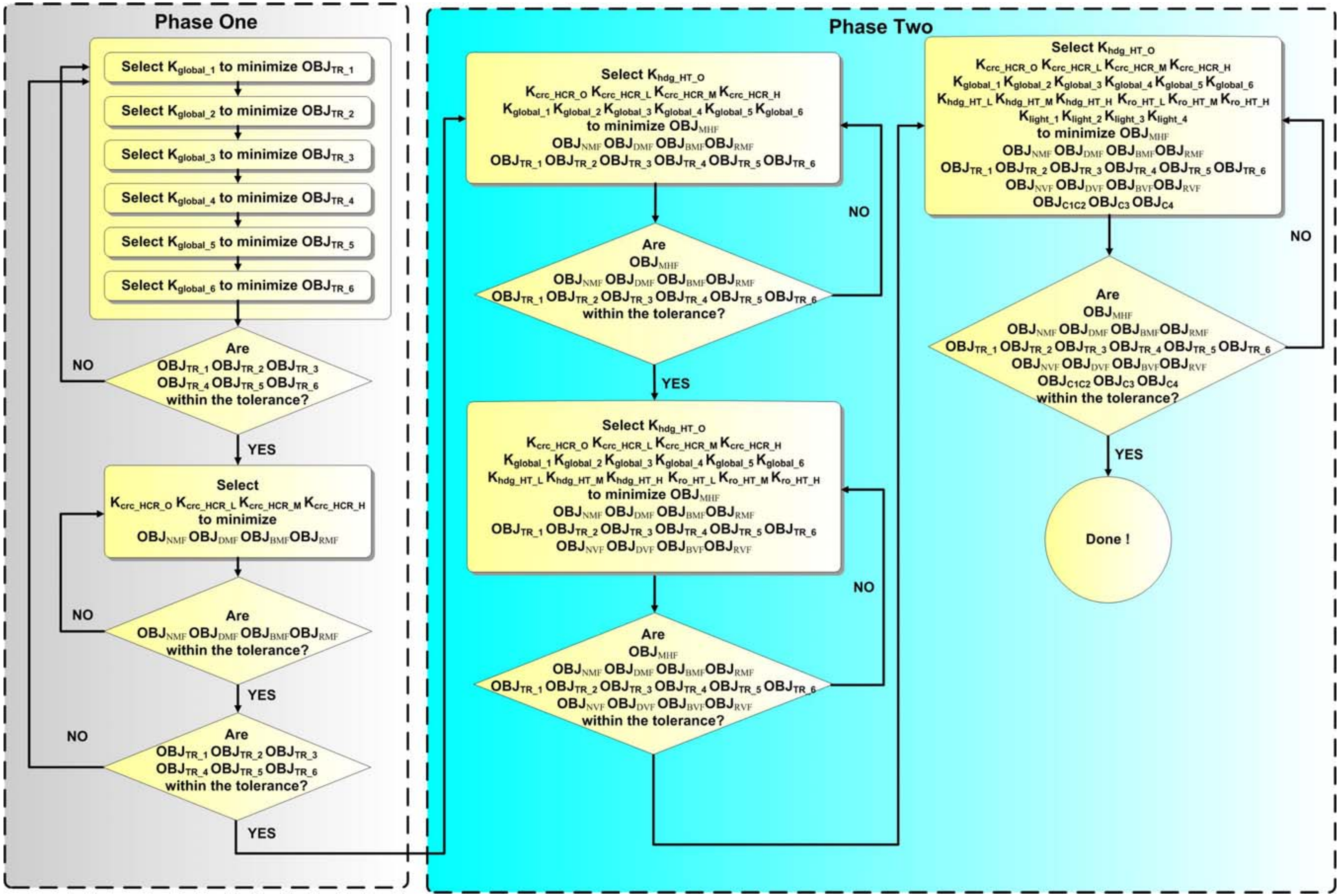

Figure 2.13 The procedure of model calibration.

### 2.4.4.2 HP HCR Reactor Model.

We describe the generalized step-by-step procedure of reactor model development in previous section. However the procedures are not applicable to the process with an unusual process flow diagram such as HP HCR process that includes two parallel reactor series. The two parallel reactor series are sharing one fractionation unit, making it unachievable to distinguish the production data from one series to the other. For example, there is no way to split heavy naphtha product into two streams to represent the performance of each reactor series. In addition, it is difficult to start with building the model of two parallel reactor series since model reconciliation of two reactor series is a time-consuming and difficult task. Therefore, we develop the following procedures to build and reconcile HP HCR reactor model:

(1) Construct an equivalent reactor to represent the two parallel reactor series;
(2) Build and reconcile the equivalent reactor model;
(3) Develop the preliminary models of the real process (two parallel reactor series);
(4) Apply the reaction activities obtained from equivalent reactor model into the reactor model of two parallel reactor series;
(5) Fine-tune the model of two parallel reactor series to match real operations and productions;

#### 2.4.4.2.1 Equivalent Reactor.

This section demonstrates the concept of equivalent reactor. Considering a system with two parallel isothermal PFRs where a first-order liquid phase reaction takes place (see Figure 2.14), the relationship between conversion and residence time of each PFR is[33]:

$$\mathrm{CONV}_1 = 1 - \mathrm{Exp}(-k\tau_1) \qquad (3)$$

$$\mathrm{CONV}_2 = 1 - \mathrm{Exp}(-k\tau_2) \qquad (4)$$

where CONV is conversion, $\tau$ is residence time, and k is rate constant. We define an equivalent reactor as a reactor that can convert the same amount of total feed flow into the same amount of total product. For the equivalent reactor, reaction conversion is represented as:

$$\mathrm{CONV_e} = 1 - \mathrm{Exp}(-k\tau_e) \tag{5}$$

Since equivalent reactor is defined by having identical total production to the two parallel isothermal PFRs, we can obtain the following equation:

$$\mathbf{F_{A\,in,T} - F_{A\,out,e} = F_{A\,in,1} - F_{Aout,1} + F_{Ain,2} - F_{Aout,2}} \tag{6}$$

Substituting the relationship between the molar flow rate and conversion:

$$\mathrm{CONV_e} = \frac{\mathrm{F_{Ain,1} - F_{Aout,1} + F_{Ain,2} - F_{Aout,2}}}{\mathrm{F_{Ain,T}}} \tag{7}$$

and letting $\theta_1 = \mathrm{F_{Ain,1}} / \mathrm{F_{Ain,T}}$ and $\theta_2 = \mathrm{F_{Ain,2}} / \mathrm{F_{Ain,T}}$ and we have:

$$\mathrm{CONV_e} = \theta_1 \times \mathrm{CONV_1} + \theta_2 \times \mathrm{CONV_2} \tag{8}$$

Substituting Eq. (3) to Eq. (5) into Eq. (8) gives:

$$1 - \mathrm{Exp}(-k\tau_e) = \theta_1 \times [1 - \mathrm{Exp}(-k\tau_1)] + \theta_2 \times [1 - \mathrm{Exp}(-k\tau_2)] \tag{9}$$

Re-arranging the equation gives:

$$\tau_e = \frac{-\ln(\theta_1 \times \mathrm{Exp}(-k\tau_1) + \theta_2 \times \mathrm{Exp}(-k\tau_2))}{k} \tag{10}$$

We can rewrite Eq. (10) into Eq. (11) in terms of space velocity (SV):

$$\mathrm{SV} = \frac{k}{-\ln(\theta_1 \times \mathrm{Exp}(-k\tau_1) + \theta_2 \times \mathrm{Exp}(-k\tau_2))} \tag{11}$$

With molar flow rate, conversion and SV, we can calculate reactor volume to conduct reactor design. The idea of equivalent reactor provides us a convenient way to understand the performance of a complex reactor system, namely, two parallel PFRs.

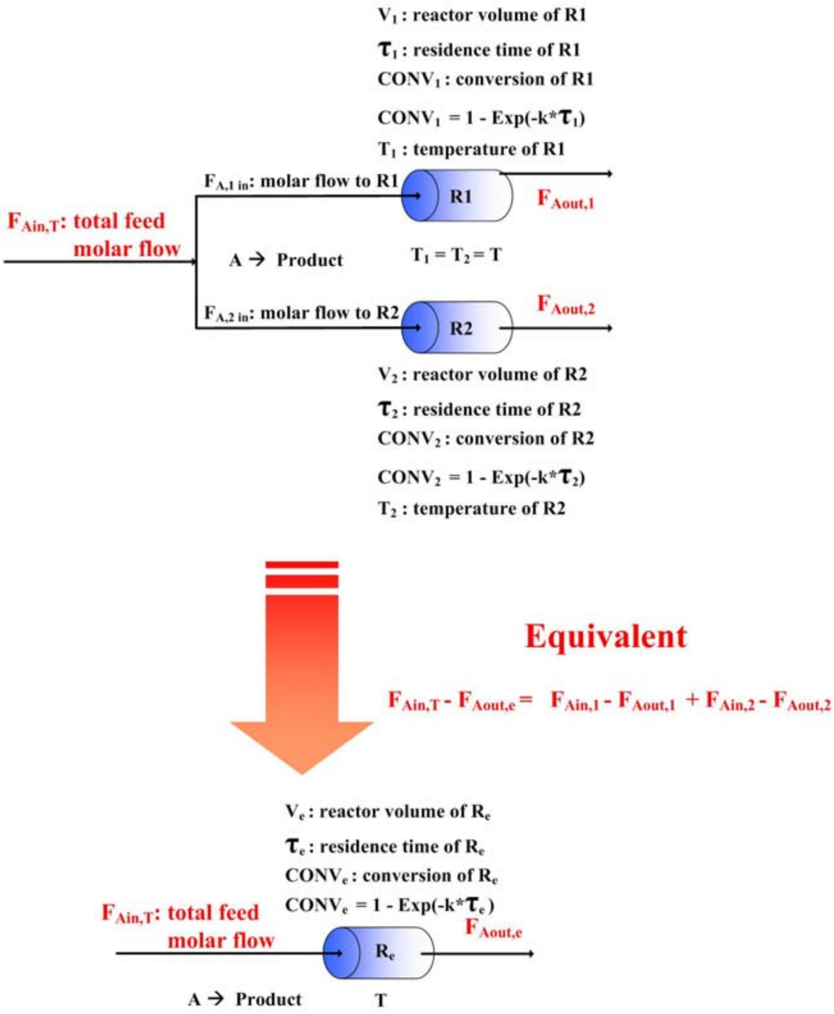

Figure 2.14 Concept of equivalent reactor

#### 2.4.4.2.2 Reconciliation of HP HCR Reactor Model.

As mentioned in previous section, there are five steps to build and reconcile the reactor model of HP HCR process. We first build an equivalent reactor model to represent the two parallel reactor series. By doing this, we can obtain good initial values of reaction activities to further model the real process. However, the difficulty of building equivalent reactor model is to assign the process variables by Eq. (11) because SV is function of rate constant. Qader and Hill[2] present a two-lump kinetic model of HCR process that characterizes feedstock and product as single lump respectively (see Figure 2.15) and apply first-order kinetics to obtain rate constant under different operating conditions. Eq. (12) represents the rate equation and they apply Arrhenius equation to correlate experimental data to obtain pre-exponential term and activation energy. Eq. (13) shows the temperature dependence of rate constant.

$$-\frac{d[\text{Gas oil}]}{dt} = k_{GO} \times [\text{Gas oil}] \tag{12}$$

$$k_{GO}\,(h^{-1}) = 1 \times 10^{7}\,(h^{-1}) \times \text{Exp}[\frac{-21100\,(\text{cal/mole})}{RT}] \tag{13}$$

where $k_{GO}$ is rate constant of gas oil HCR reaction. The experimental data were obtained at 10.34 MPa pressure, 400 – 500 ℃, 0.5 – 3.0 $h^{-1}$ SV, and a constant $H_2$/oil ratio of 500 STD $m^3/m^3$. Since they conduct experiment under similar condition as industrial reactor, it is practical to utilize kinetic data by Qader and Hill[2] to investigate the design of equivalent reactor model. We apply feed flow rates, reactor volumes, and space velocities from HP HCR process and calculate reactor volume of equivalent reactor under different rate constants. Figure 2.16 illustrates how HCR rate constant affects equivalent reactor volume. The y-axis represents the ratio of equivalent reactor volume to the sum of reactor volumes of the two parallel hydrocracking reactors ($V_e$ / ($V_1$+$V_2$)). As k approaches zero, the upper limit of 100% is also achieved. This reflects the physical limitation when no reaction takes place. On the other hand, the value of $V_e$ / ($V_1$+$V_2$) drops while k increases. Under industrial operating conditions, k value ranges from 0.5 – 3 $h^{-1}$ (corresponding reactor temperatures are 360℃ – 430℃) according to the kinetic data of Qader and Hill[2]. Therefore, typical values of $V_e$ / ($V_1$+$V_2$) should be always greater than 90%.

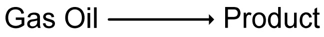

Figure 2.15 A two-lump scheme developed by Qader and Hill[2]

Because we build equivalent reactor model merely for obtaining initial values of reaction activities, we will use the sum of catalyst loading of real process to construct the equivalent reactor. We also sum up all of the material streams, namely feed flows and hydrogen quenches, to ensure mass balance of the equivalent reactor. In addition, the arithmetic averages of operating conditions such as reactor temperatures are applied for development of the equivalent reactor (see Figure 2.17 for details). During the course of model reconciliation of the equivalent reactor model, we take reactor temperature profile, flow rate of makeup hydrogen, mass and volume yields of liquid products, and light gas yields as objective functions since they are the major concerns of the HP HCR refiners. The objective functions of HP HCR process are the same as MP HCR process model, thus we follow the procedures shown in Figure 2.13 to reconcile the equivalent reactor model.

Following reconciliation of the equivalent reactor model is using real operating data to build preliminary models for real HP HCR reactors. We apply the reaction activities from the equivalent reactor model into the preliminary reactor models. It is necessary to fine tune the preliminary reactor models. By Aspen Simulation Workbook, we create a MS Excel spreadsheet (Figure 2.18) to make it feasible to simultaneously fine tune reactor models of the two parallel series. In HP HCR model, we only fine-tune hydrocracking cracking selectivity from 4.5 to 3.9 and the resulting model agrees with real operation and production well. The development equivalent reactor model reduces time and makes it achievable to develop HP HCR model of two parallel reactor series.

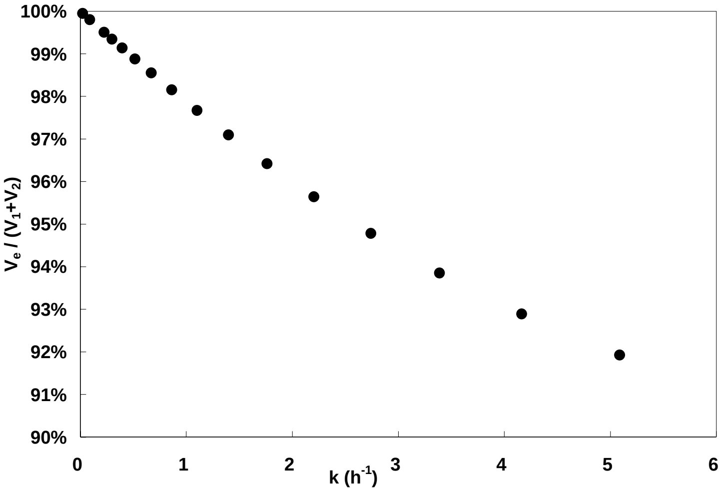

Figure 2.16 Hydrocracking rate constant vs. equivalent reactor volume

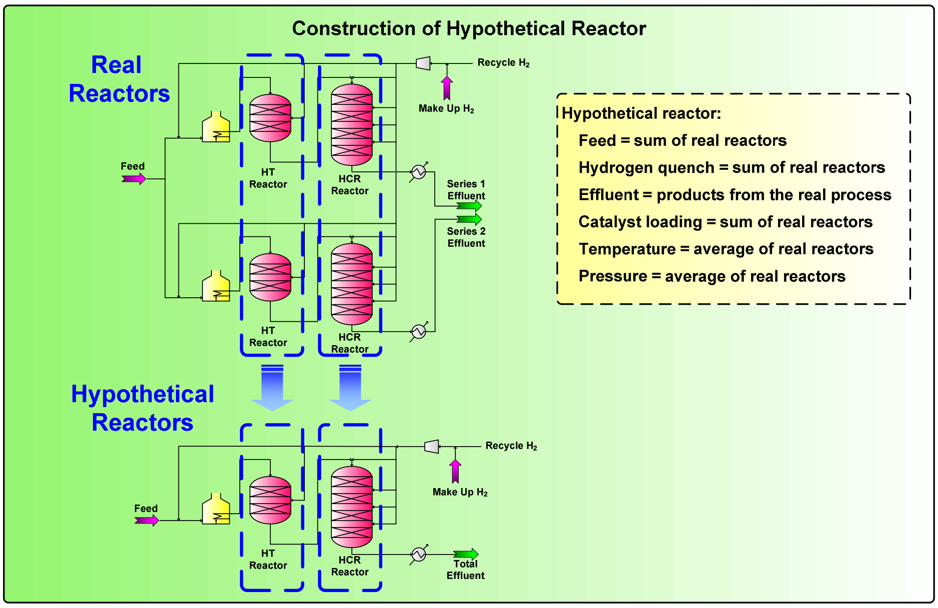

Hypothetical reactor:

Feed = sum of real reactors
Hydrogen quench = sum of real reactors
Effluent = products from the real process
Catalyst loading = sum of real reactors
Temperature = average of real reactors
Pressure = average of real reactors

Figure 2.17 Construction of the equivalent reactor

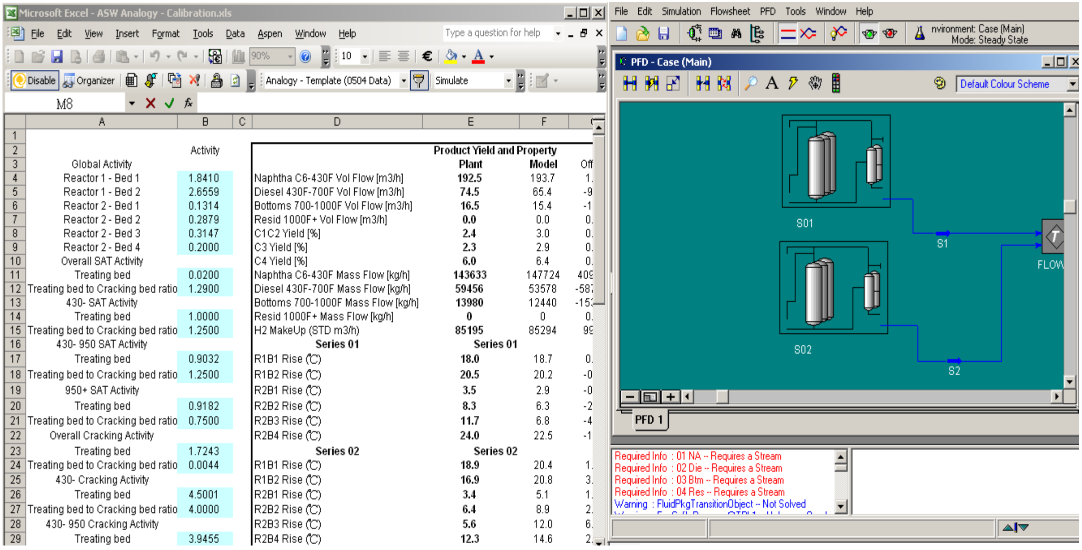

|  | A | B | C | D | E | F | G |
|---|---|---|---|---|---|---|---|
| 1 |  |  |  |  |  |  |  |
| 2 |  | Activity |  |  | Product Yield and Property |  |  |
| 3 | Global Activity |  |  |  | Plant | Model | Off |
| 4 | Reactor 1 - Bed 1 | 1.8410 |  | Naphtha C6-430F Vol Flow [m3/h] | 192.5 | 193.7 | 1. |
| 5 | Reactor 1 - Bed 2 | 2.6559 |  | Diesel 430F-700F Vol Flow [m3/h] | 74.5 | 65.4 | -9 |
| 6 | Reactor 2 - Bed 1 | 0.1314 |  | Bottoms 700-1000F Vol Flow [m3/h] | 16.5 | 15.4 | -1 |
| 7 | Reactor 2 - Bed 2 | 0.2879 |  | Resid 1000F+ Vol Flow [m3/h] | 0.0 | 0.0 | 0. |
| 8 | Reactor 2 - Bed 3 | 0.3147 |  | C1C2 Yield [%] | 2.4 | 3.0 | 0. |
| 9 | Reactor 2 - Bed 4 | 0.2000 |  | C3 Yield [%] | 2.3 | 2.9 | 0. |
| 10 | Overall SAT Activity |  |  | C4 Yield [%] | 6.0 | 6.4 | 0. |
| 11 | Treating bed | 0.0200 |  | Naphtha C6-430F Mass Flow [kg/h] | 143633 | 147724 | 409 |
| 12 | Treating bed to Cracking bed ratio | 1.2900 |  | Diesel 430F-700F Mass Flow [kg/h] | 59456 | 53578 | -58 |
| 13 | 430- SAT Activity |  |  | Bottoms 700-1000F Mass Flow [kg/h] | 13980 | 12440 | -15 |
| 14 | Treating bed | 1.0000 |  | Resid 1000F+ Mass Flow [kg/h] | 0 | 0 | 0. |
| 15 | Treating bed to Cracking bed ratio | 1.2500 |  | H2 MakeUp (STD m3/h) | 85195 | 85294 | 99 |
| 16 | 430- 950 SAT Activity |  |  | Series 01 | Series 01 |  |  |
| 17 | Treating bed | 0.9032 |  | R1B1 Rise (℃) | 18.0 | 18.7 | 0. |
| 18 | Treating bed to Cracking bed ratio | 1.2500 |  | R1B2 Rise (℃) | 20.5 | 20.2 | -0 |
| 19 | 950+ SAT Activity |  |  | R2B1 Rise (℃) | 3.5 | 2.9 | -0 |
| 20 | Treating bed | 0.9182 |  | R2B2 Rise (℃) | 8.3 | 6.3 | -2 |
| 21 | Treating bed to Cracking bed ratio | 0.7500 |  | R2B3 Rise (℃) | 11.7 | 6.8 | -4 |
| 22 | Overall Cracking Activity |  |  | R2B4 Rise (℃) | 24.0 | 22.5 | -1 |
| 23 | Treating bed | 1.7243 |  | Series 02 | Series 02 |  |  |
| 24 | Treating bed to Cracking bed ratio | 0.0044 |  | R1B1 Rise (℃) | 18.9 | 20.4 | 1. |
| 25 | 430- Cracking Activity |  |  | R1B2 Rise (℃) | 16.9 | 20.8 | 3. |
| 26 | Treating bed | 4.5001 |  | R2B1 Rise (℃) | 3.4 | 5.1 | 1. |
| 27 | Treating bed to Cracking bed ratio | 4.0000 |  | R2B2 Rise (℃) | 6.4 | 8.9 | 2. |
| 28 | 430- 950 Cracking Activity |  |  | R2B3 Rise (℃) | 5.6 | 12.0 | 6. |
| 29 | Treating bed | 3.9455 |  | R2B4 Rise (℃) | 12.3 | 14.6 | 2. |

```
Required Info  : 01 NA -- Requires a Stream
Required Info  : 02 Die -- Requires a Stream
Required Info  : 03 Btm -- Requires a Stream
Required Info  : 04 Res -- Requires a Stream
Warning  : FluidPkgTransitionObject -- Not Solved
```

Figure 2.18 Model reconciliation by MS Excel

### 2.4.5 Delumping of Reactor Model Effluent and Fractionator Model Development.

Delumping the reactor model effluent is an essential step to integrate the reactor model with the fractionator model, because kinetic lumps used in the reactor model are based on structure and carbon number, and cannot represent accurate thermodynamic behavior of the fractionator model. Since boiling point (volatility) is the most important property for distillation operation, process modelers typically use pseudo-components based on TBP curve to represent the feed oil to the HCR fractionators. We present five steps to develop pseudo-components based on boiling point (BP) ranges to represent the petroleum fraction[32, 34].

(1) Convert ASTM D86/ ASTM D1160 / simple distillation curve into the TBP curve if the curve is not available.

- We develop a spreadsheet to enable the conversion from different ASTM distillation types to the TBP curve based the correlations from ref. 35 (see Figure 2.19).

(2) Cut the entire boiling range into a number of cut-point ranges to define the BP-based pseudo-components (see Figure 2.20).

(3) Develop the density distribution of pseudo-components if only the bulk density is available:

- Assume that Waston K factor is constant throughout the entire boiling range and calculate the mean average boiling point (MeABP). We develop a spreadsheet tool to perform the iteration of estimating MeABP based on the method presented by Bollas et al.[36]

$$K_{avg} = [\mathrm{MeABP}]^{0.333} / SG_{avg} \tag{14}$$

where $K_{avg}$ is Watson K factor and $SG_{avg}$ is the bulk specific gravity 60°F/60°F

- Calculate the density distribution of the entire boiling range:

$$SG_i = [T_{i,b}]^{0.333} / K_{avg} \tag{15}$$

where $SG_i$ is the specific gravity 60°F/60°F of pseudo-component i and $T_{i,b}$ is the TBP of pseudo-component i.

(4) Estimate molecular weight distribution of the entire boiling range if it is not available. There are various correlations to estimate pseudo-component molecular weight based on standard liquid density and TBP. Riazi[37] presents a comprehensive review and comparison of published correlations.

(5) Estimate critical temperatures ($T_c$), critical pressures ($P_c$), critical volumes ($V_c$) and acentric factors ($\omega$) of pseudo-components. Refer to Riazi[37] for published correlations.

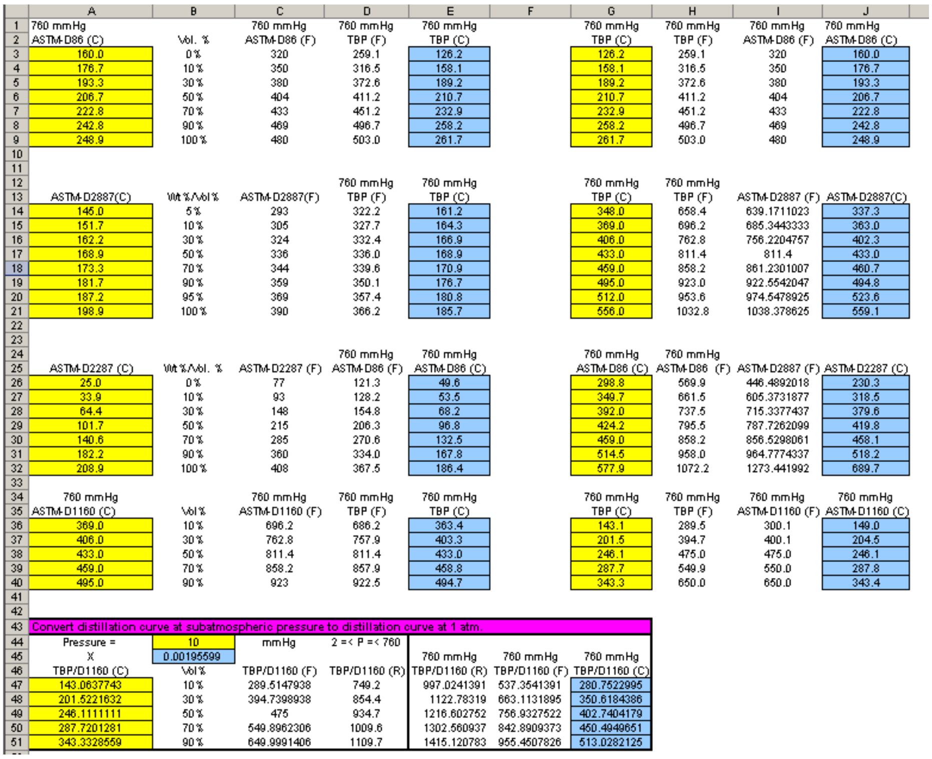

|  | A | B | C | D | E | F | G | H | I | J |
|---|---|---|---|---|---|---|---|---|---|---|
| 1 | 760 mmHg |  | 760 mmHg | 760 mmHg | 760 mmHg |  | 760 mmHg | 760 mmHg | 760 mmHg | 760 mmHg |
| 2 | ASTM-D86 (C) | Vol. % | ASTM-D86 (F) | TBP (F) | TBP (C) |  | TBP (C) | TBP (F) | ASTM-D86 (F) | ASTM-D86 (C) |
| 3 | 160.0 | 0 % | 320 | 259.1 | 126.2 |  | 126.2 | 259.1 | 320 | 160.0 |
| 4 | 176.7 | 10 % | 350 | 316.5 | 158.1 |  | 158.1 | 316.5 | 350 | 176.7 |
| 5 | 193.3 | 30 % | 380 | 372.6 | 189.2 |  | 189.2 | 372.6 | 380 | 193.3 |
| 6 | 206.7 | 50 % | 404 | 411.2 | 210.7 |  | 210.7 | 411.2 | 404 | 206.7 |
| 7 | 222.8 | 70 % | 433 | 451.2 | 232.9 |  | 232.9 | 451.2 | 433 | 222.8 |
| 8 | 242.8 | 90 % | 469 | 496.7 | 258.2 |  | 258.2 | 496.7 | 469 | 242.8 |
| 9 | 248.9 | 100 % | 480 | 503.0 | 261.7 |  | 261.7 | 503.0 | 480 | 248.9 |
| 10 |  |  |  |  |  |  |  |  |  |  |
| 11 |  |  |  |  |  |  |  |  |  |  |
| 12 |  |  |  | 760 mmHg | 760 mmHg |  | 760 mmHg | 760 mmHg |  |  |
| 13 | ASTM-D2887(C) | Wt %/Vol % | ASTM-D2887(F) | TBP (F) | TBP (C) |  | TBP (C) | TBP (F) | ASTM-D2887 (F) | ASTM-D2887(C) |
| 14 | 145.0 | 5 % | 293 | 322.2 | 161.2 |  | 348.0 | 658.4 | 639.1711023 | 337.3 |
| 15 | 151.7 | 10 % | 305 | 327.7 | 164.3 |  | 369.0 | 696.2 | 685.3443333 | 363.0 |
| 16 | 162.2 | 30 % | 324 | 332.4 | 166.9 |  | 406.0 | 762.8 | 756.2204757 | 402.3 |
| 17 | 168.9 | 50 % | 336 | 336.0 | 168.9 |  | 433.0 | 811.4 | 811.4 | 433.0 |
| 18 | 173.3 | 70 % | 344 | 339.6 | 170.9 |  | 459.0 | 858.2 | 861.2301007 | 460.7 |
| 19 | 181.7 | 90 % | 359 | 350.1 | 176.7 |  | 495.0 | 923.0 | 922.5542047 | 494.8 |
| 20 | 187.2 | 95 % | 369 | 357.4 | 180.8 |  | 512.0 | 953.6 | 974.5478925 | 523.6 |
| 21 | 198.9 | 100 % | 390 | 366.2 | 185.7 |  | 556.0 | 1032.8 | 1038.378625 | 559.1 |
| 22 |  |  |  |  |  |  |  |  |  |  |
| 23 |  |  |  |  |  |  |  |  |  |  |
| 24 |  |  |  | 760 mmHg | 760 mmHg |  | 760 mmHg | 760 mmHg |  |  |
| 25 | ASTM-D2287 (C) | Wt %/Vol. % | ASTM-D2287 (F) | ASTM-D86 (F) | ASTM-D86 (C) |  | ASTM-D86 (C) | ASTM-D86 (F) | ASTM-D2887 (F) | ASTM-D2287 (C) |
| 26 | 25.0 | 0 % | 77 | 121.3 | 49.6 |  | 298.8 | 569.9 | 446.4892018 | 230.3 |
| 27 | 33.9 | 10 % | 93 | 128.2 | 53.5 |  | 349.7 | 661.5 | 605.3731877 | 318.5 |
| 28 | 64.4 | 30 % | 148 | 154.8 | 68.2 |  | 392.0 | 737.5 | 715.3377437 | 379.6 |
| 29 | 101.7 | 50 % | 215 | 206.3 | 96.8 |  | 424.2 | 795.5 | 787.7262099 | 419.8 |
| 30 | 140.6 | 70 % | 285 | 270.6 | 132.5 |  | 459.0 | 858.2 | 856.5298061 | 458.1 |
| 31 | 182.2 | 90 % | 360 | 334.0 | 167.8 |  | 514.5 | 958.0 | 964.7774337 | 518.2 |
| 32 | 208.9 | 100 % | 408 | 367.5 | 186.4 |  | 577.9 | 1072.2 | 1273.441992 | 689.7 |
| 33 |  |  |  |  |  |  |  |  |  |  |
| 34 | 760 mmHg |  | 760 mmHg | 760 mmHg | 760 mmHg |  | 760 mmHg | 760 mmHg | 760 mmHg | 760 mmHg |
| 35 | ASTM-D1160 (C) | Vol % | ASTM-D1160 (F) | TBP (F) | TBP (C) |  | TBP (C) | TBP (F) | ASTM-D1160 (F) | ASTM-D1160 (C) |
| 36 | 369.0 | 10 % | 696.2 | 686.2 | 363.4 |  | 143.1 | 289.5 | 300.1 | 149.0 |
| 37 | 406.0 | 30 % | 762.8 | 757.9 | 403.3 |  | 201.5 | 394.7 | 400.1 | 204.5 |
| 38 | 433.0 | 50 % | 811.4 | 811.4 | 433.0 |  | 246.1 | 475.0 | 475.0 | 246.1 |
| 39 | 459.0 | 70 % | 858.2 | 857.9 | 458.8 |  | 287.7 | 549.9 | 550.0 | 287.8 |
| 40 | 495.0 | 90 % | 923 | 922.5 | 494.7 |  | 343.3 | 650.0 | 650.0 | 343.4 |
| 41 |  |  |  |  |  |  |  |  |  |  |
| 42 |  |  |  |  |  |  |  |  |  |  |
| 43 | Convert distillation curve at subatmospheric pressure to distillation curve at 1 atm. |  |  |  |  |  |  |  |  |  |
| 44 | Pressure = | 10 | mmHg | 2 =< P =< 760 |  |  |  |  |  |  |
| 45 | X | 0.00195599 |  |  | 760 mmHg | 760 mmHg | 760 mmHg |  |  |  |
| 46 | TBP/D1160 (C) | Vol % | TBP/D1160 (F) | TBP/D1160 (R) | TBP/D1160 (R) | TBP/D1160 (F) | TBP/D1160 (C) |  |  |  |
| 47 | 143.0637743 | 10 % | 289.5147938 | 749.2 | 997.0241391 | 537.3541391 | 280.7522995 |  |  |  |
| 48 | 201.5221632 | 30 % | 394.7398938 | 854.4 | 1122.78319 | 663.1131895 | 350.6184386 |  |  |  |
| 49 | 246.1111111 | 50 % | 475 | 934.7 | 1216.602752 | 756.9327522 | 402.7404179 |  |  |  |
| 50 | 287.7201281 | 70 % | 549.8962306 | 1009.6 | 1302.560937 | 842.8909373 | 450.4949651 |  |  |  |
| 51 | 343.3328559 | 90 % | 649.9991406 | 1109.7 | 1415.120783 | 955.4507826 | 513.0282125 |  |  |  |

Figure 2.19 Inter-conversion between different ASTM distillation types.

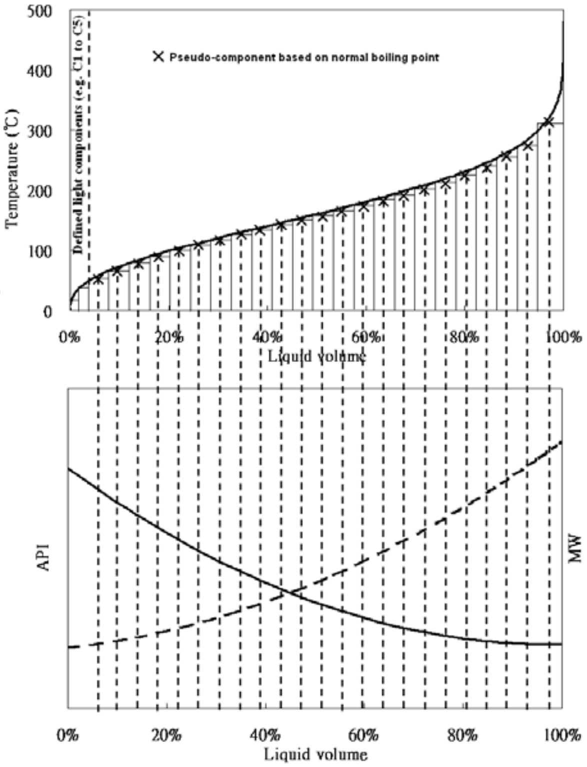

Figure 2.20 Relationship between pseudo-component properties and the TBP curve.

(redraw from ref. 32)

Because the reactor model provides the TBP curve, API gravity and molecular weight distribution of the model effluent from kinetic lumps, the major issue of developing pseudo-components in this work is to properly cut the TBP curve into numbers of BP-based pseudo-components. However, the number and boiling point ranges of cut points are arbitrary and there is no general rule to determine the cut-point ranges. Having a large number of cuts does not always lead to good representation; while having a small number of cuts may cause discontinuous prediction of column operation[32]. Additionally, the discrete nature of kinetic lumps (see Figure 2.21) makes it difficult to cut the TBP curve of the reactor model effluent to define reasonable BP-based pseudo-components. In this work, we find that applying Gauss-Legendre quadrature to cut the reactor model effluent into 20 BP-based pseudo-components works well. The rest of this section will represent the delumping we use to define these pseudo-components, how to apply tray efficiency model while building the fractionator model, and the sensitivity test of the fractionator model to verify the delumping method used in this work.

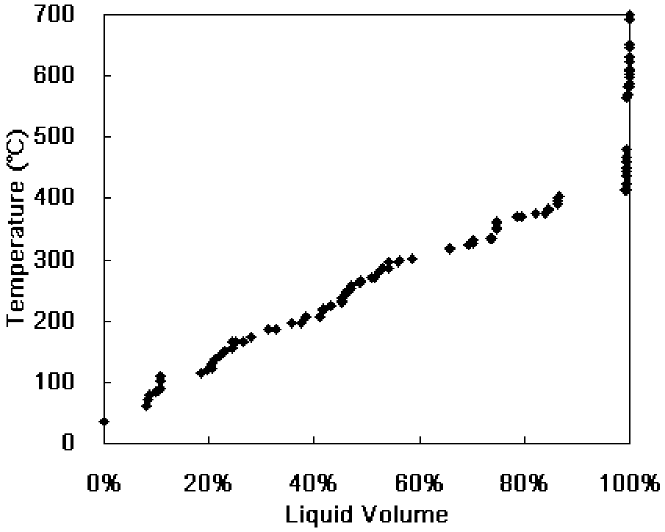

Figure 2.21 Discontinuity of C6+ kinetic lump distribution of reactor model effluent.

### 2.4.5.1 Apply the Gauss-Legendre Quadrature to Delump the Reactor Model Effluent.

Haynes and Matthews[38] apply the Gauss-Legendre quadrature to predict the vapor-liquid-equilibrium (VLE) of hydrocarbon mixture derived from a continuous equation-of-state developed by Cotterman et al.[39]. Later, Mani et al.[40] extend the work of Haynes and Matthews[38] to partition the cut-point ranges of TBP curve of a petroleum fraction to define BP-based pseudo-components, and the predicted VLE satisfactorily matches the experimental data. Hence, we extend the method represented by Mani et al.[40] to delump the reactor model effluent into BP-based pseudo-components.

In this work, we develop a method with six steps to delump the reactor model effluent into

BP-based pseudo-components by the Gauss-Legendre quadrature.

(1) Split the reactor model effluent into C6- and C6+ streams because the components below C6 are well-defined light components.

(2) Obtain TBP curve, API gravity and molecular weight distribution of C6+ stream from reactor model.

(3) Determine the number (n) of pseudo-components to be used in delumping.

■ In this work, we delump the reactor model effluent into 20 BP-based pseudo-components.

(4) We have posted on our group website the quadrature points and weight factors for the Gauss-Legendre integration which are used to partition the cut points over the TBP curve.

■ Use $F_{vi}$ calculated from the equation below to partition the cut point ($F_{vi}$) over the TBP curve of C6+ stream:

$$F_{vi} = \frac{1}{2} \times [q_i + 1] \tag{16}$$

Interpolate TBP curve to obtain the TBP associated to each cut point ($F_{vi}$). Figure 2.22 demonstrates the case of n = 6.

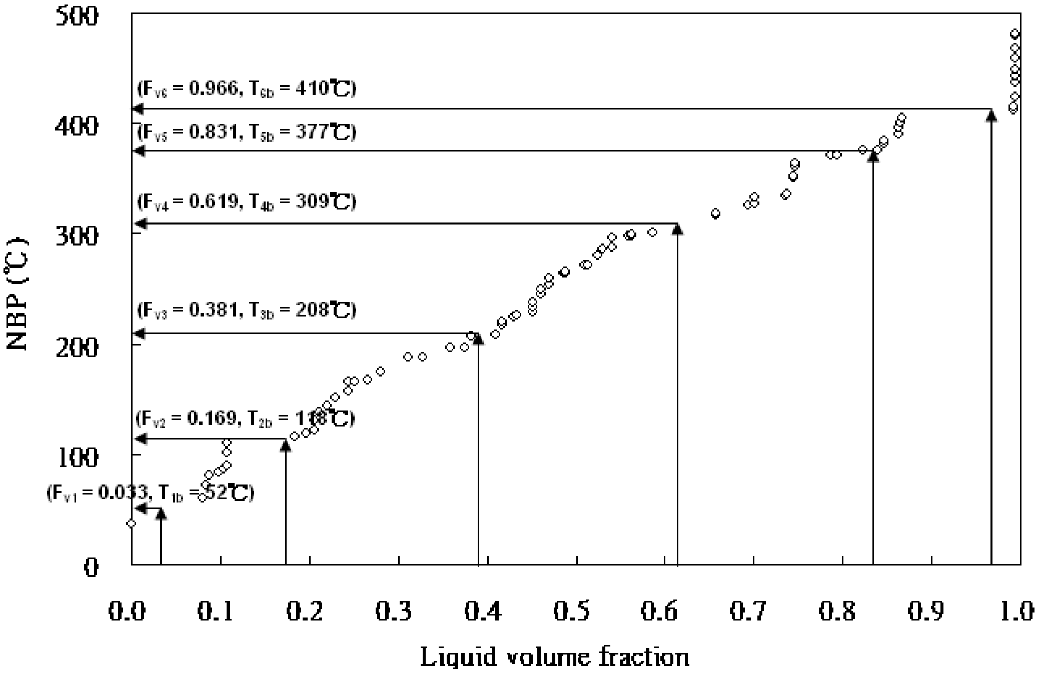

Figure 2.22 Demonstration of allocating cut point over TBP curve.

- Use the same interpolation procedure to obtain API gravities and molecular weights of the associated cut points ($F_{vi}$).

(5) Estimate $T_c$, $P_c$, $V_c$ and $\omega$ of each pseudo-component by using molecular weight and specific gravity $60^{\circ}F/60^{\circ}F$ which can be converted from API gravity.

- For $T_c$ and $P_c$, Haynes and Matthews[38] recommend to use the correlation developed by Riazi and Daubert[41]:

$$T_C\ (K) = 19.0627 \times T_b^{0.58848} \times SG^{0.3596} \tag{17}$$

$$P_C\ (atm) = 5.458 \times 10^7 \times T_b^{-2.3125} \times SG^{2.3201} \tag{18}$$

- For $\omega$, Haynes and Matthews[38] suggest to use the correlation developed by Lee and Kesler[42]:

$$\omega = \frac{(-\ln(P_c, atm) - 5.92714 + \frac{6.09648}{T_r} + 1.28862 \times T_r - 0.169347 \times T_r^6)}{(15.2518 - \frac{15.6875}{T_r} - 13.4721 \times \ln(T_r) + 0.43577 \times T_r^6)} \tag{19}$$

- For $V_c$, to be consistent with the estimations of $T_c$ and $P_c$, we also apply the correlation developed by Riazi and Daubert[41]:

$$V_C\ (cm^3/mol) = 1.7842 \times 10^{-4} \times T_b^{2.3829} \times SG^{-1.683} \tag{20}$$

(6) The last step of delumping is to calculate mole fraction ($x_i$) of each pseudo-component.

- Use the equation below to calculate mole fraction of each pseudo-component:

$$x_i = \frac{w_i \times SG_i \times MW_{avg}}{2 \times SG_{avg} \times MW_i} \tag{21}$$

where $w_i$ is the weight factor of Gauss-Legendre quadrature, $SG_i$ and MWi are the specific gravity and molecular weight of pseudo-component i which are calculated from interpolating the specific gravity and molecular weight distributions of reactor model effluent, respectively, and $SG_{avg}$ and $MW_{avg}$ are the average specific gravity and molecular weight obtained from reactor model, respectively.

- Table 2.6 lists the resulting pseudo-components and their properties and compositions for the case of n = 6.

Table 2.6 BP-based pseudo-components and their properties and compositions

| | $x_i$ | $q_i^*$ | $w_i$ | TBP (℃) | MW | SG | Tc (℃) | Pc (kPa) | Vc ($m^3$/kgmole) | $\omega$ |
|---|---|---|---|---|---|---|---|---|---|---|
| Pseudo 1 | 0.1559 | -0.932470 | 0.171324 | 52 | 84.0 | 0.6694 | 223.6 | 3373.3 | 0.340 | 0.2326 |
| Pseudo 2 | 0.2529 | -0.661209 | 0.360762 | 118 | 128.8 | 0.7904 | 314.8 | 3233.3 | 0.400 | 0.2789 |
| Pseudo 3 | 0.2550 | -0.238619 | 0.467914 | 208 | 174.9 | 0.8346 | 403.3 | 2282.8 | 0.595 | 0.4286 |
| Pseudo 4 | 0.1809 | 0.238619 | 0.467914 | 309 | 248.6 | 0.8411 | 486.3 | 1491.6 | 0.928 | 0.6792 |
| Pseudo 5 | 0.1091 | 0.661209 | 0.360762 | 377 | 318.7 | 0.8438 | 538.3 | 1163.0 | 1.201 | 0.8968 |
| Pseudo 6 | 0.0462 | 0.932470 | 0.171324 | 410 | 357.5 | 0.8438 | 562.3 | 1037.4 | 1.352 | 1.0252 |
| $MW_{avg}$ = 175, $SG_{avg}$ = 0.8084 | | | | | | | | | | |

* $q_i$ are the zeros of the Legendre polynomial of order n and $m_i$ are the associated weight factors

### 2.4.5.2 Key Issue of Building Fractionator Model: Overall Tray Efficiency Model.

In building simulation models for fractionators, simulation software users often misunderstand the concept of "tray efficiency" [32]. The theoretical column model based on rigorous thermodynamics assumes that each tray is in perfect vapor-liquid equilibrium (VLE). However, real distillation columns do not perform perfectly. The "*overall tray efficiency*", defined as (number of theoretical trays / number of actual trays), indicates the difference of a real column to a theoretical column. We can apply the overall tray efficiency to the entire column or to specific separation zones. For example, 20 theoretical trays are required to model an operating column with 40 actual trays and 50% overall tray efficiency. It is important to remember that all trays in this column still perform perfect VLE.

There are also tray efficiency models such as the "*single tray efficiency*" that considers the separation achieved on each tray independently. The most popular single tray efficiency model is the Murphree tray efficiency based on either vapor phase or liquid phase. We calculate the Murphree tray efficiency by the following equation:

$$E = \frac{y_n - y_{n+1}}{y_n^* - y_{n+1}} \quad \text{or} \quad \frac{x_n - x_{n+1}}{x_n^* - x_{n+1}} \tag{22}$$

where $y_n$ ($x_n$) is the actual composition of vapor (liquid) leaving tray n, $y_{n+1}$ ($x_{n+1}$) indicates the actual composition of vapor (liquid) leaving tray n+1, and $y_n^*$ ($x_n^*$) represents the actual composition of vapor (liquid) leaving tray n. We note that when applying a single tray efficiency model, such as the Murphree tray efficiency, the vapor and liquid leaving a tray no longer achieve VLE in the column model.

However, many simulation software users do not realize that the tray efficiency models included in commercial simulators are "single tray efficiency model" and should be careful while applying this type of tray efficiency model[32]. The non-VLE calculation of a column may cause unexpected error for heat balance. Moreover, the "single tray efficiency model" will make the resulting column simulation "no different from a fitting and useless for prediction purpose"[32]. Both Kaes[32] and Kister[43] suggest that usually it is best to apply rigorous thermodynamic calculation in column modeling, implying that we should use an "overall tray efficiency model" to account for column non-ideality instead of "single tray efficiency model". Table 2.7 lists the recommended values of tray efficiency for each separation section in distillation simulations[32] which we apply in our column models.

Table 2.7 Suggested values of tray efficiencies for distillation columns[32]

| | Typical efficiency (%) |
|---|---|
| Debutanizer (overall) | 85-90 |
| Crude distillation | |
| Stripping zone | 30 |
| Flash zone – 1st draw | 30 |
| 1st draw – 2nd draw | 45 – 50 |
| 2nd draw – 3rd draw | 50 – 55 |
| Top draw - reflux | 60 – 70 |

### 2.4.5.3 Verification of the Delumping Method

As we mentioned before, the number of cut-point ranges is arbitrarily defined. Kaes[32] states that it is necessary to perform a sensitivity test to study the relationship of side draw rate to side draw temperature and associated distillation curve to ensure if the defined BP-based pseudo-components are able to provide reasonable results. If the relationship is step-wise rather than continuous, the number of BP-based pseudo-components needs to be redefined. In this work, we cut reactor model effluent into 20 TBP pseudo-components to represent the feed to fractionators. To run the sensitivity test, we change draw rates of diesel fuel to investigate the relationship among draw rates, draw temperatures and distillation curves of products.

In order to verify that the delumping method of Gauss-Legendre quadrature with 20 BP-based pseudo-components is sufficient for column models, we perform another sensitivity test as a contrast which utilizes the even cut-point range method to cut reactor model effluent into 46 BP-based pseudo-components. The even cut-point range method is a built-in method available in Aspen HYSYS/Refining that converts the reactor model into BP-based pseudo-components with equal boiling point ranges.

Figure 2.23 to Figure 2.26 represent the results of sensitivity tests for the even cut-point range method and the Gauss-Legendre quadrature. The figures do not include initial points, end points, 90% and 95% points because modeled initial points and end points are usually not reliable[32] and the variations in 90% and 95% are too flat to provide representative results (both are less than 1%). Apparently, both methods generate smooth and continuous relationships between the draw rates and draw temperatures (see Figure 2.23 and Figure 2.24). However, Figure 2.25 and Figure 2.26 illustrate that these two methods have different performances on predicting the relationships between draw rate and distillation curve. The Gauss-Legendre quadrature is able to predict smooth and continuous relationship between draw rate and distillation curve, while the even cut-point range method is not. By using the Gauss-Legendre quadrature to delump reactor model effluent, we are able to build well-behaved column models with a few BP-based pseudo-components.

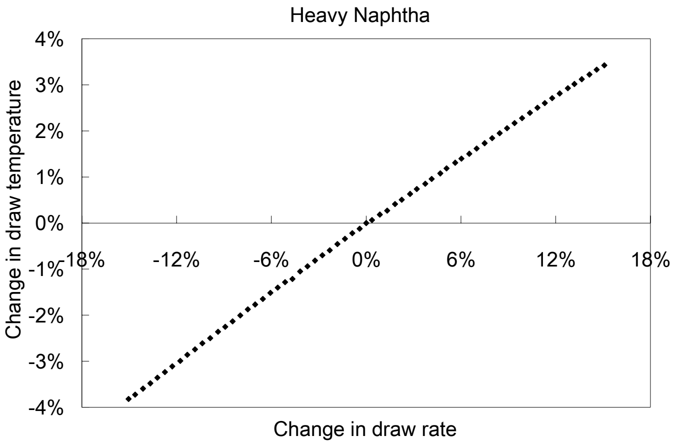

Figure 2.23 Relationship between draw rate and draw temperature of heavy naphtha

(even cut-point range method)

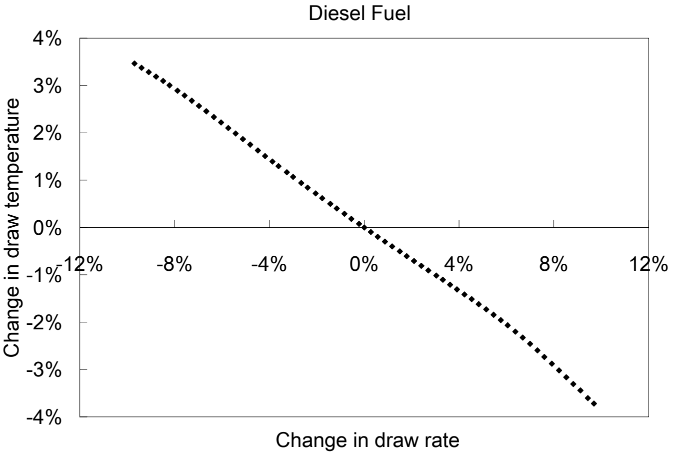

Figure 2.24 Relationship between draw rate and draw temperature of diesel fuel

(Gauss-Legendre quadrature method

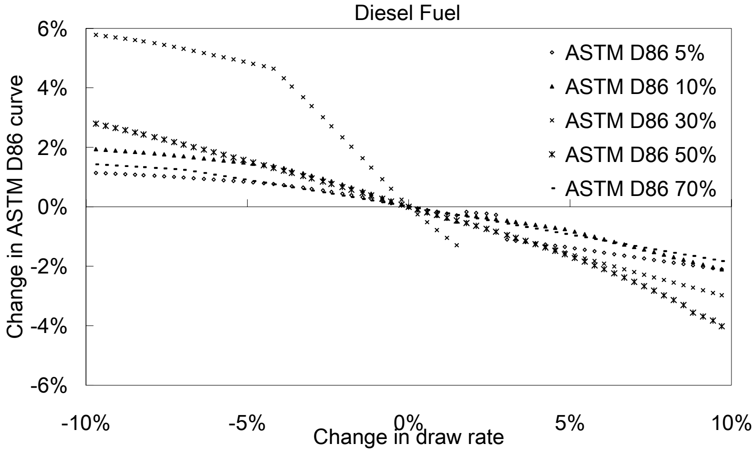

Figure 2.25 Relationship between draw rate and distillation curve of diesel fuel (even cut-point range method)

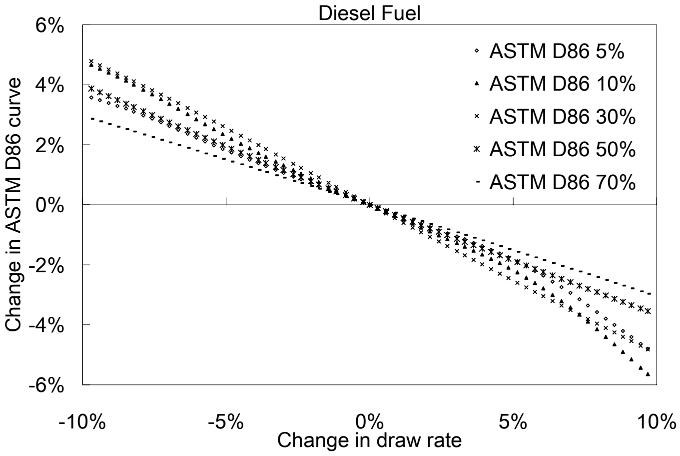

Figure 2.26 Relationship between draw rate and distillation curve of diesel fuel (Gauss-Legendre quadrature method)

### 2.4.6 Product Property Correlation.

The last important issue of building an integrated HCR model is the fuel property estimation, particularly the flash point and freezing point of diesel fuel and specific gravities of liquid products. We can estimate the specific gravities of liquid products, once we have defined the BP-based pseudo-components and calibrated the model for product flow rates (mass and volume). Flash point is defined as the lowest temperature at which a flame or spark can ignite the mixture of air and the vapors arising from oils. Flash point indicates the highest temperature at which we can store and transport the oils safely. For pure substance, freezing point is the temperature at which liquid solidifies. For petroleum fraction which is the mixture of hydrocarbons, freezing point is defined as the temperature at which solid crystals formed on cooling disappear as the temperature is increasing[35]. For both properties, we update the parameters used in API correlations[35] , Eq. (23) and Eq. (24):

$$\text{Flash Point (Fahrenheit)} = \text{A} \times 10\% \text{ of ASTM D86(Fahrenheit)} + \text{B} \tag{23}$$

$$\text{Freezing Point (R)} = \text{A} + \text{B} \times \text{SG} + \text{C} \times \frac{\text{MeABP}^{1/3}}{\text{SG}} + \text{D} \times \text{MeABP} \tag{24}$$

For MP HCR process, we apply 130 and 115 data points collected from the plant to re-fit Eq. (23) and Eq. (24) respectively. The AAD of the new correlations for flash point and freezing point are 2.7℃ and 2.3℃ and the resulting correlations are:

$$\text{Flash Point (Fahrenheit)} = 0.677 \times 10\% \text{ of ASTM D86(Fahrenheit)} - 118.2 \tag{25}$$

$$\text{Freezing Point (R)} = \text{A} + \text{B} \times \text{SG} + \text{C} \times \frac{\text{MeABP}^{1/3}}{\text{SG}} + \text{D} \times \text{MeABP} \tag{26}$$

For HP HCR process, we apply 142 and 63 data points collected from the plant to re-fit Eq. (23) and Eq. (24) respectively. The AAD of the new correlations for flash point and freezing point are 1.2℃ and 1.6℃ and the resulting correlations are:

$$\text{Flash Point (Fahrenheit)} = 0.51 \times 10\% \text{ of ASTM D86(Fahrenheit)} - 57.7 \tag{27}$$

$$\text{FreezingPoint (R)} = -857.63 + 437.16 \times \text{SG} + 41.68 \times \frac{MeABP^{1/3}}{SG} - 0.483 \times MeABP \tag{28}$$

We apply Eqs. (25) to (28) to estimate the flash points and freezing points of diesel ful in MP

HCR process and jet fuel in HP HCR process by models' predictions on distillation curve, specific gravity, and MeABP.

## 2.5 Modeling Results of MP HCR Process.

### 2.5.1 Performance of Reactor and Hydrogen Recycle System.

Our MP HCR model includes three major parts of commercial HCR process: reactors, fractionators and hydrogen recycle system. Figure 2.27 and Figure 2.28 show the model predictions of weight-average reactor temperatures (WART) of hydrotreating reactor and HCR reactor. In the reactor model, we define the inlet temperature of each catalyst bed and the model will calculate the outlet temperature of each bed. The average absolute deviations (AAD) of catalyst bed outlet temperatures of the HCR reactor is 1.9℃. The model generates good predictions on temperature profile of HCR reactor which is important for estimating product yields. However, the predictions on temperature profile of hydrotreating reactor are less accurate than those of HCR reactor. Because model calibration does not consider HDS and HDN reactions, the model is not able to estimate the reaction activity of hydrotreating reactor well. Figure 2.29 represents modeling result of makeup hydrogen flow rate and the average relative deviation (ARD) is about 8%. The error results from two factors: (1) the model is not good at predicting HDS and HDN activities, which affect the estimation of hydrogen consumption; and (2) the allocation of hydrogen recycle system of Aspen HYSYS/Refining (see Figure 2.4) is different from that of the MP HCR unit (see Figure 2.8). Aspen HYSYS/Refining considers makeup hydrogen mixes with recycle hydrogen before feeding into the hydrogen recycle system; however, in the MP HCR unit, makeup hydrogen directly mixes with feed oil and does not influence the hydrogen recycle system. This will make reactor model less accurate in calculating the hydrogen partial pressure of the reactors and cause deviation on estimating hydrogen consumption.

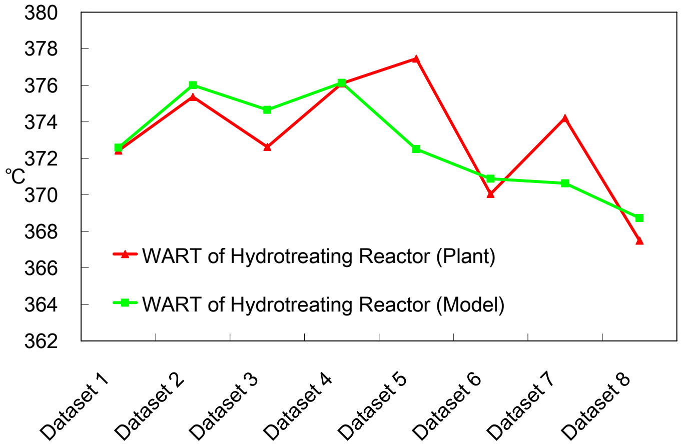

Figure 2.27 Predictions of WART of hydrotreating reactor (MP HCR Process)

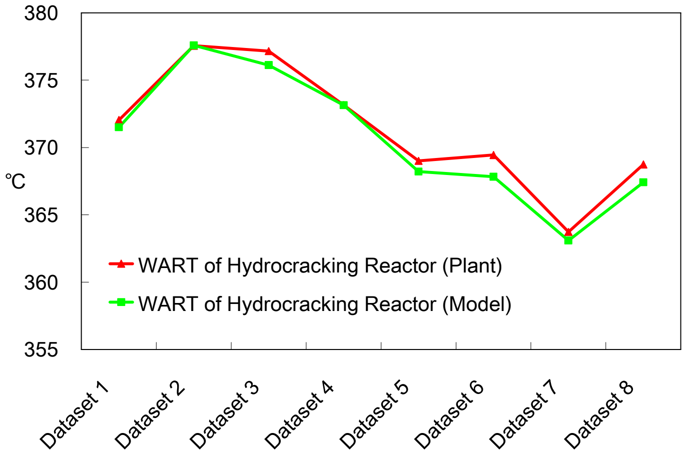

Figure 2.28 Predictions of WART of HCR reactor (MP HCR Process)

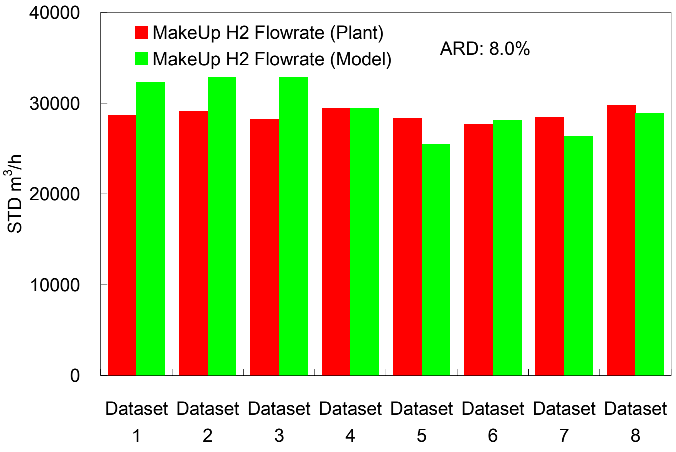

Figure 2.29 Predictions of makeup hydrogen flow rate (MP HCR)

### 2.5.2 Performance of Fractionators.

Temperature profile of distillation column is valuable for evaluating energy consumption, helping plant operation of cut-point and process optimization. Figure 2.30 to Figure 2.33 illustrate selected modeling results on temperature profiles of distillation columns. Note that we apply the overall tray efficiency model to column simulations and the resulting tray number of column model does not correspond to the tray number in the real column. Therefore, we use “top -> bottom” in Figure 2.30 to Figure 2.33 instead, showing tray number to illustrate temperature distribution from condenser to bottom of the column. Obviously, the model is able to provide good predictions on column temperature profiles.

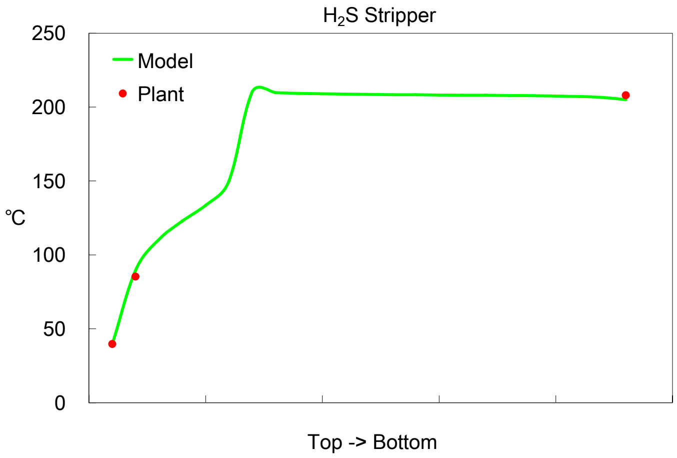

Figure 2.30 Prediction of temperature profile of $H_2S$ stripper (dataset 1 in MP HCR)

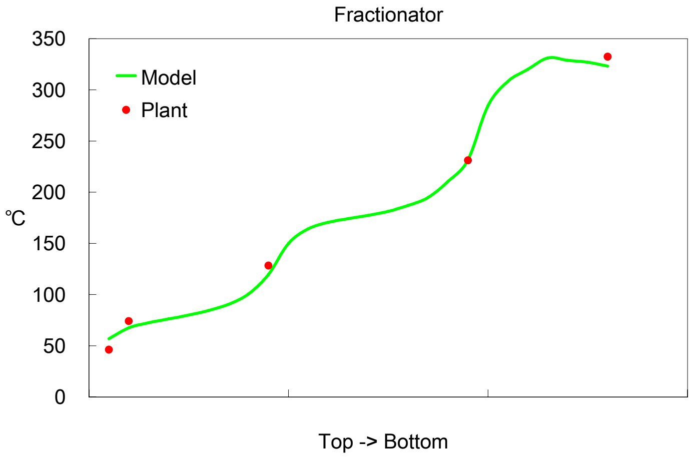

Figure 2.31 Prediction of temperature profile of fractionator (dataset 1 in MP HCR)

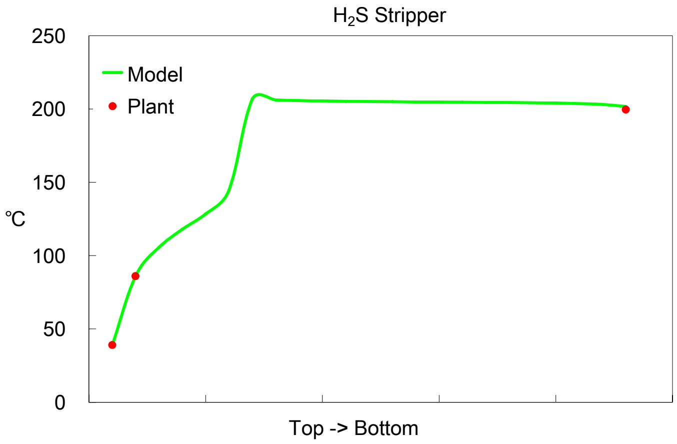

Figure 2.32 Prediction of temperature profile of $H_2S$ stripper (dataset 5 in MP HCR)

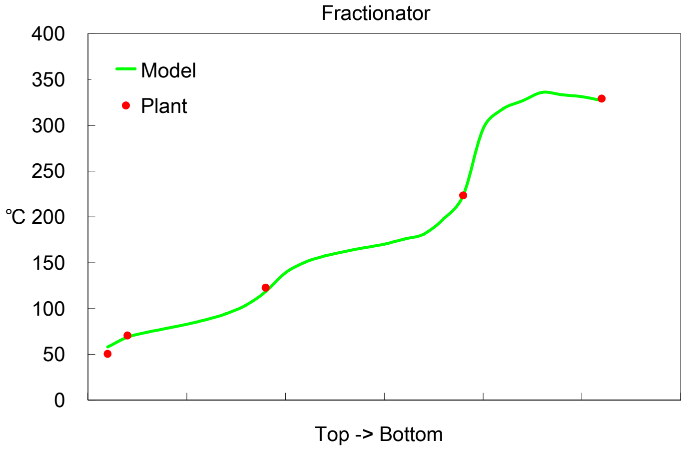

Figure 2.33 Prediction of temperature profile of fractionator (dataset 5 in MP HCR)

### 2.5.3 Product Yields.

There are seven products in the MP HCR unit as depicted in Figure 2.8, namely, low-pressure separator vapor (LPS VAP), sour gas, LPG, light naphtha, heavy naphtha, diesel fuel and bottom oil. Among these seven products, light naphtha, heavy naphtha, diesel fuel and bottom oil are major products since they account for over 95wt% of the overall production. Figure 2.34 to

Figure 2.37 illustrate the model predictions on light naphtha, heavy naphtha, diesel fuel and bottom oil and the average absolute deviations are 0.3 wt%, 3.4 wt%, 2.4 wt% and 2.4 wt%, respectively. We calculate AAD by averaging the absolute deviations (i.e. | predicted wt% - plant wt% |) of the eight datasets, since the relative deviation (i.e. | predicted wt% - plant wt% | / | plant wt% |) only represents model's prediction on each product yield rather than the overall yield, which is the key profit concern to the refinery. On the other hand, absolute deviation indicates how model affects the estimation of refinery's profit by considering the deviations in the same scale toward overall production. For example, the model shows 13% relative deviation on predicting light naphtha's mass production, but gives no clues about how model affects the overall yield. Considering that the mass yield of light naphtha is about 2.6 wt%, the 13% relative deviation has only a very small effect (0.3 wt%) on the overall yield. The model gives good prediction results on product yields when considering the average values of product yields.

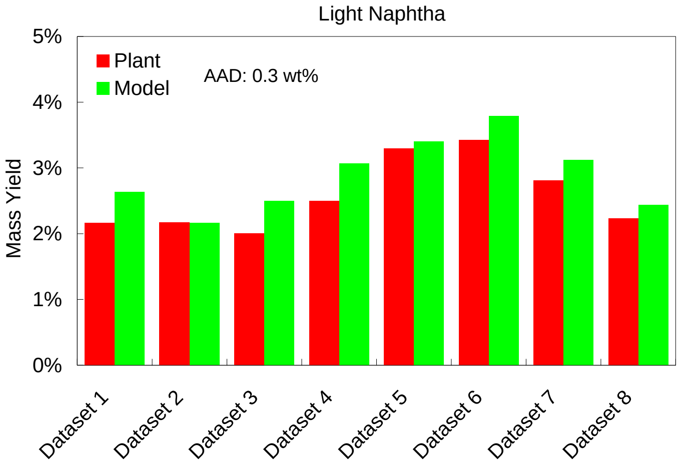

Figure 2.34 Predictions of light naphtha yield (MP HCR)

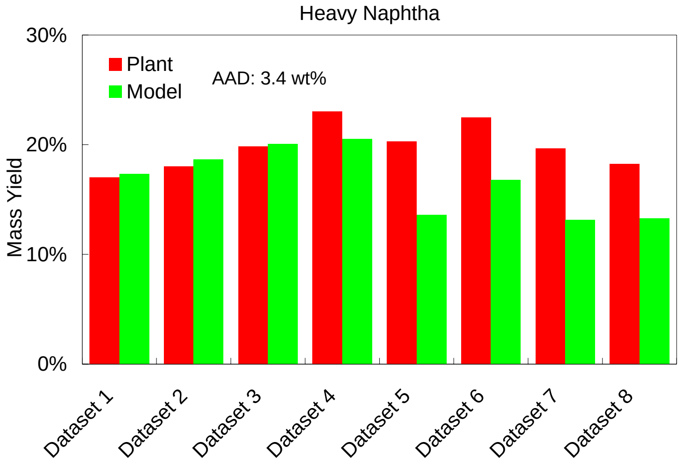

Figure 2.35 Predictions of heavy naphtha yield (MP HCR)

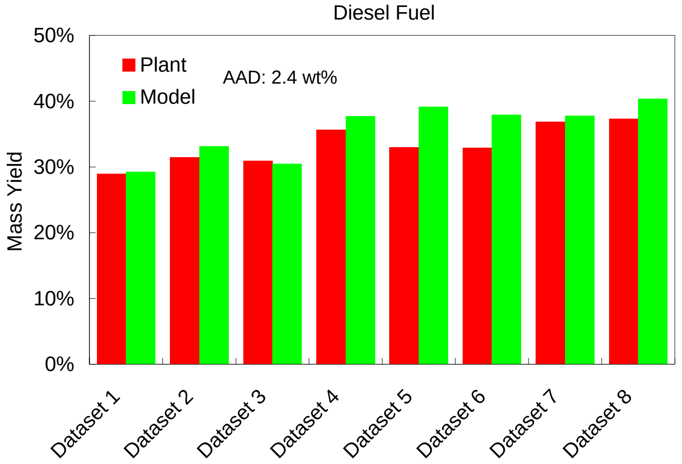

Figure 2.36 Predictions of diesel fuel yield (MP HCR)

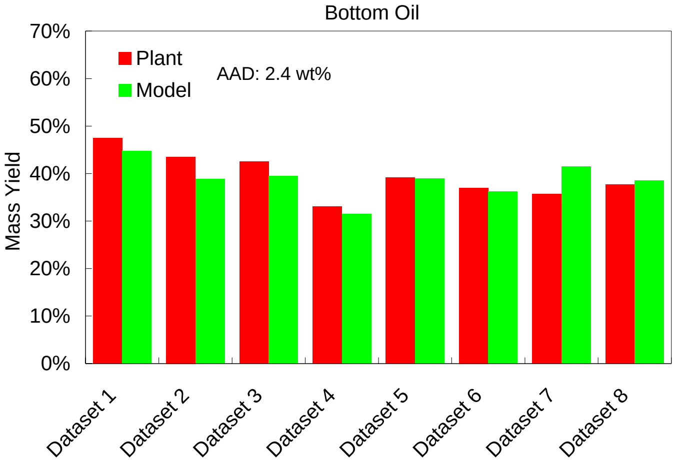

Figure 2.37 Predictions of diesel fuel yield (MP HCR)

### 2.5.4 Distillation Curves of Liquid Products.

Distillation curve displays the vaporization temperature after having a certain amount of oil fraction vaporized. Figure 2.38 and Figure 2.39 illustrate selected model predictions on distillation curves of light naphtha, heavy naphtha, diesel fuel and bottom oil. The deviations of predicting distillation curves result from two factors: (1) fractionator simulation cannot provide reliable results of the initial and final boiling points of liquid products[32]; and (2) the reactor model cannot provide accurate predictions of the boiling point distribution of reactor effluent. Although the model is able to predict accurately product yield after calibration, it does not predict the on boiling point distribution (distillation curve) of liquid product with an equal accuracy. This follows because the nature of discrete boiling point distribution of kinetic lumps. Figure 2.40 to Figure 2.42 illustrate the differences between C5+ distribution of plant reactor effluent and model prediction.

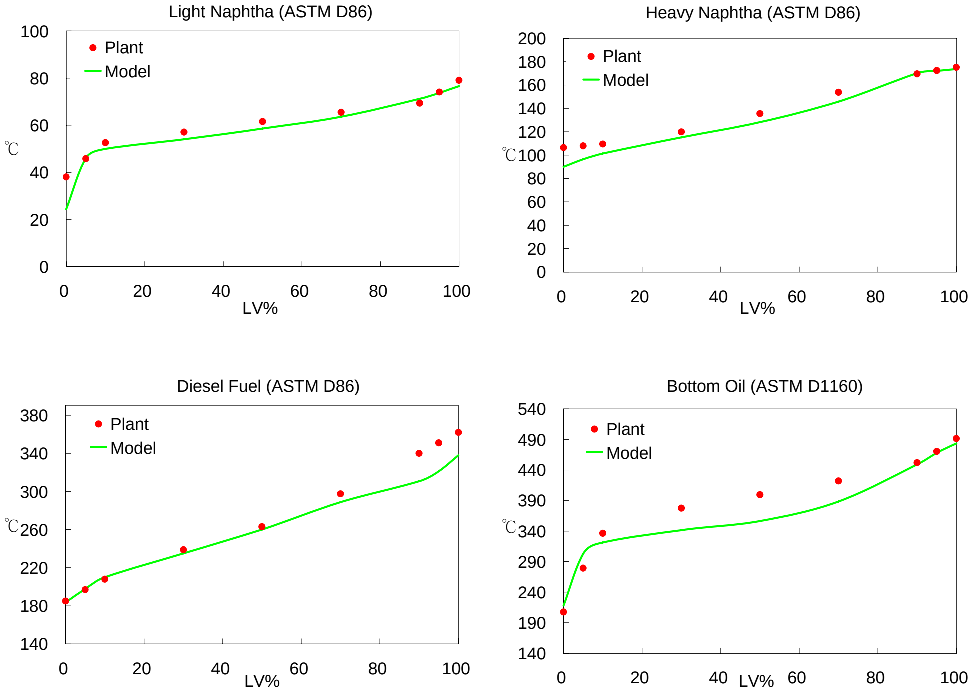

Figure 2.38 Predictions of distillation curves of liquid products (dataset 1 in MP HCR)

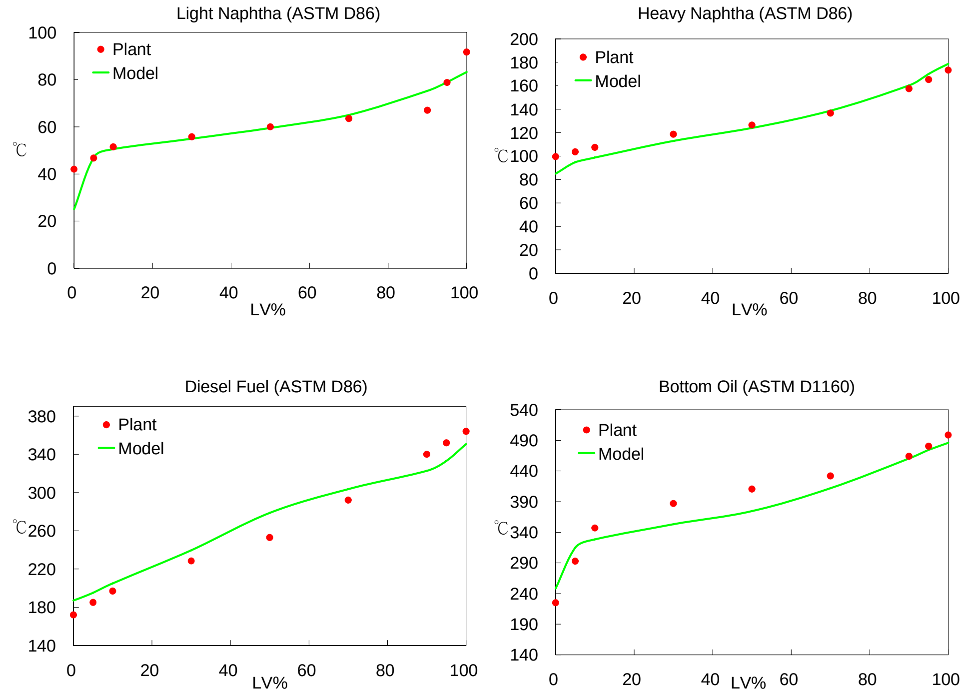

Figure 2.39 Predictions of distillation curves of liquid products (dataset 5 in MP HCR)

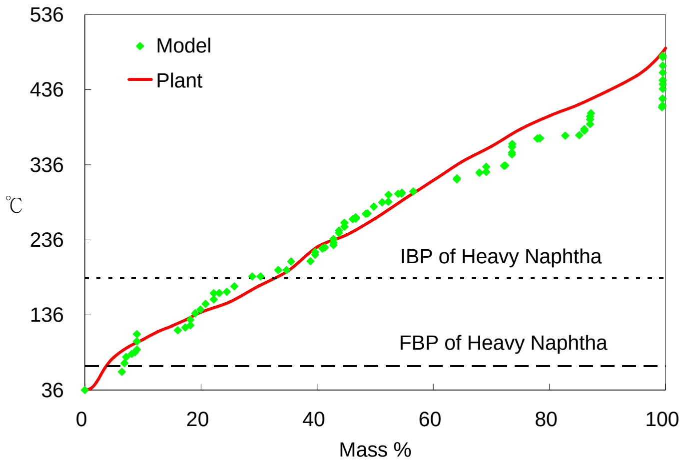

Figure 2.40 Comparison between C5+ distribution of plant reactor effluent and model prediction within the boiling point range of heavy naphtha (Dataset 4 in MP HCR).

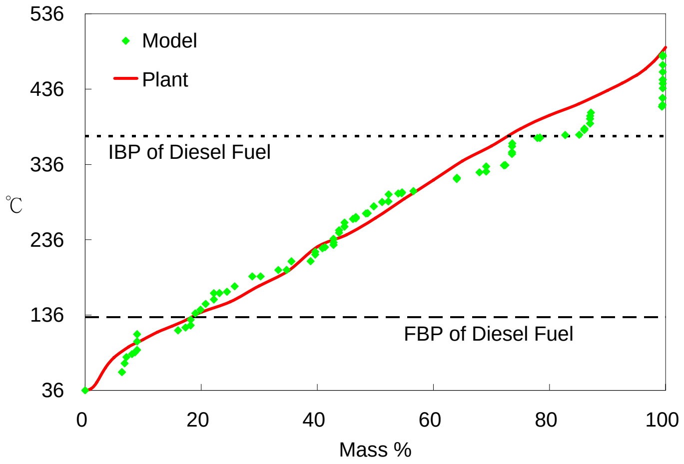

Figure 2.41 Comparison between C5+ distribution of plant reactor effluent and model prediction within the boiling point range of diesel fuel (Dataset 4 in MP HCR).

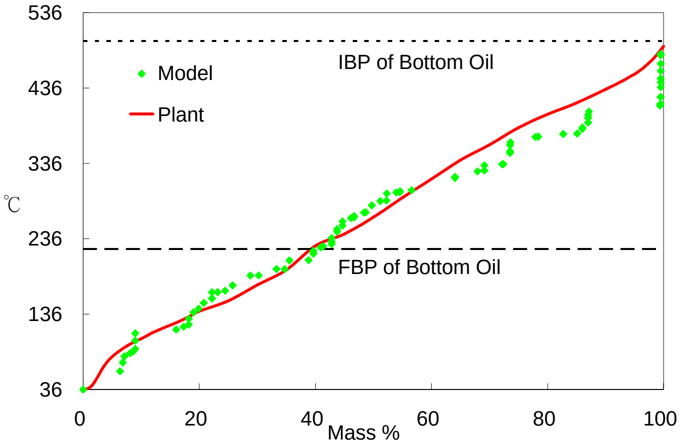

Figure 2.42 Comparison between C5+ distribution of plant reactor effluent and model prediction within the boiling point range of bottom oil (Dataset 4 in MP HCR).

### 2.5.5 Product Property.

Section 2.4.6 demonstrates the updated correlations for predicting flash point and freezing point of diesel fuel. Figure 2.43 and Figure 2.44 illustrate model predictions on flash point and freezing point of diesel fuel. The average absolute deviations are 3.6℃ and 4.1℃, which are about the same values as that obtained from correlating plant data. The integrated model collaborated with updated correlations demonstrated in Section 2.4.6 gives satisfactory predictions on flash point and freezing point of diesel fuel. Figure 2.45 to Figure 2.48 illustrate the specific gravity predictions of liquid products, which are calculated by Aspen HYSYS. The accurate predictions not only show model's predictability on specific gravity of liquid product, but also demonstrate that the delumping method we described in Section 2.4.5 is able to carry over density distribution to BP-based pseudo-components.

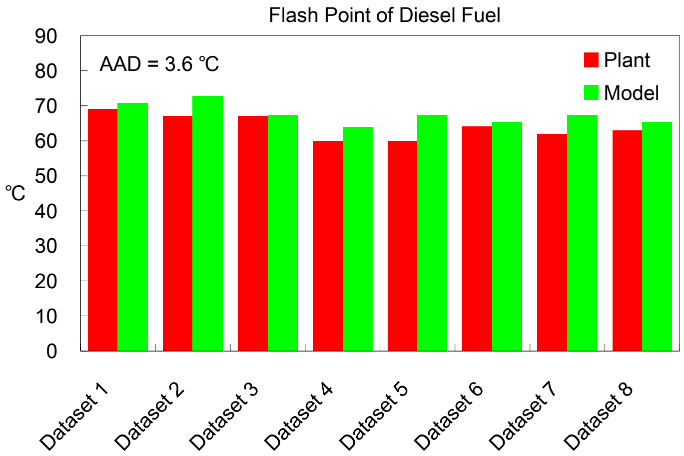

Figure 2.43 Predictions of diesel fuel's flash point (MP HCR).

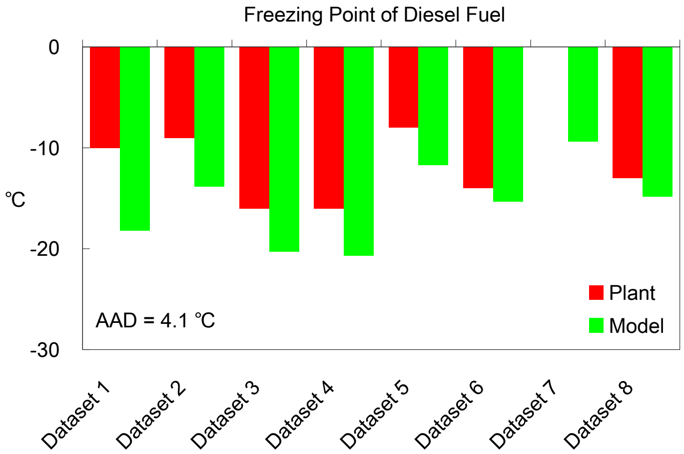

Figure 2.44 Predictions of diesel fuel's freezing point (MP HCR).

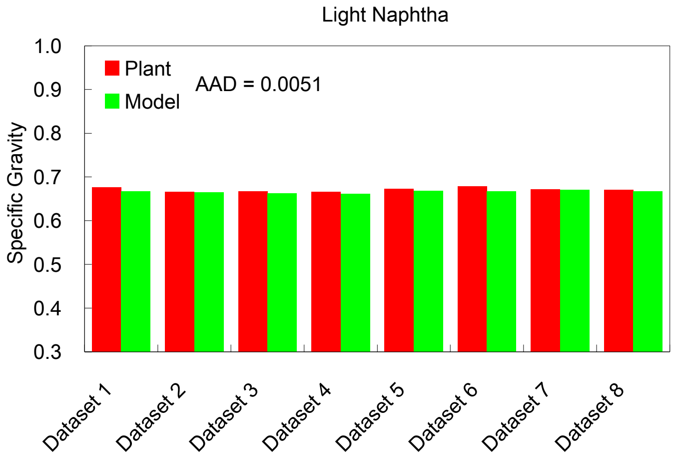

Figure 2.45 Predictions of light naphtha’s specific gravity (MP HCR).

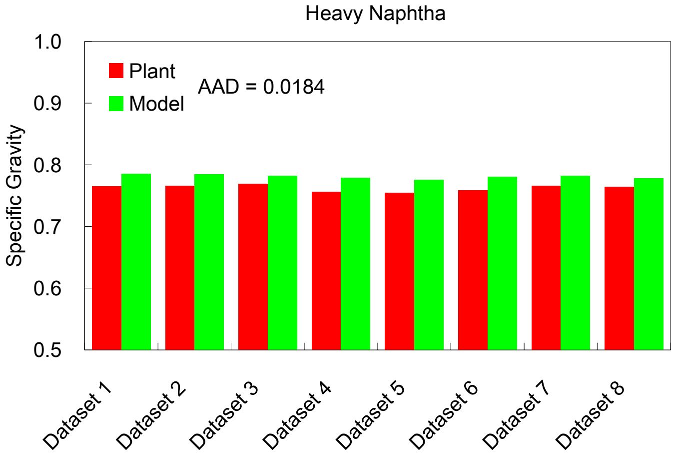

Figure 2.46 Predictions of heavy naphtha’s specific gravity (MP HCR).

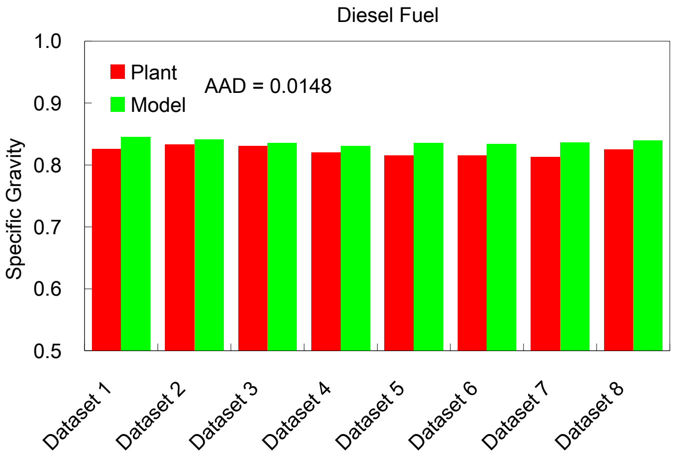

Figure 2.47 Predictions of diesel fuel's specific gravity (MP HCR).

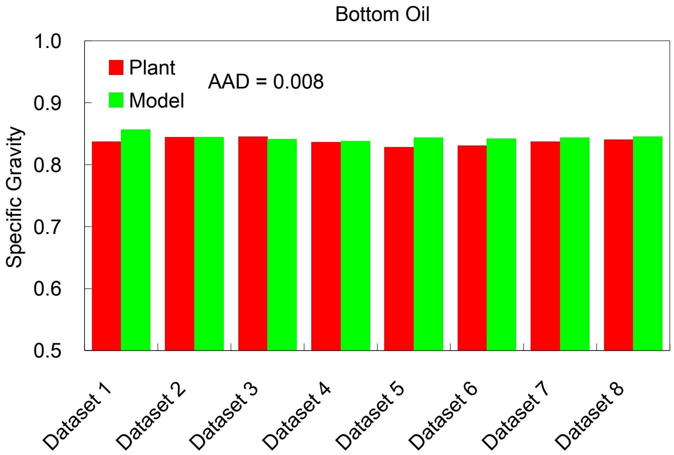

Figure 2.48 Predictions of bottom oil's specific gravity (MP HCR).

## 2.6 Modeling Results of HP HCR Process.

### 2.6.1 Performance of Reactor and Hydrogen Recycle System.

Our HP HCR model includes three major parts of commercial HCR process: reactors, fractionators and hydrogen recycle system. In the reactor model, we define the inlet temperature of each catalyst bed and the model will calculate the outlet temperature of each bed. The AADs of catalyst bed outlet temperatures of the two hydrocracking reactors are 1.8℃ and 3.2℃ for series 1 and series 2 respectively. Figure 2.49 and Figure 2.50 show the model predictions of WARTs of hydrotreating reactors and HCR reactors. The model generates good predictions on temperature profile of reactors. Figure 2.51 represents modeling result of makeup hydrogen flow rate and the average relative deviation (ARD) is only 2%.

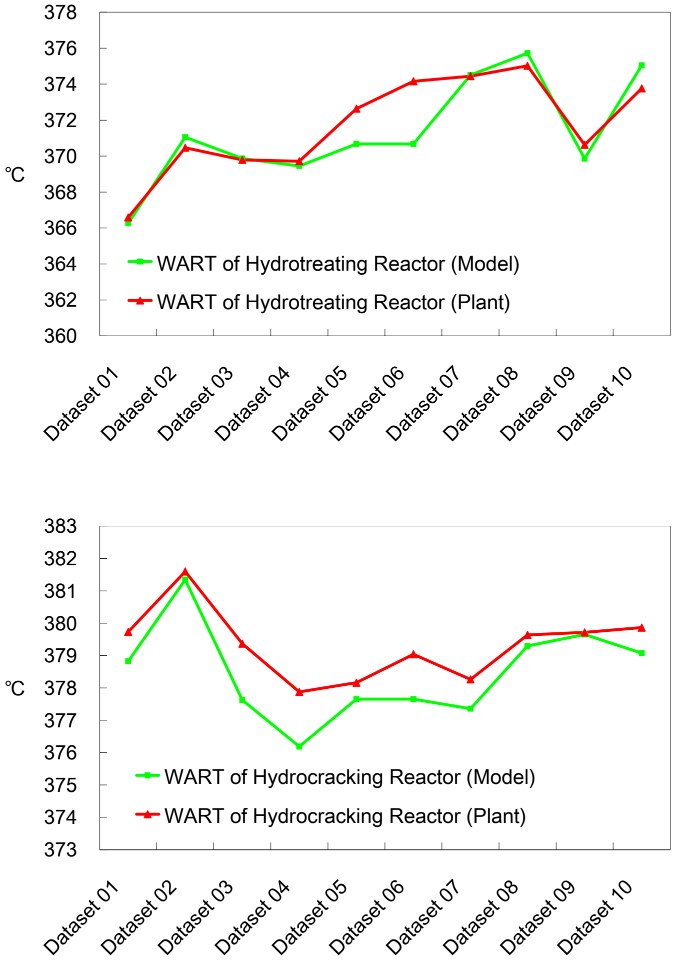

Figure 2.49 Predictions of WARTs of hydrotreating and HCR reactors

(Series 1 in HP HCR)

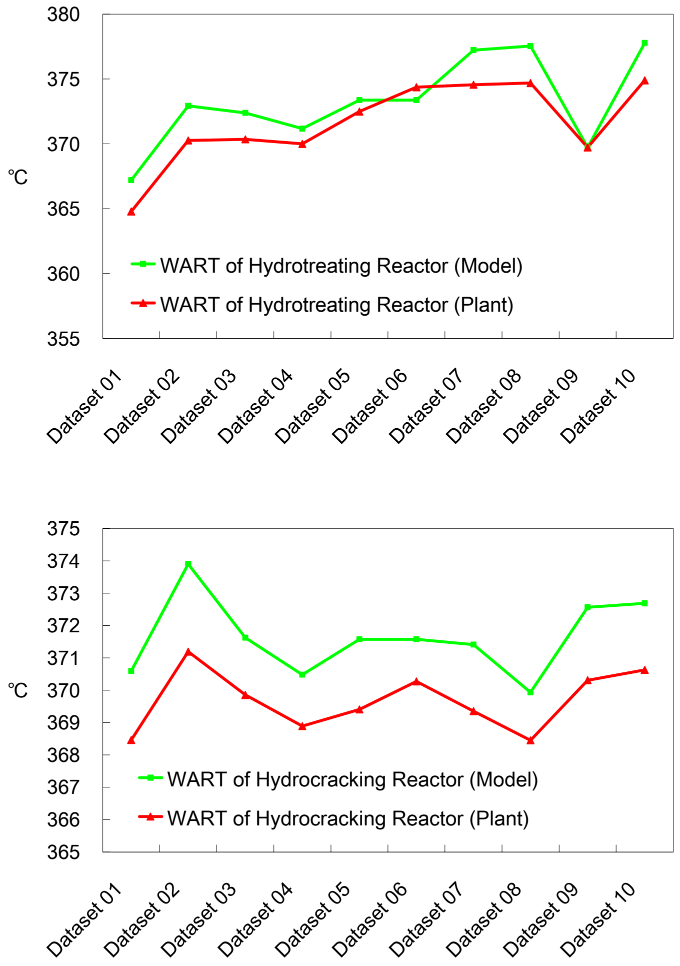

Figure 2.50 Predictions of WARTs of hydrotreating and HCR reactors

(Series 2 in HP HCR)

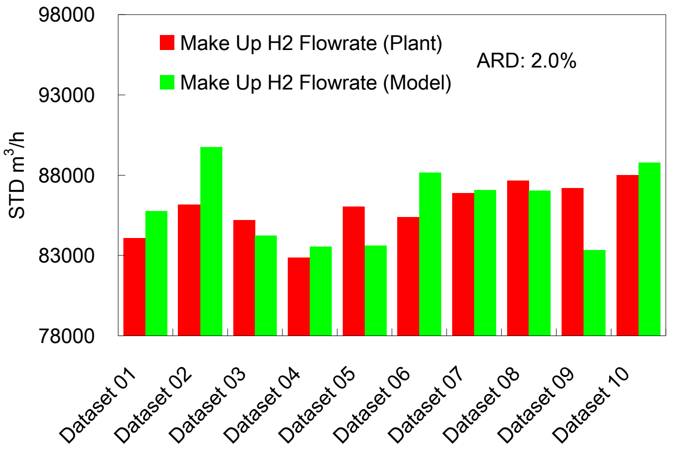

Figure 2.51 Predictions of makeup hydrogen flow rate (HP HCR)

### 2.6.2 Performance of Fractionators.

Figure 2.52 and Figure 2.53 illustrate selected modeling results on temperature profiles of distillation columns. These figures are similar to Figure 2.30 to Figure 2.33 from MP HCR.

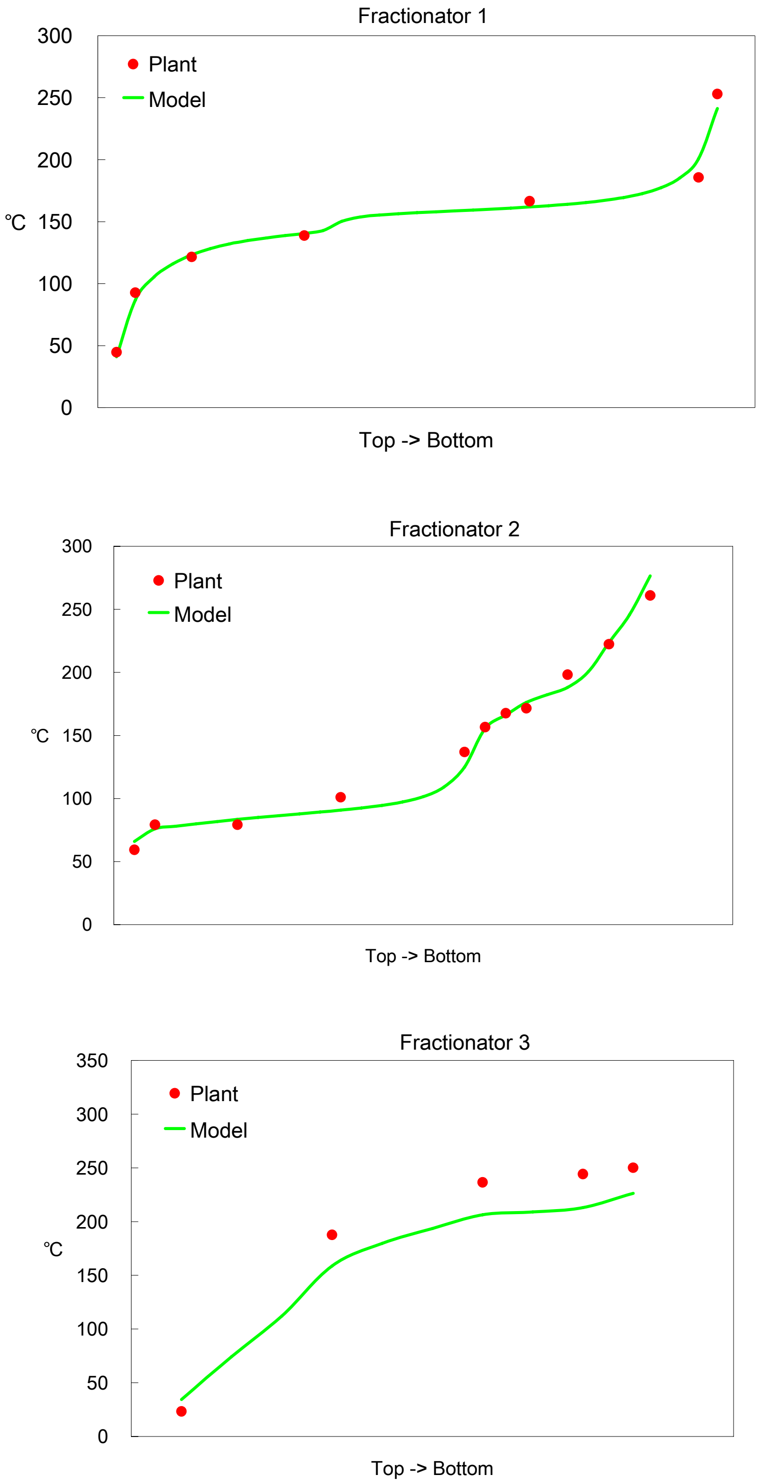

Figure 2.52 Prediction of temperature profiles of fractionators (dataset 1 in HP HCR)

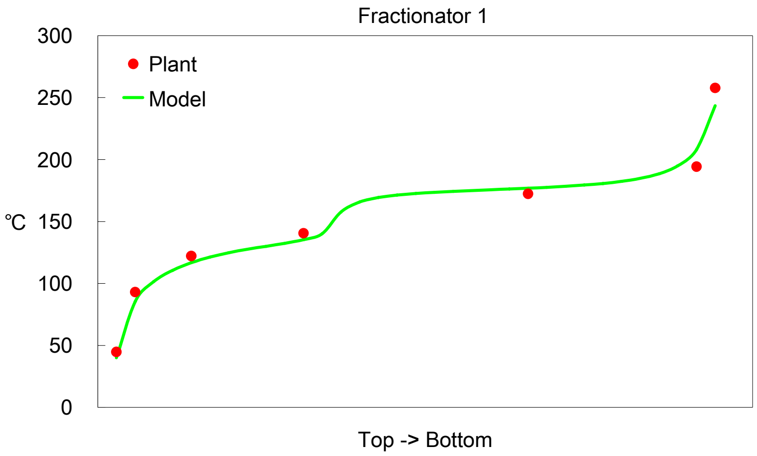

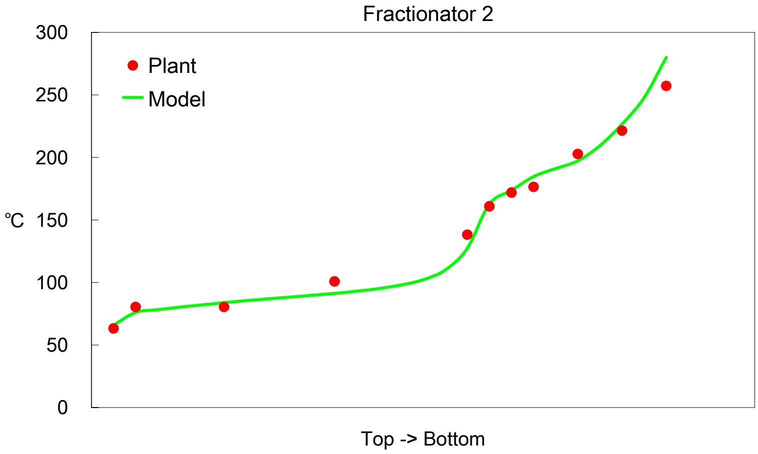

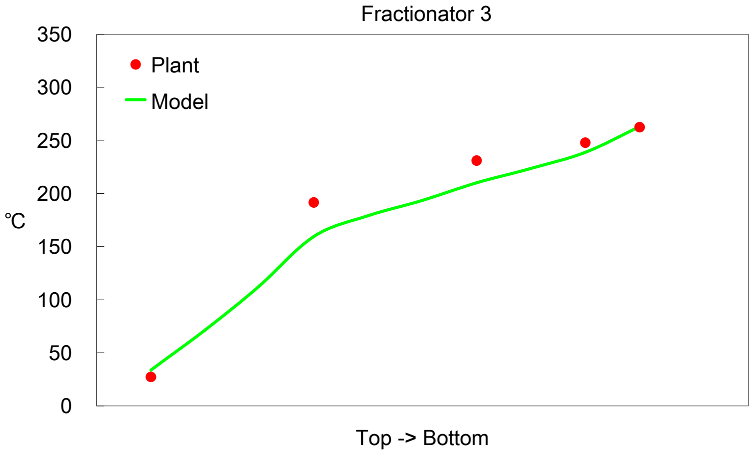

Figure 2.53 Prediction of temperature profiles of fractionators (dataset 7 in HP HCR)

### 2.6.3 Product Yields.

There are seven products in the HP HCR unit as depicted in, namely, low-pressure separator vapor (LPS VAP), dry gas, LPG, light naphtha, heavy naphtha, jet fuel and resid oil. Among these seven products, LPG, light naphtha, heavy naphtha, jet fuel and resid oil are major products since they account for over 95wt% of the overall production. Figure 2.54 to Figure 2.58 illustrate the model predictions on LPG, light naphtha, heavy naphtha, jet fuel and resid oil and the average absolute deviations (AAD) are 0.4 wt%, 0.2 wt%, 0.5 wt%, 0.4 wt% and 1.7 wt%, respectively. The model provides good prediction results on product yields when considering overall production.

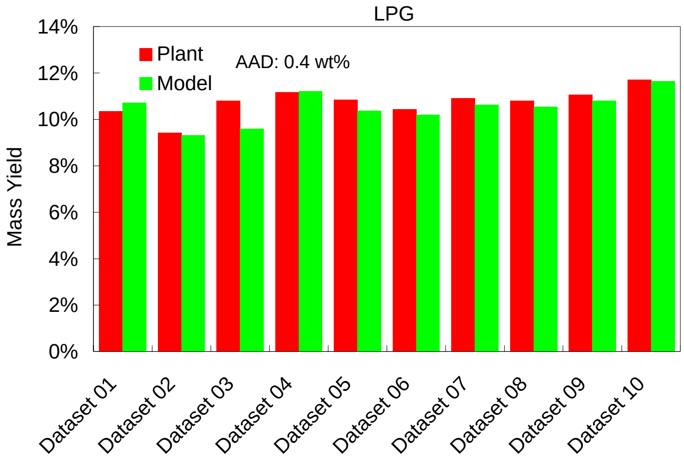

Figure 2.54 Predictions of LPG yield (HP HCR)

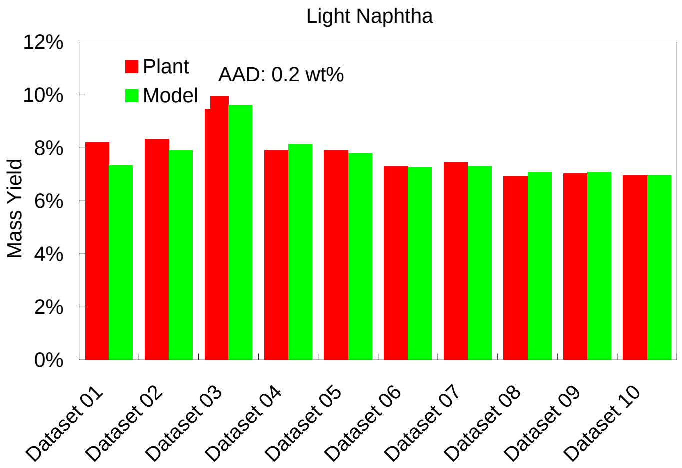

Figure 2.55 Predictions of light naphtha yield (HP HCR)

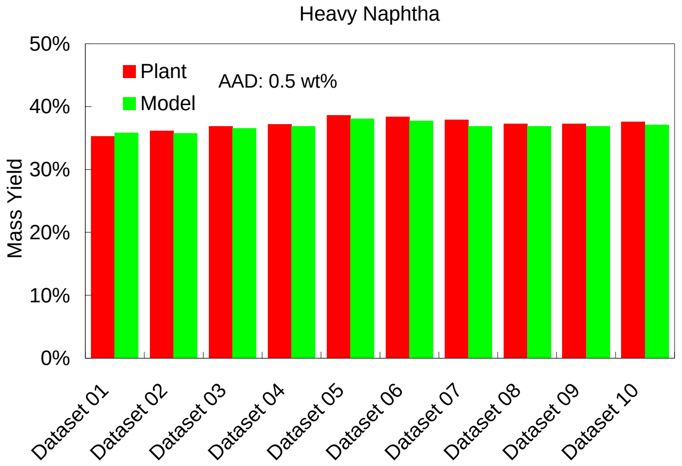

Figure 2.56 Predictions of heavy naphtha yield (HP HCR)

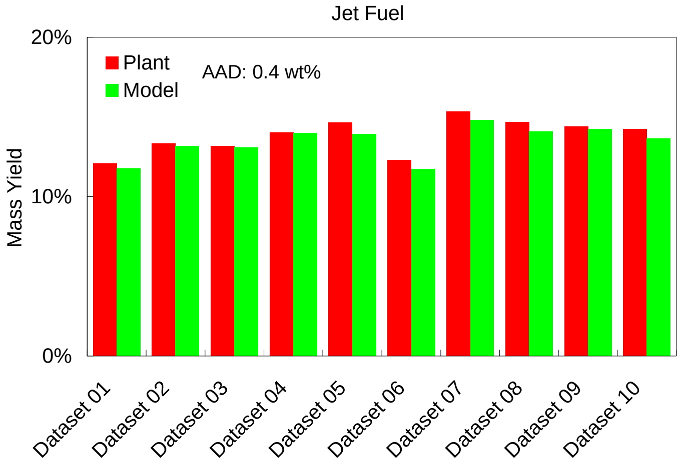

Figure 2.57 Predictions of jet fuel yield (HP HCR)

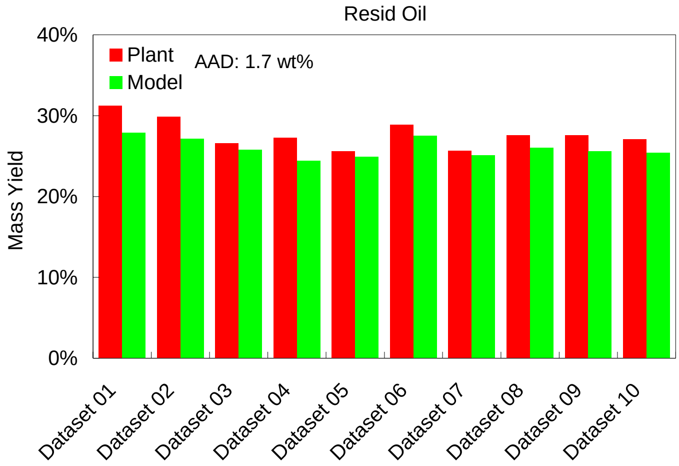

Figure 2.58 Predictions of resid oil yield (HP HCR)

### 2.6.4 LPG Composition and Distillation Curves of Liquid Products.

Composition, particularly C3 and C4, is the most important indicator to evaluate the quality of LPG product. Figure 2.59 shows selected model predictions on LPG composition with AAD of each component. For the most important components, C3 and C4, the model shows only 0.021 and 0.058 AAD in molar fraction predictions. For other liquid products, distillation curve is the most popular analysis to indicate the vaporization temperature after a certain amount of oil fraction vaporized. Figure 2.60 and Figure 2.61 illustrate selected model predictions on distillation curves of light naphtha, heavy naphtha, jet fuel and resid oil. The deviations of predicting distillation curves result from two factors: (1) fractionator simulation cannot provide reliable results of the initial and final boiling points of liquid products[32]; (2) the reactor model cannot provide accurate predictions of the boiling point distribution of reactor effluent, which causes the deviations of model's predictions on distillation curves of liquid products. Although the model is able to provide accurate prediction on product yield after calibration, it is not equivalent to say that the model is able to provide accurate predictions on boiling point distribution (distillation curve) of liquid product because the nature of discrete boiling point distribution of kinetic lumps.

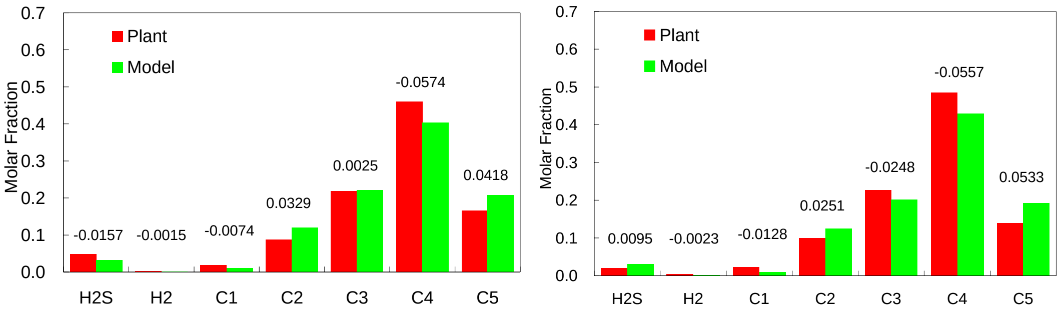

(59a) LPG composition, dataset 01 (59b) LPG composition, dataset 07

Figure 2.59 Predictions of LPG compositions (HP HCR)

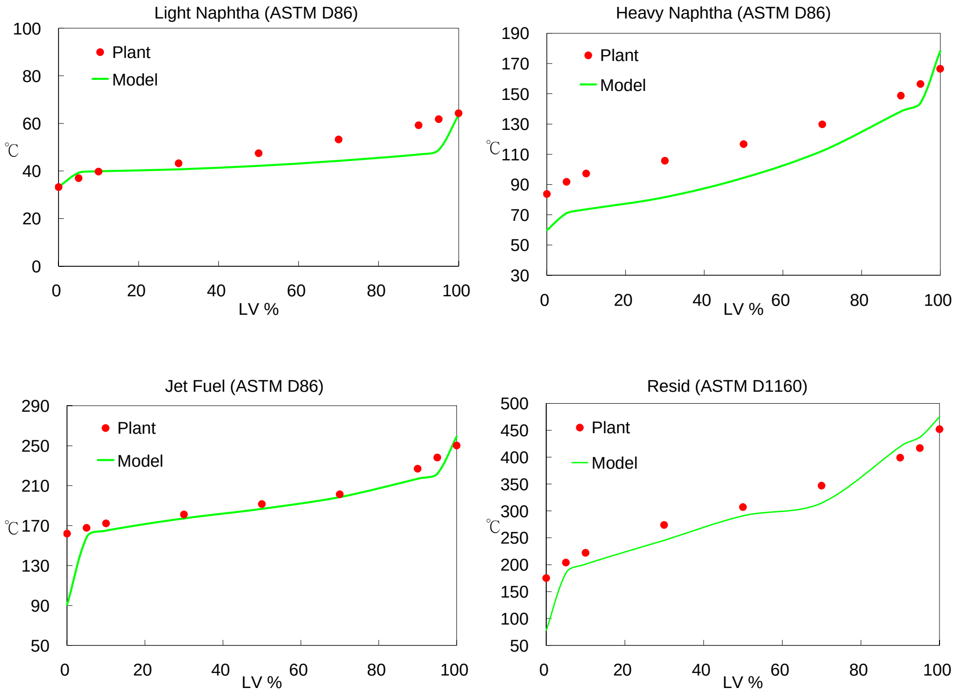

Figure 2.60 Predictions of distillation curves of liquid products (dataset 1 in HP HCR)

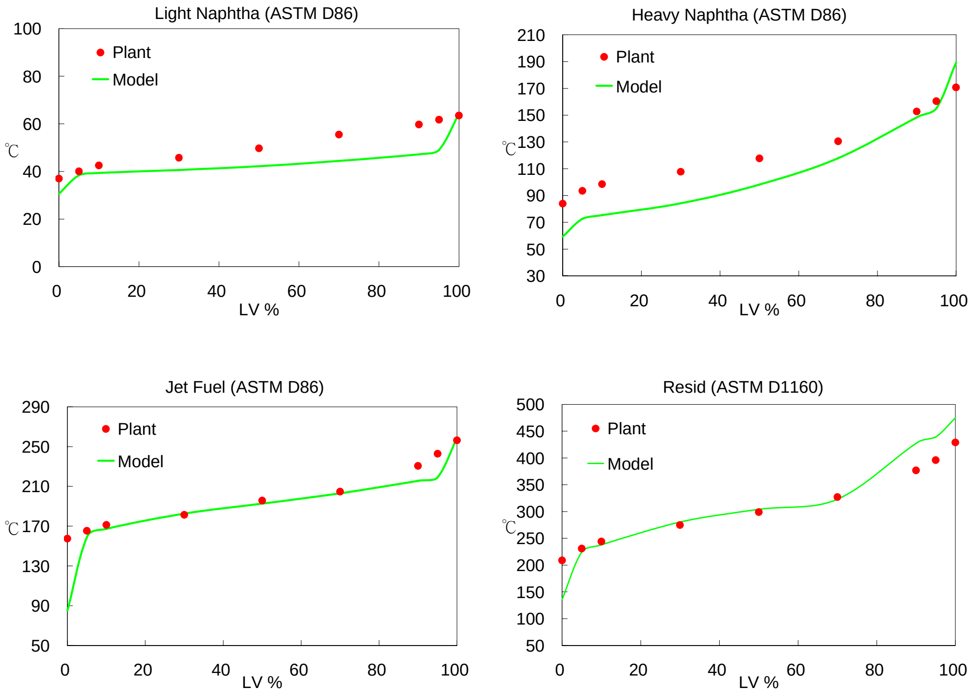

Figure 2.61 Predictions of distillation curves of liquid products (dataset 7 in HP HCR)

### 2.6.5 Product Property.

We apply the updated correlations developed in Section 2.4.6 to estimate flash point and freezing point of jet fuel. Figure 2.62 and Figure 2.63 illustrate model predictions on flash point and freezing point of jet fuel. The average absolute deviations are 1.6℃ and 2.3℃, which are about the same values as that obtained from correlating plant data. The integrated model collaborated with updated correlations provides satisfactory predictions on flash point and freezing point of jet fuel. Figure 2.64 to Figure 2.67 illustrate the specific gravity predictions of liquid products, which are calculated by Aspen HYSYS. The AADs of the specific gravity predictions for light naphtha, heavy naphtha, jet fuel, and resid oil are 0.0049, 0.0062, 0.0134, and 0.0045 respectively. The accurate predictions not only show model's predictability on specific gravity of liquid product, but also demonstrate that the delumping method we developed in Section 2.4.5 is able to carry over density distribution to NBP-based pseudo-components.

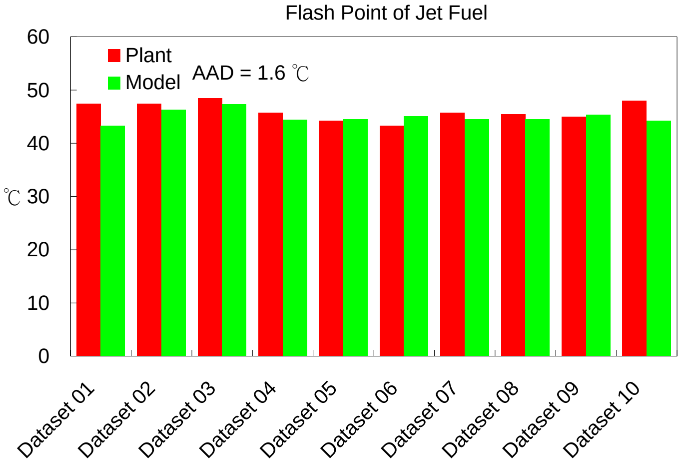

Figure 2.62 Predictions of jet fuel's flash point (HP HCR).

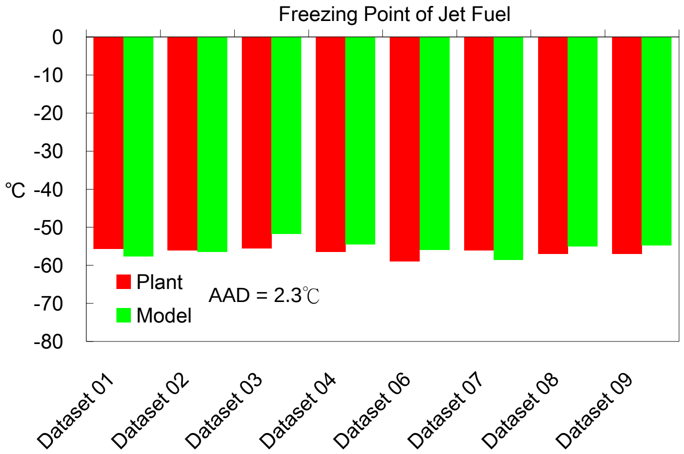

Figure 2.63 Predictions of jet fuel's freezing point (HP HCR).

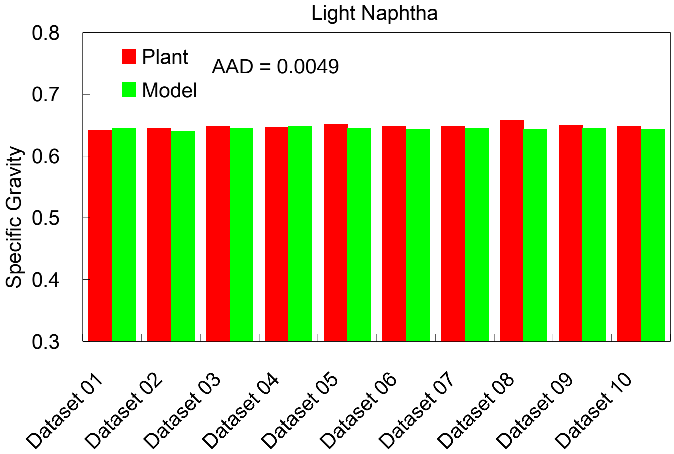

Figure 2.64 Predictions of light naphtha's specific gravity (HP HCR).

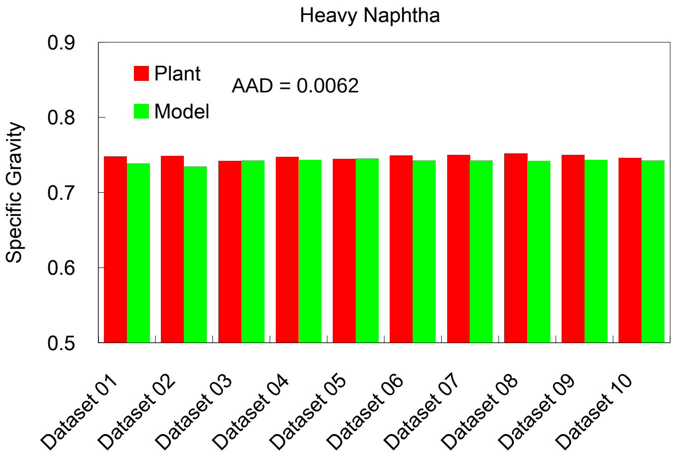

Figure 2.65 Predictions of heavy naphtha's specific gravity (HP HCR)

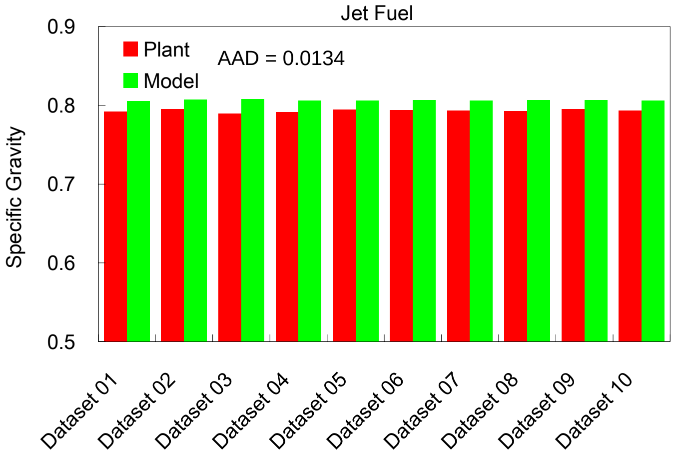

Figure 2.66 Predictions of jet fuel's specific gravity (HP HCR)

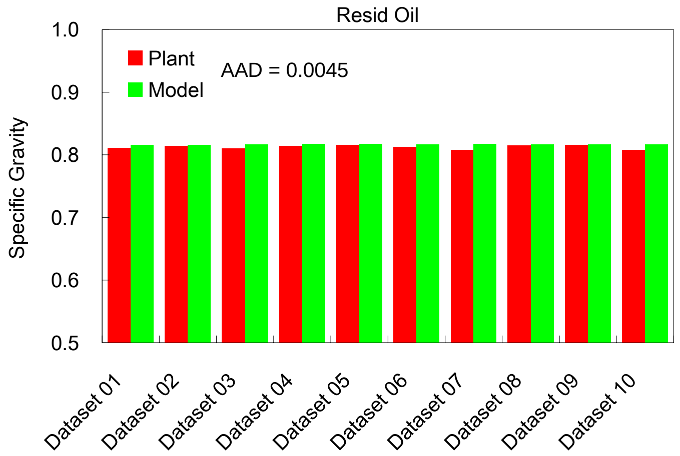

Figure 2.67 Predictions of resid oil's specific gravity (HP HCR)

## 2.7 Model Application – Simulation Experiment.

The major operating variables that affect product distribution (yield) of HCR process are reactor temperature, hydrogen partial pressure, amount of ammonia present, and residence time. For example, a change in reactor temperature can shift the maximum yield from diesel fuel to naphtha. For an industrial HCR process, the amount of ammonia present is controlled by the hydrotreating reactor and the most popular manipulations to operate the process are reactor temperature, $H_2$-to-oil ratio (equivalent to hydrogen partial pressure) and feed flow rate (residence time). In this section, we will conduct two simulation experiments using MP HCR model to demonstrate how to quantify the effects of operating variables on process performance.

### 2.7.1 $H_2$-to-oil Ratio vs. Product Distribution, Remained Catalyst Life, and Hydrogen Consumption.

Hydrogen partial pressure is one of the key operating variables for HCR process. It has two opposite effects on product distribution and process profitability. Higher hydrogen partial pressure can enhance aromatic hydrogenation, increase H/C ration of products, and extend catalyst life by reducing coke precursors (hydrogenation of multi-ring aromatics). Hydrogen also has a negative effect on paraffin hydrocracking that is crucial for product distribution[44]. In addition, higher hydrogen partial pressure leads to higher hydrogen consumption which raises the processing cost. In this section, we will conduct a simulation experiment to study the relationship among hydrogen partial pressure, product distribution, and catalyst remain life. The catalyst deactivation model is built in Aspen HYSYS/Refining that estimates the remaining catalyst life by WART at SOC (start of run), WART at EOC (end of run, provided by catalyst vendor), WART of current operation, number of days in service, coke precursors (multi-ring aromatics) in the feed, and hydrogen partial pressure. Since industrial HCR process tunes hydrogen partial pressure through changing gas-to-oil ratio, we choose gas-to-oil ratio as the operating variable rather than hydrogen partial pressure. Figure 2.68 represents the selected $H_2$-to-oil ratios in our simulation experiment and the corresponding values of hydrogen partial pressure.

Figure 2.69 illustrates the $H_2$-to-oil ratio (hydrogen partial pressure) has little effect on product distribution. The flat product distribution under various $H_2$-to-oil ratios (hydrogen partial pressures) is consistent with observations reported in the literature[45 - 47]. This implies that the current operation is around the maximum conversion and further increase/decrease in hydrogen partial pressure will not change the yields of valuable products such as heavy naphtha and diesel. Even so, $H_2$-to-oil ratio is still a double-edged knife for process profitability because it affects the hydrogen consumption and remaining catalyst life. Figure 2.70 represents how $H_2$-to-oil ratio affects hydrogen consumption and remaining catalyst life. Obviously, $H_2$-to-oil ratio has a positive effect on both variables. However, the two variables have opposite effects on process profitability and we can use the model to study the optimal operating point.

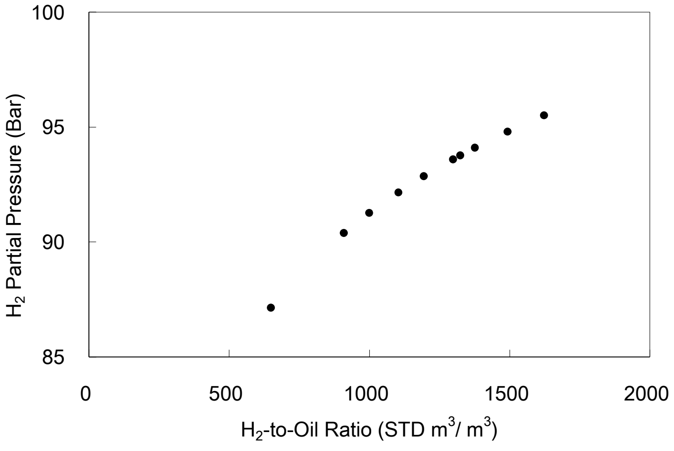

Figure 2.68 $H_2$-to-oil ratios and the corresponding values of $H_2$ partial pressure

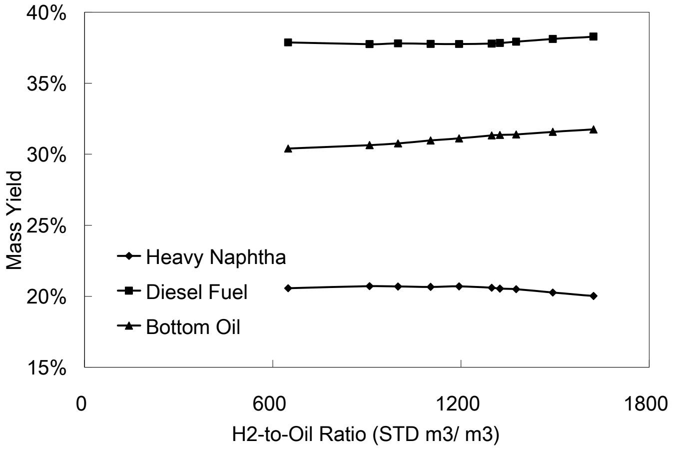

Figure 2.69 $H_2$-to-oil ratios and the corresponding values of $H_2$ partial pressure

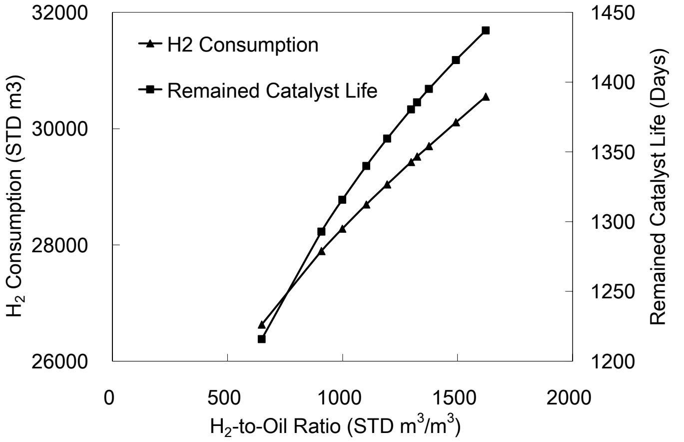

Figure 2.70 The effects of $H_2$-to-oil ratio on $H_2$ consumption and catalyst life

### 2.7.2 WART vs. Feed Flow Rate vs. Product Distribution.

The most important operating variable for HCR process is reactor temperature. Increasing the reactor temperature increases reaction conversion and shift product distribution from heavier to lighter products. However, increasing the reactor temperature does not always benefit the refinery and may generate process safety issue. This follows because high reactor temperature will accelerate coke formation, and the secondary hydrocracking of middle distillate oils (such as gasoline and diesel) will increase product yield of gas products which are less profitable. Thus, the refiners intend to raise reactor temperature gradually to produce desirable product distribution. For instance, the 2 months' operating data of the MP HCR unit show that the WART of HCR reactor varies within ±8℃ from base dataset.

Figure 2.71 to Figure 2.73 illustrate the effects of feed flow rate and WART (HCR reactor) on product distribution (yields). The heavy naphtha yield increases significantly while WART increases and/or feed flow decreases, because the rising HCR reactor temperature enhances hydrocracking reactions and the decreasing feed flow implies longer residence time that also enhances hydrocracking reactions. On the other side, the bottom oil yield presents the opposite trend to that of heavy naphtha yield. This follows because bottom oil is the heaviest product and the higher severity of cracking reactions resulted from rising WART and/or falling feed flow rate, the lower bottom oil yield is. However, the most interesting observation comes from Figure 2.72 that represents the diesel fuel yield reaches maximum value at some operating point. Both Tippett et al.[48] and Rossi[49] et al. report that in a HCR process, the yield of middle distillate fraction (diesel fuel in this case) would approach a maximum value with increasing reactor temperature, because of secondary hydrocracking reactions of middle distillate paraffins. We can conclude that with lower feed flow rate, the diesel fuel yield tends to approach maximum when increasing WART of HCR reactor. By performing this simulation experiment, refiners can determine the optimal reactor temperature and feed flow rate to achieve maximum profits under various supply-and-demand situations.

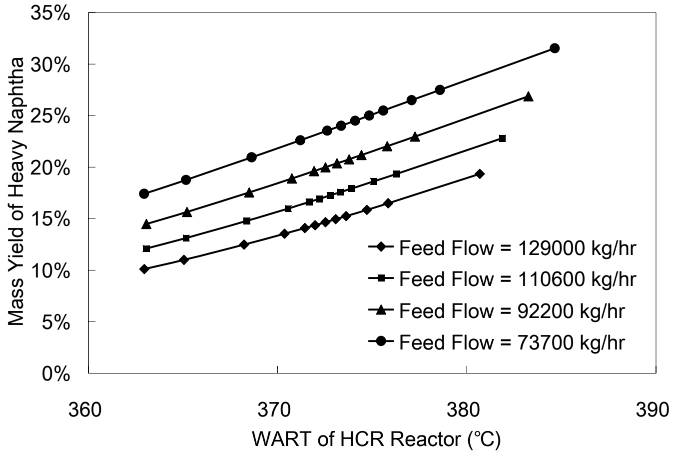

Figure 2.71 Effect of feed flow rate and WART of HCR reactor on heavy naphtha yield.

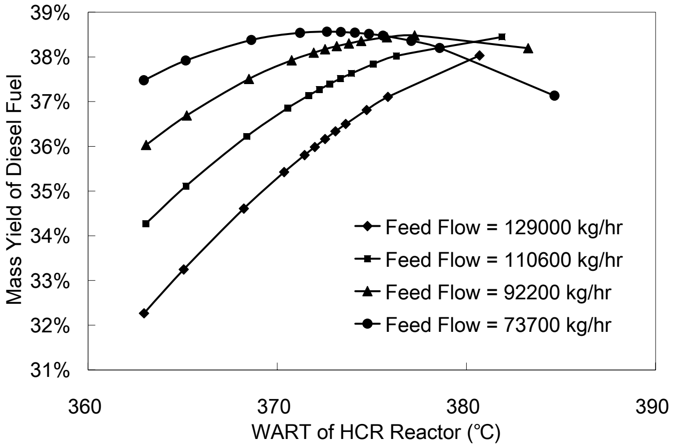

Figure 2.72 Effect of feed flow rate and WART of HCR reactor on diesel fuel yield.

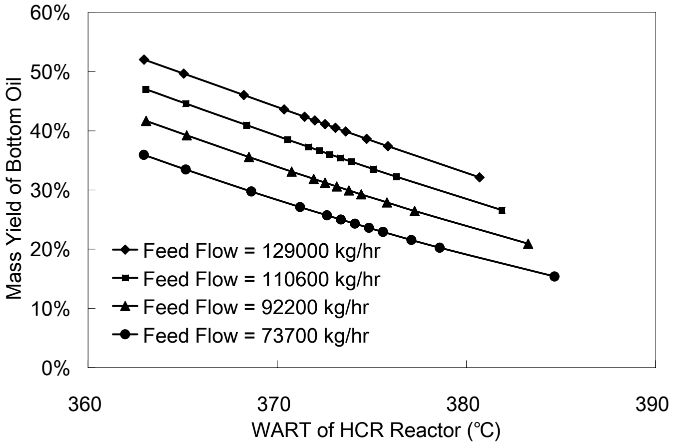

Figure 2.73 Effect of feed flow rate and WART of HCR reactor on bottom oil yield.

## 2.8 Model Application – Delta-Base Vector Generation.

Refining industry started to investigate the application of linear programming (LP) based model since 1950s[50]. Nowadays LP based model is the most important optimized tool to schedule production, evaluate feedstock, study new process configuration, and adjust production plan after operational upsets. For a given refinery, the LP based model is a combination of economic and technical databanks. The economic databank requires the availability and price of feedstocks, the demand and price of refining products, and operating cost of process units. The technical databank needs process product yields, product properties, product specifications, operating constraints, and use of utility.

Modern refiners gather and update most of the required information from market research, government regulation, design data, and operating history except for product yields. Instead of adopting historic data, refiners apply process model to generate required information of product yields for LP based model. However, actual refining reaction processes are highly nonlinear and the responses of product yields to process variables such as operating conditions and feed properties are usually complex. Figure 2.74 illustrates the nonlinear relation between HCR reactor temperature and product distribution (redraw from ref.51). Yield of each product represents nonlinear variation along with the change of reactor temperature. To integrate the nonlinear relationship between product yields and process variables with LP based model, refiners linearize product yields over a small range of process variables as illustrated in Figure 2.75a. The linear relationship between product yields and process variables is so called "delta-base" technology in modern refinery production planning.

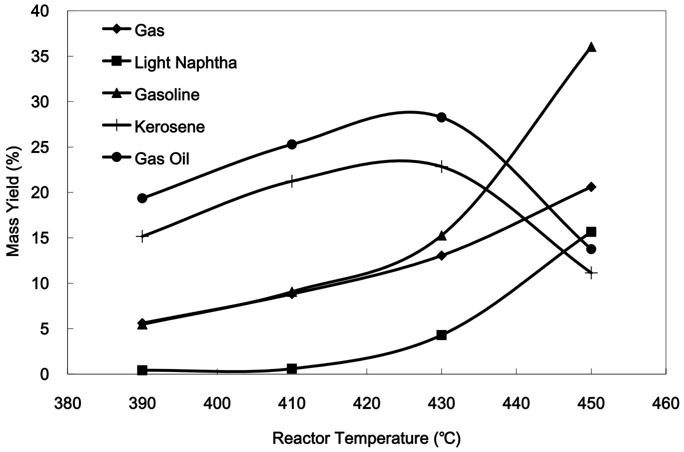

Figure 2.74 Nonlinear relationship between product distribution & reactor temperature

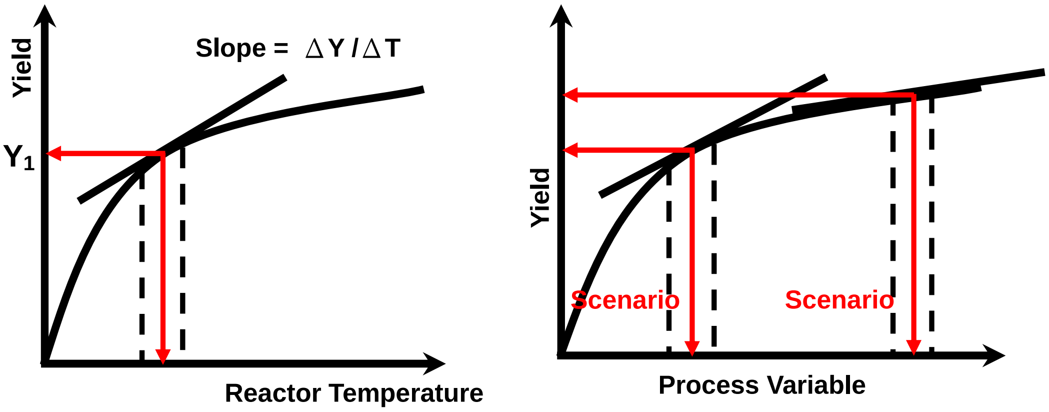

(75a) Linearization of process performance (75b) Scenarios for different operations

Figure 2.75 Linearization of production yield's response on process variable

As shown in Eq. (29), refiners use delta-base technology to construct the linear representation of product yield's ( $Y$ ) response to the change of process variable ( $X - \overline{X} = \Delta X$ ), namely, delta vector. Base vector ( $\overline{Y}$ ) represents the product yield under a selected operating condition and feedstock quality ( $\overline{X}$ ). Delta-base vector ( $\Delta Y/\Delta X$ ) indicates the departure of product yield ( $\Delta Y$ ) from base vector ( $\overline{Y}$ ) corresponding to the per unit change of process variable ( $\Delta X$ ).

The delta-base technology simplifies the nonlinearity of refining process and allows LP based product planning to take product yield into account. However, the resulting LP based model only provides good prediction of product yield over a small range of operating condition and feedstock qualities. To extend the application of LP based model, refiners generate different sets of delta-base vectors to reflect various production scenarios as shown in Figure 2.75b. By doing this, the LP based production planning can switch over delta-base vectors according to the production scenario. Figure 2.76 represents multi-scenario delta-base vectors of a catalytic reforming process used in Aspen PIMS. The delta-base vector inside each red box indicates a scenario producing gasoline product with varying research octant number (RON).

$$\begin{bmatrix} Y_1 \\ Y_2 \\ \vdots \\ \vdots \\ Y_m \end{bmatrix} = \begin{bmatrix} \overline{Y}_1 \\ \overline{Y}_2 \\ \vdots \\ \vdots \\ \overline{Y}_m \end{bmatrix} + \begin{bmatrix} \frac{\Delta Y_1}{\Delta X_1} & \frac{\Delta Y_1}{\Delta X_2} & \cdots & \frac{\Delta Y_1}{\Delta X_n} \\ \frac{\Delta Y_2}{\Delta X_1} & \frac{\Delta Y_2}{\Delta X_2} & \cdots & \frac{\Delta Y_2}{\Delta X_n} \\ \vdots & & & \vdots \\ \vdots & & & \vdots \\ \frac{\Delta Y_m}{\Delta X_1} & \frac{\Delta Y_m}{\Delta X_2} & \cdots & \frac{\Delta Y_m}{\Delta X_n} \end{bmatrix} \bullet \begin{bmatrix} X_1 - \overline{X}_1 \\ X_2 - \overline{X}_2 \\ \vdots \\ \vdots \\ X_n - \overline{X}_n \end{bmatrix} \tag{29}$$

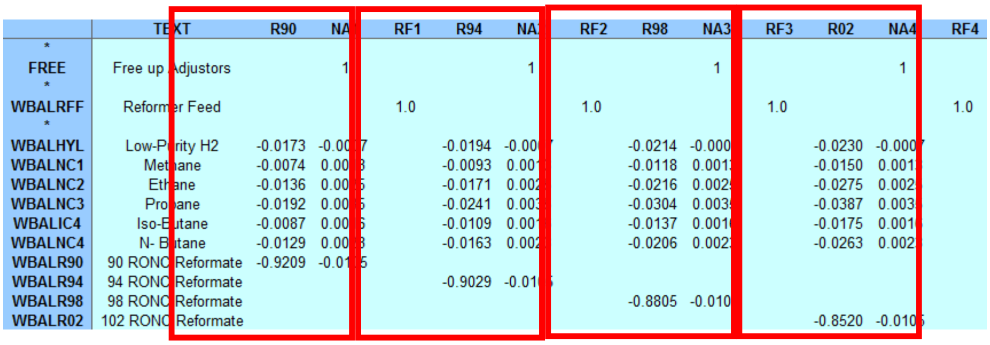

| | TEXT | R90 | NA | RF1 | R94 | NA | RF2 | R98 | NA3 | RF3 | R02 | NA4 | RF4 |
|---|---|---|---|---|---|---|---|---|---|---|---|---|---|
| * | | | | | | | | | | | | | |
| FREE | Free up Adjustors | | 1 | | | 1 | | | 1 | | | 1 | |
| * | | | | | | | | | | | | | |
| WBALRFF | Reform r Feed | | | 1.0 | | | 1.0 | | | 1.0 | | | 1.0 |
| * | | | | | | | | | | | | | |
| WBALHYL | Low-P rity H2 | -0.0173 | -0.00 7 | | -0.0194 | -0.000 | | -0.0214 | -0.000 | | -0.0230 | -0.000 | |
| WBALNC1 | Met ane | -0.0074 | 0.00 3 | | -0.0093 | 0.001 | | -0.0118 | 0.001 | | -0.0150 | 0.001 | |
| WBALNC2 | Eth ane | -0.0136 | 0.00 5 | | -0.0171 | 0.002 | | -0.0216 | 0.002 | | -0.0275 | 0.002 | |
| WBALNC3 | Pro ane | -0.0192 | 0.00 5 | | -0.0241 | 0.003 | | -0.0304 | 0.003 | | -0.0387 | 0.003 | |
| WBALIC4 | Iso- utane | -0.0087 | 0.00 6 | | -0.0109 | 0.001 | | -0.0137 | 0.001 | | -0.0175 | 0.001 | |
| WBALNC4 | N- B tane | -0.0129 | 0.00 3 | | -0.0163 | 0.002 | | -0.0206 | 0.002 | | -0.0263 | 0.002 | |
| WBALR90 | 90 RONC Reformate | -0.9209 | -0.01 5 | | | | | | | | | | |
| WBALR94 | 94 RONC Reformate | | | | -0.9029 | -0.01 | | | | | | | |
| WBALR98 | 98 RONC Reformate | | | | | | | -0.8805 | -0.010 | | | | |
| WBALR02 | 102 RONC Reformate | | | | | | | | | | -0.8520 | -0.010 | |

Figure 2.76 Multi-scenario delta-base vectors in a catalytic reforming process

To generate delta-base vector, refiners produce case studies by running process model under varied feed and operating conditions by the following procedures:

1. Run the process model;
2. Choose the process variables to produce case studies;
   - In real practice, feedstock qualities rather than operating conditions are chosen such as specific gravity, Watson K, PNA etc.
3. Record base yields (base vector, $\overline{Y}$ in Eq. (29)) and the values of the selected process variables ( $\overline{X}$ in Eq. (29)) in the process model;
4. Produce case studies by running the process model with changing selected process variable(s);
5. Record the changes of process variables ($\Delta X$ in Eq. (29)) and the corresponding yields ( $Y$ in Eq. (29));
6. Apply Eq. (29) to run linear regression to obtain delta-base vector;

In this section, we use HP HCR model to demonstrate how to generate delta-base vector from computer simulation. We choose sulfur content, Watson K factor, and API gravity of feed oil as process variables to perform case study and generate delta-base vector. The product yields calculated from the base case of HP HCR model are defined as base vector ( $\overline{Y}$ in Eq. (29)). Then we input different feed analyses obtained from the refinery into the HP HCR model to produce case studies. We regress Eq. (29) with base vector ( $\overline{Y}$ in Eq. (29)), the recorded product yields ( $Y$ in Eq. (29)), and the corresponding change of process variable ($\Delta X$, $X-\overline{X}$ in Eq. (29)) from 15 case studies to obtain delta-base vector. Figure 2.77 represents the resulting delta-base vector for HP HCR process. We generate one set of delta-base vector because the plant data collected for build the HP HCR model are based on the same production scenario.

The resulting delta-base vector shows that sulfur content of feed oil has positive effect on the yields of light products and negative effect on heavier liquid product, because more $H_2S$ is produced with increasing sulfur compounds of feed oil. Hu et al. [52] also report that sulfur content of feed oil has opposite effects on light and heavy products. However, the trends of API gravity and Watson K factor on product yields are irregular. This follows because API factor and Watson factor are not independent and the resulting delta-base vector will represent the mutual effect of there two variables on product yields as well. It is worthy noting that API gravity and Watson K factor are not good enough to generate delta-base vector of HCR process because they provide little information of feed composition such as PNA content that is important to HCR modeling. The attributes relevant to feed composition should be included to obtain more precise delta-base vector. Although we only use API gravity and Watson K factor to generate delta-base vector due to the limitation of plant data, HP HCR model's good predictability among two and half months of plant data can promise the application of delta-base vector.

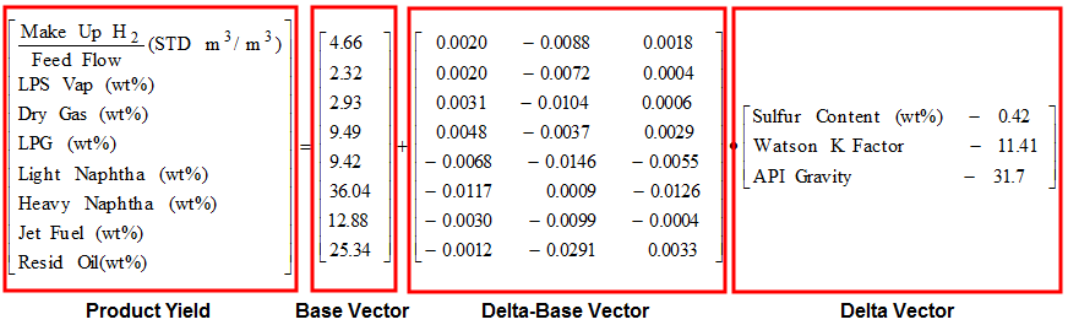

$$\begin{bmatrix} \frac{\text{Make Up } H_2}{\text{Feed Flow}} (\text{STD } m^3/m^3) \\ \text{LPS Vap (wt\%)} \\ \text{Dry Gas (wt\%)} \\ \text{LPG (wt\%)} \\ \text{Light Naphtha (wt\%)} \\ \text{Heavy Naphtha (wt\%)} \\ \text{Jet Fuel (wt\%)} \\ \text{Resid Oil(wt\%)} \end{bmatrix} = \begin{bmatrix} 4.66 \\ 2.32 \\ 2.93 \\ 9.49 \\ 9.42 \\ 36.04 \\ 12.88 \\ 25.34 \end{bmatrix} + \begin{bmatrix} 0.0020 & -0.0088 & 0.0018 \\ 0.0020 & -0.0072 & 0.0004 \\ 0.0031 & -0.0104 & 0.0006 \\ 0.0048 & -0.0037 & 0.0029 \\ -0.0068 & -0.0146 & -0.0055 \\ -0.0117 & 0.0009 & -0.0126 \\ -0.0030 & -0.0099 & -0.0004 \\ -0.0012 & -0.0291 & 0.0033 \end{bmatrix} \bullet \begin{bmatrix} \text{Sulfur Content (wt\%)} - 0.42 \\ \text{Watson K Factor} - 11.41 \\ \text{API Gravity} - 31.7 \end{bmatrix}$$

Figure 2.77 Delta-base vector of HP HCR process generated in this work.

## 2.9 Conclusion.

HCR process models are usually very sophisticated since their complex feedstocks and highly coupled reaction mechanisms make it difficult to build a plantwide HCR process simulation. However, refiners are most concerned about maximizing profit under steady operations which imply small changes of the process operations and feedstock varieties. Therefore, a good operating model of refining process only needs to match key product yields, qualities and process operations under small process changes.

In this work, we develop two operating models of large-scale HCR processes to satisfy the key considerations of the refiners. The two models only require typical operating conditions, and routine analysis of feedstock and products. We validate the models' capabilities of predicting product yields, product qualities and unit operations with two months of plant data. We also show key applications of HCR models, namely simulation experiment and delta-base vector generation. We summarize the key achievements of this work as follows:

(1) We develop two integrated HCR process models which include reactors, fractionators and hydrogen recycle systems.

(2) We provide the step-by-step guideline of model development that has not been reported in the literature.

(3) We apply the Gauss-Legendre Quadrature to convert kinetic lumps into pseudo-components based on boiling point ranges (delumping) for rigorous fractionator simulation.

(4) Our delumping method gives a continuous response to changes in fractionator specification such as distillate rate.

(5) We update API correlations of flash point and freezing point to plant operation and production.

(6) The integrated HCR process models are able to predict accurately the product yields, distillation curves of liquid products, and temperature profiles of reactors and fractionators.

(7) The integrated HCR process models also gives good estimations on liquid product qualities – density, flash point and freezing point of diesel fuel (MP HCR) and jet fuel (HP HCR) – by using updated API correlations.

(8) We apply the integrated MP HCR process model to conduct simulation experiment to

quantify the effects of operating variables on product yields.

(9) We apply the integrated HP HCR process model to generate delta-base vector for LP based production planning.

This work represents the workflow to build integrated HCR process model by using Aspen HYSYS/Refining and only routine measurements for feed characterization in the refinery. We also use routine measurements of products to calibrate the model. To further improve our models, we may include Apply SimDist analysis for feed characterization, and to incorporate detailed molecular information for feed characterization and customize our feed lump distribution if these measurements are available regularly. We can also to customize the calibration environment to include product property and product composition as objective functions if detailed molecular information of product is available.

## 2.10 Workshop 1 – Build Preliminary Reactor Model of HCR Process.

This workshop provides step-by-step guidelines to demonstrate how to build a preliminary reactor model of HCR process.

Step 1: Define the process type (single-stage or two-tage), the number of reactors of each stage and the corresponding reaction beds and the number of high-pressure separators and if amine treatment is included in the model.

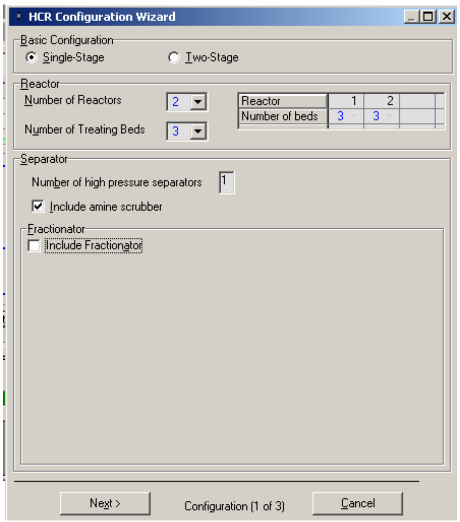

Basic Configuration

● Single-Stage ○ Two-Stage

Reactor

Number of Reactors: 2

Number of Treating Beds: 3

| Reactor | 1 | 2 |
|---|---|---|
| Number of beds | 3 | 3 |

Separator

Number of high pressure separators: 1

☑ Include amine scrubber

Fractionator

☐ Include Fractionator

Figure 2.78 Define reactors in HCR process

Step 2: Assign the dimensions and catalyst loading information of each reaction bed.

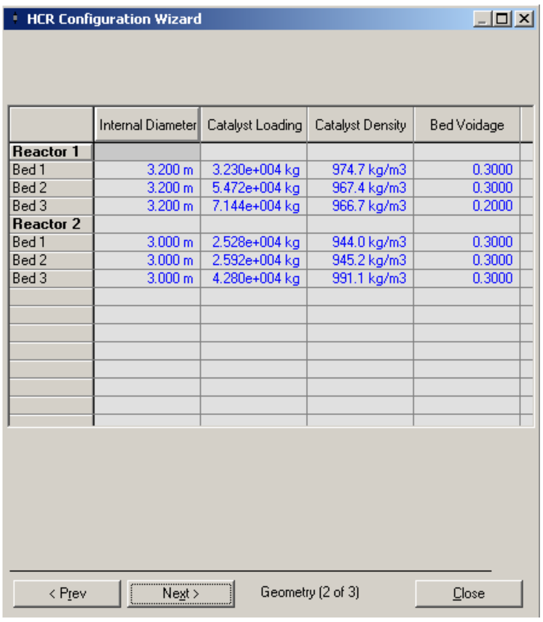

| | Internal Diameter | Catalyst Loading | Catalyst Density | Bed Voidage |
|---|---|---|---|---|
| **Reactor 1** | | | | |
| Bed 1 | 3.200 m | 3.230e+004 kg | 974.7 kg/m3 | 0.3000 |
| Bed 2 | 3.200 m | 5.472e+004 kg | 967.4 kg/m3 | 0.3000 |
| Bed 3 | 3.200 m | 7.144e+004 kg | 966.7 kg/m3 | 0.2000 |
| **Reactor 2** | | | | |
| Bed 1 | 3.000 m | 2.528e+004 kg | 944.0 kg/m3 | 0.3000 |
| Bed 2 | 3.000 m | 2.592e+004 kg | 945.2 kg/m3 | 0.3000 |
| Bed 3 | 3.000 m | 4.280e+004 kg | 991.1 kg/m3 | 0.3000 |

Figure 2.79 Define catalyst bed

Step 3: Select a dataset of reaction activity. Suggest to use the "Default" option when building a preliminary model from scratch.

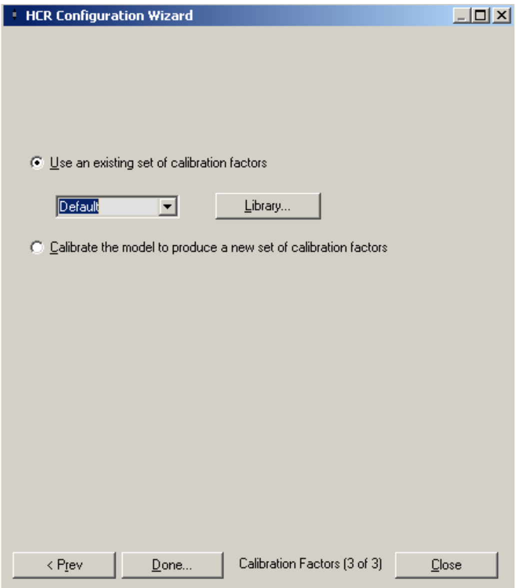

● Use an existing set of calibration factors

Default

○ Calibrate the model to produce a new set of calibration factors

Figure 2.80 Choose a set of reaction activity factors

Step 4: Input the required feed analysis

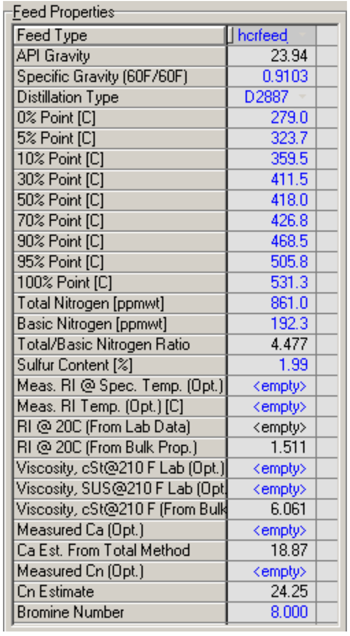
Feed Properties

| | |
|---|---|
| Feed Type | hcrfeed |
| API Gravity | 23.94 |
| Specific Gravity (60F/60F) | 0.9103 |
| Distillation Type | D2887 |
| 0% Point [C] | 279.0 |
| 5% Point [C] | 323.7 |
| 10% Point [C] | 359.5 |
| 30% Point [C] | 411.5 |
| 50% Point [C] | 418.0 |
| 70% Point [C] | 426.8 |
| 90% Point [C] | 468.5 |
| 95% Point [C] | 505.8 |
| 100% Point [C] | 531.3 |
| Total Nitrogen [ppmwt] | 861.0 |
| Basic Nitrogen [ppmwt] | 192.3 |
| Total/Basic Nitrogen Ratio | 4.477 |
| Sulfur Content [%] | 1.99 |
| Meas. RI @ Spec. Temp. (Opt.) | <empty> |
| Meas. RI Temp. (Opt.) [C] | <empty> |
| RI @ 20C (From Lab Data) | <empty> |
| RI @ 20C (From Bulk Prop.) | 1.511 |
| Viscosity, cSt@210 F Lab (Opt.) | <empty> |
| Viscosity, SUS@210 F Lab (Opt | <empty> |
| Viscosity, cSt@210 F (From Bulk | 6.061 |
| Measured Ca (Opt.) | <empty> |
| Ca Est. From Total Method | 18.87 |
| Measured Cn (Opt.) | <empty> |
| Cn Estimate | 24.25 |
| Bromine Number | 8.000 |

Figure 2.81 Feed analysis sheet

Step 5: Select an appropriate feed fingerprint

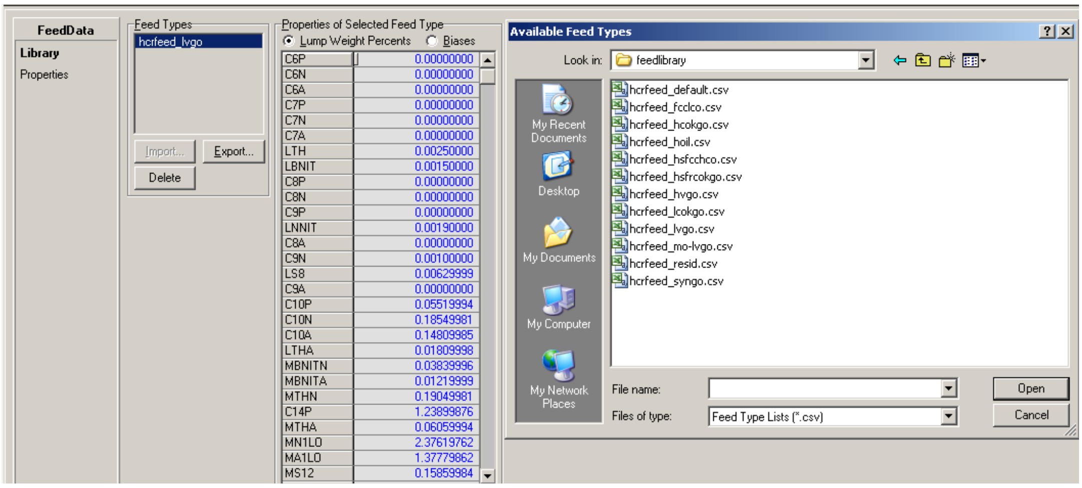

Feed Types: hcrfeed_lvgo

Properties of Selected Feed Type

● Lump Weight Percents ○ Biases

| | |
|---|---|
| C6P | 0.00000000 |
| C6N | 0.00000000 |
| C6A | 0.00000000 |
| C7P | 0.00000000 |
| C7N | 0.00000000 |
| C7A | 0.00000000 |
| LTH | 0.00250000 |
| LBNIT | 0.00150000 |
| C8P | 0.00000000 |
| C8N | 0.00000000 |
| C9P | 0.00000000 |
| LNNIT | 0.00190000 |
| C8A | 0.00000000 |
| C9N | 0.00100000 |
| LS8 | 0.00629999 |
| C9A | 0.00000000 |
| C10P | 0.05519994 |
| C10N | 0.18549981 |
| C10A | 0.14809985 |
| LTHA | 0.01809998 |
| MBNITN | 0.03839996 |
| MBNITA | 0.01219999 |
| MTHN | 0.19049981 |
| C14P | 1.23899876 |
| MTHA | 0.06059994 |
| MN1LO | 2.37619762 |
| MA1LO | 1.37779862 |
| MS12 | 0.15859984 |

Look in: feedlibrary

- hcrfeed_default.csv
- hcrfeed_fcclco.csv
- hcrfeed_hcokgo.csv
- hcrfeed_hoil.csv
- hcrfeed_hsfcchco.csv
- hcrfeed_hsfrcokgo.csv
- hcrfeed_hvgo.csv
- hcrfeed_lcokgo.csv
- hcrfeed_lvgo.csv
- hcrfeed_mo-lvgo.csv
- hcrfeed_resid.csv
- hcrfeed_syngo.csv

Files of type: Feed Type Lists (*.csv)

Figure 2.82 Fingerprint type

Step 6: Input the conditions of feed streams. The temperature and pressure input here only affect the flash calculation of feed stream and have no influence on reactor conditions. However, it is important to input the correct data of hydrogen flow.

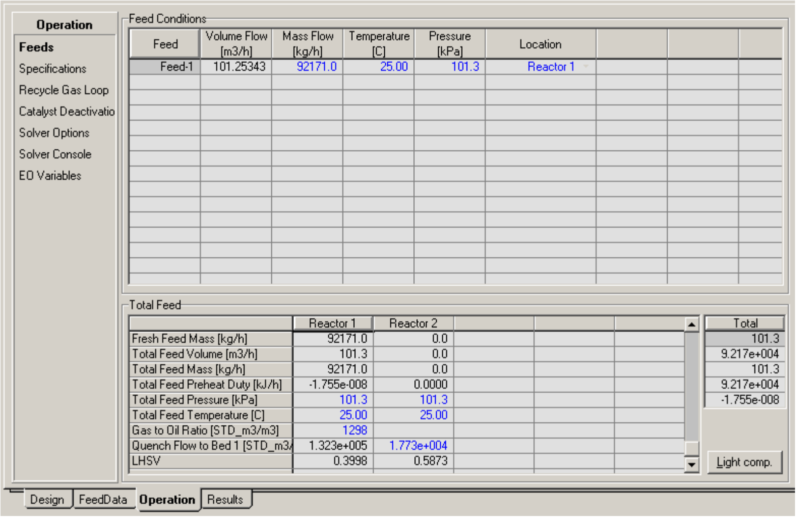

Feed Conditions

| Feed | Volume Flow [m3/h] | Mass Flow [kg/h] | Temperature [C] | Pressure [kPa] | Location |
|---|---|---|---|---|---|
| Feed-1 | 101.25343 | 92171.0 | 25.00 | 101.3 | Reactor 1 |

Total Feed

| | Reactor 1 | Reactor 2 |
|---|---|---|
| Fresh Feed Mass [kg/h] | 92171.0 | 0.0 |
| Total Feed Volume [m3/h] | 101.3 | 0.0 |
| Total Feed Mass [kg/h] | 92171.0 | 0.0 |
| Total Feed Preheat Duty [kJ/h] | -1.755e-008 | 0.0000 |
| Total Feed Pressure [kPa] | 101.3 | 101.3 |
| Total Feed Temperature [C] | 25.00 | 25.00 |
| Gas to Oil Ratio [STD_m3/m3] | 1298 | |
| Quench Flow to Bed 1 [STD_m3/ | 1.323e+005 | 1.773e+004 |
| LHSV | 0.3998 | 0.5873 |

| Total |
|---|
| 101.3 |
| 9.217e+004 |
| 101.3 |
| 9.217e+004 |
| -1.755e-008 |

Figure 2.83 Define flow conditions

Step 7: Input the inlet temperature of each reaction bed

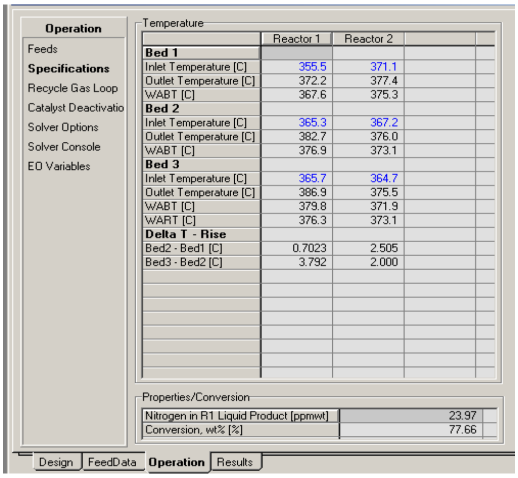

Temperature

| | Reactor 1 | Reactor 2 |
|---|---|---|
| **Bed 1** | | |
| Inlet Temperature [C] | 355.5 | 371.1 |
| Outlet Temperature [C] | 372.2 | 377.4 |
| WABT [C] | 367.6 | 375.3 |
| **Bed 2** | | |
| Inlet Temperature [C] | 365.3 | 367.2 |
| Outlet Temperature [C] | 382.7 | 376.0 |
| WABT [C] | 376.9 | 373.1 |
| **Bed 3** | | |
| Inlet Temperature [C] | 365.7 | 364.7 |
| Outlet Temperature [C] | 386.9 | 375.5 |
| WABT [C] | 379.8 | 371.9 |
| WART [C] | 376.3 | 373.1 |
| **Delta T - Rise** | | |
| Bed2 - Bed1 [C] | 0.7023 | 2.505 |
| Bed3 - Bed2 [C] | 3.792 | 2.000 |

Properties/Conversion

| | |
|---|---|
| Nitrogen in R1 Liquid Product [ppmwt] | 23.97 |
| Conversion, wt% [%] | 77.66 |

Figure 2.84 Assign reactor temperature

Step 8: Input the operating data of recycle hydrogen system. It is crucial to ensure the “outlet pressure of compressor” and “delta P to reactor inlet” are correct because they are used to calculate the inlet pressure of reactor.

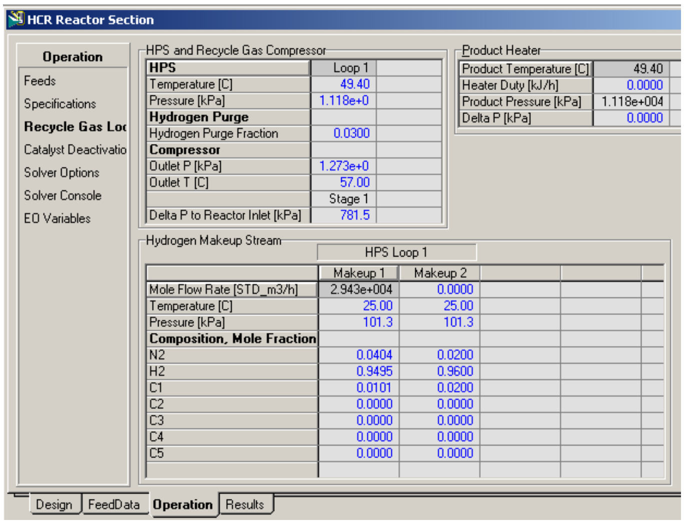

HPS and Recycle Gas Compressor

| **HPS** | Loop 1 |
|---|---|
| Temperature [C] | 49.40 |
| Pressure [kPa] | 1.118e+0 |
| **Hydrogen Purge** | |
| Hydrogen Purge Fraction | 0.0300 |
| **Compressor** | |
| Outlet P [kPa] | 1.273e+0 |
| Outlet T [C] | 57.00 |
| | Stage 1 |
| Delta P to Reactor Inlet [kPa] | 781.5 |

Product Heater

| | |
|---|---|
| Product Temperature [C] | 49.40 |
| Heater Duty [kJ/h] | 0.0000 |
| Product Pressure [kPa] | 1.118e+004 |
| Delta P [kPa] | 0.0000 |

Hydrogen Makeup Stream

| | HPS Loop 1 | |
|---|---|---|
| | Makeup 1 | Makeup 2 |
| Mole Flow Rate [STD_m3/h] | 2.943e+004 | 0.0000 |
| Temperature [C] | 25.00 | 25.00 |
| Pressure [kPa] | 101.3 | 101.3 |
| **Composition, Mole Fraction** | | |
| N2 | 0.0404 | 0.0200 |
| H2 | 0.9495 | 0.9600 |
| C1 | 0.0101 | 0.0200 |
| C2 | 0.0000 | 0.0000 |
| C3 | 0.0000 | 0.0000 |
| C4 | 0.0000 | 0.0000 |
| C5 | 0.0000 | 0.0000 |

Figure 2.85 Define hydrogen recycle system

Step 9: Input the catalyst information provided by vendor. After completing this step, Aspen RefSYS will solve the model automatically.

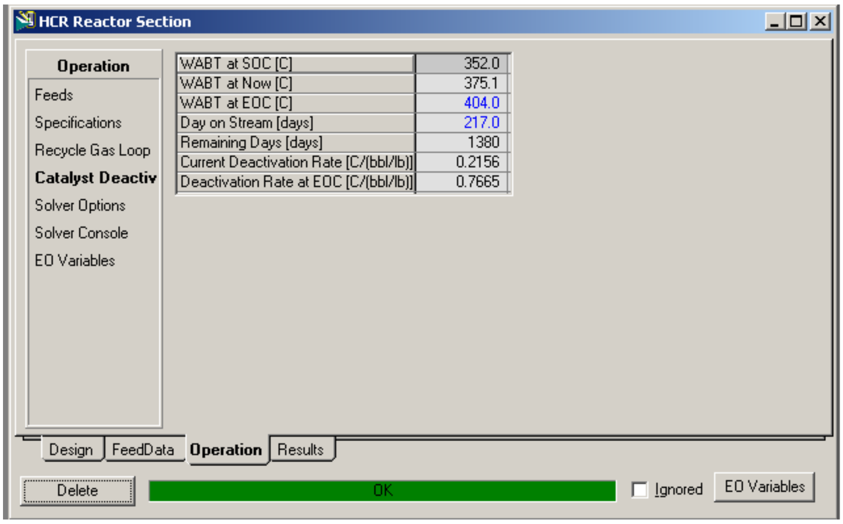

| | |
|---|---|
| WABT at SOC [C] | 352.0 |
| WABT at Now [C] | 375.1 |
| WABT at EOC [C] | 404.0 |
| Day on Stream [days] | 217.0 |
| Remaining Days [days] | 1380 |
| Current Deactivation Rate [C/(bbl/lb)] | 0.2156 |
| Deactivation Rate at EOC [C/(bbl/lb)] | 0.7665 |

Figure 2.86 Catalyst deactivation information

Step 10: Increase the number of iterations and reduce the step size of creep step parameters to enhance model convergence.

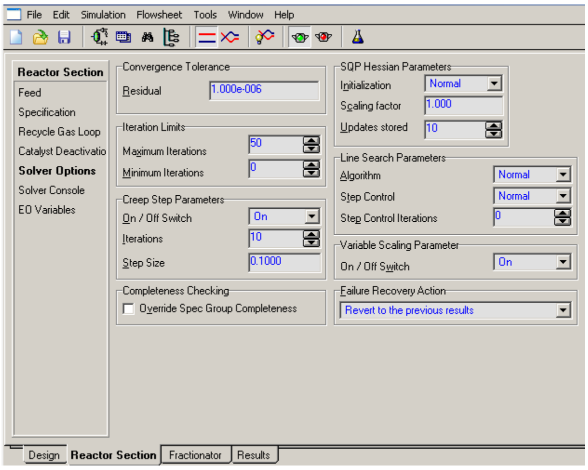

Convergence Tolerance
Residual 1.000e-006

Iteration Limits
Maximum Iterations 50
Minimum Iterations 0

Creep Step Parameters
On / Off Switch On
Iterations 10
Step Size 0.1000

Completeness Checking
☐ Override Spec Group Completeness

SQP Hessian Parameters
Initialization Normal
Scaling factor 1.000
Updates stored 10

Line Search Parameters
Algorithm Normal
Step Control Normal
Step Control Iterations 0

Variable Scaling Parameter
On / Off Switch On

Failure Recovery Action
Revert to the previous results

Figure 2.87 Select an algorithm for model convergence

Step 11: Check model results such as the product yields and reactor temperature profile.

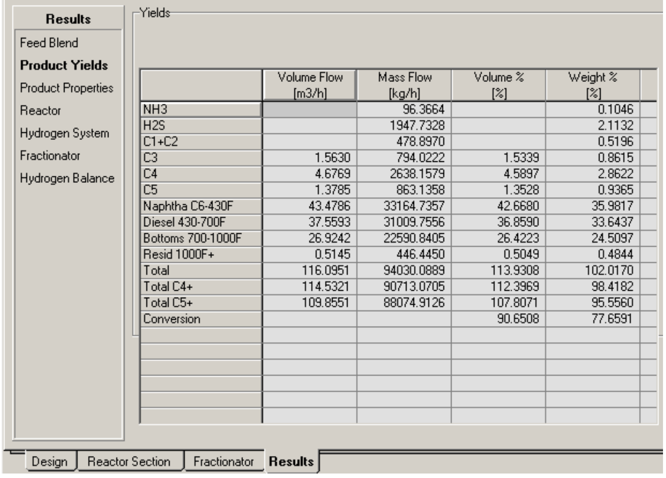

| | Volume Flow [m3/h] | Mass Flow [kg/h] | Volume % [%] | Weight % [%] |
|---|---|---|---|---|
| NH3 | | 96.3664 | | 0.1046 |
| H2S | | 1947.7328 | | 2.1132 |
| C1+C2 | | 478.8970 | | 0.5196 |
| C3 | 1.5630 | 794.0222 | 1.5339 | 0.8615 |
| C4 | 4.6769 | 2638.1579 | 4.5897 | 2.8622 |
| C5 | 1.3785 | 863.1358 | 1.3528 | 0.9365 |
| Naphtha C6-430F | 43.4786 | 33164.7357 | 42.6680 | 35.9817 |
| Diesel 430-700F | 37.5593 | 31009.7556 | 36.8590 | 33.6437 |
| Bottoms 700-1000F | 26.9242 | 22590.8405 | 26.4223 | 24.5097 |
| Resid 1000F+ | 0.5145 | 446.4450 | 0.5049 | 0.4844 |
| Total | 116.0951 | 94030.0889 | 113.9308 | 102.0170 |
| Total C4+ | 114.5321 | 90713.0705 | 112.3969 | 98.4182 |
| Total C5+ | 109.8551 | 88074.9126 | 107.8071 | 95.5560 |
| Conversion | | | 90.6508 | 77.6591 |

Figure 2.88 Model results – product yield

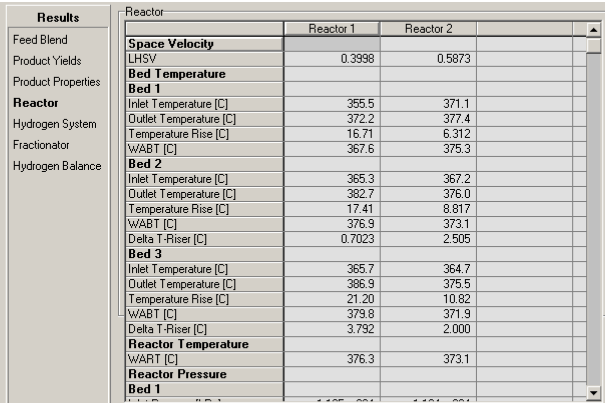

| | Reactor 1 | Reactor 2 |
|---|---|---|
| **Space Velocity** | | |
| LHSV | 0.3998 | 0.5873 |
| **Bed Temperature** | | |
| **Bed 1** | | |
| Inlet Temperature [C] | 355.5 | 371.1 |
| Outlet Temperature [C] | 372.2 | 377.4 |
| Temperature Rise [C] | 16.71 | 6.312 |
| WABT [C] | 367.6 | 375.3 |
| **Bed 2** | | |
| Inlet Temperature [C] | 365.3 | 367.2 |
| Outlet Temperature [C] | 382.7 | 376.0 |
| Temperature Rise [C] | 17.41 | 8.817 |
| WABT [C] | 376.9 | 373.1 |
| Delta T-Riser [C] | 0.7023 | 2.505 |
| **Bed 3** | | |
| Inlet Temperature [C] | 365.7 | 364.7 |
| Outlet Temperature [C] | 386.9 | 375.5 |
| Temperature Rise [C] | 21.20 | 10.82 |
| WABT [C] | 379.8 | 371.9 |
| Delta T-Riser [C] | 3.792 | 2.000 |
| **Reactor Temperature** | | |
| WART [C] | 376.3 | 373.1 |
| **Reactor Pressure** | | |
| **Bed 1** | | |

Figure 2.89 Model results – reactor performance

## 2.11 Workshop 2 – Calibrate the Preliminary Reactor Model to Match Plant Data.

After completing preliminary model, it is necessary to calibrate the model to match plant measurements. The following section will represent a step-by-step guideline to calibrating a preliminary model to match plant measurements of reactor temperature profile and product yields.

Step 1: Enter the “calibration” environment.

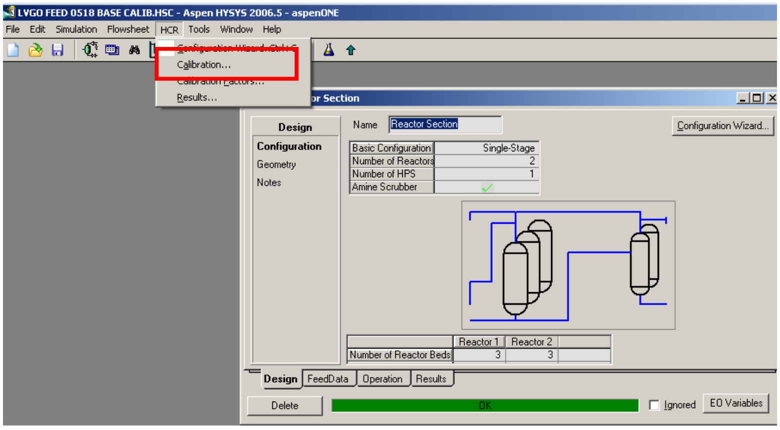

Name: Reactor Section

| Basic Configuration | Single-Stage |
|---|---|
| Number of Reactors | 2 |
| Number of HPS | 1 |
| Amine Scrubber | ✓ |

|  | Reactor 1 | Reactor 2 |
|---|---|---|
| Number of Reactor Beds | 3 | 3 |

Figure 2.90 Enter calibration environment

Step 2: Click the button of “pull data from simulation” to import the results of the preliminary model.

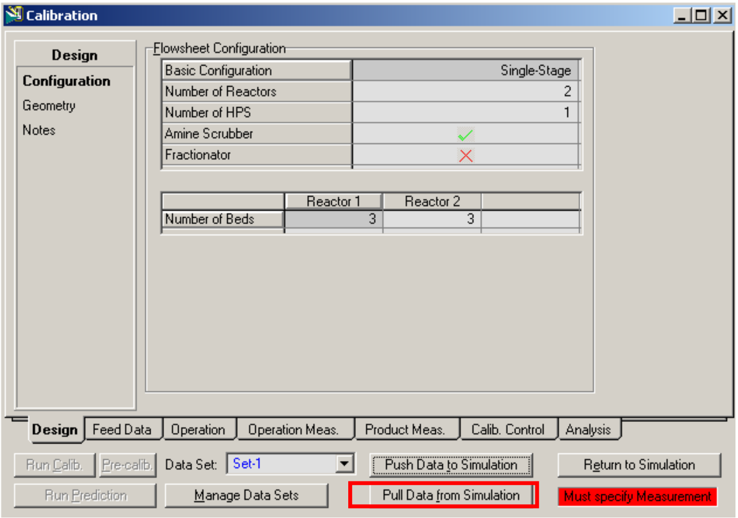

| Basic Configuration | Single-Stage |
|---|---|
| Number of Reactors | 2 |
| Number of HPS | 1 |
| Amine Scrubber | ✓ |
| Fractionator | ✗ |

|  | Reactor 1 | Reactor 2 |
|---|---|---|
| Number of Beds | 3 | 3 |

Figure 2.91 Extract data from simulation

Step 3: Input the temperature rise and pressure drop of each reaction bed.

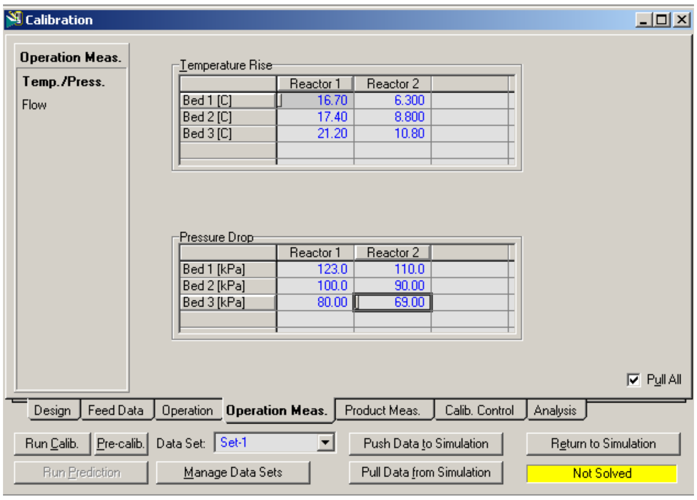

Temperature Rise

| | Reactor 1 | Reactor 2 |
|---|---|---|
| Bed 1 [C] | 16.70 | 6.300 |
| Bed 2 [C] | 17.40 | 8.800 |
| Bed 3 [C] | 21.20 | 10.80 |

Pressure Drop

| | Reactor 1 | Reactor 2 |
|---|---|---|
| Bed 1 [kPa] | 123.0 | 110.0 |
| Bed 2 [kPa] | 100.0 | 90.00 |
| Bed 3 [kPa] | 80.00 | 69.00 |

Figure 2.92 Input reactor variables

Step 4: Input the quench flow of each reaction bed, sour gas removal, makeup hydrogen rate, chemical hydrogen consumption, nitrogen content in the first reactor’s effluent and composition of purge gas.

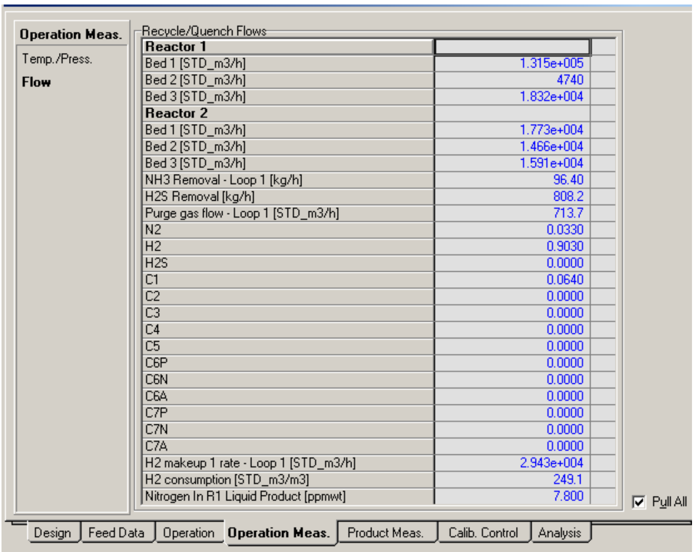

Recycle/Quench Flows

| **Reactor 1** | |
|---|---|
| Bed 1 [STD_m3/h] | 1.315e+005 |
| Bed 2 [STD_m3/h] | 4740 |
| Bed 3 [STD_m3/h] | 1.832e+004 |
| **Reactor 2** | |
| Bed 1 [STD_m3/h] | 1.773e+004 |
| Bed 2 [STD_m3/h] | 1.466e+004 |
| Bed 3 [STD_m3/h] | 1.591e+004 |
| NH3 Removal - Loop 1 [kg/h] | 96.40 |
| H2S Removal [kg/h] | 808.2 |
| Purge gas flow - Loop 1 [STD_m3/h] | 713.7 |
| N2 | 0.0330 |
| H2 | 0.9030 |
| H2S | 0.0000 |
| C1 | 0.0640 |
| C2 | 0.0000 |
| C3 | 0.0000 |
| C4 | 0.0000 |
| C5 | 0.0000 |
| C6P | 0.0000 |
| C6N | 0.0000 |
| C6A | 0.0000 |
| C7P | 0.0000 |
| C7N | 0.0000 |
| C7A | 0.0000 |
| H2 makeup 1 rate - Loop 1 [STD_m3/h] | 2.943e+004 |
| H2 consumption [STD_m3/m3] | 249.1 |
| Nitrogen In R1 Liquid Product [ppmwt] | 7.800 |

Figure 2.93 Input process data

Step 5: Define the number of cuts in each distillate range.

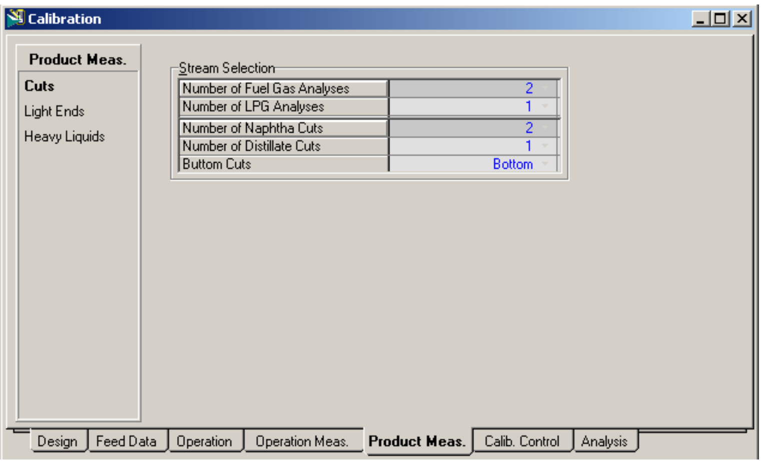

Stream Selection

| | |
|---|---|
| Number of Fuel Gas Analyses | 2 |
| Number of LPG Analyses | 1 |
| Number of Naphtha Cuts | 2 |
| Number of Distillate Cuts | 1 |
| Buttom Cuts | Bottom |

Figure 2.94 Define plant cuts

Step 6: Input compositional analyses and flow rates of light ends. These are important to calculate the composition of naphtha cuts.

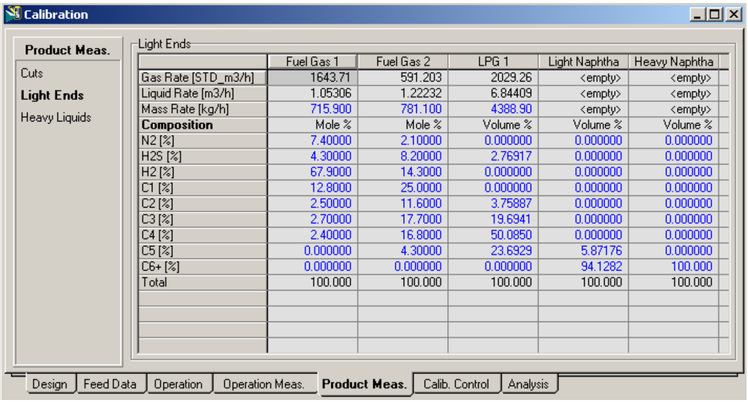

Light Ends

| | Fuel Gas 1 | Fuel Gas 2 | LPG 1 | Light Naphtha | Heavy Naphtha |
|---|---|---|---|---|---|
| Gas Rate [STD_m3/h] | 1643.71 | 591.203 | 2029.26 | <empty> | <empty> |
| Liquid Rate [m3/h] | 1.05306 | 1.22232 | 6.84409 | <empty> | <empty> |
| Mass Rate [kg/h] | 715.900 | 781.100 | 4388.90 | <empty> | <empty> |
| **Composition** | Mole % | Mole % | Volume % | Volume % | Volume % |
| N2 [%] | 7.40000 | 2.10000 | 0.000000 | 0.000000 | 0.000000 |
| H2S [%] | 4.30000 | 8.20000 | 2.76917 | 0.000000 | 0.000000 |
| H2 [%] | 67.9000 | 14.3000 | 0.000000 | 0.000000 | 0.000000 |
| C1 [%] | 12.8000 | 25.0000 | 0.000000 | 0.000000 | 0.000000 |
| C2 [%] | 2.50000 | 11.6000 | 3.75887 | 0.000000 | 0.000000 |
| C3 [%] | 2.70000 | 17.7000 | 19.6941 | 0.000000 | 0.000000 |
| C4 [%] | 2.40000 | 16.8000 | 50.0850 | 0.000000 | 0.000000 |
| C5 [%] | 0.000000 | 4.30000 | 23.6929 | 5.87176 | 0.000000 |
| C6+ [%] | 0.000000 | 0.000000 | 0.000000 | 94.1282 | 100.000 |
| Total | 100.000 | 100.000 | 100.000 | 100.000 | 100.000 |

Figure 2.95 Input product yields and analyses (light products)

Step 7: Input distillation curves, elemental analyses, specific gravities and flow rates of liquid products. Distillation curves and flow rates are the most important properties and they have to be accurate to ensure that the model works well. Specific gravity affects model's prediction on hydrogenation reaction rate. Elemental analysis only affects the severity of HDN and HDS reactions and hydrogen balance which have little effect on the yield prediction of HCR model.

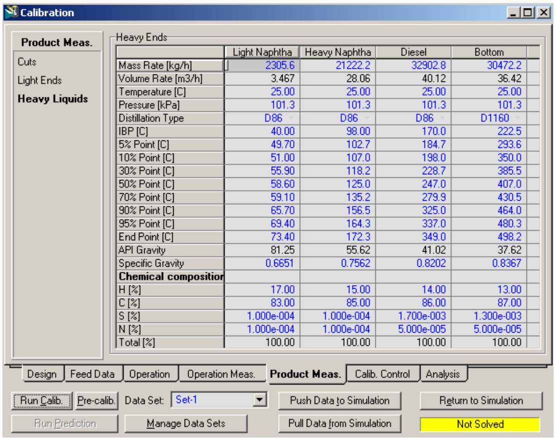

Data Set: Set-1

Heavy Ends

| | Light Naphtha | Heavy Naphtha | Diesel | Bottom |
|---|---|---|---|---|
| Mass Rate [kg/h] | 2305.6 | 21222.2 | 32902.8 | 30472.2 |
| Volume Rate [m3/h] | 3.467 | 28.06 | 40.12 | 36.42 |
| Temperature [C] | 25.00 | 25.00 | 25.00 | 25.00 |
| Pressure [kPa] | 101.3 | 101.3 | 101.3 | 101.3 |
| Distillation Type | D86 | D86 | D86 | D1160 |
| IBP [C] | 40.00 | 98.00 | 170.0 | 222.5 |
| 5% Point [C] | 49.70 | 102.7 | 184.7 | 293.6 |
| 10% Point [C] | 51.00 | 107.0 | 198.0 | 350.0 |
| 30% Point [C] | 55.90 | 118.2 | 228.7 | 385.5 |
| 50% Point [C] | 58.60 | 125.0 | 247.0 | 407.0 |
| 70% Point [C] | 59.10 | 135.2 | 279.9 | 430.5 |
| 90% Point [C] | 65.70 | 156.5 | 325.0 | 464.0 |
| 95% Point [C] | 69.40 | 164.3 | 337.0 | 480.3 |
| End Point [C] | 73.40 | 172.3 | 349.0 | 498.2 |
| API Gravity | 81.25 | 55.62 | 41.02 | 37.62 |
| Specific Gravity | 0.6651 | 0.7562 | 0.8202 | 0.8367 |
| **Chemical compositior** | | | | |
| H [%] | 17.00 | 15.00 | 14.00 | 13.00 |
| C [%] | 83.00 | 85.00 | 86.00 | 87.00 |
| S [%] | 1.000e-004 | 1.000e-004 | 1.700e-003 | 1.300e-003 |
| N [%] | 1.000e-004 | 1.000e-004 | 5.000e-005 | 5.000e-005 |
| Total [%] | 100.00 | 100.00 | 100.00 | 100.00 |

Figure 2.96 Input product yields and analyses (heavy products)

Step 8: Change the iteration scheme to enhance model’s convergence.

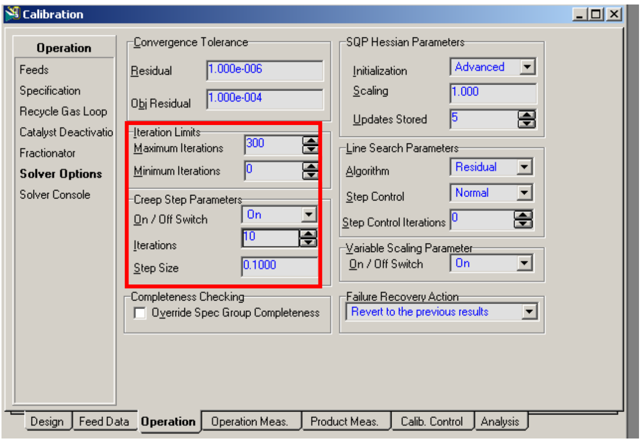

Convergence Tolerance
Residual 1.000e-006
Obj Residual 1.000e-004

Iteration Limits
Maximum Iterations 300
Minimum Iterations 0

Creep Step Parameters
On / Off Switch On
Iterations 10
Step Size 0.1000

Completeness Checking
☐ Override Spec Group Completeness

SQP Hessian Parameters
Initialization Advanced
Scaling 1.000
Updates Stored 5

Line Search Parameters
Algorithm Residual
Step Control Normal
Step Control Iterations 0

Variable Scaling Parameter
On / Off Switch On

Failure Recovery Action
Revert to the previous results

Figure 2.97 Iteration algorithm for model convergence

Step 9: Check all of the boxes in “object function” sheet so that we are able to probe into how significantly the model results deviate from plant data.

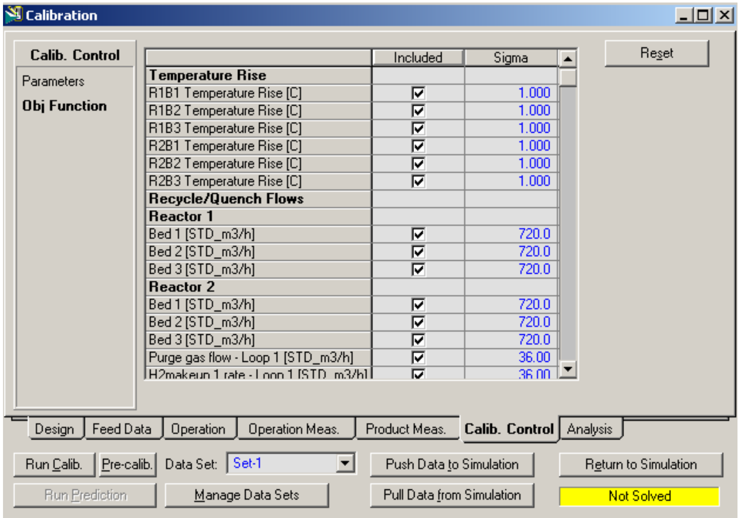

Data Set: Set-1

|  | Included | Sigma |
|---|---|---|
| **Temperature Rise** |  |  |
| R1B1 Temperature Rise [C] | ☑ | 1.000 |
| R1B2 Temperature Rise [C] | ☑ | 1.000 |
| R1B3 Temperature Rise [C] | ☑ | 1.000 |
| R2B1 Temperature Rise [C] | ☑ | 1.000 |
| R2B2 Temperature Rise [C] | ☑ | 1.000 |
| R2B3 Temperature Rise [C] | ☑ | 1.000 |
| **Recycle/Quench Flows** |  |  |
| **Reactor 1** |  |  |
| Bed 1 [STD_m3/h] | ☑ | 720.0 |
| Bed 2 [STD_m3/h] | ☑ | 720.0 |
| Bed 3 [STD_m3/h] | ☑ | 720.0 |
| **Reactor 2** |  |  |
| Bed 1 [STD_m3/h] | ☑ | 720.0 |
| Bed 2 [STD_m3/h] | ☑ | 720.0 |
| Bed 3 [STD_m3/h] | ☑ | 720.0 |
| Purge gas flow - Loop 1 [STD_m3/h] | ☑ | 36.00 |
| H2makeup 1 rate - Loop 1 [STD_m3/h] | ☑ | 36.00 |

Figure 2.98 Objective function sheet

Step 10: We can use this sheet to select the reaction activities to be adjusted during automatic calibration by clicking “run calib” and change the lower and upper bounds of the selected reaction activities. In this step, we click the button of “pre-calib” to run the model with current reaction activities which are also default values.

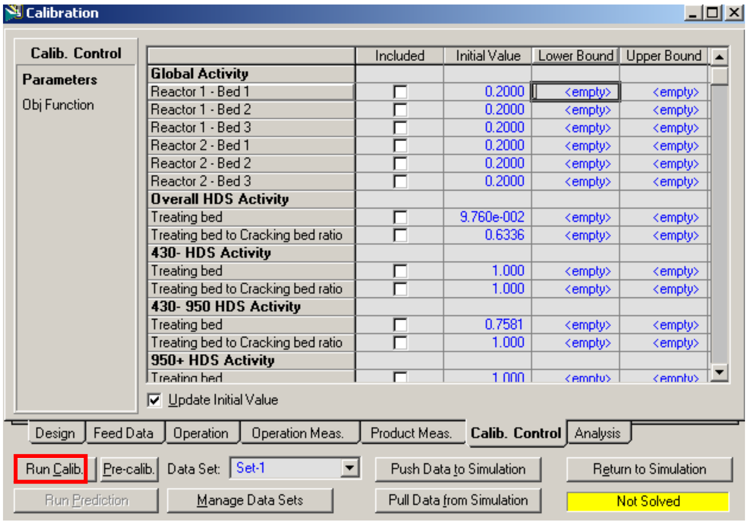

Data Set: Set-1

|  | Included | Initial Value | Lower Bound | Upper Bound |
|---|---|---|---|---|
| **Global Activity** |  |  |  |  |
| Reactor 1 - Bed 1 | ☐ | 0.2000 | <empty> | <empty> |
| Reactor 1 - Bed 2 | ☐ | 0.2000 | <empty> | <empty> |
| Reactor 1 - Bed 3 | ☐ | 0.2000 | <empty> | <empty> |
| Reactor 2 - Bed 1 | ☐ | 0.2000 | <empty> | <empty> |
| Reactor 2 - Bed 2 | ☐ | 0.2000 | <empty> | <empty> |
| Reactor 2 - Bed 3 | ☐ | 0.2000 | <empty> | <empty> |
| **Overall HDS Activity** |  |  |  |  |
| Treating bed | ☐ | 9.760e-002 | <empty> | <empty> |
| Treating bed to Cracking bed ratio | ☐ | 0.6336 | <empty> | <empty> |
| **430- HDS Activity** |  |  |  |  |
| Treating bed | ☐ | 1.000 | <empty> | <empty> |
| Treating bed to Cracking bed ratio | ☐ | 1.000 | <empty> | <empty> |
| **430- 950 HDS Activity** |  |  |  |  |
| Treating bed | ☐ | 0.7581 | <empty> | <empty> |
| Treating bed to Cracking bed ratio | ☐ | 1.000 | <empty> | <empty> |
| **950+ HDS Activity** |  |  |  |  |
| Treating bed | ☐ | 1.000 | <empty> | <empty> |

☑ Update Initial Value

Figure 2.99 Reaction activity factor sheet

Step 11: Analysis sheet represents the results after running calibration. It also shows the comparisons between model results from current reaction activities and plant data.

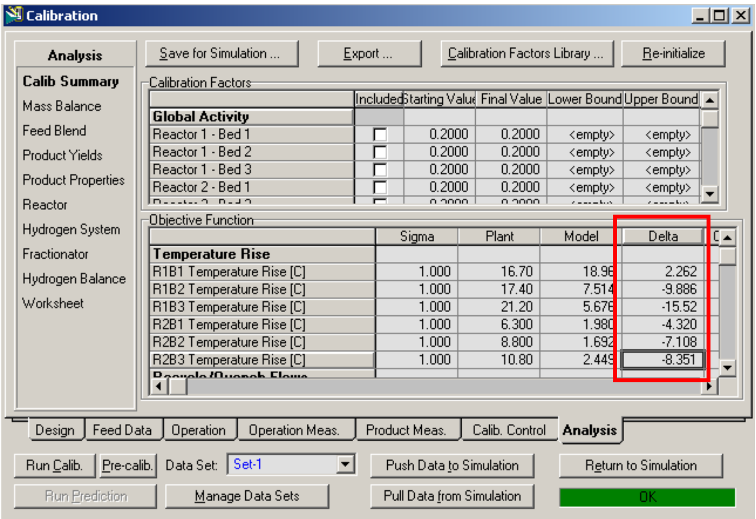

Calibration Factors

| | Included | Starting Value | Final Value | Lower Bound | Upper Bound |
|---|---|---|---|---|---|
| **Global Activity** | | | | | |
| Reactor 1 - Bed 1 | ☐ | 0.2000 | 0.2000 | <empty> | <empty> |
| Reactor 1 - Bed 2 | ☐ | 0.2000 | 0.2000 | <empty> | <empty> |
| Reactor 1 - Bed 3 | ☐ | 0.2000 | 0.2000 | <empty> | <empty> |
| Reactor 2 - Bed 1 | ☐ | 0.2000 | 0.2000 | <empty> | <empty> |

Objective Function

| | Sigma | Plant | Model | Delta |
|---|---|---|---|---|
| **Temperature Rise** | | | | |
| R1B1 Temperature Rise [C] | 1.000 | 16.70 | 18.96 | 2.262 |
| R1B2 Temperature Rise [C] | 1.000 | 17.40 | 7.514 | -9.886 |
| R1B3 Temperature Rise [C] | 1.000 | 21.20 | 5.676 | -15.52 |
| R2B1 Temperature Rise [C] | 1.000 | 6.300 | 1.980 | -4.320 |
| R2B2 Temperature Rise [C] | 1.000 | 8.800 | 1.692 | -7.108 |
| R2B3 Temperature Rise [C] | 1.000 | 10.80 | 2.449 | -8.351 |

Data Set: Set-1

Figure 2.100 Calibration result sheet

Step 12: Select “R1B1 Temperature Rise” in “Obj. Function” sheet.

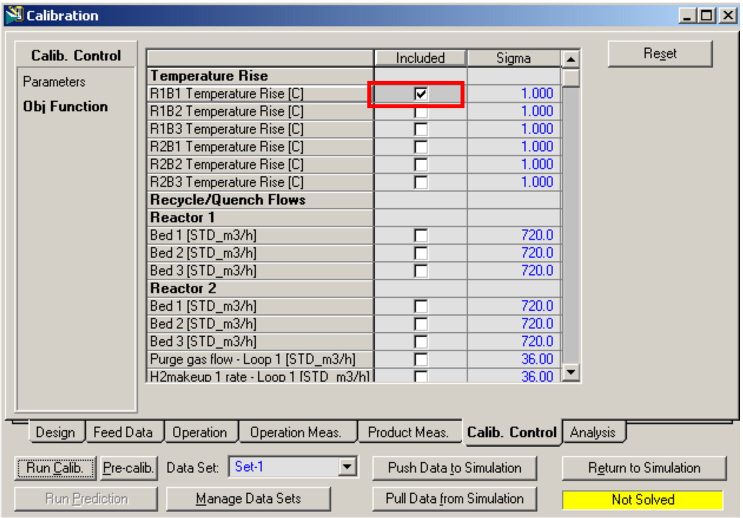

| | Included | Sigma |
|---|---|---|
| **Temperature Rise** | | |
| R1B1 Temperature Rise [C] | ☑ | 1.000 |
| R1B2 Temperature Rise [C] | ☐ | 1.000 |
| R1B3 Temperature Rise [C] | ☐ | 1.000 |
| R2B1 Temperature Rise [C] | ☐ | 1.000 |
| R2B2 Temperature Rise [C] | ☐ | 1.000 |
| R2B3 Temperature Rise [C] | ☐ | 1.000 |
| **Recycle/Quench Flows** | | |
| **Reactor 1** | | |
| Bed 1 [STD_m3/h] | ☐ | 720.0 |
| Bed 2 [STD_m3/h] | ☐ | 720.0 |
| Bed 3 [STD_m3/h] | ☐ | 720.0 |
| **Reactor 2** | | |
| Bed 1 [STD_m3/h] | ☐ | 720.0 |
| Bed 2 [STD_m3/h] | ☐ | 720.0 |
| Bed 3 [STD_m3/h] | ☐ | 720.0 |
| Purge gas flow - Loop 1 [STD_m3/h] | ☐ | 36.00 |
| H2makeup 1 rate - Loop 1 [STD_m3/h] | ☐ | 36.00 |

Data Set: Set-1

Figure 2.101 Define objective function (1st bed)

Step 13: Select “Global activity – Reactor 1 – Bed 1” and assign appropriate lower and upper bounds. We suggest that the lower and upper bounds are ±25% up and down around current value (i.e. initial value). By doing steps 12 and 13, the model will tune “Global activity – Reactor 1 – Bed 1” within the assigned range to minimize the deviation between model result of “R1B1 Temperature Rise” and plant measurement.

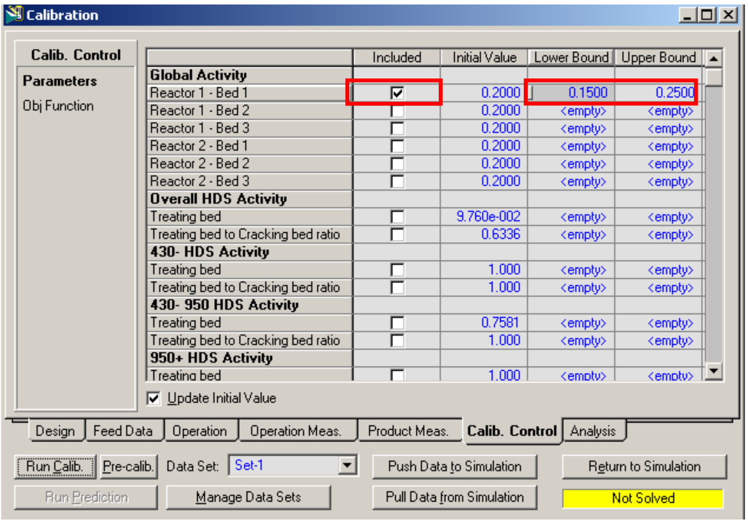

| | Included | Initial Value | Lower Bound | Upper Bound |
|---|---|---|---|---|
| **Global Activity** | | | | |
| Reactor 1 - Bed 1 | ☑ | 0.2000 | 0.1500 | 0.2500 |
| Reactor 1 - Bed 2 | ☐ | 0.2000 | <empty> | <empty> |
| Reactor 1 - Bed 3 | ☐ | 0.2000 | <empty> | <empty> |
| Reactor 2 - Bed 1 | ☐ | 0.2000 | <empty> | <empty> |
| Reactor 2 - Bed 2 | ☐ | 0.2000 | <empty> | <empty> |
| Reactor 2 - Bed 3 | ☐ | 0.2000 | <empty> | <empty> |
| **Overall HDS Activity** | | | | |
| Treating bed | ☐ | 9.760e-002 | <empty> | <empty> |
| Treating bed to Cracking bed ratio | ☐ | 0.6336 | <empty> | <empty> |
| **430- HDS Activity** | | | | |
| Treating bed | ☐ | 1.000 | <empty> | <empty> |
| Treating bed to Cracking bed ratio | ☐ | 1.000 | <empty> | <empty> |
| **430- 950 HDS Activity** | | | | |
| Treating bed | ☐ | 0.7581 | <empty> | <empty> |
| Treating bed to Cracking bed ratio | ☐ | 1.000 | <empty> | <empty> |
| **950+ HDS Activity** | | | | |
| Treating bed | ☐ | 1.000 | <empty> | <empty> |

☑ Update Initial Value

Data Set: Set-1

Not Solved

Figure 2.102 Select tuning activity factor (1st global activity)

Step 14: Check the results in "Analysis" sheet. Repeat step 14 to assign new lower and upper bounds to calibrate the model again if the model results are not good enough.

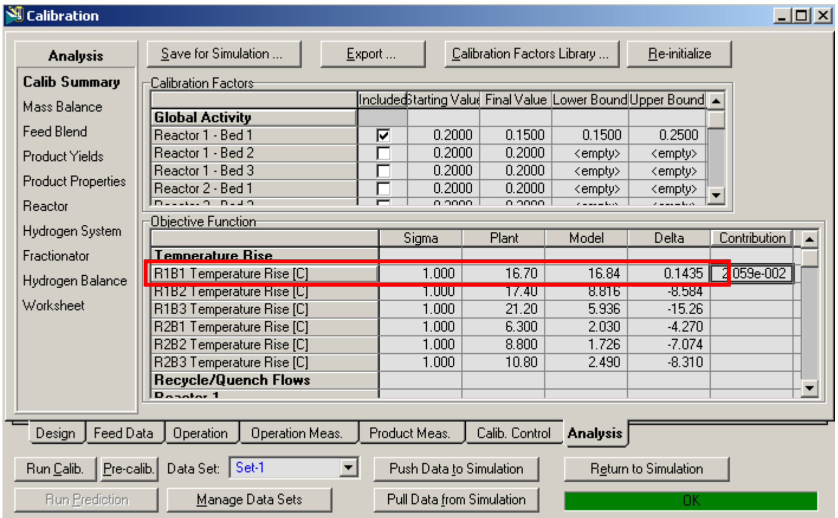

Calibration Factors

| | Included | Starting Value | Final Value | Lower Bound | Upper Bound |
|---|---|---|---|---|---|
| **Global Activity** | | | | | |
| Reactor 1 - Bed 1 | ☑ | 0.2000 | 0.1500 | 0.1500 | 0.2500 |
| Reactor 1 - Bed 2 | ☐ | 0.2000 | 0.2000 | <empty> | <empty> |
| Reactor 1 - Bed 3 | ☐ | 0.2000 | 0.2000 | <empty> | <empty> |
| Reactor 2 - Bed 1 | ☐ | 0.2000 | 0.2000 | <empty> | <empty> |

Objective Function

| | Sigma | Plant | Model | Delta | Contribution |
|---|---|---|---|---|---|
| **Temperature Rise** | | | | | |
| R1B1 Temperature Rise [C] | 1.000 | 16.70 | 16.84 | 0.1435 | 2.059e-002 |
| R1B2 Temperature Rise [C] | 1.000 | 17.40 | 8.816 | -8.584 | |
| R1B3 Temperature Rise [C] | 1.000 | 21.20 | 5.936 | -15.26 | |
| R2B1 Temperature Rise [C] | 1.000 | 6.300 | 2.030 | -4.270 | |
| R2B2 Temperature Rise [C] | 1.000 | 8.800 | 1.726 | -7.074 | |
| R2B3 Temperature Rise [C] | 1.000 | 10.80 | 2.490 | -8.310 | |
| **Recycle/Quench Flows** | | | | | |

Data Set: Set-1

OK

Figure 2.103 Calibration result (1st bed)

Step 15: After obtaining satisfactory result of "R1B1 Temperature Rise", uncheck the selections of "R1B1 Temperature Rise" and "Global activity – Reactor 1 – Bed 1". Next, repeat steps 12 to 14 for the other reaction beds and corresponding reaction activities one by one.

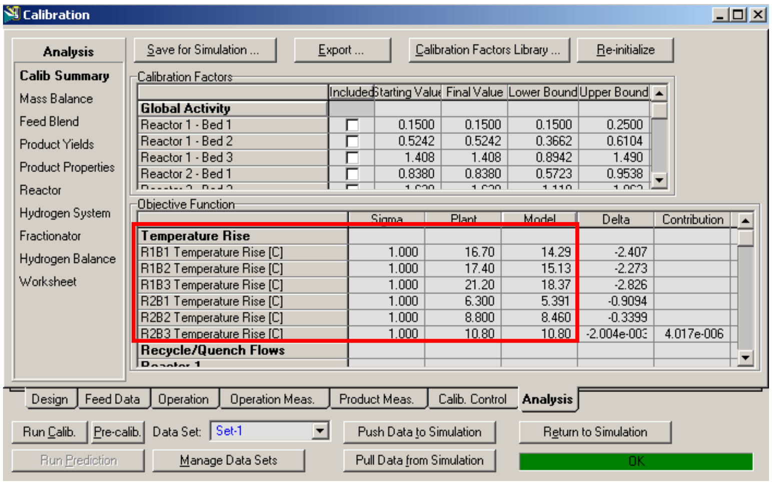

Calibration Factors

| | Included | Starting Value | Final Value | Lower Bound | Upper Bound |
|---|---|---|---|---|---|
| **Global Activity** | | | | | |
| Reactor 1 - Bed 1 | ☐ | 0.1500 | 0.1500 | 0.1500 | 0.2500 |
| Reactor 1 - Bed 2 | ☐ | 0.5242 | 0.5242 | 0.3662 | 0.6104 |
| Reactor 1 - Bed 3 | ☐ | 1.408 | 1.408 | 0.8942 | 1.490 |
| Reactor 2 - Bed 1 | ☐ | 0.8380 | 0.8380 | 0.5723 | 0.9538 |

Objective Function

| | Sigma | Plant | Model | Delta | Contribution |
|---|---|---|---|---|---|
| **Temperature Rise** | | | | | |
| R1B1 Temperature Rise [C] | 1.000 | 16.70 | 14.29 | -2.407 | |
| R1B2 Temperature Rise [C] | 1.000 | 17.40 | 15.13 | -2.273 | |
| R1B3 Temperature Rise [C] | 1.000 | 21.20 | 18.37 | -2.826 | |
| R2B1 Temperature Rise [C] | 1.000 | 6.300 | 5.391 | -0.9094 | |
| R2B2 Temperature Rise [C] | 1.000 | 8.800 | 8.460 | -0.3399 | |
| R2B3 Temperature Rise [C] | 1.000 | 10.80 | 10.80 | -2.004e-003 | 4.017e-006 |
| **Recycle/Quench Flows** | | | | | |

Data Set: Set-1

OK

Figure 2.104 Fitted activity factor (1st global activity)

Step 16: In most cases, the reactor temperature profile obtained from step 15 will show similar trend as plant measurement rather than perfect agreement. To make model's prediction on reactor temperature profile matches plant measurement well, we select all of the "temperature rise" variables as objective functions, assign new tuning ranges to and tune all of the "global reaction activities".

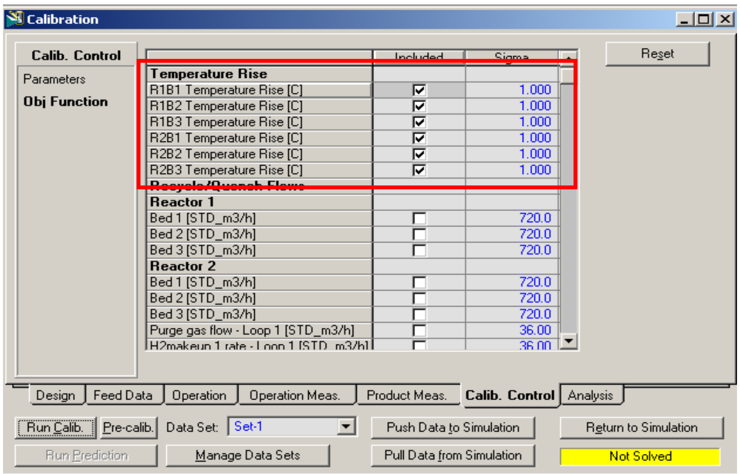

| | Included | Sigma |
|---|---|---|
| **Temperature Rise** | | |
| R1B1 Temperature Rise [C] | ☑ | 1.000 |
| R1B2 Temperature Rise [C] | ☑ | 1.000 |
| R1B3 Temperature Rise [C] | ☑ | 1.000 |
| R2B1 Temperature Rise [C] | ☑ | 1.000 |
| R2B2 Temperature Rise [C] | ☑ | 1.000 |
| R2B3 Temperature Rise [C] | ☑ | 1.000 |
| **Recycle/Quench Flows** | | |
| **Reactor 1** | | |
| Bed 1 [STD_m3/h] | ☐ | 720.0 |
| Bed 2 [STD_m3/h] | ☐ | 720.0 |
| Bed 3 [STD_m3/h] | ☐ | 720.0 |
| **Reactor 2** | | |
| Bed 1 [STD_m3/h] | ☐ | 720.0 |
| Bed 2 [STD_m3/h] | ☐ | 720.0 |
| Bed 3 [STD_m3/h] | ☐ | 720.0 |
| Purge gas flow - Loop 1 [STD_m3/h] | ☐ | 36.00 |
| H2makeup 1 rate - Loop 1 [STD_m3/h] | ☐ | 36.00 |

Data Set: Set-1

Not Solved

Figure 2.105 Define objective function (all beds)

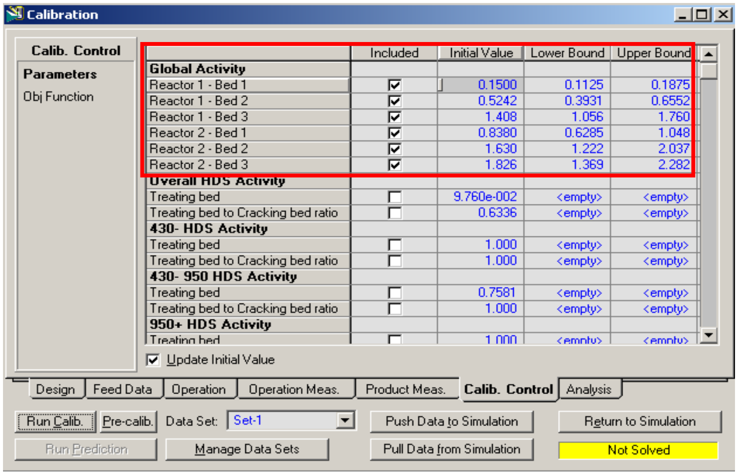

| | Included | Initial Value | Lower Bound | Upper Bound |
|---|---|---|---|---|
| **Global Activity** | | | | |
| Reactor 1 - Bed 1 | ☑ | 0.1500 | 0.1125 | 0.1875 |
| Reactor 1 - Bed 2 | ☑ | 0.5242 | 0.3931 | 0.6552 |
| Reactor 1 - Bed 3 | ☑ | 1.408 | 1.056 | 1.760 |
| Reactor 2 - Bed 1 | ☑ | 0.8380 | 0.6285 | 1.048 |
| Reactor 2 - Bed 2 | ☑ | 1.630 | 1.222 | 2.037 |
| Reactor 2 - Bed 3 | ☑ | 1.826 | 1.369 | 2.282 |
| **Overall HDS Activity** | | | | |
| Treating bed | ☐ | 9.760e-002 | <empty> | <empty> |
| Treating bed to Cracking bed ratio | ☐ | 0.6336 | <empty> | <empty> |
| **430- HDS Activity** | | | | |
| Treating bed | ☐ | 1.000 | <empty> | <empty> |
| Treating bed to Cracking bed ratio | ☐ | 1.000 | <empty> | <empty> |
| **430- 950 HDS Activity** | | | | |
| Treating bed | ☐ | 0.7581 | <empty> | <empty> |
| Treating bed to Cracking bed ratio | ☐ | 1.000 | <empty> | <empty> |
| **950+ HDS Activity** | | | | |
| Treating bed | ☐ | 1.000 | <empty> | <empty> |

☑ Update Initial Value

Data Set: Set-1

Not Solved

Figure 2.106 Select tuning activity factor (all global activities)

Step 17: Repeat step 16 until model's prediction on reactor temperature profile satisfactorily agrees with plant measurement.

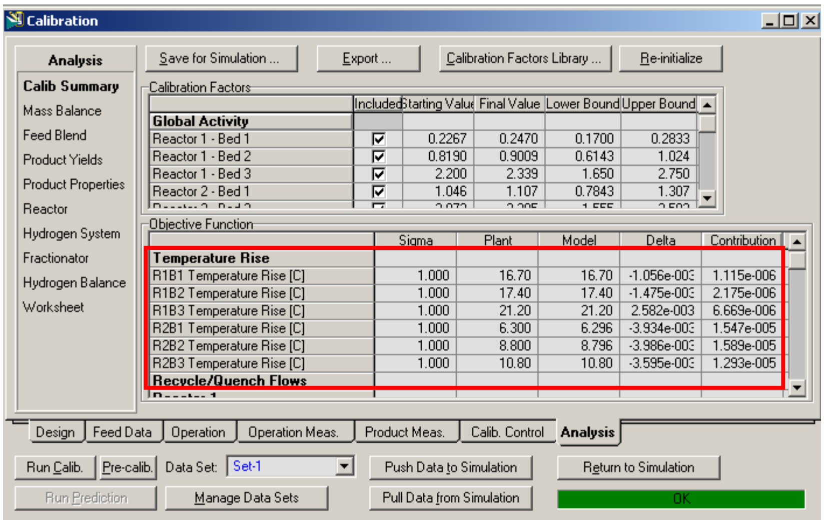

Calibration Factors

| | Included | Starting Value | Final Value | Lower Bound | Upper Bound |
|---|---|---|---|---|---|
| **Global Activity** | | | | | |
| Reactor 1 - Bed 1 | ☑ | 0.2267 | 0.2470 | 0.1700 | 0.2833 |
| Reactor 1 - Bed 2 | ☑ | 0.8190 | 0.9009 | 0.6143 | 1.024 |
| Reactor 1 - Bed 3 | ☑ | 2.200 | 2.339 | 1.650 | 2.750 |
| Reactor 2 - Bed 1 | ☑ | 1.046 | 1.107 | 0.7843 | 1.307 |

Objective Function

| | Sigma | Plant | Model | Delta | Contribution |
|---|---|---|---|---|---|
| **Temperature Rise** | | | | | |
| R1B1 Temperature Rise [C] | 1.000 | 16.70 | 16.70 | -1.056e-003 | 1.115e-006 |
| R1B2 Temperature Rise [C] | 1.000 | 17.40 | 17.40 | -1.475e-003 | 2.175e-006 |
| R1B3 Temperature Rise [C] | 1.000 | 21.20 | 21.20 | 2.582e-003 | 6.669e-006 |
| R2B1 Temperature Rise [C] | 1.000 | 6.300 | 6.296 | -3.934e-003 | 1.547e-005 |
| R2B2 Temperature Rise [C] | 1.000 | 8.800 | 8.796 | -3.986e-003 | 1.589e-005 |
| R2B3 Temperature Rise [C] | 1.000 | 10.80 | 10.80 | -3.595e-003 | 1.293e-005 |
| **Recycle/Quench Flows** | | | | | |

Data Set: Set-1

OK

Figure 2.107 Calibration result (all beds)

Step 18: Even thought the reactor temperature profile from model satisfactorily agrees with plant measurement, model's prediction on product yields still significantly deviates from real operation. By observing the comparison between model results and plant measurement, the model has significant predicting deviations on diesel and bottom yields. Additionally, real production does not include any fraction within the boiling range over 1000°F (square cut residue oil).

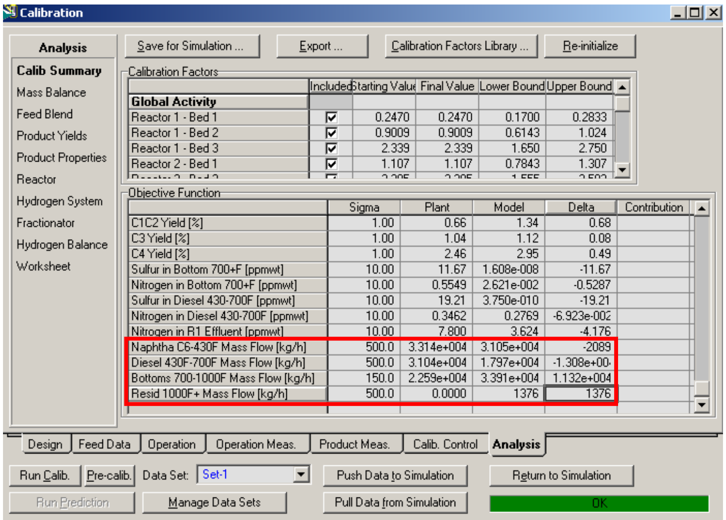

Data Set: Set-1

| | Included | Starting Value | Final Value | Lower Bound | Upper Bound |
|---|---|---|---|---|---|
| **Global Activity** | | | | | |
| Reactor 1 - Bed 1 | ☑ | 0.2470 | 0.2470 | 0.1700 | 0.2833 |
| Reactor 1 - Bed 2 | ☑ | 0.9009 | 0.9009 | 0.6143 | 1.024 |
| Reactor 1 - Bed 3 | ☑ | 2.339 | 2.339 | 1.650 | 2.750 |
| Reactor 2 - Bed 1 | ☑ | 1.107 | 1.107 | 0.7843 | 1.307 |

| | Sigma | Plant | Model | Delta | Contribution |
|---|---|---|---|---|---|
| C1C2 Yield [%] | 1.00 | 0.66 | 1.34 | 0.68 | |
| C3 Yield [%] | 1.00 | 1.04 | 1.12 | 0.08 | |
| C4 Yield [%] | 1.00 | 2.46 | 2.95 | 0.49 | |
| Sulfur in Bottom 700+F [ppmwt] | 10.00 | 11.67 | 1.608e-008 | -11.67 | |
| Nitrogen in Bottom 700+F [ppmwt] | 10.00 | 0.5549 | 2.621e-002 | -0.5287 | |
| Sulfur in Diesel 430-700F [ppmwt] | 10.00 | 19.21 | 3.750e-010 | -19.21 | |
| Nitrogen in Diesel 430-700F [ppmwt] | 10.00 | 0.3462 | 0.2769 | -6.923e-002 | |
| Nitrogen in R1 Effluent [ppmwt] | 10.00 | 7.800 | 3.624 | -4.176 | |
| Naphtha C6-430F Mass Flow [kg/h] | 500.0 | 3.314e+004 | 3.105e+004 | -2089 | |
| Diesel 430F-700F Mass Flow [kg/h] | 500.0 | 3.104e+004 | 1.797e+004 | -1.308e+00 | |
| Bottoms 700-1000F Mass Flow [kg/h] | 150.0 | 2.259e+004 | 3.391e+004 | 1.132e+004 | |
| Resid 1000F+ Mass Flow [kg/h] | 500.0 | 0.0000 | 1376 | 1376 | |

Figure 2.108 Calibration result (product yields)

Step 19: Select the following objective functions and reaction activities to calibrate the model (by clicking the button of "run calib"). Repeat this step until the model matches plant measurements on reactor temperature profile and product yields.

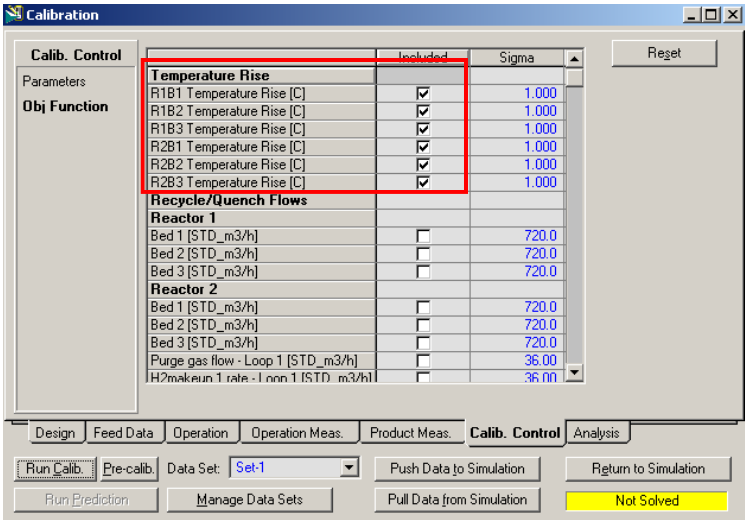

Data Set: Set-1

| | Included | Sigma |
|---|---|---|
| **Temperature Rise** | | |
| R1B1 Temperature Rise [C] | ☑ | 1.000 |
| R1B2 Temperature Rise [C] | ☑ | 1.000 |
| R1B3 Temperature Rise [C] | ☑ | 1.000 |
| R2B1 Temperature Rise [C] | ☑ | 1.000 |
| R2B2 Temperature Rise [C] | ☑ | 1.000 |
| R2B3 Temperature Rise [C] | ☑ | 1.000 |
| **Recycle/Quench Flows** | | |
| **Reactor 1** | | |
| Bed 1 [STD_m3/h] | ☐ | 720.0 |
| Bed 2 [STD_m3/h] | ☐ | 720.0 |
| Bed 3 [STD_m3/h] | ☐ | 720.0 |
| **Reactor 2** | | |
| Bed 1 [STD_m3/h] | ☐ | 720.0 |
| Bed 2 [STD_m3/h] | ☐ | 720.0 |
| Bed 3 [STD_m3/h] | ☐ | 720.0 |
| Purge gas flow - Loop 1 [STD_m3/h] | ☐ | 36.00 |
| H2makeup 1 rate - Loop 1 [STD_m3/h] | ☐ | 36.00 |

Figure 2.109 Define objective function (all beds)

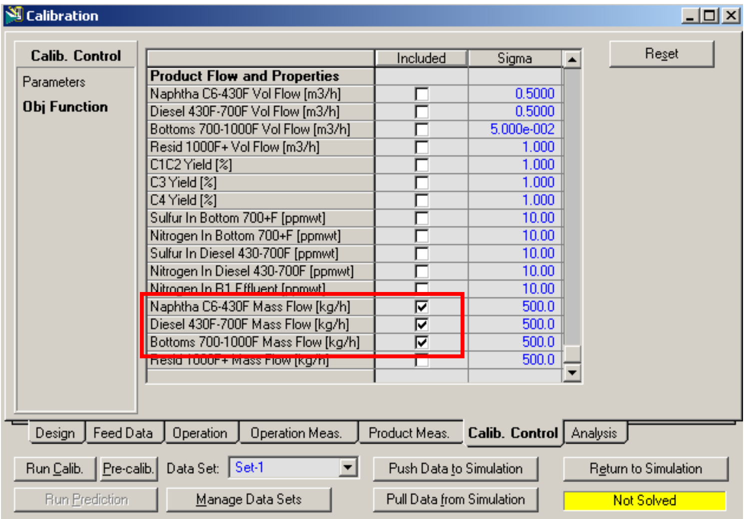

| | Included | Sigma |
|---|---|---|
| **Product Flow and Properties** | | |
| Naphtha C6-430F Vol Flow [m3/h] | ☐ | 0.5000 |
| Diesel 430F-700F Vol Flow [m3/h] | ☐ | 0.5000 |
| Bottoms 700-1000F Vol Flow [m3/h] | ☐ | 5.000e-002 |
| Resid 1000F+ Vol Flow [m3/h] | ☐ | 1.000 |
| C1C2 Yield [%] | ☐ | 1.000 |
| C3 Yield [%] | ☐ | 1.000 |
| C4 Yield [%] | ☐ | 1.000 |
| Sulfur In Bottom 700+F [ppmwt] | ☐ | 10.00 |
| Nitrogen In Bottom 700+F [ppmwt] | ☐ | 10.00 |
| Sulfur In Diesel 430-700F [ppmwt] | ☐ | 10.00 |
| Nitrogen In Diesel 430-700F [ppmwt] | ☐ | 10.00 |
| Nitrogen In R1 Effluent [ppmwt] | ☐ | 10.00 |
| Naphtha C6-430F Mass Flow [kg/h] | ☑ | 500.0 |
| Diesel 430F-700F Mass Flow [kg/h] | ☑ | 500.0 |
| Bottoms 700-1000F Mass Flow [kg/h] | ☑ | 500.0 |
| Resid 1000F+ Mass Flow [kg/h] | ☐ | 500.0 |

Figure 2.110 Define objective function (all mass yields except for resid)

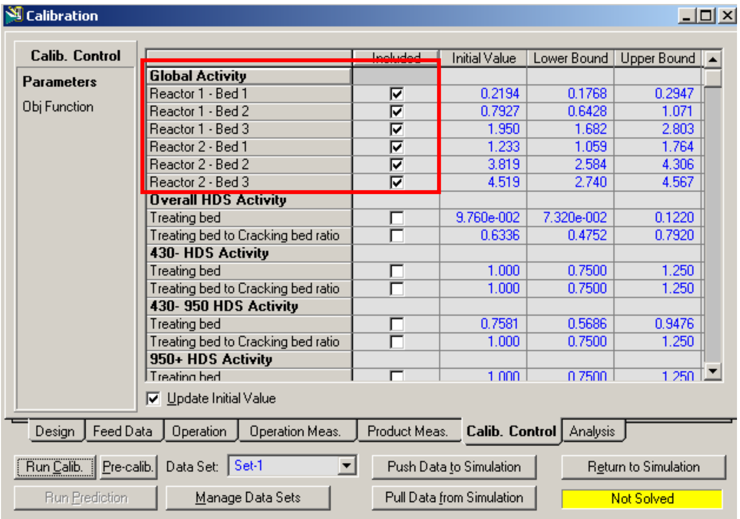

| | Included | Initial Value | Lower Bound | Upper Bound |
|---|---|---|---|---|
| **Global Activity** | | | | |
| Reactor 1 - Bed 1 | ☑ | 0.2194 | 0.1768 | 0.2947 |
| Reactor 1 - Bed 2 | ☑ | 0.7927 | 0.6428 | 1.071 |
| Reactor 1 - Bed 3 | ☑ | 1.950 | 1.682 | 2.803 |
| Reactor 2 - Bed 1 | ☑ | 1.233 | 1.059 | 1.764 |
| Reactor 2 - Bed 2 | ☑ | 3.819 | 2.584 | 4.306 |
| Reactor 2 - Bed 3 | ☑ | 4.519 | 2.740 | 4.567 |
| **Overall HDS Activity** | | | | |
| Treating bed | ☐ | 9.760e-002 | 7.320e-002 | 0.1220 |
| Treating bed to Cracking bed ratio | ☐ | 0.6336 | 0.4752 | 0.7920 |
| **430- HDS Activity** | | | | |
| Treating bed | ☐ | 1.000 | 0.7500 | 1.250 |
| Treating bed to Cracking bed ratio | ☐ | 1.000 | 0.7500 | 1.250 |
| **430- 950 HDS Activity** | | | | |
| Treating bed | ☐ | 0.7581 | 0.5686 | 0.9476 |
| Treating bed to Cracking bed ratio | ☐ | 1.000 | 0.7500 | 1.250 |
| **950+ HDS Activity** | | | | |
| Treating bed | ☐ | 1.000 | 0.7500 | 1.250 |

☑ Update Initial Value

Figure 2.111 Select tuning activity factor (all global activities)

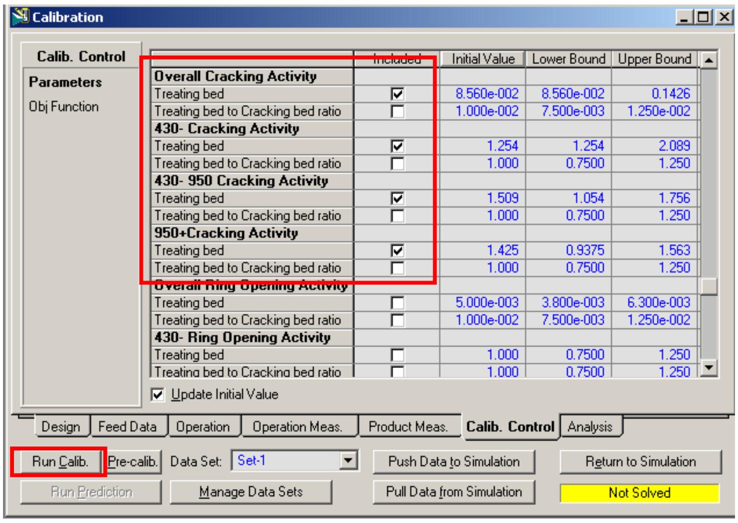

|  | Included | Initial Value | Lower Bound | Upper Bound |
|---|---|---|---|---|
| **Overall Cracking Activity** |  |  |  |  |
| Treating bed | ☑ | 8.560e-002 | 8.560e-002 | 0.1426 |
| Treating bed to Cracking bed ratio | ☐ | 1.000e-002 | 7.500e-003 | 1.250e-002 |
| **430- Cracking Activity** |  |  |  |  |
| Treating bed | ☑ | 1.254 | 1.254 | 2.089 |
| Treating bed to Cracking bed ratio | ☐ | 1.000 | 0.7500 | 1.250 |
| **430- 950 Cracking Activity** |  |  |  |  |
| Treating bed | ☑ | 1.509 | 1.054 | 1.756 |
| Treating bed to Cracking bed ratio | ☐ | 1.000 | 0.7500 | 1.250 |
| **950+Cracking Activity** |  |  |  |  |
| Treating bed | ☑ | 1.425 | 0.9375 | 1.563 |
| Treating bed to Cracking bed ratio | ☐ | 1.000 | 0.7500 | 1.250 |
| **Overall Ring Opening Activity** |  |  |  |  |
| Treating bed | ☐ | 5.000e-003 | 3.800e-003 | 6.300e-003 |
| Treating bed to Cracking bed ratio | ☐ | 1.000e-002 | 7.500e-003 | 1.250e-002 |
| **430- Ring Opening Activity** |  |  |  |  |
| Treating bed | ☐ | 1.000 | 0.7500 | 1.250 |
| Treating bed to Cracking bed ratio | ☐ | 1.000 | 0.7500 | 1.250 |

☑ Update Initial Value

Data Set: Set-1

Not Solved

Figure 2.112 Select tuning activity factor (all cracking activities on cracking beds)

Step 20: In some cases, the model's predictions match most of the plant measurements except for one or two process variables. We suggest not to run automatic calibration but manually reconcile the model that allows "creep" moving by small step in each run. For example, the figure below shows that the model only fails to predict the third bed temperature of first reactor (R1B3).

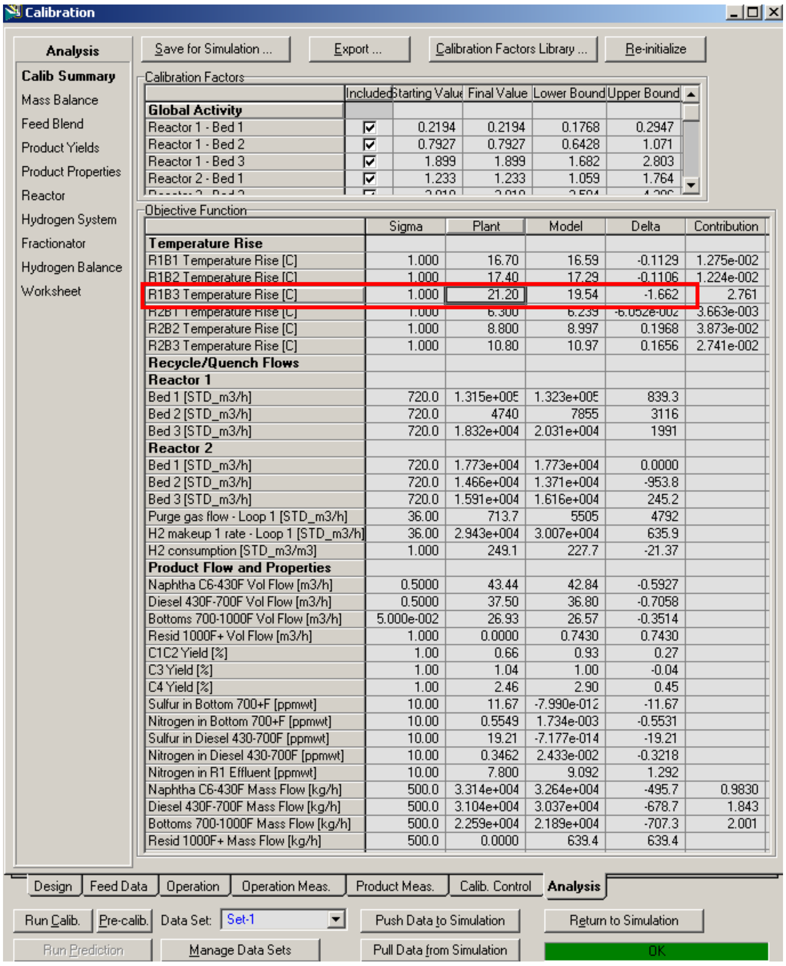

Calibration Factors

| | Included | Starting Valu | Final Value | Lower Bound | Upper Bound |
|---|---|---|---|---|---|
| **Global Activity** | | | | | |
| Reactor 1 - Bed 1 | ☑ | 0.2194 | 0.2194 | 0.1768 | 0.2947 |
| Reactor 1 - Bed 2 | ☑ | 0.7927 | 0.7927 | 0.6428 | 1.071 |
| Reactor 1 - Bed 3 | ☑ | 1.899 | 1.899 | 1.682 | 2.803 |
| Reactor 2 - Bed 1 | ☑ | 1.233 | 1.233 | 1.059 | 1.764 |

Objective Function

| | Sigma | Plant | Model | Delta | Contribution |
|---|---|---|---|---|---|
| **Temperature Rise** | | | | | |
| R1B1 Temperature Rise [C] | 1.000 | 16.70 | 16.59 | -0.1129 | 1.275e-002 |
| R1B2 Temperature Rise [C] | 1.000 | 17.40 | 17.29 | -0.1106 | 1.224e-002 |
| R1B3 Temperature Rise [C] | 1.000 | 21.20 | 19.54 | -1.662 | 2.761 |
| R2B1 Temperature Rise [C] | 1.000 | 6.300 | 6.239 | -6.052e-002 | 3.663e-003 |
| R2B2 Temperature Rise [C] | 1.000 | 8.800 | 8.997 | 0.1968 | 3.873e-002 |
| R2B3 Temperature Rise [C] | 1.000 | 10.80 | 10.97 | 0.1656 | 2.741e-002 |
| **Recycle/Quench Flows** | | | | | |
| **Reactor 1** | | | | | |
| Bed 1 [STD_m3/h] | 720.0 | 1.315e+005 | 1.323e+005 | 839.3 | |
| Bed 2 [STD_m3/h] | 720.0 | 4740 | 7855 | 3116 | |
| Bed 3 [STD_m3/h] | 720.0 | 1.832e+004 | 2.031e+004 | 1991 | |
| **Reactor 2** | | | | | |
| Bed 1 [STD_m3/h] | 720.0 | 1.773e+004 | 1.773e+004 | 0.0000 | |
| Bed 2 [STD_m3/h] | 720.0 | 1.466e+004 | 1.371e+004 | -953.8 | |
| Bed 3 [STD_m3/h] | 720.0 | 1.591e+004 | 1.616e+004 | 245.2 | |
| Purge gas flow - Loop 1 [STD_m3/h] | 36.00 | 713.7 | 5505 | 4792 | |
| H2 makeup 1 rate - Loop 1 [STD_m3/h] | 36.00 | 2.943e+004 | 3.007e+004 | 635.9 | |
| H2 consumption [STD_m3/m3] | 1.000 | 249.1 | 227.7 | -21.37 | |
| **Product Flow and Properties** | | | | | |
| Naphtha C6-430F Vol Flow [m3/h] | 0.5000 | 43.44 | 42.84 | -0.5927 | |
| Diesel 430F-700F Vol Flow [m3/h] | 0.5000 | 37.50 | 36.80 | -0.7058 | |
| Bottoms 700-1000F Vol Flow [m3/h] | 5.000e-002 | 26.93 | 26.57 | -0.3514 | |
| Resid 1000F+ Vol Flow [m3/h] | 1.000 | 0.0000 | 0.7430 | 0.7430 | |
| C1C2 Yield [%] | 1.00 | 0.66 | 0.93 | 0.27 | |
| C3 Yield [%] | 1.00 | 1.04 | 1.00 | -0.04 | |
| C4 Yield [%] | 1.00 | 2.46 | 2.90 | 0.45 | |
| Sulfur in Bottom 700+F [ppmwt] | 10.00 | 11.67 | -7.990e-012 | -11.67 | |
| Nitrogen in Bottom 700+F [ppmwt] | 10.00 | 0.5549 | 1.734e-003 | -0.5531 | |
| Sulfur in Diesel 430-700F [ppmwt] | 10.00 | 19.21 | -7.177e-014 | -19.21 | |
| Nitrogen in Diesel 430-700F [ppmwt] | 10.00 | 0.3462 | 2.433e-002 | -0.3218 | |
| Nitrogen in R1 Effluent [ppmwt] | 10.00 | 7.800 | 9.092 | 1.292 | |
| Naphtha C6-430F Mass Flow [kg/h] | 500.0 | 3.314e+004 | 3.264e+004 | -495.7 | 0.9830 |
| Diesel 430F-700F Mass Flow [kg/h] | 500.0 | 3.104e+004 | 3.037e+004 | -678.7 | 1.843 |
| Bottoms 700-1000F Mass Flow [kg/h] | 500.0 | 2.259e+004 | 2.189e+004 | -707.3 | 2.001 |
| Resid 1000F+ Mass Flow [kg/h] | 500.0 | 0.0000 | 639.4 | 639.4 | |

Data Set: Set-1

Figure 2.113 Calibration results

Step 21: To manually reconcile the model, assign a new value to the related reaction activity. In this case, the predicted temperature is lower than plant measurement and we expect a bigger value of the related reaction reactivity. Thus, we change “global activity reactor 1 bed 3” from current value (1.899) to 1.91 and click the button of “pre-calib” to run the model with current values of reaction activities.

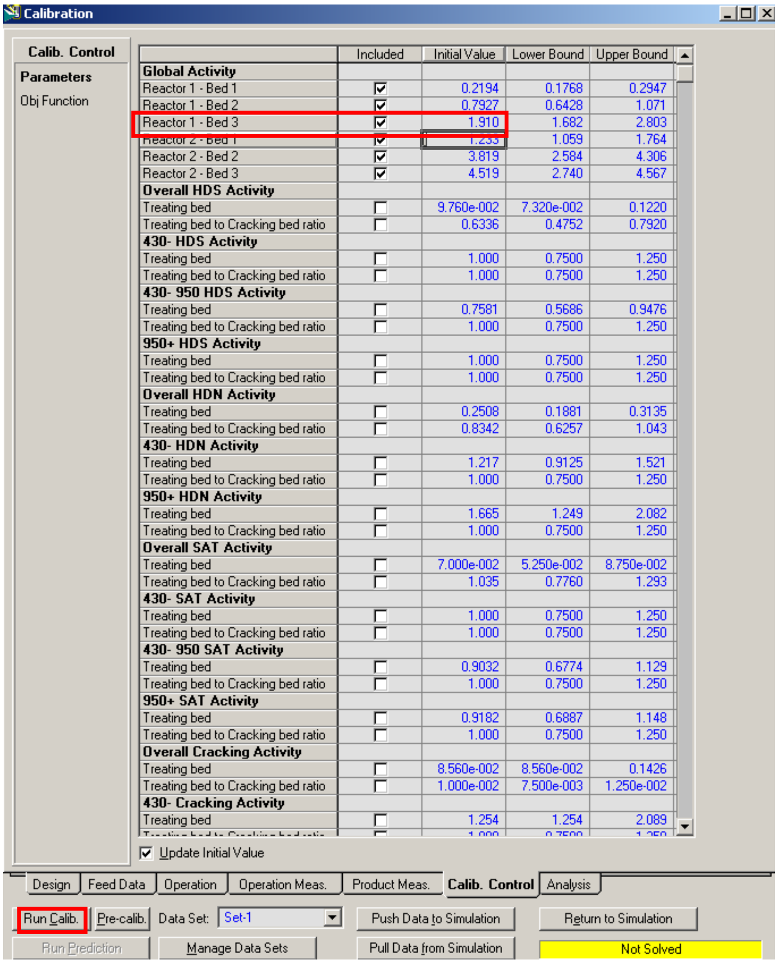

|  | Included | Initial Value | Lower Bound | Upper Bound |
|---|---|---|---|---|
| **Global Activity** |  |  |  |  |
| Reactor 1 - Bed 1 | ☑ | 0.2194 | 0.1768 | 0.2947 |
| Reactor 1 - Bed 2 | ☑ | 0.7927 | 0.6428 | 1.071 |
| Reactor 1 - Bed 3 | ☑ | 1.910 | 1.682 | 2.803 |
| Reactor 2 - Bed 1 | ☑ | 1.233 | 1.059 | 1.764 |
| Reactor 2 - Bed 2 | ☑ | 3.819 | 2.584 | 4.306 |
| Reactor 2 - Bed 3 | ☑ | 4.519 | 2.740 | 4.567 |
| **Overall HDS Activity** |  |  |  |  |
| Treating bed | ☐ | 9.760e-002 | 7.320e-002 | 0.1220 |
| Treating bed to Cracking bed ratio | ☐ | 0.6336 | 0.4752 | 0.7920 |
| **430- HDS Activity** |  |  |  |  |
| Treating bed | ☐ | 1.000 | 0.7500 | 1.250 |
| Treating bed to Cracking bed ratio | ☐ | 1.000 | 0.7500 | 1.250 |
| **430- 950 HDS Activity** |  |  |  |  |
| Treating bed | ☐ | 0.7581 | 0.5686 | 0.9476 |
| Treating bed to Cracking bed ratio | ☐ | 1.000 | 0.7500 | 1.250 |
| **950+ HDS Activity** |  |  |  |  |
| Treating bed | ☐ | 1.000 | 0.7500 | 1.250 |
| Treating bed to Cracking bed ratio | ☐ | 1.000 | 0.7500 | 1.250 |
| **Overall HDN Activity** |  |  |  |  |
| Treating bed | ☐ | 0.2508 | 0.1881 | 0.3135 |
| Treating bed to Cracking bed ratio | ☐ | 0.8342 | 0.6257 | 1.043 |
| **430- HDN Activity** |  |  |  |  |
| Treating bed | ☐ | 1.217 | 0.9125 | 1.521 |
| Treating bed to Cracking bed ratio | ☐ | 1.000 | 0.7500 | 1.250 |
| **950+ HDN Activity** |  |  |  |  |
| Treating bed | ☐ | 1.665 | 1.249 | 2.082 |
| Treating bed to Cracking bed ratio | ☐ | 1.000 | 0.7500 | 1.250 |
| **Overall SAT Activity** |  |  |  |  |
| Treating bed | ☐ | 7.000e-002 | 5.250e-002 | 8.750e-002 |
| Treating bed to Cracking bed ratio | ☐ | 1.035 | 0.7760 | 1.293 |
| **430- SAT Activity** |  |  |  |  |
| Treating bed | ☐ | 1.000 | 0.7500 | 1.250 |
| Treating bed to Cracking bed ratio | ☐ | 1.000 | 0.7500 | 1.250 |
| **430- 950 SAT Activity** |  |  |  |  |
| Treating bed | ☐ | 0.9032 | 0.6774 | 1.129 |
| Treating bed to Cracking bed ratio | ☐ | 1.000 | 0.7500 | 1.250 |
| **950+ SAT Activity** |  |  |  |  |
| Treating bed | ☐ | 0.9182 | 0.6887 | 1.148 |
| Treating bed to Cracking bed ratio | ☐ | 1.000 | 0.7500 | 1.250 |
| **Overall Cracking Activity** |  |  |  |  |
| Treating bed | ☐ | 8.560e-002 | 8.560e-002 | 0.1426 |
| Treating bed to Cracking bed ratio | ☐ | 1.000e-002 | 7.500e-003 | 1.250e-002 |
| **430- Cracking Activity** |  |  |  |  |
| Treating bed | ☐ | 1.254 | 1.254 | 2.089 |

☑ Update Initial Value

Data Set: Set-1

Not Solved

Figure 2.114 Manual calibration

Step 22: By observing the results, the temperature of R1B3 is closer to plant measurement. To obtain better result, repeat step 21 until the temperature profile is within the tolerance. Meanwhile, watch out for all of the other objective process variables – other reaction bed temperatures and product yields. Repeat steps 16 to 21 if the model's predictions fails in other objective process variables during manual calibration.

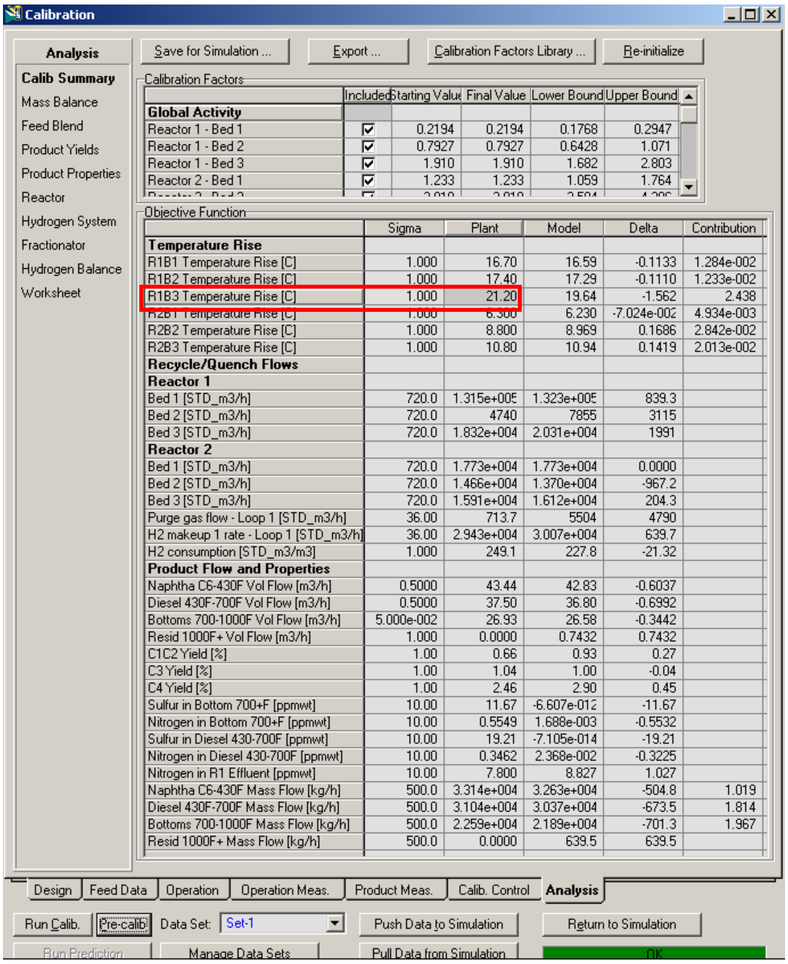

Data Set: Set-1

Calibration Factors

| | Included | Starting Value | Final Value | Lower Bound | Upper Bound |
|---|---|---|---|---|---|
| **Global Activity** | | | | | |
| Reactor 1 - Bed 1 | ☑ | 0.2194 | 0.2194 | 0.1768 | 0.2947 |
| Reactor 1 - Bed 2 | ☑ | 0.7927 | 0.7927 | 0.6428 | 1.071 |
| Reactor 1 - Bed 3 | ☑ | 1.910 | 1.910 | 1.682 | 2.803 |
| Reactor 2 - Bed 1 | ☑ | 1.233 | 1.233 | 1.059 | 1.764 |

Objective Function

| | Sigma | Plant | Model | Delta | Contribution |
|---|---|---|---|---|---|
| **Temperature Rise** | | | | | |
| R1B1 Temperature Rise [C] | 1.000 | 16.70 | 16.59 | -0.1133 | 1.284e-002 |
| R1B2 Temperature Rise [C] | 1.000 | 17.40 | 17.29 | -0.1110 | 1.233e-002 |
| R1B3 Temperature Rise [C] | 1.000 | 21.20 | 19.64 | -1.562 | 2.438 |
| R2B1 Temperature Rise [C] | 1.000 | 6.300 | 6.230 | -7.024e-002 | 4.934e-003 |
| R2B2 Temperature Rise [C] | 1.000 | 8.800 | 8.969 | 0.1686 | 2.842e-002 |
| R2B3 Temperature Rise [C] | 1.000 | 10.80 | 10.94 | 0.1419 | 2.013e-002 |
| **Recycle/Quench Flows** | | | | | |
| **Reactor 1** | | | | | |
| Bed 1 [STD_m3/h] | 720.0 | 1.315e+005 | 1.323e+005 | 839.3 | |
| Bed 2 [STD_m3/h] | 720.0 | 4740 | 7855 | 3115 | |
| Bed 3 [STD_m3/h] | 720.0 | 1.832e+004 | 2.031e+004 | 1991 | |
| **Reactor 2** | | | | | |
| Bed 1 [STD_m3/h] | 720.0 | 1.773e+004 | 1.773e+004 | 0.0000 | |
| Bed 2 [STD_m3/h] | 720.0 | 1.466e+004 | 1.370e+004 | -967.2 | |
| Bed 3 [STD_m3/h] | 720.0 | 1.591e+004 | 1.612e+004 | 204.3 | |
| Purge gas flow - Loop 1 [STD_m3/h] | 36.00 | 713.7 | 5504 | 4790 | |
| H2 makeup 1 rate - Loop 1 [STD_m3/h] | 36.00 | 2.943e+004 | 3.007e+004 | 639.7 | |
| H2 consumption [STD_m3/m3] | 1.000 | 249.1 | 227.8 | -21.32 | |
| **Product Flow and Properties** | | | | | |
| Naphtha C6-430F Vol Flow [m3/h] | 0.5000 | 43.44 | 42.83 | -0.6037 | |
| Diesel 430F-700F Vol Flow [m3/h] | 0.5000 | 37.50 | 36.80 | -0.6992 | |
| Bottoms 700-1000F Vol Flow [m3/h] | 5.000e-002 | 26.93 | 26.58 | -0.3442 | |
| Resid 1000F+ Vol Flow [m3/h] | 1.000 | 0.0000 | 0.7432 | 0.7432 | |
| C1C2 Yield [%] | 1.00 | 0.66 | 0.93 | 0.27 | |
| C3 Yield [%] | 1.00 | 1.04 | 1.00 | -0.04 | |
| C4 Yield [%] | 1.00 | 2.46 | 2.90 | 0.45 | |
| Sulfur in Bottom 700+F [ppmwt] | 10.00 | 11.67 | -6.607e-012 | -11.67 | |
| Nitrogen in Bottom 700+F [ppmwt] | 10.00 | 0.5549 | 1.688e-003 | -0.5532 | |
| Sulfur in Diesel 430-700F [ppmwt] | 10.00 | 19.21 | -7.105e-014 | -19.21 | |
| Nitrogen in Diesel 430-700F [ppmwt] | 10.00 | 0.3462 | 2.368e-002 | -0.3225 | |
| Nitrogen in R1 Effluent [ppmwt] | 10.00 | 7.800 | 8.827 | 1.027 | |
| Naphtha C6-430F Mass Flow [kg/h] | 500.0 | 3.314e+004 | 3.263e+004 | -504.8 | 1.019 |
| Diesel 430F-700F Mass Flow [kg/h] | 500.0 | 3.104e+004 | 3.037e+004 | -673.5 | 1.814 |
| Bottoms 700-1000F Mass Flow [kg/h] | 500.0 | 2.259e+004 | 2.189e+004 | -701.3 | 1.967 |
| Resid 1000F+ Mass Flow [kg/h] | 500.0 | 0.0000 | 639.5 | 639.5 | |

Figure 2.115 Calibration results after manual calibration

Step 23: The following shows the calibration results in this workshop.

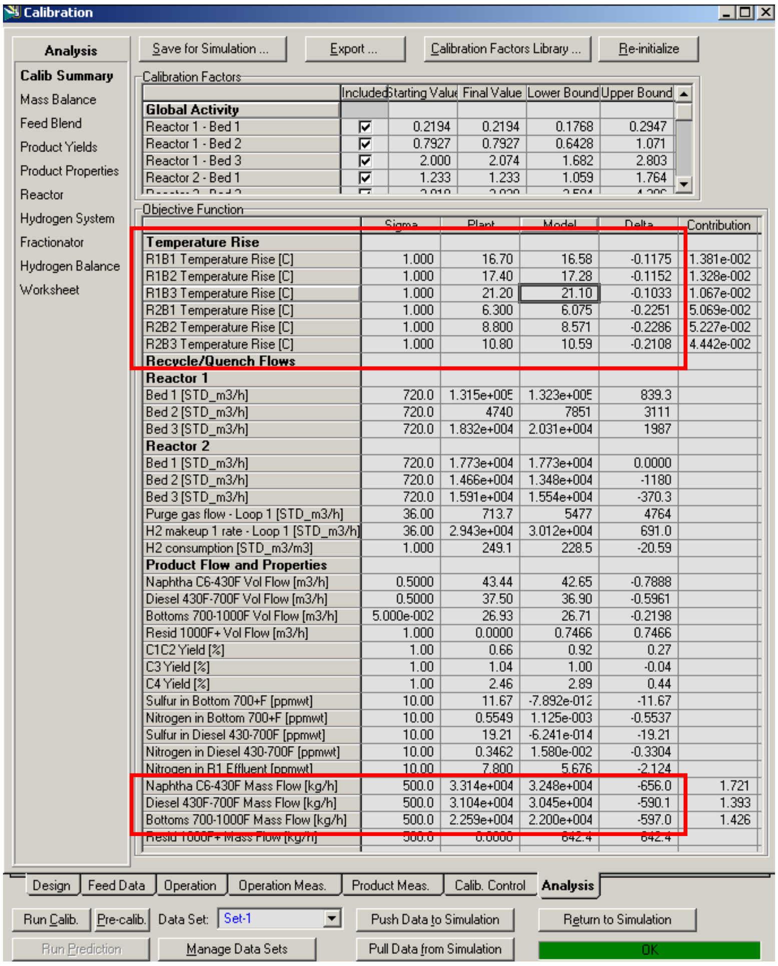

Calibration Factors

| | Included | Starting Value | Final Value | Lower Bound | Upper Bound |
|---|---|---|---|---|---|
| **Global Activity** | | | | | |
| Reactor 1 - Bed 1 | ☑ | 0.2194 | 0.2194 | 0.1768 | 0.2947 |
| Reactor 1 - Bed 2 | ☑ | 0.7927 | 0.7927 | 0.6428 | 1.071 |
| Reactor 1 - Bed 3 | ☑ | 2.000 | 2.074 | 1.682 | 2.803 |
| Reactor 2 - Bed 1 | ☑ | 1.233 | 1.233 | 1.059 | 1.764 |

Objective Function

| | Sigma | Plant | Model | Delta | Contribution |
|---|---|---|---|---|---|
| **Temperature Rise** | | | | | |
| R1B1 Temperature Rise [C] | 1.000 | 16.70 | 16.58 | -0.1175 | 1.381e-002 |
| R1B2 Temperature Rise [C] | 1.000 | 17.40 | 17.28 | -0.1152 | 1.328e-002 |
| R1B3 Temperature Rise [C] | 1.000 | 21.20 | 21.10 | -0.1033 | 1.067e-002 |
| R2B1 Temperature Rise [C] | 1.000 | 6.300 | 6.075 | -0.2251 | 5.069e-002 |
| R2B2 Temperature Rise [C] | 1.000 | 8.800 | 8.571 | -0.2286 | 5.227e-002 |
| R2B3 Temperature Rise [C] | 1.000 | 10.80 | 10.59 | -0.2108 | 4.442e-002 |
| **Recycle/Quench Flows** | | | | | |
| **Reactor 1** | | | | | |
| Bed 1 [STD_m3/h] | 720.0 | 1.315e+005 | 1.323e+005 | 839.3 | |
| Bed 2 [STD_m3/h] | 720.0 | 4740 | 7851 | 3111 | |
| Bed 3 [STD_m3/h] | 720.0 | 1.832e+004 | 2.031e+004 | 1987 | |
| **Reactor 2** | | | | | |
| Bed 1 [STD_m3/h] | 720.0 | 1.773e+004 | 1.773e+004 | 0.0000 | |
| Bed 2 [STD_m3/h] | 720.0 | 1.466e+004 | 1.348e+004 | -1180 | |
| Bed 3 [STD_m3/h] | 720.0 | 1.591e+004 | 1.554e+004 | -370.3 | |
| Purge gas flow - Loop 1 [STD_m3/h] | 36.00 | 713.7 | 5477 | 4764 | |
| H2 makeup 1 rate - Loop 1 [STD_m3/h] | 36.00 | 2.943e+004 | 3.012e+004 | 691.0 | |
| H2 consumption [STD_m3/m3] | 1.000 | 249.1 | 228.5 | -20.59 | |
| **Product Flow and Properties** | | | | | |
| Naphtha C6-430F Vol Flow [m3/h] | 0.5000 | 43.44 | 42.65 | -0.7888 | |
| Diesel 430F-700F Vol Flow [m3/h] | 0.5000 | 37.50 | 36.90 | -0.5961 | |
| Bottoms 700-1000F Vol Flow [m3/h] | 5.000e-002 | 26.93 | 26.71 | -0.2198 | |
| Resid 1000F+ Vol Flow [m3/h] | 1.000 | 0.0000 | 0.7466 | 0.7466 | |
| C1C2 Yield [%] | 1.00 | 0.66 | 0.92 | 0.27 | |
| C3 Yield [%] | 1.00 | 1.04 | 1.00 | -0.04 | |
| C4 Yield [%] | 1.00 | 2.46 | 2.89 | 0.44 | |
| Sulfur in Bottom 700+F [ppmwt] | 10.00 | 11.67 | -7.892e-012 | -11.67 | |
| Nitrogen in Bottom 700+F [ppmwt] | 10.00 | 0.5549 | 1.125e-003 | -0.5537 | |
| Sulfur in Diesel 430-700F [ppmwt] | 10.00 | 19.21 | -6.241e-014 | -19.21 | |
| Nitrogen in Diesel 430-700F [ppmwt] | 10.00 | 0.3462 | 1.580e-002 | -0.3304 | |
| Nitrogen in R1 Effluent [ppmwt] | 10.00 | 7.800 | 5.676 | -2.124 | |
| Naphtha C6-430F Mass Flow [kg/h] | 500.0 | 3.314e+004 | 3.248e+004 | -656.0 | 1.721 |
| Diesel 430F-700F Mass Flow [kg/h] | 500.0 | 3.104e+004 | 3.045e+004 | -590.1 | 1.393 |
| Bottoms 700-1000F Mass Flow [kg/h] | 500.0 | 2.259e+004 | 2.200e+004 | -597.0 | 1.426 |
| Resid 1000F+ Mass Flow [kg/h] | 500.0 | 0.0000 | 642.4 | 642.4 | |

Data Set: Set-1

Figure 2.116 Calibration results of this workshop

Step 24: After completing model calibration, click the button of "push data to simulation" to export the updated reaction activities into the HCR simulation environment.

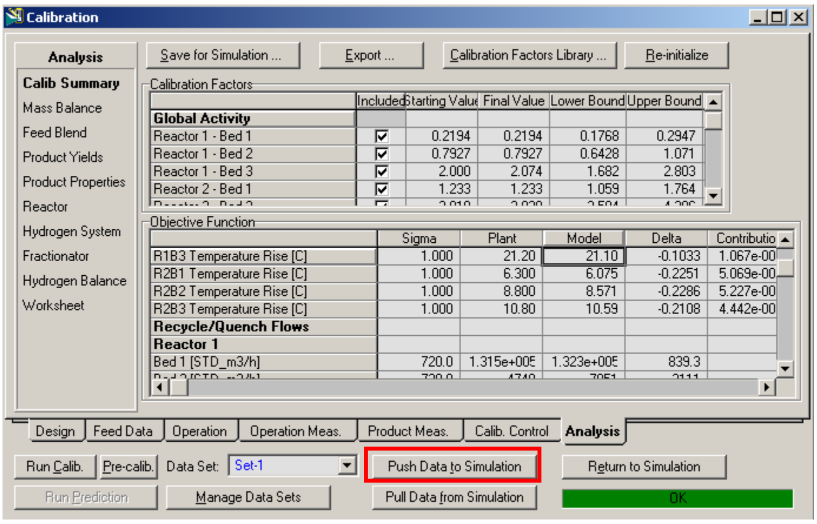

Data Set: Set-1

Calibration Factors

| | Included | Starting Value | Final Value | Lower Bound | Upper Bound |
|---|---|---|---|---|---|
| **Global Activity** | | | | | |
| Reactor 1 - Bed 1 | ☑ | 0.2194 | 0.2194 | 0.1768 | 0.2947 |
| Reactor 1 - Bed 2 | ☑ | 0.7927 | 0.7927 | 0.6428 | 1.071 |
| Reactor 1 - Bed 3 | ☑ | 2.000 | 2.074 | 1.682 | 2.803 |
| Reactor 2 - Bed 1 | ☑ | 1.233 | 1.233 | 1.059 | 1.764 |

Objective Function

| | Sigma | Plant | Model | Delta | Contributio |
|---|---|---|---|---|---|
| R1B3 Temperature Rise [C] | 1.000 | 21.20 | 21.10 | -0.1033 | 1.067e-00 |
| R2B1 Temperature Rise [C] | 1.000 | 6.300 | 6.075 | -0.2251 | 5.069e-00 |
| R2B2 Temperature Rise [C] | 1.000 | 8.800 | 8.571 | -0.2286 | 5.227e-00 |
| R2B3 Temperature Rise [C] | 1.000 | 10.80 | 10.59 | -0.2108 | 4.442e-00 |
| **Recycle/Quench Flows** | | | | | |
| **Reactor 1** | | | | | |
| Bed 1 [STD_m3/h] | 720.0 | 1.315e+005 | 1.323e+005 | 839.3 | |

Figure 2.117 Export calibrated activity factors and results into simulation

## 2.12 Workshop 3 – Simulation Experiment.

One of HCR model's applications is used to investigate different operating scenarios and help answering what-if question by running simulation experiments. This workshop demonstrates how to use the developed Aspen RefSYS HCR model to investigate the effect of WART of HCR reactor and feed flow rate on product distribution. In real operation, the only way to tune WART is to change inlet temperature of reaction bed. In this workshop, we will change inlet temperatures of the three HCR beds at the same time to perform case study.

Step 1: Hold the model to avoid automatic calculation while defining variables for simulation experiment.

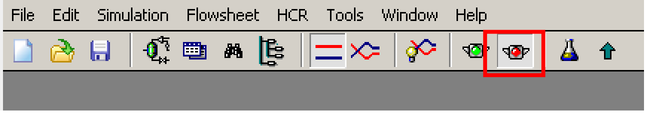

Figure 2.118 Deactivation button

Step 2: We need to add a "spreadsheet" in Aspen HYSYS to make tuning three inlet temperatures possible. Click "flowsheet" → "add operation" or click "F12". And then, choose spreadsheet to add.

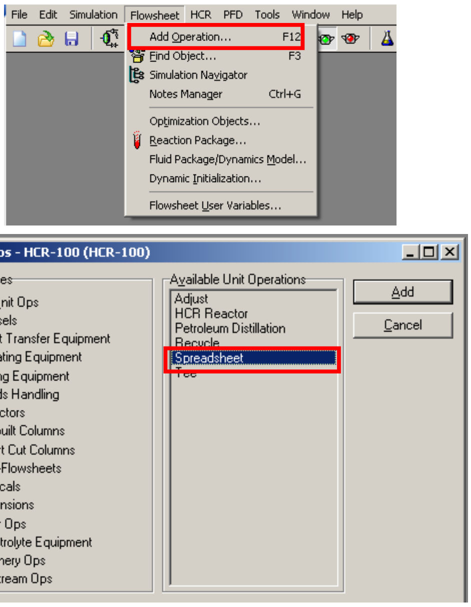

Figure 2.119 Add spreadsheet in Aspen HYSYS

Step 3: Open the spreadsheet tab and input current values of the three HCR beds' inlet temperatures.

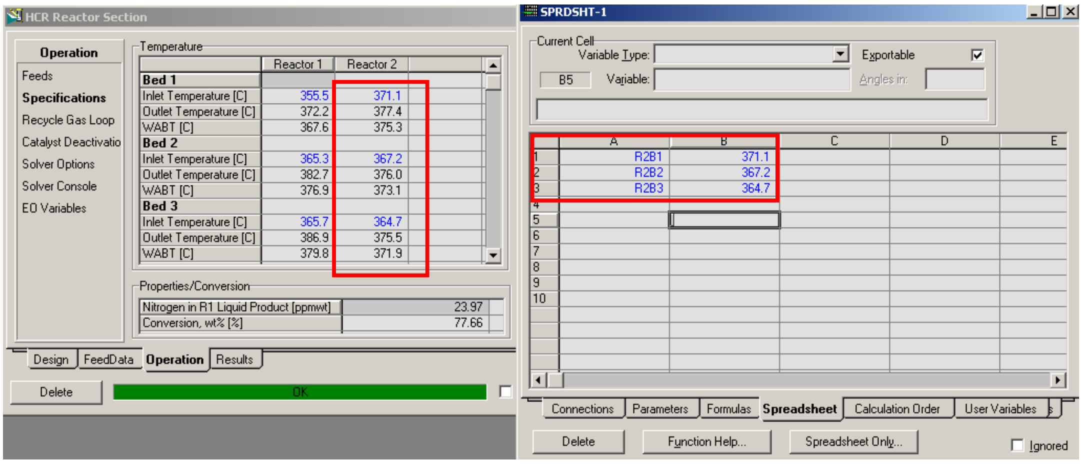

Temperature

| | Reactor 1 | Reactor 2 |
|---|---|---|
| **Bed 1** | | |
| Inlet Temperature [C] | 355.5 | 371.1 |
| Outlet Temperature [C] | 372.2 | 377.4 |
| WABT [C] | 367.6 | 375.3 |
| **Bed 2** | | |
| Inlet Temperature [C] | 365.3 | 367.2 |
| Outlet Temperature [C] | 382.7 | 376.0 |
| WABT [C] | 376.9 | 373.1 |
| **Bed 3** | | |
| Inlet Temperature [C] | 365.7 | 364.7 |
| Outlet Temperature [C] | 386.9 | 375.5 |
| WABT [C] | 379.8 | 371.9 |

Properties/Conversion

| | |
|---|---|
| Nitrogen in R1 Liquid Product [ppmwt] | 23.97 |
| Conversion, wt% [%] | 77.66 |

| | A | B | C | D | E |
|---|---|---|---|---|---|
| 1 | R2B1 | 371.1 | | | |
| 2 | R2B2 | 367.2 | | | |
| 3 | R2B3 | 364.7 | | | |
| 4 | | | | | |
| 5 | | | | | |
| 6 | | | | | |
| 7 | | | | | |
| 8 | | | | | |
| 9 | | | | | |
| 10 | | | | | |

Figure 2.120 Export reactor temperature into spreadsheet

Step 4: Add a cell called "temp increment" which will be used as an operator to allow for a step change of inlet temperature during the simulation experiment.

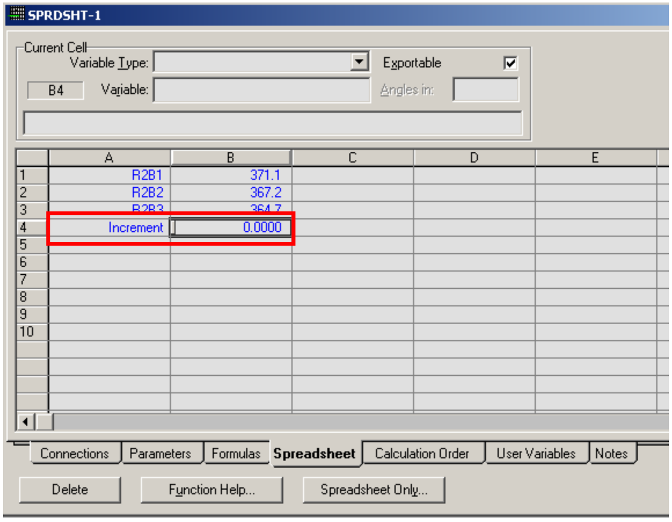

B4

|  | A | B | C | D | E |
|---|---|---|---|---|---|
| 1 | R2B1 | 371.1 |  |  |  |
| 2 | R2B2 | 367.2 |  |  |  |
| 3 | R2B3 | 364.7 |  |  |  |
| 4 | Increment | 0.0000 |  |  |  |
| 5 |  |  |  |  |  |
| 6 |  |  |  |  |  |
| 7 |  |  |  |  |  |
| 8 |  |  |  |  |  |
| 9 |  |  |  |  |  |
| 10 |  |  |  |  |  |

Figure 2.121 Add an increment factor to enable step change

Step 5: Input current value of feed mass flow rate and add a cell called “feed increment” which will be used as an operator to allow step change of feed flow rate during simulation experiment.

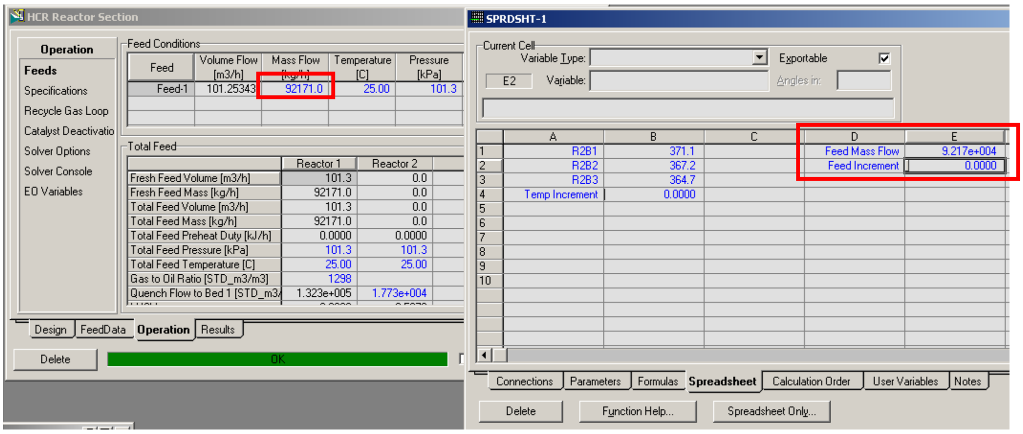

Feed Conditions

| Feed | Volume Flow [m3/h] | Mass Flow [kg/h] | Temperature [C] | Pressure [kPa] |
|---|---|---|---|---|
| Feed-1 | 101.25343 | 92171.0 | 25.00 | 101.3 |

Total Feed

|  | Reactor 1 | Reactor 2 |
|---|---|---|
| Fresh Feed Volume [m3/h] | 101.3 | 0.0 |
| Fresh Feed Mass [kg/h] | 92171.0 | 0.0 |
| Total Feed Volume [m3/h] | 101.3 | 0.0 |
| Total Feed Mass [kg/h] | 92171.0 | 0.0 |
| Total Feed Preheat Duty [kJ/h] | 0.0000 | 0.0000 |
| Total Feed Pressure [kPa] | 101.3 | 101.3 |
| Total Feed Temperature [C] | 25.00 | 25.00 |
| Gas to Oil Ratio [STD_m3/m3] | 1298 |  |
| Quench Flow to Bed 1 [STD_m3/ | 1.323e+005 | 1.773e+004 |

E2

|  | A | B | C | D | E |
|---|---|---|---|---|---|
| 1 | R2B1 | 371.1 |  | Feed Mass Flow | 9.217e+004 |
| 2 | R2B2 | 367.2 |  | Feed Increment | 0.0000 |
| 3 | R2B3 | 364.7 |  |  |  |
| 4 | Temp Increment | 0.0000 |  |  |  |
| 5 |  |  |  |  |  |
| 6 |  |  |  |  |  |
| 7 |  |  |  |  |  |
| 8 |  |  |  |  |  |
| 9 |  |  |  |  |  |
| 10 |  |  |  |  |  |

Figure 2.122 Export feed flow into spreadsheet

Step 6: Add equations to cell C1, C2, C3, and F1 to calculate the new process variables (inlet temperature of HCR bed and feed mass flow rate) while running the case study. C1: B1+B4, C2: B2+B4, C3: B3+B4, F1: E1+E2.

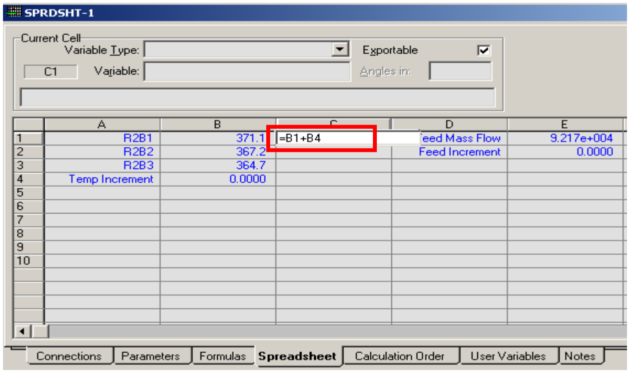

Variable Type:

C1 Variable:

Exportable ☑

Angles in:

|  | A | B | C | D | E |
|---|---|---|---|---|---|
| 1 | R2B1 | 371.1 | =B1+B4 | eed Mass Flow | 9.217e+004 |
| 2 | R2B2 | 367.2 |  | Feed Increment | 0.0000 |
| 3 | R2B3 | 364.7 |  |  |  |
| 4 | Temp Increment | 0.0000 |  |  |  |

Figure 2.123 Add equations to allow the three reactor temperatures to be tuned at once

Step 7: After inputting the equations, the cells show “empty” because values of the cells are not exported yet.

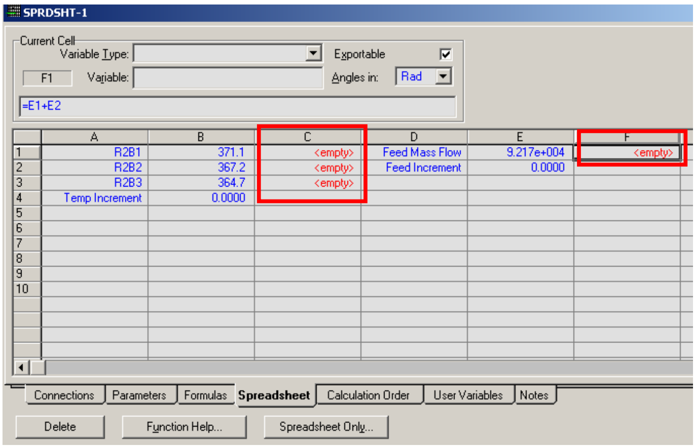

Variable Type:

F1 Variable:

Exportable ☑

Angles in: Rad

=E1+E2

|  | A | B | C | D | E | F |
|---|---|---|---|---|---|---|
| 1 | R2B1 | 371.1 | <empty> | Feed Mass Flow | 9.217e+004 | <empty> |
| 2 | R2B2 | 367.2 | <empty> | Feed Increment | 0.0000 |  |
| 3 | R2B3 | 364.7 | <empty> |  |  |  |
| 4 | Temp Increment | 0.0000 |  |  |  |  |

Figure 2.124 Cells are empty until exporting the results

Step 8: Right-click on cell C1 and click “export formula result”.

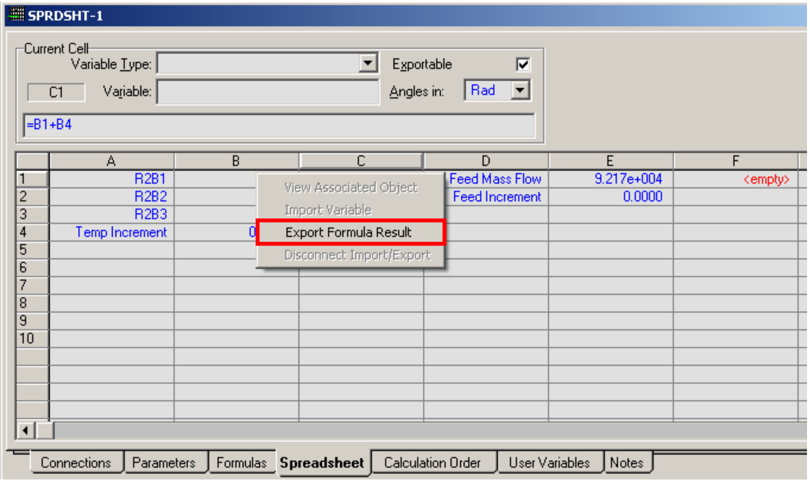

SPRDSHT-1

Current Cell

C1

Variable Type:

Variable:

Exportable ☑

Angles in: Rad

=B1+B4

|  | A | B | C | D | E | F |
|---|---|---|---|---|---|---|
| 1 | R2B1 |  |  | Feed Mass Flow | 9.217e+004 | <empty> |
| 2 | R2B2 |  |  | Feed Increment | 0.0000 |  |
| 3 | R2B3 |  |  |  |  |  |
| 4 | Temp Increment | 0 |  |  |  |  |
| 5 |  |  |  |  |  |  |
| 6 |  |  |  |  |  |  |
| 7 |  |  |  |  |  |  |
| 8 |  |  |  |  |  |  |
| 9 |  |  |  |  |  |  |
| 10 |  |  |  |  |  |  |

Figure 2.125 Export formula results

Step 9: Select the inlet temperature of R2B1 to export the calculated temperature.

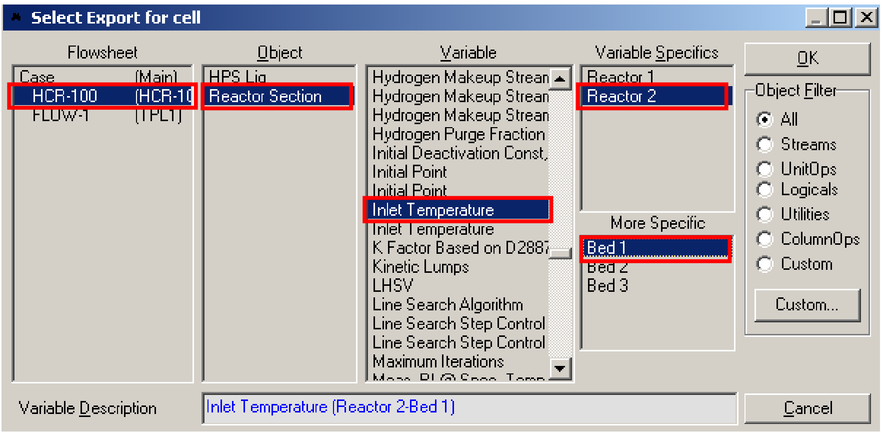

Select Export for cell

Flowsheet: HCR-100 (HCR-10

Object: Reactor Section

Variable: Inlet Temperature

Variable Specifics: Reactor 2

More Specific: Bed 1

Object Filter: ● All

Variable Description: Inlet Temperature (Reactor 2-Bed 1)

Figure 2.126 Select the variables to export formula results

Step 10: Repeat steps 8 and 9 to export calculated temperatures and feed mass flow rate to R1B2, R2B3 and feed mass flow.

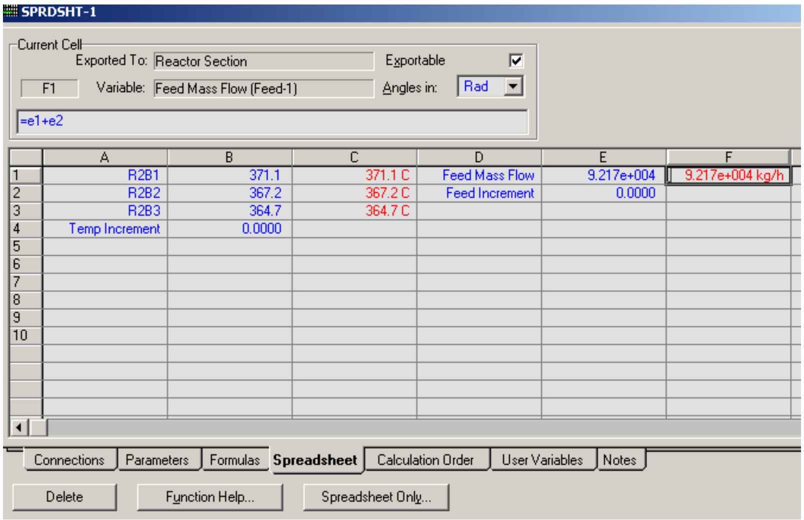
SPRDSHT-1

Current Cell

Exported To: Reactor Section

Exportable ☑

F1

Variable: Feed Mass Flow (Feed-1)

Angles in: Rad

=e1+e2

| | A | B | C | D | E | F |
|---|---|---|---|---|---|---|
| 1 | R2B1 | 371.1 | 371.1 C | Feed Mass Flow | 9.217e+004 | 9.217e+004 kg/h |
| 2 | R2B2 | 367.2 | 367.2 C | Feed Increment | 0.0000 | |
| 3 | R2B3 | 364.7 | 364.7 C | | | |
| 4 | Temp Increment | 0.0000 | | | | |
| 5 | | | | | | |
| 6 | | | | | | |
| 7 | | | | | | |
| 8 | | | | | | |
| 9 | | | | | | |
| 10 | | | | | | |

Figure 2.127 Exported formula results in spreadsheet

Step 11: Add a new “databook”

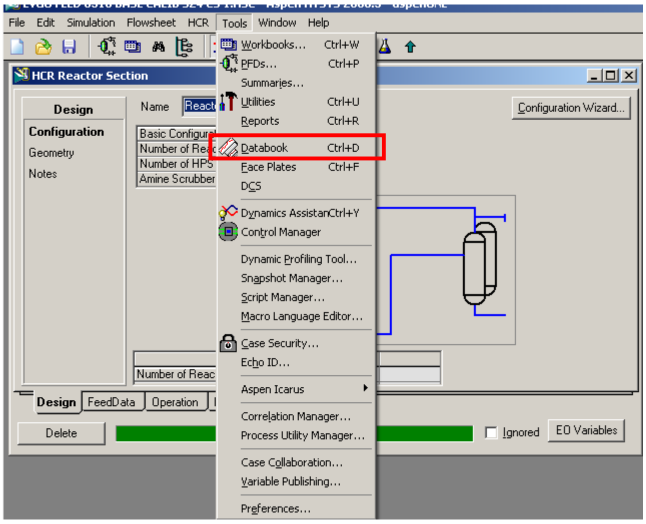

Figure 2.128 New databook

Step 12: Insert B4 and E2 into the databook from the spreadsheet.

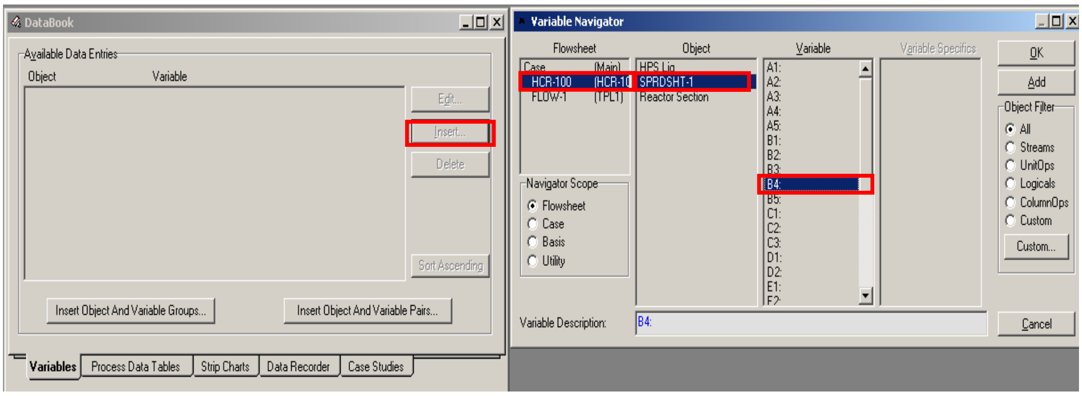

| Flowsheet | |
|---|---|
| Case | (Main) |
| HCR-100 | (HCR-10 |
| FLOW-1 | (TPL1) |

Object: HPS Liq, SPRDSHT-1, Reactor Section

Variable: A1:, A2:, A3:, A4:, A5:, B1:, B2:, B3:, B4:, B5:, C1:, C2:, C3:, D1:, D2:, E1:, F2:

Variable Description: B4:

Figure 2.129 Insert the cells of spreadsheet into databook

Step 13: Insert WART of reactor 2 (HCR reactor) and feed mass flow.

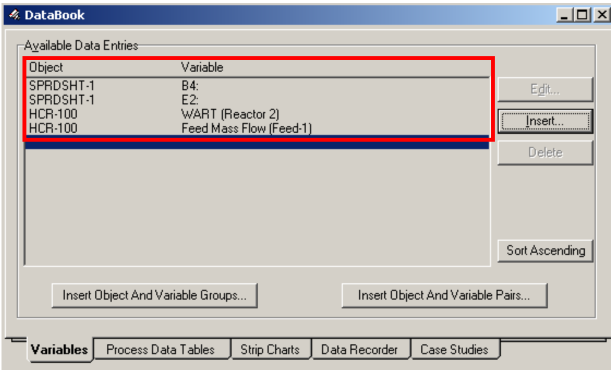

| Object | Variable |
|---|---|
| SPRDSHT-1 | B4: |
| SPRDSHT-1 | E2: |
| HCR-100 | WART (Reactor 2) |
| HCR-100 | Feed Mass Flow (Feed-1) |

Figure 2.130 Insert process variables into databook

Step 14: Insert mass yields of naphtha, diesel and bottom.

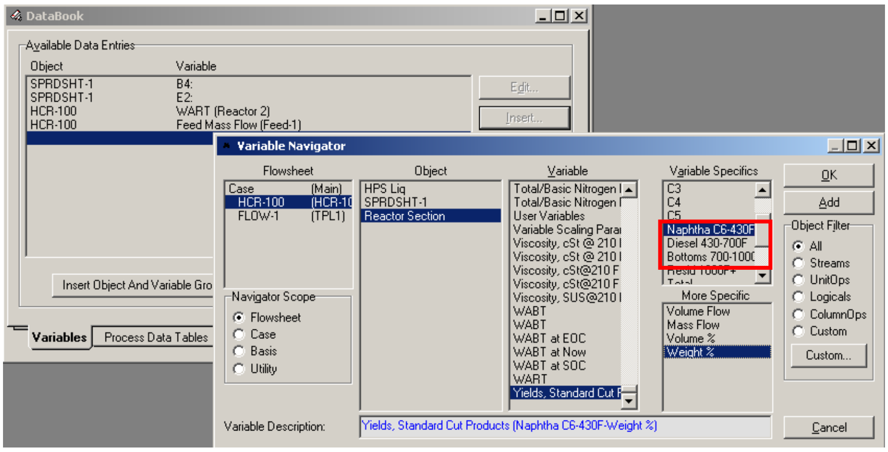

| Object | Variable |
|---|---|
| SPRDSHT-1 | B4: |
| SPRDSHT-1 | E2: |
| HCR-100 | WART (Reactor 2) |
| HCR-100 | Feed Mass Flow (Feed-1) |

| Flowsheet | |
|---|---|
| Case | (Main) |
| HCR-100 | (HCR-10 |
| FLOW-1 | (TPL1) |

Object: HPS Liq, SPRDSHT-1, Reactor Section

Variable: Total/Basic Nitrogen I, Total/Basic Nitrogen I, User Variables, Variable Scaling Parai, Viscosity, cSt @ 210 I, Viscosity, cSt @ 210 I, Viscosity, cSt@210 F, Viscosity, cSt@210 F, Viscosity, SUS@210 I, WABT, WABT, WABT at EOC, WABT at Now, WABT at SOC, WART, Yields, Standard Cut F

Variable Specifics: C3, C4, C5, Naphtha C6-430F, Diesel 430-700F, Bottoms 700-1000, Resid 1000F+, Total

More Specific: Volume Flow, Mass Flow, Volume %, Weight %

Variable Description: Yields, Standard Cut Products (Naphtha C6-430F-Weight %)

Figure 2.131 Insert product yields into databook

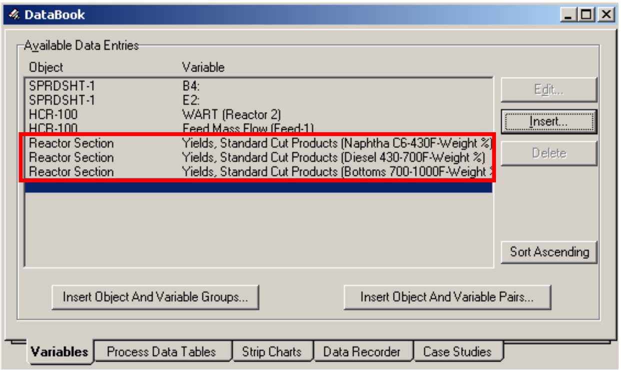

| Object | Variable |
|---|---|
| SPRDSHT-1 | B4: |
| SPRDSHT-1 | E2: |
| HCR-100 | WART (Reactor 2) |
| HCR-100 | Feed Mass Flow (Feed-1) |
| Reactor Section | Yields, Standard Cut Products (Naphtha C6-430F-Weight %) |
| Reactor Section | Yields, Standard Cut Products (Diesel 430-700F-Weight %) |
| Reactor Section | Yields, Standard Cut Products (Bottoms 700-1000F-Weight |

Figure 2.132 Variables in databook

Step 15: Go to “case studies” tab and add a new case study.

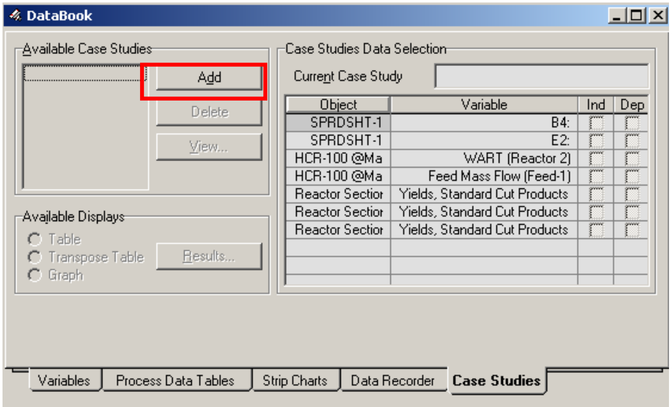

| Object | Variable | Ind | Dep |
|---|---|---|---|
| SPRDSHT-1 | B4: | ☐ | ☐ |
| SPRDSHT-1 | E2: | ☐ | ☐ |
| HCR-100 @Ma | WART (Reactor 2) | ☐ | ☐ |
| HCR-100 @Ma | Feed Mass Flow (Feed-1) | ☐ | ☐ |
| Reactor Sectior | Yields, Standard Cut Products | ☐ | ☐ |
| Reactor Sectior | Yields, Standard Cut Products | ☐ | ☐ |
| Reactor Sectior | Yields, Standard Cut Products | ☐ | ☐ |

Figure 2.133 Add a case study

Step 16: Define B4 and E2 as independent variables because they are operators to change WART and feed mass flow while running case study. On the other hand, define all of the other variables as dependent variables.

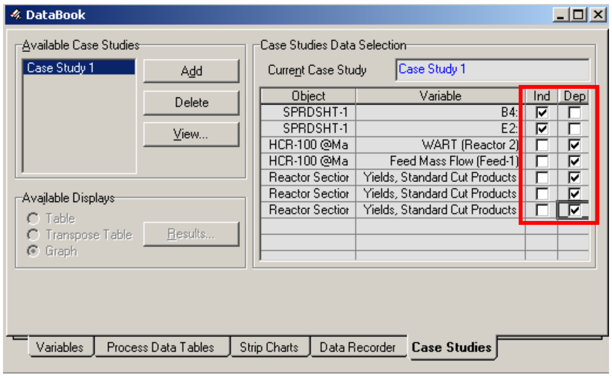

Current Case Study: Case Study 1

| Object | Variable | Ind | Dep |
|---|---|---|---|
| SPRDSHT-1 | B4: | ☑ | ☐ |
| SPRDSHT-1 | E2: | ☑ | ☐ |
| HCR-100 @Ma | WART (Reactor 2) | ☐ | ☑ |
| HCR-100 @Ma | Feed Mass Flow (Feed-1) | ☐ | ☑ |
| Reactor Sectior | Yields, Standard Cut Products | ☐ | ☑ |
| Reactor Sectior | Yields, Standard Cut Products | ☐ | ☑ |
| Reactor Sectior | Yields, Standard Cut Products | ☐ | ☑ |

Figure 2.134 Define independent and dependent variables in case study

Step 17: Click “view” to open a new window to assign lower and upper bounds that allows WART and feed mass flow to change during running the simulation experiment. Next, click “start” to run the case study.

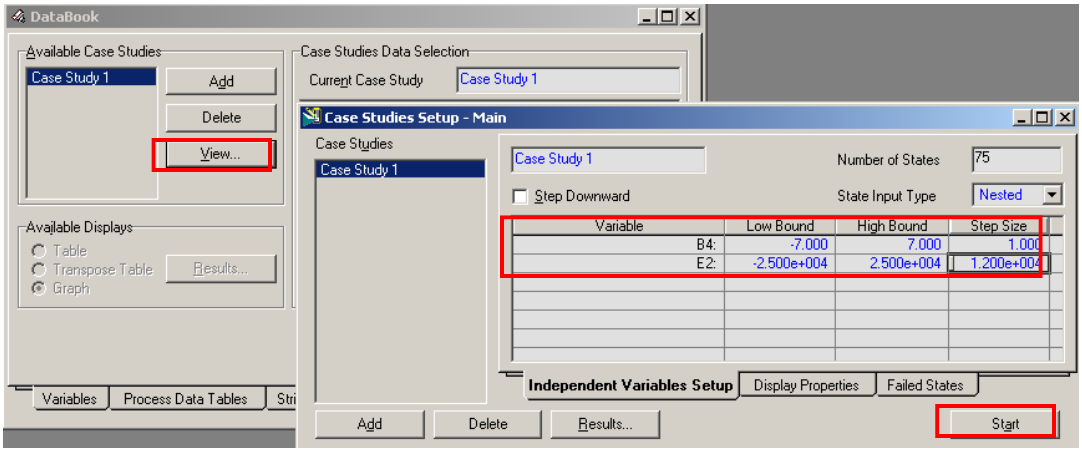

Current Case Study: Case Study 1

Case Study 1

Number of States: 75

☐ Step Downward

State Input Type: Nested

| Variable | Low Bound | High Bound | Step Size |
|---|---|---|---|
| B4: | -7.000 | 7.000 | 1.000 |
| E2: | -2.500e+004 | 2.500e+004 | 1.200e+004 |

Figure 2.135 Define lower and upper bounds of independent variables

Step 18: Click “results” to check the results of case studies.

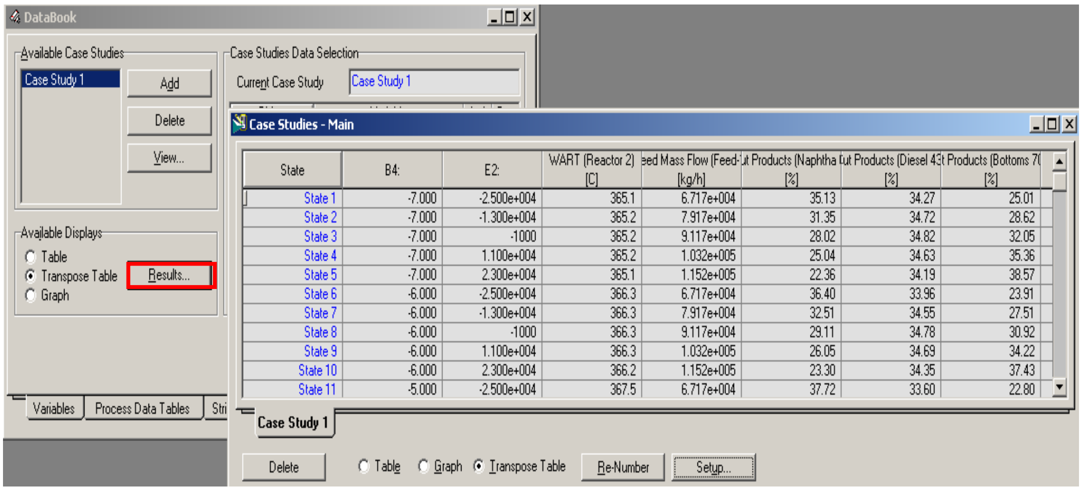

Current Case Study: Case Study 1

○ Table ○ Graph ● Transpose Table

| State | B4: | E2: | WART (Reactor 2) [C] | ed Mass Flow (Feed- [kg/h] | ut Products (Naphtha [%] | ut Products (Diesel 4 [%] | Products (Bottoms 7 [%] |
|---|---|---|---|---|---|---|---|
| State 1 | -7.000 | -2.500e+004 | 365.1 | 6.717e+004 | 35.13 | 34.27 | 25.01 |
| State 2 | -7.000 | -1.300e+004 | 365.2 | 7.917e+004 | 31.35 | 34.72 | 28.62 |
| State 3 | -7.000 | -1000 | 365.2 | 9.117e+004 | 28.02 | 34.82 | 32.05 |
| State 4 | -7.000 | 1.100e+004 | 365.2 | 1.032e+005 | 25.04 | 34.63 | 35.36 |
| State 5 | -7.000 | 2.300e+004 | 365.1 | 1.152e+005 | 22.36 | 34.19 | 38.57 |
| State 6 | -6.000 | -2.500e+004 | 366.3 | 6.717e+004 | 36.40 | 33.96 | 23.91 |
| State 7 | -6.000 | -1.300e+004 | 366.3 | 7.917e+004 | 32.51 | 34.55 | 27.51 |
| State 8 | -6.000 | -1000 | 366.3 | 9.117e+004 | 29.11 | 34.78 | 30.92 |
| State 9 | -6.000 | 1.100e+004 | 366.3 | 1.032e+005 | 26.05 | 34.69 | 34.22 |
| State 10 | -6.000 | 2.300e+004 | 366.2 | 1.152e+005 | 23.30 | 34.35 | 37.43 |
| State 11 | -5.000 | -2.500e+004 | 367.5 | 6.717e+004 | 37.72 | 33.60 | 22.80 |

Figure 2.136 The results of case study

## 2.13 Workshop 4 – Connect Reactor Model to Fractionator Simulation.

This workshop demonstrates how to delump the effluent of HCR reactor model and build fractionator simulation.

Step 1: Open the developed HCR reactor model in Aspen HYSYS

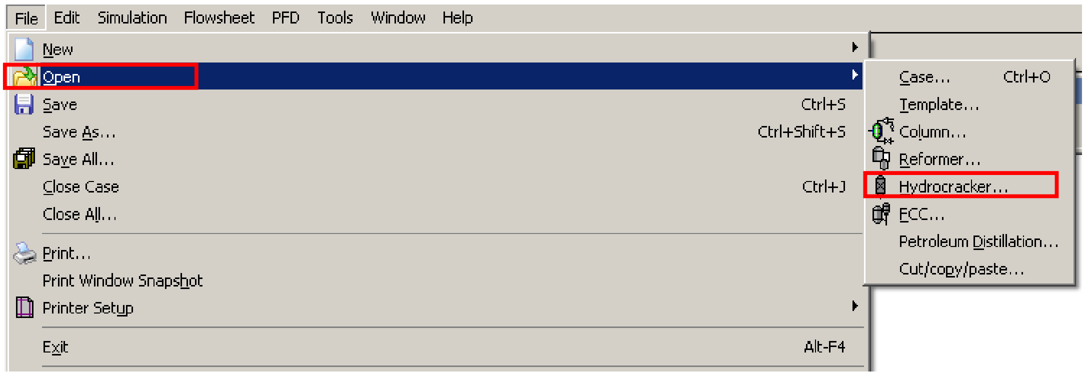

Figure 2.137 Open HCR model in Aspen HYSYS environment

Step 2: Type "HPS Liq HCR" to export stream results of HCR reactor model to HYSYS environment.

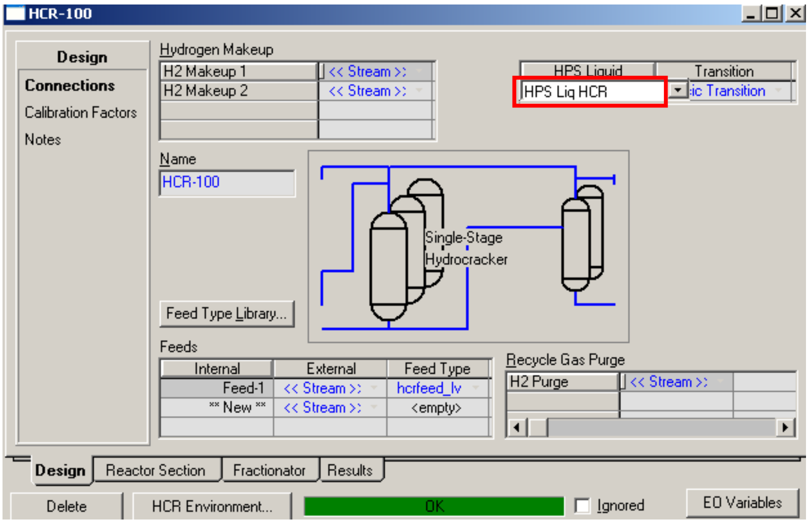

Figure 2.138 Export HCR model result into Aspen HYSYS environment

Step 3: Right-click to open the tool bar to import "trans.hfl" that is included in the CD-ROM.

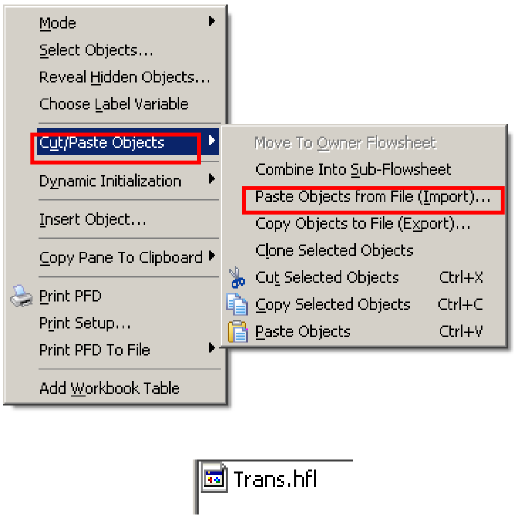

Figure 2.139 Insert the template to read stream results

Step 4: Double-click the icon of “trans” and select “HPS Liq HCR” in external stream cell. Next, click the button of “sub-flowsheet environment” to enter the sub-flowsheet.

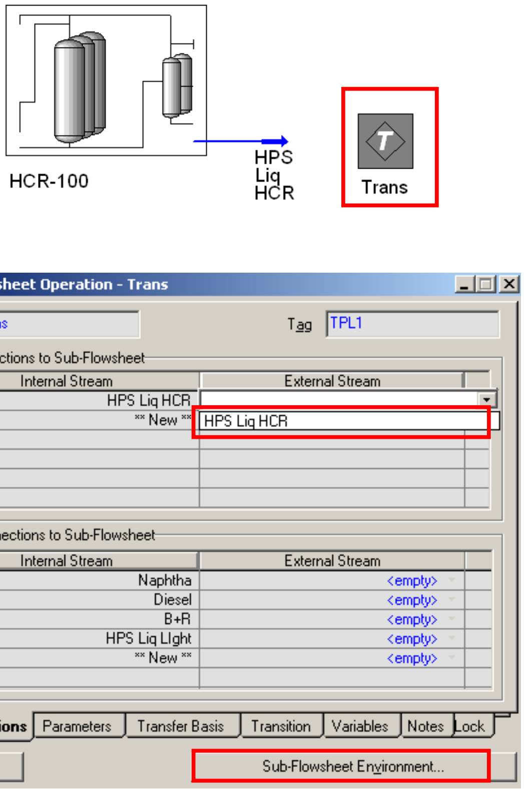

Name Trans
Tag TPL1

Inlet Connections to Sub-Flowsheet

| Internal Stream | External Stream |
|---|---|
| HPS Liq HCR | HPS Liq HCR |
| ** New ** | |

Outlet Connections to Sub-Flowsheet

| Internal Stream | External Stream |
|---|---|
| Naphtha | <empty> |
| Diesel | <empty> |
| B+R | <empty> |
| HPS Liq Light | <empty> |
| ** New ** | <empty> |

Figure 2.140 Flowsheet after inserting the template mentioned above

Step 5: Open delump.xls in the CD-ROM

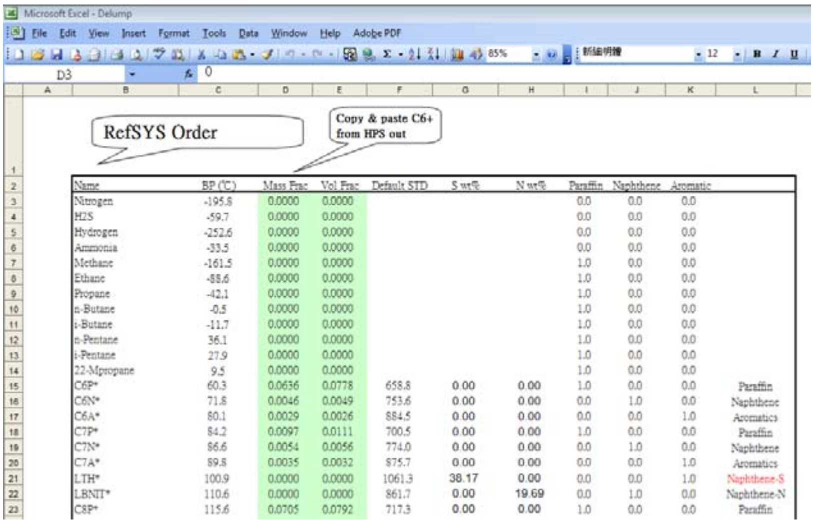

| Name | BP (℃) | Mass Frac | Vol Frac | Default STD | S wt% | N wt% | Paraffin | Naphthene | Aromatic | |
|---|---|---|---|---|---|---|---|---|---|---|
| Nitrogen | -195.8 | 0.0000 | 0.0000 | | | | 0.0 | 0.0 | 0.0 | |
| H2S | -59.7 | 0.0000 | 0.0000 | | | | 0.0 | 0.0 | 0.0 | |
| Hydrogen | -252.6 | 0.0000 | 0.0000 | | | | 0.0 | 0.0 | 0.0 | |
| Ammonia | -33.5 | 0.0000 | 0.0000 | | | | 0.0 | 0.0 | 0.0 | |
| Methane | -161.5 | 0.0000 | 0.0000 | | | | 1.0 | 0.0 | 0.0 | |
| Ethane | -88.6 | 0.0000 | 0.0000 | | | | 1.0 | 0.0 | 0.0 | |
| Propane | -42.1 | 0.0000 | 0.0000 | | | | 1.0 | 0.0 | 0.0 | |
| n-Butane | -0.5 | 0.0000 | 0.0000 | | | | 1.0 | 0.0 | 0.0 | |
| i-Butane | -11.7 | 0.0000 | 0.0000 | | | | 1.0 | 0.0 | 0.0 | |
| n-Pentane | 36.1 | 0.0000 | 0.0000 | | | | 1.0 | 0.0 | 0.0 | |
| i-Pentane | 27.9 | 0.0000 | 0.0000 | | | | 1.0 | 0.0 | 0.0 | |
| 22-Mpropane | 9.5 | 0.0000 | 0.0000 | | | | 1.0 | 0.0 | 0.0 | |
| C6P* | 60.3 | 0.0636 | 0.0778 | 658.8 | 0.00 | 0.00 | 1.0 | 0.0 | 0.0 | Paraffin |
| C6N* | 71.8 | 0.0046 | 0.0049 | 753.6 | 0.00 | 0.00 | 0.0 | 1.0 | 0.0 | Naphthene |
| C6A* | 80.1 | 0.0029 | 0.0026 | 884.5 | 0.00 | 0.00 | 0.0 | 0.0 | 1.0 | Aromatics |
| C7P* | 84.2 | 0.0097 | 0.0111 | 700.5 | 0.00 | 0.00 | 1.0 | 0.0 | 0.0 | Paraffin |
| C7N* | 86.6 | 0.0054 | 0.0056 | 774.0 | 0.00 | 0.00 | 0.0 | 1.0 | 0.0 | Naphthene |
| C7A* | 89.8 | 0.0035 | 0.0032 | 875.7 | 0.00 | 0.00 | 0.0 | 0.0 | 1.0 | Aromatics |
| LTH* | 100.9 | 0.0000 | 0.0000 | 1061.3 | 38.17 | 0.00 | 0.0 | 0.0 | 1.0 | Naphthene-S |
| LBNIT* | 110.6 | 0.0000 | 0.0000 | 861.7 | 0.00 | 19.69 | 0.0 | 1.0 | 0.0 | Naphthene-N |
| C8P* | 115.6 | 0.0705 | 0.0792 | 717.3 | 0.00 | 0.00 | 1.0 | 0.0 | 0.0 | Paraffin |

Figure 2.141 Delumping spreadsheet

Step 6: Double-click “HPS Liq Heavy” stream to open stream compositions.

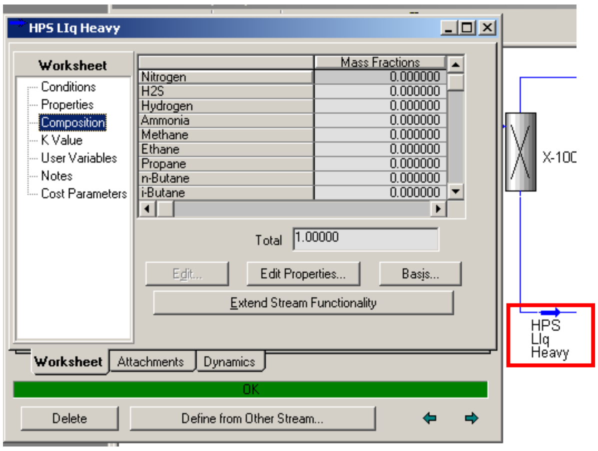

| | Mass Fractions |
|---|---|
| Nitrogen | 0.000000 |
| H2S | 0.000000 |
| Hydrogen | 0.000000 |
| Ammonia | 0.000000 |
| Methane | 0.000000 |
| Ethane | 0.000000 |
| Propane | 0.000000 |
| n-Butane | 0.000000 |
| i-Butane | 0.000000 |

Total 1.00000

Figure 2.142 Stream property of C6+ of HCR reactor effluent

Step 7: Copy stream composition (mass fraction and liquid volume fraction) into delump.xls as follows:

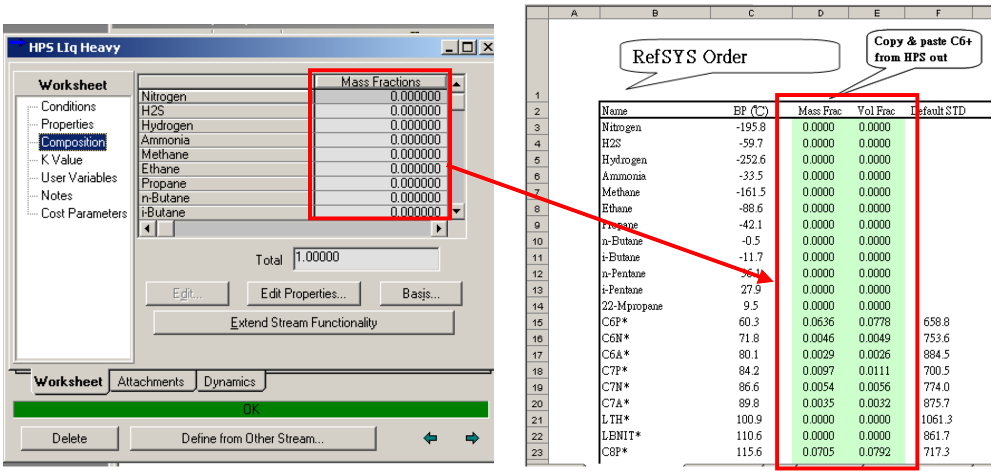

|  | Mass Fractions |
|---|---|
| Nitrogen | 0.000000 |
| H2S | 0.000000 |
| Hydrogen | 0.000000 |
| Ammonia | 0.000000 |
| Methane | 0.000000 |
| Ethane | 0.000000 |
| Propane | 0.000000 |
| n-Butane | 0.000000 |
| i-Butane | 0.000000 |

Total 1.00000

RefSYS Order

Copy & paste C6+ from HPS out

| Name | BP (C) | Mass Frac | Vol Frac | Default STD |
|---|---|---|---|---|
| Nitrogen | -195.8 | 0.0000 | 0.0000 |  |
| H2S | -59.7 | 0.0000 | 0.0000 |  |
| Hydrogen | -252.6 | 0.0000 | 0.0000 |  |
| Ammonia | -33.5 | 0.0000 | 0.0000 |  |
| Methane | -161.5 | 0.0000 | 0.0000 |  |
| Ethane | -88.6 | 0.0000 | 0.0000 |  |
| Propane | -42.1 | 0.0000 | 0.0000 |  |
| n-Butane | -0.5 | 0.0000 | 0.0000 |  |
| i-Butane | -11.7 | 0.0000 | 0.0000 |  |
| n-Pentane | 36.1 | 0.0000 | 0.0000 |  |
| i-Pentane | 27.9 | 0.0000 | 0.0000 |  |
| 22-Mpropane | 9.5 | 0.0000 | 0.0000 |  |
| C6P* | 60.3 | 0.0636 | 0.0778 | 658.8 |
| C6N* | 71.8 | 0.0046 | 0.0049 | 753.6 |
| C6A* | 80.1 | 0.0029 | 0.0026 | 884.5 |
| C7P* | 84.2 | 0.0097 | 0.0111 | 700.5 |
| C7N* | 86.6 | 0.0054 | 0.0056 | 774.0 |
| C7A* | 89.8 | 0.0035 | 0.0032 | 875.7 |
| LTH* | 100.9 | 0.0000 | 0.0000 | 1061.3 |
| LBNIT* | 110.6 | 0.0000 | 0.0000 | 861.7 |
| C8P* | 115.6 | 0.0705 | 0.0792 | 717.3 |

Figure 2.143 Copy stream properties into delumping spreadsheet

Step 8: Click “properties” to open the spreadsheet which includes the required properties extracted from HCR reactor model for delumping.

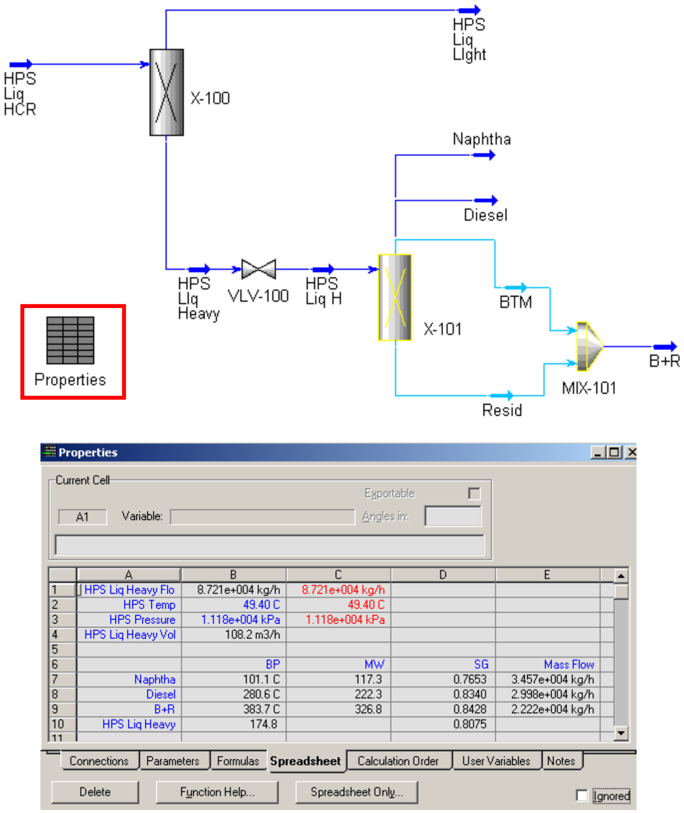

|  | A | B | C | D | E |
|---|---|---|---|---|---|
| 1 | HPS Liq Heavy Flo | 8.721e+004 kg/h | 8.721e+004 kg/h |  |  |
| 2 | HPS Temp | 49.40 C | 49.40 C |  |  |
| 3 | HPS Pressure | 1.118e+004 kPa | 1.118e+004 kPa |  |  |
| 4 | HPS Liq Heavy Vol | 108.2 m3/h |  |  |  |
| 5 |  |  |  |  |  |
| 6 |  | BP | MW | SG | Mass Flow |
| 7 | Naphtha | 101.1 C | 117.3 | 0.7653 | 3.457e+004 kg/h |
| 8 | Diesel | 280.6 C | 222.3 | 0.8340 | 2.998e+004 kg/h |
| 9 | B+R | 383.7 C | 326.8 | 0.8428 | 2.222e+004 kg/h |
| 10 | HPS Liq Heavy | 174.8 |  | 0.8075 |  |
| 11 |  |  |  |  |  |

Figure 2.144 Property template includes stream results from reactor model

Step 9: Copy required properties and conditions (BP, MW, SG and Mass flow) from “properties” to “delump.xls” as following:

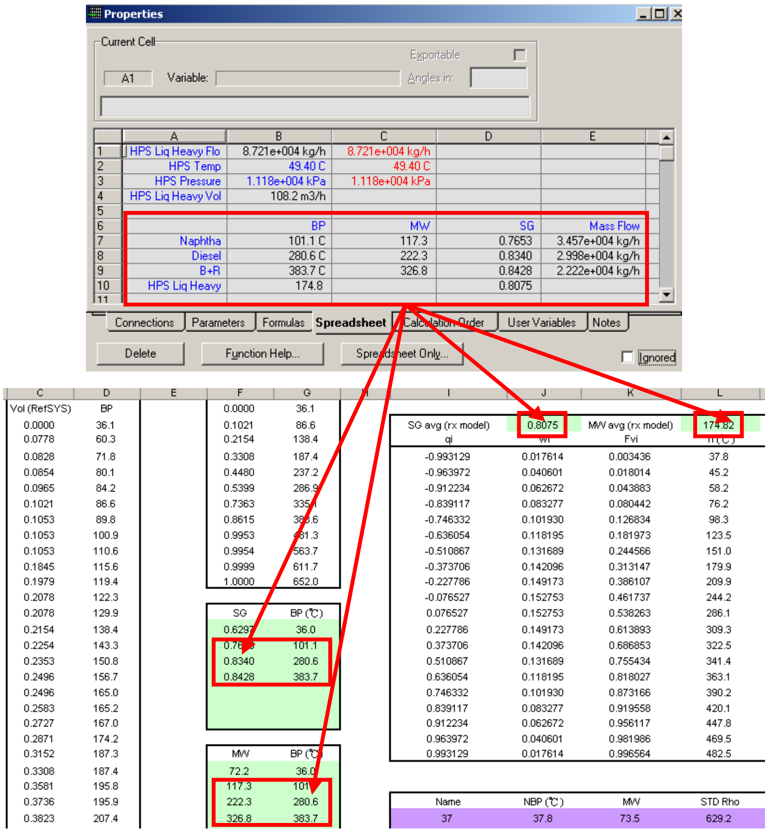

A1 Variable:

|  | A | B | C | D | E |
|---|---|---|---|---|---|
| 1 | HPS Liq Heavy Flo | 8.721e+004 kg/h | 8.721e+004 kg/h |  |  |
| 2 | HPS Temp | 49.40 C | 49.40 C |  |  |
| 3 | HPS Pressure | 1.118e+004 kPa | 1.118e+004 kPa |  |  |
| 4 | HPS Liq Heavy Vol | 108.2 m3/h |  |  |  |
| 5 |  |  |  |  |  |
| 6 |  | BP | MW | SG | Mass Flow |
| 7 | Naphtha | 101.1 C | 117.3 | 0.7653 | 3.457e+004 kg/h |
| 8 | Diesel | 280.6 C | 222.3 | 0.8340 | 2.998e+004 kg/h |
| 9 | B+R | 383.7 C | 326.8 | 0.8428 | 2.222e+004 kg/h |
| 10 | HPS Liq Heavy | 174.8 |  | 0.8075 |  |
| 11 |  |  |  |  |  |

| Vol (RefSYS) | BP |
|---|---|
| 0.0000 | 36.1 |
| 0.0778 | 60.3 |
| 0.0828 | 71.8 |
| 0.0854 | 80.1 |
| 0.0965 | 84.2 |
| 0.1021 | 86.6 |
| 0.1053 | 89.8 |
| 0.1053 | 100.9 |
| 0.1053 | 110.6 |
| 0.1845 | 115.6 |
| 0.1979 | 119.4 |
| 0.2078 | 122.3 |
| 0.2078 | 129.9 |
| 0.2154 | 138.4 |
| 0.2254 | 143.3 |
| 0.2353 | 150.8 |
| 0.2496 | 156.7 |
| 0.2496 | 165.0 |
| 0.2583 | 165.2 |
| 0.2727 | 167.0 |
| 0.2871 | 174.2 |
| 0.3152 | 187.3 |
| 0.3308 | 187.4 |
| 0.3581 | 195.8 |
| 0.3736 | 195.9 |
| 0.3823 | 207.4 |

| F | G |
|---|---|
| 0.0000 | 36.1 |
| 0.1021 | 86.6 |
| 0.2154 | 138.4 |
| 0.3308 | 187.4 |
| 0.4480 | 237.2 |
| 0.5399 | 286.9 |
| 0.7363 | 335.1 |
| 0.8615 | [illegible] |
| 0.9953 | [illegible] |
| 0.9954 | 563.7 |
| 0.9999 | 611.7 |
| 1.0000 | 652.0 |

| SG | BP (℃) |
|---|---|
| 0.6297 | 36.0 |
| [illegible] | 101.1 |
| 0.8340 | 280.6 |
| 0.8428 | 383.7 |

| MW | BP (℃) |
|---|---|
| 72.2 | 36.0 |
| 117.3 | [illegible] |
| 222.3 | 280.6 |
| 326.8 | 383.7 |

| SG avg (rx model) | 0.8075 | MW avg (rx model) | 174.82 |
|---|---|---|---|
| qi | wi | Fvi | [illegible] |
| -0.993129 | 0.017614 | 0.003436 | 37.8 |
| -0.963972 | 0.040601 | 0.018014 | 45.2 |
| -0.912234 | 0.062672 | 0.043883 | 58.2 |
| -0.839117 | 0.083277 | 0.080442 | 76.2 |
| -0.746332 | 0.101930 | 0.126834 | 98.3 |
| -0.636054 | 0.118195 | 0.181973 | 123.5 |
| -0.510867 | 0.131689 | 0.244566 | 151.0 |
| -0.373706 | 0.142096 | 0.313147 | 179.9 |
| -0.227786 | 0.149173 | 0.386107 | 209.9 |
| -0.076527 | 0.152753 | 0.461737 | 244.2 |
| 0.076527 | 0.152753 | 0.538263 | 286.1 |
| 0.227786 | 0.149173 | 0.613893 | 309.3 |
| 0.373706 | 0.142096 | 0.686853 | 322.5 |
| 0.510867 | 0.131689 | 0.755434 | 341.4 |
| 0.636054 | 0.118195 | 0.818027 | 363.1 |
| 0.746332 | 0.101930 | 0.873166 | 390.2 |
| 0.839117 | 0.083277 | 0.919558 | 420.1 |
| 0.912234 | 0.062672 | 0.956117 | 447.8 |
| 0.963972 | 0.040601 | 0.981986 | 469.5 |
| 0.993129 | 0.017614 | 0.996564 | 482.5 |

| Name | NBP (℃) | MW | STD Rho |
|---|---|---|---|
| 37 | 37.8 | 73.5 | 629.2 |

Figure 2.145 Copy essential stream properties into delumping spreadsheet

Step 10: The cells with purple represent the calculated properties of pseudo-components and corresponding composition to represent HCR reactor effluent.

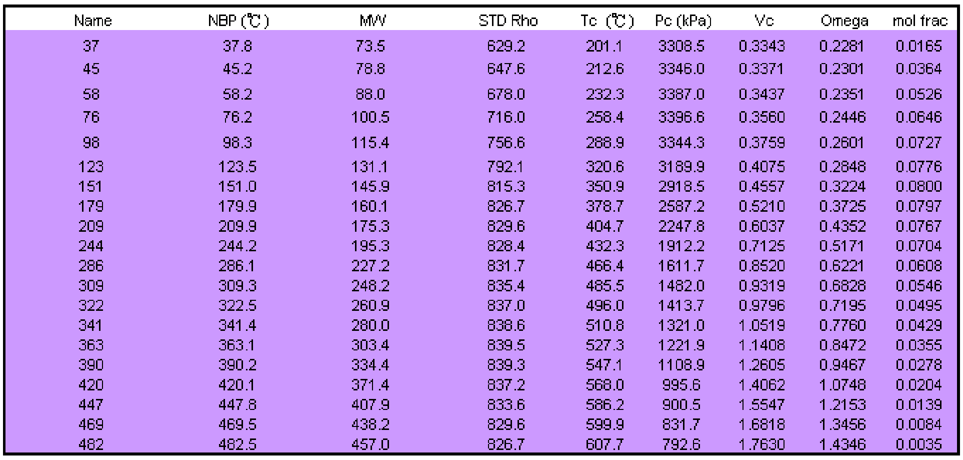

| Name | NBP (℃) | MW | STD Rho | Tc (℃) | Pc (kPa) | Vc | Omega | mol frac |
|---|---|---|---|---|---|---|---|---|
| 37 | 37.8 | 73.5 | 629.2 | 201.1 | 3308.5 | 0.3343 | 0.2281 | 0.0165 |
| 45 | 45.2 | 78.8 | 647.6 | 212.6 | 3346.0 | 0.3371 | 0.2301 | 0.0364 |
| 58 | 58.2 | 88.0 | 678.0 | 232.3 | 3387.0 | 0.3437 | 0.2351 | 0.0526 |
| 76 | 76.2 | 100.5 | 716.0 | 258.4 | 3396.6 | 0.3560 | 0.2446 | 0.0646 |
| 98 | 98.3 | 115.4 | 756.6 | 288.9 | 3344.3 | 0.3759 | 0.2601 | 0.0727 |
| 123 | 123.5 | 131.1 | 792.1 | 320.6 | 3189.9 | 0.4075 | 0.2848 | 0.0776 |
| 151 | 151.0 | 145.9 | 815.3 | 350.9 | 2918.5 | 0.4557 | 0.3224 | 0.0800 |
| 179 | 179.9 | 160.1 | 826.7 | 378.7 | 2587.2 | 0.5210 | 0.3725 | 0.0797 |
| 209 | 209.9 | 175.3 | 829.6 | 404.7 | 2247.8 | 0.6037 | 0.4352 | 0.0767 |
| 244 | 244.2 | 195.3 | 828.4 | 432.3 | 1912.2 | 0.7125 | 0.5171 | 0.0704 |
| 286 | 286.1 | 227.2 | 831.7 | 466.4 | 1611.7 | 0.8520 | 0.6221 | 0.0608 |
| 309 | 309.3 | 248.2 | 835.4 | 485.5 | 1482.0 | 0.9319 | 0.6828 | 0.0546 |
| 322 | 322.5 | 260.9 | 837.0 | 496.0 | 1413.7 | 0.9796 | 0.7195 | 0.0495 |
| 341 | 341.4 | 280.0 | 838.6 | 510.8 | 1321.0 | 1.0519 | 0.7760 | 0.0429 |
| 363 | 363.1 | 303.4 | 839.5 | 527.3 | 1221.9 | 1.1408 | 0.8472 | 0.0355 |
| 390 | 390.2 | 334.4 | 839.3 | 547.1 | 1108.9 | 1.2605 | 0.9467 | 0.0278 |
| 420 | 420.1 | 371.4 | 837.2 | 568.0 | 995.6 | 1.4062 | 1.0748 | 0.0204 |
| 447 | 447.8 | 407.9 | 833.6 | 586.2 | 900.5 | 1.5547 | 1.2153 | 0.0139 |
| 469 | 469.5 | 438.2 | 829.6 | 599.9 | 831.7 | 1.6818 | 1.3456 | 0.0084 |
| 482 | 482.5 | 457.0 | 826.7 | 607.7 | 792.6 | 1.7630 | 1.4346 | 0.0035 |

Figure 2.146 Properties of generated pseudo-components

Step 11: Go to "basis environment".

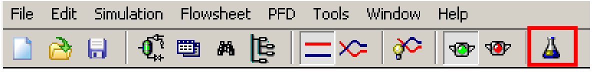

Figure 2.147 Enter basis environment

Step 12: Add a new component list called "GL20".

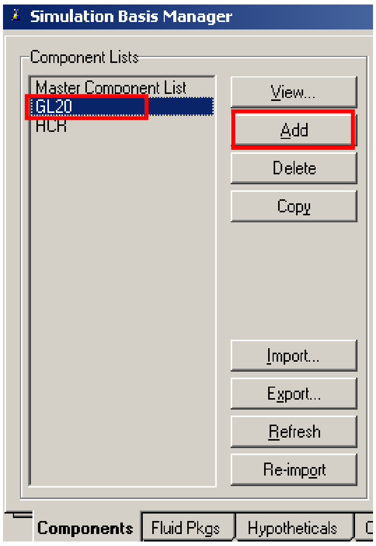

Master Component List
GL20
HCR

Figure 2.148 Add new component list

Step 13: Add the following components into "GL20" list.

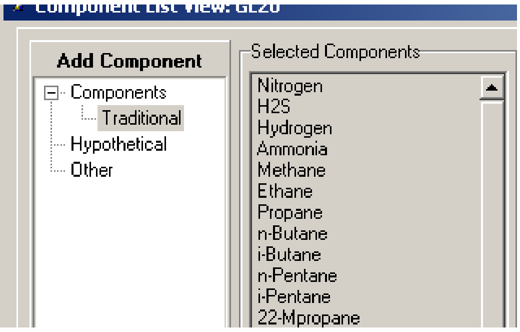

Nitrogen
H2S
Hydrogen
Ammonia
Methane
Ethane
Propane
n-Butane
i-Butane
n-Pentane
i-Pentane
22-Mpropane

Figure 2.149 Add light components

Step 14: Go to "Hypotheticals" tab and add a new hypo list called "GL20".

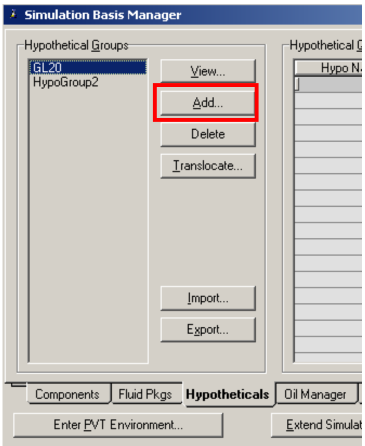

Figure 2.150 Create new hypo list for pseudo-components generated by delumping

Step 15: Click "view" to add pseudo-components. Obtain the required properties of pseudo-components from "delump.xls" (please refer to step 10).

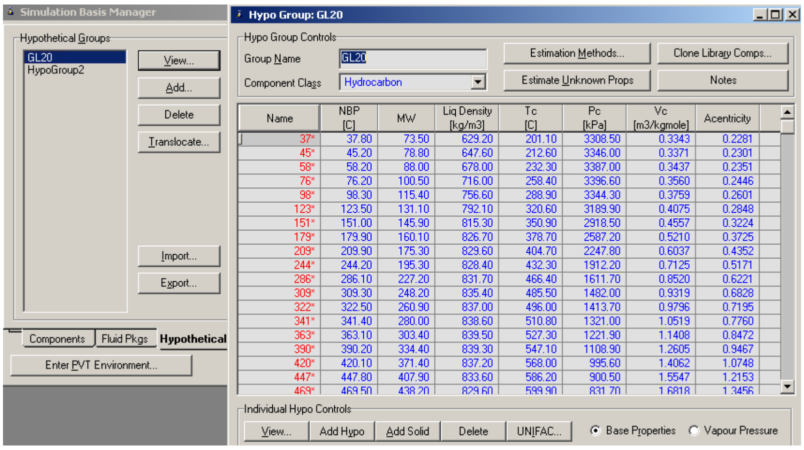

Group Name: GL20

Component Class: Hydrocarbon

| Name | NBP [C] | MW | Liq Density [kg/m3] | Tc [C] | Pc [kPa] | Vc [m3/kgmole] | Acentricity |
|---|---|---|---|---|---|---|---|
| 37* | 37.80 | 73.50 | 629.20 | 201.10 | 3308.50 | 0.3343 | 0.2281 |
| 45* | 45.20 | 78.80 | 647.60 | 212.60 | 3346.00 | 0.3371 | 0.2301 |
| 58* | 58.20 | 88.00 | 678.00 | 232.30 | 3387.00 | 0.3437 | 0.2351 |
| 76* | 76.20 | 100.50 | 716.00 | 258.40 | 3396.60 | 0.3560 | 0.2446 |
| 98* | 98.30 | 115.40 | 756.60 | 288.90 | 3344.30 | 0.3759 | 0.2601 |
| 123* | 123.50 | 131.10 | 792.10 | 320.60 | 3189.90 | 0.4075 | 0.2848 |
| 151* | 151.00 | 145.90 | 815.30 | 350.90 | 2918.50 | 0.4557 | 0.3224 |
| 179* | 179.90 | 160.10 | 826.70 | 378.70 | 2587.20 | 0.5210 | 0.3725 |
| 209* | 209.90 | 175.30 | 829.60 | 404.70 | 2247.80 | 0.6037 | 0.4352 |
| 244* | 244.20 | 195.30 | 828.40 | 432.30 | 1912.20 | 0.7125 | 0.5171 |
| 286* | 286.10 | 227.20 | 831.70 | 466.40 | 1611.70 | 0.8520 | 0.6221 |
| 309* | 309.30 | 248.20 | 835.40 | 485.50 | 1482.00 | 0.9319 | 0.6828 |
| 322* | 322.50 | 260.90 | 837.00 | 496.00 | 1413.70 | 0.9796 | 0.7195 |
| 341* | 341.40 | 280.00 | 838.60 | 510.80 | 1321.00 | 1.0519 | 0.7760 |
| 363* | 363.10 | 303.40 | 839.50 | 527.30 | 1221.90 | 1.1408 | 0.8472 |
| 390* | 390.20 | 334.40 | 839.30 | 547.10 | 1108.90 | 1.2605 | 0.9467 |
| 420* | 420.10 | 371.40 | 837.20 | 568.00 | 995.60 | 1.4062 | 1.0748 |
| 447* | 447.80 | 407.90 | 833.60 | 586.20 | 900.50 | 1.5547 | 1.2153 |
| 469* | 469.50 | 438.20 | 829.60 | 599.90 | 831.70 | 1.6818 | 1.3456 |

● Base Properties ○ Vapour Pressure

Figure 2.151 The pseudo-components and relevant properties

Step 16: Go back to the simulation environment.

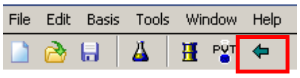

Figure 2.152 Enter simulation environment

Step 17: Create two streams called "HPS Liq C6-" and "HPS Liq C6+" to represent the light and heavy parts of liquid effluent of high-pressure separator.

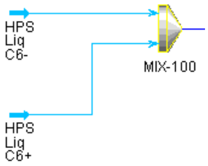

Figure 2.153 Flowsheet for mixing light and heavy parts of reactor effluent

Step 18: The flow rate and composition of “HPS Liq 6-“ can be obtained from reactor model (please refer to “HPS Liq Light” in step 8).

Step 19: The flow rate of “HPS Liq 6+“ can be obtained from reactor model (please refer to “HPS Liq Heavy” in step 8).

Step 20: The composition of “HPS Liq 6+“ can be obtained from “delump.xls” (please refer to step 10).

Step 21: Build the following flowsheet:

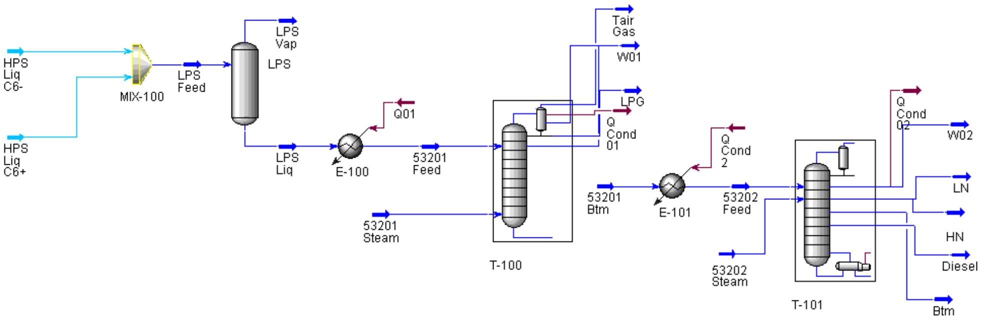

Figure 2.154 The resulting process flowsheet

Step 22: The specifications corresponding to the flowsheet above are listed below:

LPS: Temperature = 49.5℃, Pressure = 1451 kPa

E100: Outlet temperature = 221℃, Delta pressure: 0 kPa

E101: Outlet temperature = 340℃, Outlet pressure: 151.3 kPa

53201 Steam: Flow rate = 680 kg/hr, Temperature = 345℃, Pressure =1101 kPa

53202 Steam: Flow rate = 350 kg/hr, Temperature = 345℃, Pressure =1101 kPa

T-100:

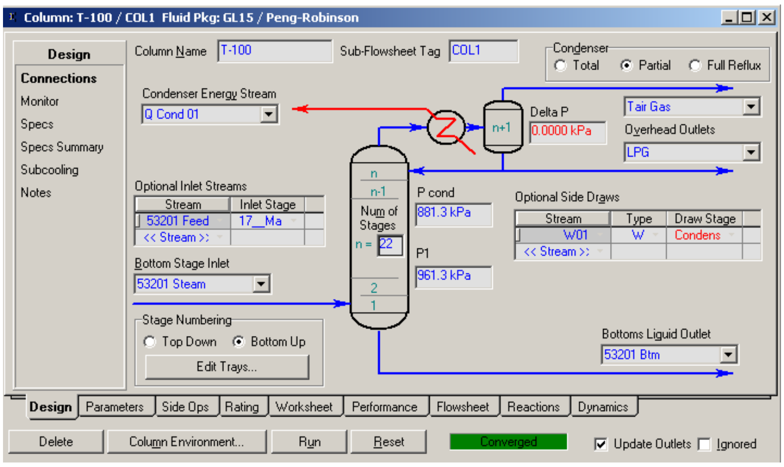

Column: T-100 / COL1 Fluid Pkg: GL15 / Peng-Robinson

Column Name: T-100

Sub-Flowsheet Tag: COL1

Condenser: ○ Total ● Partial ○ Full Reflux

Condenser Energy Stream: Q Cond 01

Delta P: 0.0000 kPa

Overhead Outlets: Tair Gas, LPG

Optional Inlet Streams

| Stream | Inlet Stage |
|---|---|
| 53201 Feed | 17__Ma |
| << Stream >> | |

Bottom Stage Inlet: 53201 Steam

Num of Stages: n = 22

P cond: 881.3 kPa

P1: 961.3 kPa

Optional Side Draws

| Stream | Type | Draw Stage |
|---|---|---|
| W01 | W | Condens |
| << Stream >> | | |

Bottoms Liquid Outlet: 53201 Btm

Stage Numbering: ○ Top Down ● Bottom Up

☑ Update Outlets ☐ Ignored

Figure 2.155 Definitions of T-100

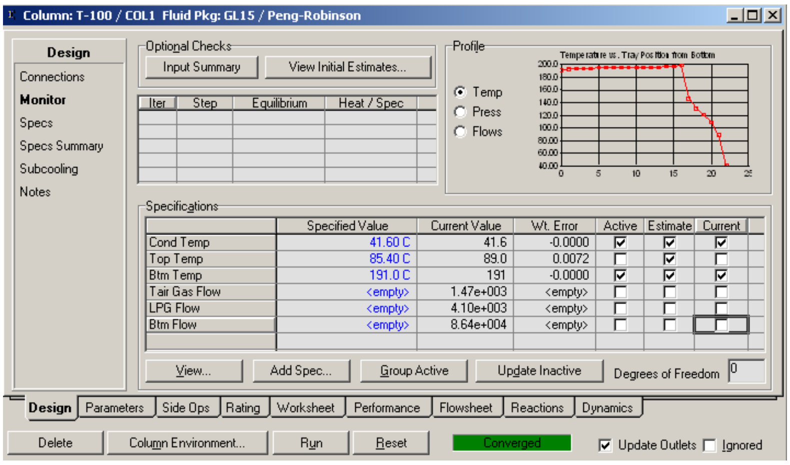

Column: T-100 / COL1 Fluid Pkg: GL15 / Peng-Robinson

Profile: ● Temp ○ Press ○ Flows

Specifications

| | Specified Value | Current Value | Wt. Error | Active | Estimate | Current |
|---|---|---|---|---|---|---|
| Cond Temp | 41.60 C | 41.6 | -0.0000 | ☑ | ☑ | ☑ |
| Top Temp | 85.40 C | 89.0 | 0.0072 | ☐ | ☑ | ☐ |
| Btm Temp | 191.0 C | 191 | -0.0000 | ☑ | ☑ | ☑ |
| Tair Gas Flow | <empty> | 1.47e+003 | <empty> | ☐ | ☐ | ☐ |
| LPG Flow | <empty> | 4.10e+003 | <empty> | ☐ | ☐ | ☐ |
| Btm Flow | <empty> | 8.64e+004 | <empty> | ☐ | ☐ | ☐ |

Degrees of Freedom: 0

☑ Update Outlets ☐ Ignored

Figure 2.156 Specifications of T-100

T-101:

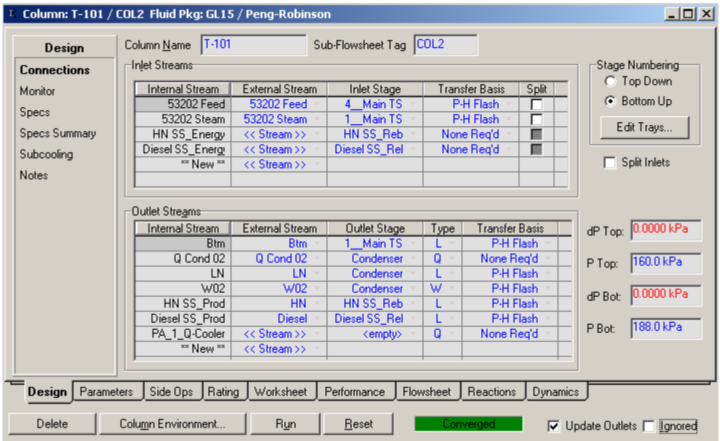

Column: T-101 / COL2 Fluid Pkg: GL15 / Peng-Robinson

Column Name: T-101

Sub-Flowsheet Tag: COL2

Inlet Streams

| Internal Stream | External Stream | Inlet Stage | Transfer Basis | Split |
|---|---|---|---|---|
| 53202 Feed | 53202 Feed | 4__Main TS | P-H Flash | ☐ |
| 53202 Steam | 53202 Steam | 1__Main TS | P-H Flash | ☐ |
| HN SS_Energy | << Stream >> | HN SS_Reb | None Req'd | ▨ |
| Diesel SS_Energ | << Stream >> | Diesel SS_Rel | None Req'd | ▨ |
| ** New ** | << Stream >> | | | |

Stage Numbering: ○ Top Down ● Bottom Up

☐ Split Inlets

Outlet Streams

| Internal Stream | External Stream | Outlet Stage | Type | Transfer Basis |
|---|---|---|---|---|
| Btm | Btm | 1__Main TS | L | P-H Flash |
| Q Cond 02 | Q Cond 02 | Condenser | Q | None Req'd |
| LN | LN | Condenser | L | P-H Flash |
| W02 | W02 | Condenser | W | P-H Flash |
| HN SS_Prod | HN | HN SS_Reb | L | P-H Flash |
| Diesel SS_Prod | Diesel | Diesel SS_Rel | L | P-H Flash |
| PA_1_Q-Cooler | << Stream >> | <empty> | Q | None Req'd |
| ** New ** | << Stream >> | | | |

dP Top: 0.0000 kPa

P Top: 160.0 kPa

dP Bot: 0.0000 kPa

P Bot: 188.0 kPa

☑ Update Outlets ☐ Ignored

Figure 2.157 Definitions of T-101

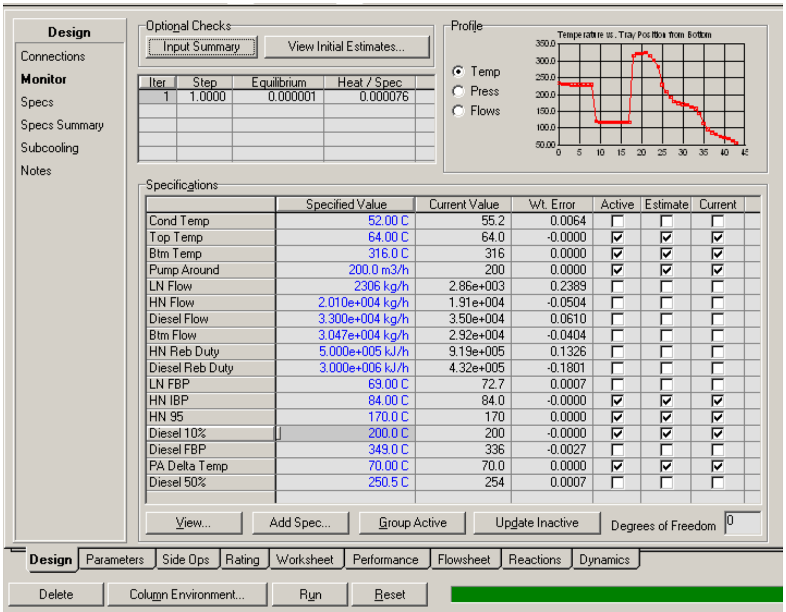

● Temp ○ Press ○ Flows

| Iter | Step | Equilibrium | Heat / Spec |
|---|---|---|---|
| 1 | 1.0000 | 0.000001 | 0.000076 |

| | Specified Value | Current Value | Wt. Error | Active | Estimate | Current |
|---|---|---|---|---|---|---|
| Cond Temp | 52.00 C | 55.2 | 0.0064 | ☐ | ☐ | ☐ |
| Top Temp | 64.00 C | 64.0 | -0.0000 | ☑ | ☑ | ☑ |
| Btm Temp | 316.0 C | 316 | 0.0000 | ☑ | ☑ | ☑ |
| Pump Around | 200.0 m3/h | 200 | 0.0000 | ☑ | ☑ | ☑ |
| LN Flow | 2306 kg/h | 2.86e+003 | 0.2389 | ☐ | ☐ | ☐ |
| HN Flow | 2.010e+004 kg/h | 1.91e+004 | -0.0504 | ☐ | ☐ | ☐ |
| Diesel Flow | 3.300e+004 kg/h | 3.50e+004 | 0.0610 | ☐ | ☐ | ☐ |
| Btm Flow | 3.047e+004 kg/h | 2.92e+004 | -0.0404 | ☐ | ☐ | ☐ |
| HN Reb Duty | 5.000e+005 kJ/h | 9.19e+005 | 0.1326 | ☐ | ☐ | ☐ |
| Diesel Reb Duty | 3.000e+006 kJ/h | 4.32e+005 | -0.1801 | ☐ | ☐ | ☐ |
| LN FBP | 69.00 C | 72.7 | 0.0007 | ☐ | ☐ | ☐ |
| HN IBP | 84.00 C | 84.0 | -0.0000 | ☑ | ☑ | ☑ |
| HN 95 | 170.0 C | 170 | 0.0000 | ☑ | ☑ | ☑ |
| Diesel 10% | 200.0 C | 200 | -0.0000 | ☑ | ☑ | ☑ |
| Diesel FBP | 349.0 C | 336 | -0.0027 | ☐ | ☐ | ☐ |
| PA Delta Temp | 70.00 C | 70.0 | 0.0000 | ☑ | ☑ | ☑ |
| Diesel 50% | 250.5 C | 254 | 0.0007 | ☐ | ☐ | ☐ |

Degrees of Freedom 0

Figure 2.158 Specifications of T-101

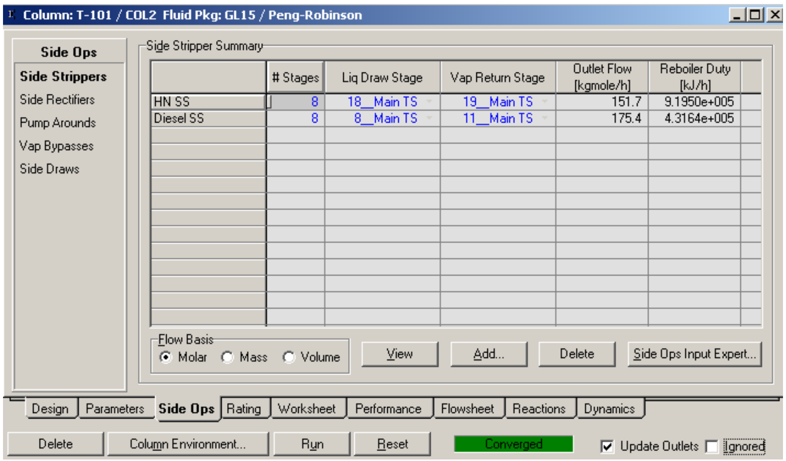
Column: T-101 / COL2 Fluid Pkg: GL15 / Peng-Robinson

| | # Stages | Liq Draw Stage | Vap Return Stage | Outlet Flow [kgmole/h] | Reboiler Duty [kJ/h] |
|---|---|---|---|---|---|
| HN SS | 8 | 18__Main TS | 19__Main TS | 151.7 | 9.1950e+005 |
| Diesel SS | 8 | 8__Main TS | 11__Main TS | 175.4 | 4.3164e+005 |

Flow Basis: ● Molar ○ Mass ○ Volume

Converged

☑ Update Outlets ☐ Ignored

Figure 2.159 Side strippers in T-101

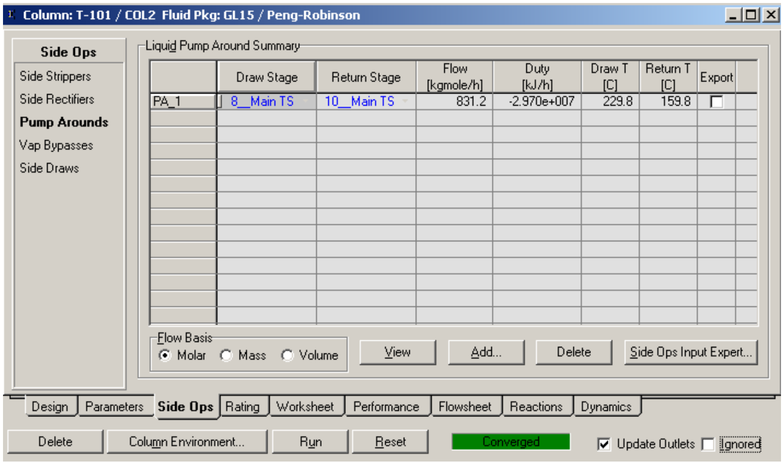

Liquid Pump Around Summary

| | Draw Stage | Return Stage | Flow [kgmole/h] | Duty [kJ/h] | Draw T [C] | Return T [C] | Export |
|---|---|---|---|---|---|---|---|
| PA_1 | 8__Main TS | 10__Main TS | 831.2 | -2.970e+007 | 229.8 | 159.8 | ☐ |

Flow Basis: ● Molar ○ Mass ○ Volume

☑ Update Outlets ☐ Ignored

Figure 2.160 Pump arounds in T-101

## 2.14 Acknowledgement.

We thank Mr. Stephen Dziuk of Aspen Technology for his valuable review comments. We thank Alliant Techsystems, Aspen Technology, China Petroleum and Chemical Corporation (SINOPEC), Milliken Chemical, Novozymes Biological, and Mid-Atlantic Technology, Research and Innovation Center for supporting our educational programs in computer-aided design and process system engineering at Virginia Tech

## 2.15 Nomenclature.

| | |
|---|---|
| CONV | Conversion (—) |
| E | Murphree tray efficiency (—) |
| F | Molar flow (mole/hr) |
| $F_{vi}$ | The i cut point while applying Gauss-Legendre quadrature into delump |
| $I_m$ | Inhibition factor in LHHW mechanism (m = $NH_3$, $H_2S$ and organic nitrogen compounds) (—) |
| $K_{avg}$ | Watson K factor (—) |
| $K_{ADS}$ | LHHW adsorption constants of hydrocarbon ($kPa^{-1}$) |

| | |
|---|---|
| $K_{eq}$ | Equilibrium constant of reversible reaction (—) |
| $K_{total}$ | Overall activity of reaction group (—) |
| $K_{global\_i}$ | Global activity for the i catalyst bed (—) |
| $K_{sul\_i\_j}$ | Hydrodesulfurization activity of the j distillate cut (j = whole fraction, 430°F-, 430 to 950°F, and 950°F+) in the i reactor (i = hydrotreating, and hydrocracking reactor) (—) |
| $K_{crc\_i\_j}$ | Hydrocracking activity of the j distillate cut (j = whole fraction, 430°F-, 430 to 950°F, and 950°F+) in the i reactor (i = hydrotreating, and hydrocracking reactor) (—) |
| $K_{hdg\_i\_j}$ | Aromatic hydrogenation activity of the j distillate cut (j = whole fraction, 430°F-, 430 to 950°F, and 950°F+) in the i reactor (i = hydrotreating, and hydrocracking reactor) (—) |
| $K_{ro\_i\_j}$ | Ring opening activity of the j distillate cut (j = whole fraction, 430°F-, 430 to 950°F, and 950°F+) in the i reactor (i = hydrotreating, and hydrocracking reactor) (—) |
| $K_{light\_i}$ | Light gas distributing factor (i = C1, C2, C3, and C4) (—) |
| k | Intrinsic rate constant of reaction ($hr^{-1}$) |
| MeABP | Mean average boiling point (Rankine) |
| MW | Molecular weight (—) |
| $OBJ_{TR}$ | The predicting error of temperature rise of catalyst bed (℃) |
| $OBJ_{HQ}$ | The predicting error of hydrogen quench of catalyst bed (STD $m^3/h$) |
| $OBJ_{PGF}$ | The predicting error of flow rate of purge gas (STD $m^3/h$) |
| $OBJ_{MHF}$ | The predicting error of flow rate of makeup $H_2$ (STD $m^3/h$) |
| $OBJ_{HC}$ | The predicting error $H_2$ consumption (STD $m^3/m^3$) |

| | |
|---|---|
| $OBJ_{NVF}$ | The predicting error of C6 to 430°F cut (naphtha) volume flow ($m^3$/h) |
| $OBJ_{DVF}$ | The predicting error of 430 to 700°F cut (diesel) volume flow ($m^3$/h) |
| $OBJ_{BVF}$ | The predicting error of 700 to 1000°F cut (bottom) volume flow ($m^3$/h) |
| $OBJ_{RVF}$ | The predicting error of 1000°F+ cut (resid) volume flow ($m^3$/h) |
| $OBJ_{NMF}$ | The predicting error of C6 to 430°F cut (naphtha) mass flow (kg/h) |
| $OBJ_{DMF}$ | The predicting error of 430 to 700°F cut (diesel) mass flow (kg/h) |
| $OBJ_{BMF}$ | The predicting error of 700 to 1000°F cut (bottom) mass flow (kg/h) |
| $OBJ_{RMF}$ | The predicting error of 1000°F+ cut (resid) mass flow (kg/h) |
| $OBJ_{C1C2}$ | The predicting error of C1C2 mass yield (wt%) |
| $OBJ_{C3}$ | The predicting error of C3 mass yield (wt%) |
| $OBJ_{C4}$ | The predicting error of C4 mass yield (wt%) |
| $OBJ_{SD}$ | The predicting error of sulfur content of 430 to 700°F cut (wt%) |
| $OBJ_{SB}$ | The predicting error of sulfur content of 700 to 1000°F cut (wt%) |
| $OBJ_{ND}$ | The predicting error of nitrogen content of 430 to 700°F cut (ppmwt) |
| $OBJ_{NB}$ | The predicting error of nitrogen content of 700 to 1000°F cut (ppmwt) |
| $OBJ_{NR1}$ | The predicting error of nitrogen content in reactor 1 effluent (ppmwt) |
| $P_c$ | Critical pressure (kPa) |
| $P_{H2}$ | Partial pressure of hydrogen (kPa) |
| $q_i$ | The zeros of the Legendre polynomial (－) |
| SG | Specific gravity 60°F/60°F(－) |
| SV | Space velocity (1/hr) |
| T | Temperature (℃) |
| $T_b$ | Normal boiling point (℃) |
| $T_c$ | Critical temperature (℃) |

| | |
|---|---|
| $T_r$ | Reduced temperature (－) |
| V | Volume ($m^3$) |
| $V_c$ | Critical volume ($m^3$) |
| $w_i$ | Weight factor of Gauss-Legendre quadrature (－) |
| $\omega$ | Acentric factor (－) |
| $\theta$ | Feed ratio of feed 1 to feed 2 (－) |
| $\tau$ | Residence time (hr) |

## 2.16 Literature Cited.

1. Aye, M. M. S.; Zhang, N. A Novel Methodology in Transforming Bulk Properties of Refining Streams into Molecular Information, *Chem. Eng. Sci.* **2005**, 60, 6702.
2. Qader, S. A.; Hill, G. R. Hydrocracking of Gas Oil, *Ind. Eng. Chem. Proc. Des. Dev.* **1969**, 8, 98.
3. Quann, R. J.; Jaffe, S. B. Structure-Oriented Lumping: Describing the Chemistry of Complex Hydrocarbon Mixtures, *Ind. Eng. Chem. Res.* **1992**, 31, 2483.
4. Quann, R. J.; Jaffe, S. B. Building Useful Models of Complex Reaction Systems in Petroleum Refining, *Chem. Eng. Sci.* **1996**, 51, 1615.
5. Quann, R. R. Modeling the Chemistry of Complex Petroleum Mixtures, *Environ. Health Perspect. Suppl.* **1998**, 106, 1501.
6. Froment, G. F. Single Event Kinetic Modeling of Complex Catalytic Processes, *Catal. Rev.-Sci. Eng.* **2005**, 47, 83.
7. Ghosh, P.; Andrews A. T.; Quann, R. J.; Halbert, T. R. Detailed Kinetic Model for the Hydro-desulfurization of FCC Naphtha *Energy Fuels* **2009**, 23, 5743.
8. Christensen, G.; Apelian, M. R.; Karlton, J. H.; Jaffe, S. B. Future directions in modeling the FCC process: An emphasis on product quality *Chem. Eng. Sci.* **1999**, 54, 2753.

9. Kumar, H.; Froment, G. F. Mechanistic Kinetic Modeling of the Hydrocracking of Complex Feedstocks, Such as Vacuum Gas Oils, *Ind. Eng. Chem. Res.* **2007**, 46, 5881.
10. Ancheyta, J.; Sánchez, S.; Rodríguez, M. A. Kinetic Modeling of Hydrocracking of Heavy Oil Fractions: A Review, *Catal. Today* **2005**, 109, 76.
11. Ho, T. C. Kinetic Modeling of Large-Scale Reaction Systems, *Catal. Rev. Sci. Eng.* **2008**, 50, 287.
12. Valavarasu, G.; Bhaskar, M.; Sairam, B. A Four Lump Kinetic Model for the Simulation of the Hydrocracking Process, *Petrol. Sci. Technol.* **2005**, 23, 1323.
13. Sánchez, S.; Rodríguez, M. A.; Ancheyta, J. Kinetic Model for Moderate Hydrocracking of Heavy Oils, *Ind. Eng. Chem. Res.* **2005**, 44, 9409.
14. Verstraete, J. J.; Le Lannic, K.; Guibard, I. Modeling Fixed-bed Residue Hydrotreating Processes, *Chem. Eng. Sci.* **2007**, 62, 5402.
15. Stangeland, B. E. A Kinetic Model for the Prediction of Hydrocracker Yields, *Ind. Eng. Chem. Proc. Des. Dev.* **1974**, 13, 71.
16. Mohanty, S.; Saraf, D. N.; Kunzru, D. Modeling of a Hydrocracking Reactor, *Fuel Process Technol.* **1991**, 29, 1.
17. Pacheco, M. A.; Dassori, C. G. Hydrocracking: An improved Kinetic Model and Reactor Modeling, *Chem. Eng. Commun.* **2002**, 189, 1684.
18. Bhutani, N.; Ray, A. K.; Rangaiah, G. P. Modeling, Simulation, and Multi-objective Optimization of an Industrial Hydrocracking Unit, *Ind. Eng. Chem. Res.* **2006**, 45, 1354.
19. Laxminarasimhan, C. S.; Verma, R. P.; Ramachandran, P. A. Continuous Lumping Model for Simulation of Hydrocracking, *AIChE J.* **1996**, 42, 2645.
20. Basak, K.; Sau, M.; Manna, U.; Verma, R. P. Industrial Hydrocracker Model Based on Novel Continuum Lumping Approach for Optimization in Petroleum Refinery, *Catal. Today*

**2004**, 98, 253.

21. Fukuyama, H.; Terai, S. Kinetic Study on the Hydrocracking Reaction of Vacuum Residue Using a Lumping Model, *Petrol. Sci. Technol.* **2007**, 25, 277.
22. Aspen HYSYS/Refining Option Guide, AspenTech, Cambridge, MA (2006).
23. Korre, S. C.; Klein, M. T.; Quann, R. J. Hydorcracking of Polynuclear Aromatic Hydrocarbons. Development of Rate Laws through Inhibition Studies, *Ind. Eng. Chem. Res.* **1997**, 36, 2041.
24. Jacob, S. M.; Quann, R. J.; Sanchez, E.; Wells, M. E. Compositional Modeling Reduces Crude-Analysis Time, Predicts Yields, *Oil & Gas J.* **1998**, July 6, 51.
25. Filimonov, V.A.; Popov, A.A.; Khavkin, V.A.; Perezhigina, I.Ya.; Osipov, L.N.; Rogov, S.P.; Agafonov, A.V. *International Chemical Engineering* **1972**, 12, 21.
26. Jacobs, P.A. Hydrocracking of n-Alkane Mixtures on Pt/H-Y Zeolite: Chain Length Dependence of the Adsorption and the Kinetic Constants, *Ind. Eng. Chem. Res.* **1997**, 36, 3242.
27. Brown, J. M.; Sundaram, A.; Saeger, R. B.; Wellons, H. S.; Kennedy, H. S.; Jaffe, S. B. Estimating Compositional Information from Limited Analytical Data, WO2009051742, **2009**.
28. Gomez-Prado, J.; Zhang, N.; Theodoropoulos, C. Characterization of Heavy Petroleum Fractions Using Modified Molecular-Type Homologous Series (MTHS) Representation *Energy* **2008**, 33, 974.
29. Aspen Plus Hydrocracker User’s Guide, AspenTech, Cambridge, MA (2006).
30. Mudt, D. R.; Pedersen, C. C.; Jett, M. D.; Karur, S.; McIntyre, B.; Robinson, P. R. Refinery-wide Optimization with Rigorous Models, In *Practical Advances in Petroleum Processing*, Hsu, C. S.; Robinson, P. R. (Eds.), Springer: New York, NY, 2006.

31. Satterfield, C. N. Trickle-Bed Reactors, *AIChE J.* **1975**, 21, 209.

32. Kaes, G. L. *Refinery Process Modeling A Practical Guide to Steady State Modeling of Petroleum Processes*; The Athens Printing Company: Athens, GA, 2000.

33. Fogler, H. S. *Elements of Chemical Reaction Engineering*, 4th ed.; Prentice Hall: Upper Saddle River, NJ, 2005.

34. Aspen HYSYS Simulation Basis, AspenTech, Cambridge, MA (2006).

35. Daubert, T. E.; Danner, R. P. *API Technical Data Book – Petroleum Refining*, 6th ed., American Petroleum Institute: Washington D.C., 1997.

36. Bollas, G. M.; Vasalos, I. A.; Lappas, A. A.; Iatridis, D. K.; Tsioni, G. K. Bulk Molecular Characterization Approach for the Simulation of FCC Feedstocks, *Ind. Eng. Chem. Res.* **2004**, 43, 3270.

37. Riazi, M. R. *Characterization and Properties of Petroleum Fractions*; 1st ed., American Society for Testing and Materials: West Conshohocken, PA, 2005.

38. Haynes, H. W. Jr.; Matthews, M. A. Continuous-Mixture Vapor-Liquid Equilibria Computations Based on True Boiling Point Distillations, *Ind. Eng. Chem. Res.* **1991**, 30, 1911.

39. Cotterman, R. L.; Bender, R.; Prausnitz, J. M. Phase Equilibria for Mixtures Containing Very Many Components. Development and Application of Continuous Thermodynamics for Chemical Process Design, *Ind. Eng. Chem. Proc. Des. Dev.* **1985**, 24, 194.

40. Mani, K. C.; Mathews, M. A.; Haynes, H. W. Jr. Continuous Approach Optimizes Vapor-Liquid Equilibrium Calculation, *Oil & Gas J.* **1993**, Feb 15, 76.

41. Riazi, M. R.; Daubert, T. E. Simplify Property Predictions, *Hydrocarbon Processing* **1980**, Mar, 115.

42. Lee, B. I.; Kesler, M. A. A Generalized Thermodynamic Correlation Based on

Three-Parameter Corresponding States. *AIChE J.* **1985**, 31, 1136.

43. Kister, H. Z. *Distillation Design*; McGraw-Hill, Inc.: New York, NY, 1992.
44. Roussel, M.; Norsica, S.; Lemberton, J. L.; Guinet, M.; Cseri, T.; Benazzi, E. Hydrocracking of n-Decane on a Bifunctional Sulfided NiW/Silica-Alumina Catalyst: Effect of the Operating Conditions, *Appl. Catal.* **2005**, 279, 53.
45. Dufresne, P.; Bigeard, P. H.; Bilon, A. New Development in Hydrocracking: Low Pressure High-Conversion Hydrocracking, Catal. Today **1987**, 1, 367.
46. Scherzer, J.; Gruia, A. J. *Hydrocracking Science and Technology*; Marcel Dekker: New York, NY, 1996.
47. Hu, Z. H.; Xiong, Z. L.; Shi, Y. H.; Li, D. D. Investigation on the Reaction Pressure of Hydrocracking Unit, *Petroleum Processing and Petrochemicals* **2005**, 36, 35. (Chinese)
48. Tippett, T. W.; Ward, J. W. Mild Hydrocracking for Middle Distillate Production, *National Petroleum Refiners Association (NPRA) Annual Meeting, 24 Mar 1985*, 24 Mar 1985, AM-85-43.
49. Rossi, V. J.; Mayer, J. F.; Powell, B. E. To Up Hydrocracking Conversion, *Hydrocarbon Processing* **1978**, Oct 15, 123.
50. Bodington, C. E.; Baker, T. E. A History of Mathematical Programming in the Petroleum Industry, *Interfaces* **1990**, 20, 117.
51. El-Kady, F. Y. Hydrocracking of Vacuum Distillate Fraction over Bifunctional Molybdenum – Nickel/Silica – Alumina Catalyst, *Indian J. Technol.* **1979**, 17, 176.
52. Hu, M. C.; Powell, R. T.; Kidd, N. F. Develop LP Models Using a Steady-State Simulator, *Hydrocarbon Processing* **1997**, 76 (6), 81.

# Chapter 3 Integrated Process Modeling and Product Design of Biodiesel Manufacturing

## Abstract

Biodiesel, i.e., a mixture of fatty acid methyl esters (FAMEs), produced from reacting triglyceride with methanol by alkali-catalyzed transesterification, has attracted much attention as an important renewable energy source. To aid in the optimization of biodiesel manufacturing, a number of published studies have applied commercial process simulators to quantify the effects of operating conditions on the process performance. Significantly, all of the reported simulation models are design models for new processes by fixing some level of equipment performance such as the conversion of transesterification reaction. Most models assume the feed oil as pure triolein and the biodiesel fuel as pure methyl oleate, and pay insufficient attention to the feed oil characterization, thermophysical property estimation, rigorous reaction kinetics, phase equilibrium for separation and purification units, and prediction of essential biodiesel fuel qualities. This paper presents first a comprehensive review of published literature pertaining to developing an integrated process modeling and product design of biodiesel manufacturing, and identifies those deficient areas for further development.

This paper then presents new modeling tools and a methodology for the integrated process modeling and product design of an entire biodiesel manufacturing train (including transesterification reactor, methanol recovery and recycle, water wash, biodiesel recovery, and glycerol separation, etc.). We demonstrate the methodology by simulating an integrated process to predict reactor and separator performance, stream conditions, and product qualities with different feedstocks. The results show that the methodology is effective not only for the rating and optimization of an existing biodiesel manufacturing, and but also for the design of a new process to produce biodiesel with specified fuel properties.

## 3.1 Biodiesel Production by Transesterification Process.

The American Society for Testing and Materials (ASTM) defines biodiesel as a fuel comprised exclusively of mono-alkyl esters of long-chain fatty acids derived from vegetable oils or animal fats, designated B100 (100% pure biodiesel), and meeting the requirements of ASTM designation D6751[1]. Transesterification process is the most well-known biodiesel production technology that essentially involves the reaction of alcohol with triglyceride (from vegetable oils or animal fats) to produce FAMEs, the biodiesel fuel.

Alkali-catalyzed transesterification is the most common manufacturing method because of its faster rate and less corrosive to industrial equipment[2]. Methanol is most popular alcohol used because of its low cost and suitable properties[3], and the corresponding product is a mixture of FAMEs. This article focuses on alkali-catalyzed transesterification of methanol with triglyceride. Figure 3.1 shows a simplified flowsheet of an alkali-catalyzed transesterification process. There are many options for the separation and purification processes following the transesterification step[4].

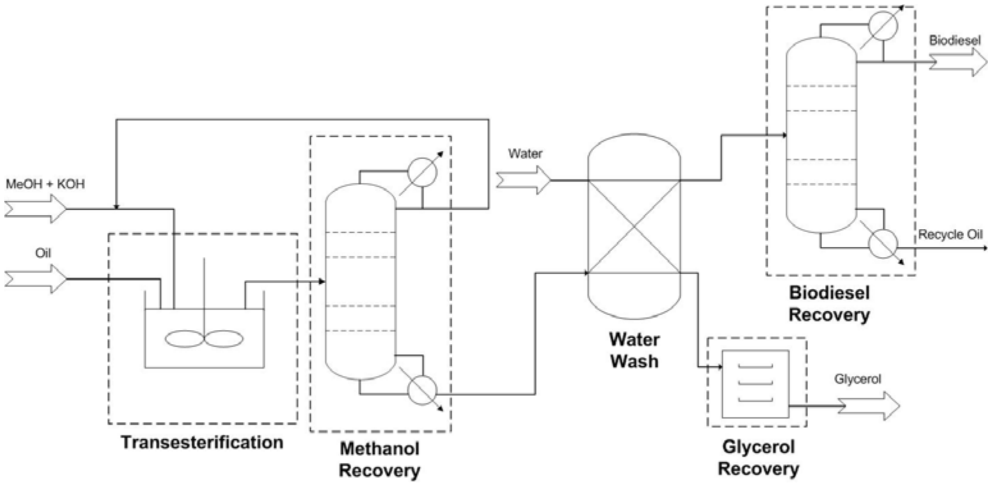

Figure 3.1 A simplified flowsheet of an alkali-catalyzed transesterification process

## 3.2 Integrated Process Modeling and Product Design.

Many of the alkali-catalyzed transesterification process models[4,5,6,7,8,9,10,11,12] are developed by flowsheet simulators such as Aspen Plus and Aspen HYSYS. Table 3.1 summarizes the key features of the process models in the literature. We distinguish the reported simulation models into *design* mode and *rating* mode. In the design mode, we develop simulation models by assuming some level of equipment performance (e.g., reactors with known component conversion, or with product yields calculated according to Gibbs thermodynamic equilibrium), and then design the equipment to meet this level of performance. In the rating mode, however, the equipment already exists and we develop simulation models with quantitative rate equations (e.g., reactors with known reaction equations and kinetic parameters) to predict how the equipment will perform under a variety of process conditions.

Significantly, all of the reported simulation models are design mode, fixing the conversion of transesterification reaction. Most models assume the feed oil as pure triolein and the biodiesel fuel as pure methyl oleate, and ignore the saponification reaction which is important only when the reactor feed is crude or used oil containing much water and free fatty acids initially. The reported models pay insufficient attention to the characterization and thermophysical properties of feed oil, and to the prediction of essential product fuel qualities. This paper focuses on those issues that are not well covered or essentially ignored in reported studies.

Table 3.1 Key features of reported simulation models

| Reference | Feed/Product Characterization | | Reactor Model | | Calculation of Fuel Properties of Biodiesel | Thermodynamic Model of Biodiesel Purification Unit | Program | Mode |
|---|---|---|---|---|---|---|---|---|
| | Feed/product definition | Description of thermophysical property models | Kinetics | Saponification | | | | |
| Myint & El-Halwagi[4] | Feed: pure triolein + oleic acid<br>Product: methyl-oleate | None | Yield model | Included | None | NRTL (non-random two-liquid) activity coefficient model with RKS (Redlich-Kwong-Soave) equation of state;<br>UNIFAC for estimating missing parameters | Aspen Plus | Design |
| West et al.[5] | Feed: pure triolein + oleic acid<br>Product: methyl-oleate | None | Yield model | Not included | None | NRTL<br>UNIFAC for estimating missing parameters<br>& fixed efficiency for centrifuge | Aspen HYSYS | Design |
| Zhang et al.[6] | Feed: pure triolein<br>Product: methyl-oleate | None | Yield model | Not included | None | NRTL<br>UNIFAC for estimating missing parameters<br>& fixed efficiency for centrifuge | Aspen HYSYS | Design |
| Harding et al.[7] | Feed: pure triolein<br>Product: methyl-oleate | None | Yield model | Not included | None | No description | Aspen Plus | Design |
| Haas et al.[8] | Feed: pure triolein<br>Product: methyl-oleate | None | Yield model | Not included | None | Fixed efficiency for centrifuge | Aspen Plus | Design |
| Tapasvi et al.[9] | Feed: mixture of simple triglycerides<br>Product: mixture of FAMEs | None | Yield model | Included | None | Fixed efficiency for centrifuge | MS Excel | Design |
| Kapilakarn & Peutong[10] | Feed: no description<br>Product: no description | None | Rigorous model | Not included | None | Fixed efficiency for centrifuge | Aspen HYSYS | Design |
| Stiefel & Dassori[11] | Feed: pure triolein<br>Product: methyl-oleate + diolein + monoolein | None | Rigorous model | Not included | None | Fixed efficiency | Aspen Plus | Design |
| Apostolakou et al.[12] | Feed: pure triolein<br>Product: methyl-oleate | Tang et al.[13] | Yield model | Not included | None | NRTL<br>UNIFAC for estimating missing parameters<br>& Fixed efficiency for centrifuge | Aspen HYSYS | Design |

## 3.3 Reaction Kinetics.

The raw materials of transesterification reaction, vegetable oil and animal fat, are mixtures of several oils and fats, and the compositions vary with oil sources and growth conditions. The major feed component is triglyceride (TG) in which glycerol (GL) is esterified with fatty acids. Figure 3.2 shows the structure of TG:

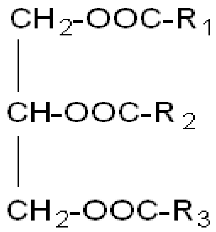

$$\begin{array}{l} CH_2\text{-}OOC\text{-}R_1 \\ | \\ CH\text{-}OOC\text{-}R_2 \\ | \\ CH_2\text{-}OOC\text{-}R_3 \end{array}$$

Figure 3.2 Chemical structure of triglyceride (TG)

where R1, R2 and R3 are long fatty acid chains. Vegetable oil and animal fat usually contain small amounts of water and free fatty acids[14]. Table 3.2 lists the chemical structures of common fatty acid chains[14, 15].

Table 3.2 Chemical structure of common fatty acid chains*

| Fatty acid chain | Structure | Common acronym |
|---|---|---|
| Lauric acid | $HOOC\text{-}(CH_2)_{10}\text{-}CH_3$ | C12:0 |
| Myristic acid | $HOOC\text{-}(CH_2)_{12}\text{-}CH_3$ | C14:0 |
| Palmitic acid | $HOOC\text{-}(CH_2)_{14}\text{-}CH_3$ | C16:0 |
| Stearic acid | $HOOC\text{-}(CH_2)_{16}\text{-}CH_3$ | C18:0 |
| Oleic acid | $HOOC\text{-}(CH_2)_7\text{-}CH{=}CH\text{-}(CH_2)_7\text{-}CH_3$ | C18:1 |
| Linoleic acid | $HOOC\text{-}(CH_2)_7\text{-}CH{=}CH\text{-}CH_2\text{-}CH{=}CH\text{-}(CH_2)_4\text{-}CH_3$ | C18:2 |
| Linolenic acid | $HOOC\text{-}(CH_2)_7\text{-}(CH{=}CH\text{-}CH_2)_3\text{-}CH_3$ | C18:3 |
| Arachidic acid | $HOOC\text{-}(CH_2)_{18}\text{-}CH_3$ | C20:0 |
| Bechnic acid | $HOOC\text{-}(CH_2)_{20}\text{-}CH_3$ | C22:0 |
| Lignoceric acid | $HOOC\text{-}(CH_2)_{22}\text{-}CH_3$ | C24:0 |

*Note: By replacing the H atom in the HOOC- group with $CH_3$ group, we have the structure of the fatty acid methyl ester (FAME). For example, the structure of lauric acid methyl ester is $CH_3\text{-}OOC\text{-}(CH_2)_{10}\text{-}CH_3$.

In the common acronym column in Table 3.2, the first number denotes the number of carbon atoms in the chain and the second number indicates the number of double bonds. The number of carbon atoms includes the carboxylic carbon. Table 3.3 shows the typical compositions of various oil sources.

Table 3.3 Compositions (wt %) of various oil sources[15]

| Fatty acid chain | Common acronym | Palm | Olive | Peanut | Rape | Soybean | Sunflower | Grape | Almond | Corn |
|---|---|---|---|---|---|---|---|---|---|---|
| Lauric acid chain | C12:0 | 0.10 | 0.00 | 0.00 | 0.00 | 0.00 | 0.00 | 0.00 | 0.00 | 0.00 |
| Myristic acid chain | C14:0 | 0.70 | 0.00 | 0.10 | 0.00 | 0.00 | 0.00 | 0.10 | 0.00 | 0.00 |
| Palmitic acid chain | C16:0 | 36.70 | 11.60 | 8.00 | 4.90 | 11.30 | 6.20 | 6.90 | 10.40 | 6.50 |
| Palmitoleic acid chain | C16:1 | 0.10 | 1.00 | 0.00 | 0.00 | 0.10 | 0.10 | 0.10 | 0.50 | 0.60 |
| Stearic acid chain | C18:0 | 6.60 | 3.10 | 1.80 | 1.60 | 3.60 | 3.70 | 4.00 | 2.90 | 1.40 |
| Oleic acid chain | C18:1 | 46.10 | 75.00 | 53.30 | 33.00 | 24.90 | 25.20 | 19.00 | 77.10 | 65.60 |
| Linoleic acid chain | C18:2 | 8.60 | 7.80 | 28.40 | 20.40 | 53.00 | 63.10 | 69.10 | 7.60 | 25.20 |
| Linolenic acid chain | C18:3 | 0.30 | 0.60 | 0.30 | 7.90 | 6.10 | 0.20 | 0.30 | 0.80 | 0.10 |
| Arachidic acid chain | C20:0 | 0.40 | 0.30 | 0.90 | 0.00 | 0.30 | 0.30 | 0.30 | 0.30 | 0.10 |
| Eicosenoic acid chain | C20:1 | 0.20 | 0.00 | 2.40 | 9.30 | 0.30 | 0.20 | 0.00 | 0.00 | 0.10 |
| Behenic acid chain | C22:0 | 0.10 | 0.10 | 3.00 | 0.00 | 0.00 | 0.70 | 0.00 | 0.10 | 0.00 |
| Erucic acid chain | C22:1 | 0.00 | 0.00 | 0.00 | 23.00 | 0.30 | 0.10 | 0.00 | 0.00 | 0.10 |
| Liqnoceric acid chain | C24:0 | 0.10 | 0.50 | 1.80 | 0.00 | 0.10 | 0.20 | 0.00 | 0.20 | 0.10 |
| Nervonic acid chain | C24:1 | 0.00 | 0.00 | 0.00 | 0.00 | 0.00 | 0.00 | 0.00 | 0.40 | 0.00 |

Freedman et al.[2] show the overall reaction scheme of transesterification of methanol with triglyceride (TG) to give the fatty acid methyl ester (FAME), i.e., the biodiesel, and byproduct, glycerol (GL). See Figure 3.3 .

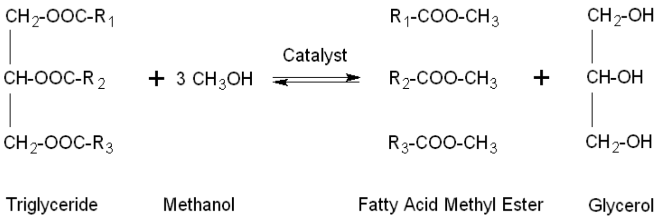

Figure 3.3 Overall reaction scheme of transesterification

Figure 3.4 represents the stepwise reaction scheme which includes reaction intermediates, monoglyceride (MG) and diglyceride (DG) [2] and fatty acid methyl esters (FAMEs).

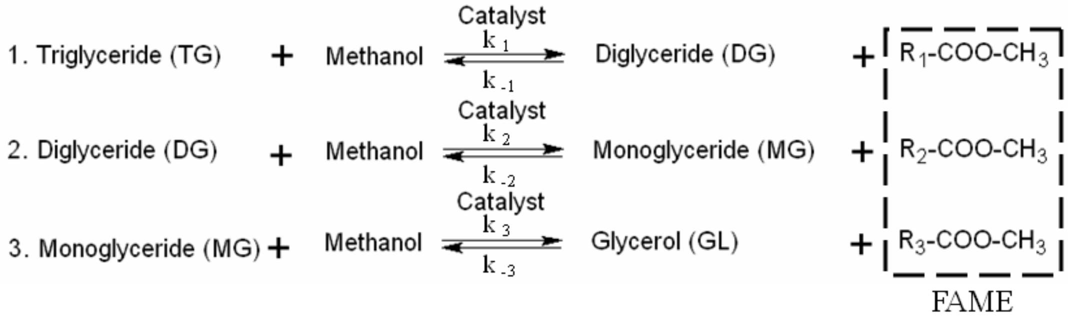

Figure 3.4 Stepwise reaction scheme of transesterification

The reaction takes place through three stages: (1) slow mass-transfer stage, (2) fast kinetic stage, and (3) slow chemical-equilibrium stage[16,17,18,19,20,21]. The slow mass-transfer stage at the beginning results from the immiscibility of oil and methanol. The reaction rate is limited by the mass transfer of TG to methanol and oil phases. The fast kinetic stage occurs, when the reaction intermediates, MG and DG, act as surfactants and stabilize the methanol drops in the continuous oil phase[18]. The increasing interfacial area between oil and methanol phases makes the mass transfer of TG to methanol and oil phases no longer limiting the reaction rate. In the last stage, the reaction approaches chemical equilibrium and the reaction rate slows down. In addition, saponification of free fatty acid and TG with hydroxide ion ($OH^-$) may also occur in the reaction system[4]:

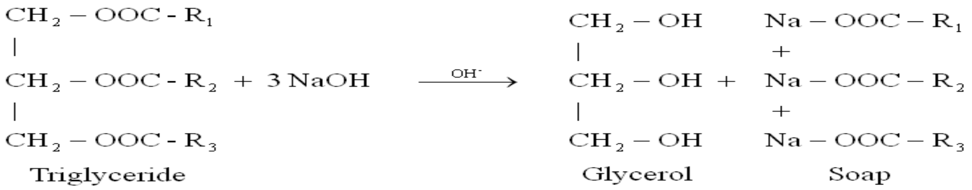

Figure 3.5 Saponification of triglyceride with NaOH

$$\underset{\text{Free Fatty Acid}}{R - COOH} + NaOH \longrightarrow H_2O + \underset{\text{Soap}}{R\text{-}COO\text{-}Na}$$

Figure 3.6 Saponification of free fatty acid with NaOH

Saponification leads to lower production of biodiesel and higher cost of purification process[4]. For the alkali-catalyzed transesterification of methanol with oils, Freedman et al.[20] demonstrate that at 60 ℃ or higher, 1 wt% NaOH, methanol/oil molar ratio at least 6:1 and fully refined oil (free fatty acid < 5%) give the optimum conversion within 1 hour. Many of the kinetic models[21,22,23,24,25,26,27] show good performances near optimal operating conditions by ignoring the mass-transfer stage and applying the second-order kinetics to characterize the reaction. The mass-transfer stage is much shorter than the other two stages and is negligible when the mixing is intense[20,21] and reaction temperature is higher than 30℃[17]. Slinn and Kendall[28] demonstrate that the drop size affects the reaction rate and develop a mass-transfer-limited kinetic model. However, most reported studies neglect saponification because of its small extent when the raw material is well refined[20,29]. According to the kinetic scheme in Figure 3.4, the second-order kinetics obeys the following governing equations.

$$\frac{d[TG]}{dt} = -k_1[TG][MeOH] + k_2[DG][FAME] \tag{1}$$

$$\frac{d[DG]}{dt} = k_1[TG][MeOH] - k_2[DG][FAME] - k_3[DG][MeOH] + k_4[MG][FAME] \tag{2}$$

$$\frac{d[MG]}{dt} = k_3[DG][MeOH] - k4[MG][FAME] - k_5[MG][MeOH] + k_6[GL][FAME] \tag{3}$$

$$\frac{d[GL]}{dt} = k_5[MG][MeOH] - k_6[GL][FAME] \tag{4}$$

$$\begin{aligned}\frac{d[FAME]}{dt} = {} & k_1[TG][MeOH] - k_2[DG][FAME] + k_3[DG][MeOH] - k4[MG][FAME] \\ & + k_5[MG][MeOH] - k_6[GL][FAME]\end{aligned} \tag{5}$$

$$\frac{d[MeOH]}{dt} = -\frac{d[FAME]}{dt} \tag{6}$$

For alkali-catalyzed transesterification, Wu et al.[30], and Table 3 in Canakci and Gerpen[31] show that fatty acid compositions of biodiesel fuels are essentially identical to those of their corresponding vegetable oils. This implies that the various fatty acid chains of the TG have an essentially identical reactivity toward methanol. Table 3.4 summarizes the apparent rate constants of the second-order kinetics from the literature. The rate constants and activation energies follow the Arrhenius equation:

$$\ln\frac{k}{k_0} = \frac{E_a}{R}\cdot\left(\frac{1}{T_0} - \frac{1}{T}\right) \quad \text{or} \quad k = A\cdot e^{-\frac{E_a}{RT}} \tag{7}$$

where k is rate constant, $E_a$ is activation energy and A is pre-exponential factor.

Table 3.4 Apparent kinetic parameters of the second-order kinetics

| Data Source | Noureddini and Zhu[22] | Narvaez et al.[25] | Bambase et al.[27] | Leevijit et al.[24] |
|---|---|---|---|---|
| Feed Oil Type | Soybean oil | Palm Oil | Sunflower Oil | Palm Oil |
| Temperature Range (℃) | 30-70 | 50-60 | 25-60 | 60 |
| Catalyst | NaOH | NaOH | NaOH | NaOH |
| Catalyst wt% (based on oil) | 0.2 | 0.2 | 0.5 | 1 |
| Rate Constant (L/mol-min ) | at 50 ℃ ($T_0$) | at 50 ℃ ($T_0$) | at 60 ℃ ($T_0$) | |

| | | | | |
|---|---|---|---|---|
| $k_1$ | 0.050 | 0.049 | 0.090 | 0.634 |
| $k_{-1}$ | 0.110 | 0.112 | 0.009 | 0.000 |
| $k_2$ | 0.215 | 0.226 | 0.348 | 7.104 |
| $k_{-2}$ | 1.228 | 0.133 | 0.129 | 4.912 |
| $k_3$ | 0.242 | 0.122 | 0.488 | 7.860 |
| $k_{-3}$ | 0.007 | 0.016 | 0.038 | 0.121 |
| Activation Energy (kcal/mol) | | | | |
| $E_1$ | 13.145 | 13.500 | 14.040 | |
| $E_{-1}$ | 9.932 | 10.300 | 10.739 | |
| $E_2$ | 19.860 | 17.400 | 16.049 | |
| $E_{-2}$ | 14.639 | 16.200 | 13.907 | |
| $E_3$ | 6.421 | 6.200 | 7.173 | |
| $E_{-3}$ | 9.588 | 11.900 | 10.997 | |

Vicente et al.[21,26] develop the intrinsic catalyzed kinetics by correlating catalyst concentration with apparent rate constants. They propose the following relationship:

$$k_i = k_i^{intrinsic} \times C_{CAT} \tag{8}$$

where $k_i^{intrinsic}$ is the intrinsic catalyzed rate constant which follows the Arrhenius equation, $k_i$ is the apparent rate constant and $C_{CAT}$ is the catalyst concentration. The activation energies and pre-exponential factors reported by Vincente et al.[21] are log-based Arrhenius equation and we re-fit their data to obtain a new set of activation energies and pre-exponential factors based on natural log (see Table 3.5 ).

Table 3.5 Intrinsic catalyzed kinetic parameters

| Data Source | Vicente et al.[21] | Vicente et al.[26] |
|---|---|---|
| Feed Oil Type | Sunflower oil | Brassica carinata oil |
| Temperature Range (℃) | 25-65 | 25-65 |
| Catalyst | KOH | KOH |
| Catalyst wt% (based on oil) | 0.5 - 1.5 | 0.5 - 1.5 |

| | | |
|---|---|---|
| Pre-exponential Factor ($L^2/mol^2$-min) | | |
| $A_1$ | 3.5093E+12 | 5.1600E+17 |
| $A_{-1}$ | 1.1542E+13 | 9.0000E+12 |
| $A_2$ | 4.9432E+17 | 6.6000E+16 |
| $A_{-2}$ | 1.2895E+17 | 1.6800E+13 |
| $A_3$ | 6.2713E+02 | 2.7600E+02 |
| $A_{-3}$* | | |
| Activation Energy (J/mol) | | |
| $E_1$ | 7.2963E+04 | 1.0476E+05 |
| $E_{-1}$ | 7.1648E+04 | 7.0976E+04 |
| $E_2$ | 9.7825E+04 | 9.2432E+04 |
| $E_{-2}$ | 9.4770E+04 | 7.0657E+04 |
| $E_3$ | 1.4070E+04 | 1.2020E+04 |
| $E_{-3}$ | | |

* $A_{-3}$ and $E_{-3}$ are ignored in the original studies due to insignificant values

### 3.4 Characterization and Thermophysical Property of Feed Oil and Biodiesel Fuel.

The compounds involved in the alkali-catalyzed transesterification process are feed oil (mixture of triglycerides), diglyceride (by-product), monoglyceride (by-product), fatty acid, methanol, water, base, glycerol and biodiesel fuel (mixture of FAMEs). The thermophysical property data of methanol, water, base, glycerol, fatty acids and FAMEs are available in National Institute of Science and Technology ThermoData Engine[32], or NIST TDE (http://trc.nist.gov/tde.html), which is the most comprehensive database and integrated with Aspen Plus 2006 and subsequent versions. Appendix A illustrates how the reader can access the NIST TDE when applying Aspen Plus to develop a biodiesel process model. Because only a few studies of diglyceride and monoglyceride are available in the literature, we focus mainly on the characterization and thermophysical property calculations of triglyceride, FAME, feed oil and biodiesel fuel.

#### 3.4.1 Minimum Requirements of Thermophysical Properties.

The required thermophysical properties depend on which thermodynamic model is selected.

Because of the presence of polar components (e.g., methanol) in a biodiesel process, we choose activity coefficient model for modeling thermodynamic equilibrium. Therefore, the minimum required thermophysical properties are normal boiling point ($T_b$), critical temperature ($T_c$), critical pressure ($P_c$,), acentric factor ($\omega$), liquid density ($\rho_L$) or liquid molar volume ($V_L$), ideal gas heat capacity ($C_{P, G}$), liquid heat capacity ($C_{P, L}$), heat of vaporization ($\triangle H_{vap}$) and vapor pressure ($P_{vap}$).

### 3.4.2 Triglycerides.

Triglyerides can be classified into two groups – simple triglyceride and mixed triglyceride. The simple triglyceride is composed of three identical fatty acid chains, but these fatty acid chains of mixed triglyceride are not identical. This section focuses on the simple triglyceride. Because thermal decomposition at high temperature makes the experimental measurements unattainable, it is necessary to predict $T_b$, $P_c$, $T_c$ and $\omega$ for long-chain triglycerides. There are many prediction methods of $T_b$, $P_c$, $T_c$ and $\omega$ for organic liquids in the literature, but many of the methods are unsuitable for triglycerides because of their structures and high molecular weights. For example, Figure 3.7 demonstrates that the Joback method significantly over-estimates the normal boiling points of pure triglycerides.

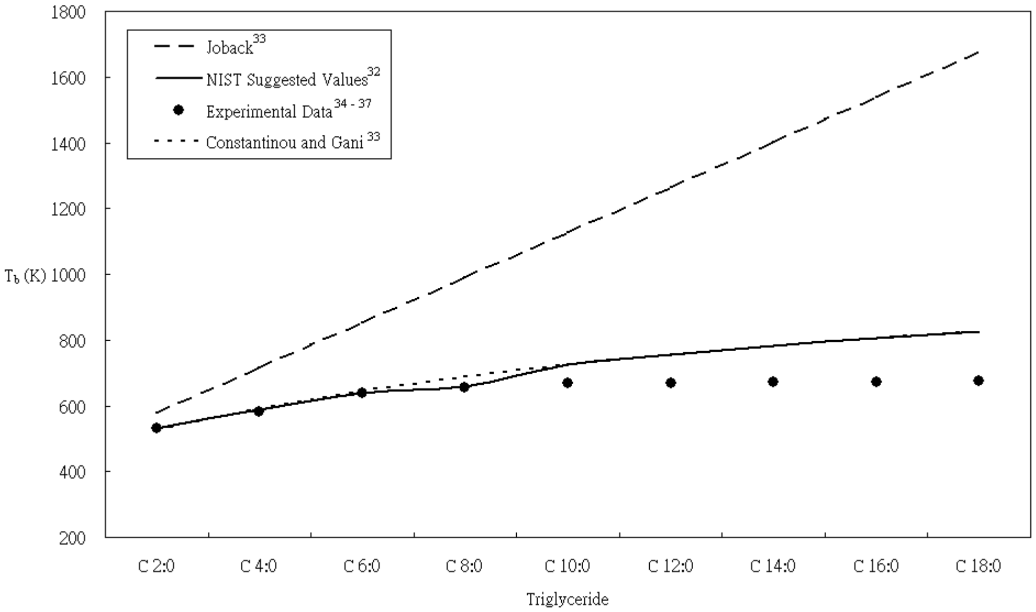

Figure 3.7 Comparison of normal boiling points of pure triglycerides predicted by different methods with experimental data

In addition to $T_b$, $P_c$, $T_c$ and $\omega$, it is necessary to estimate the missing values of $V_L$, $C_{P,G}$, $C_{P,L}$, $\triangle H_{vap}$ and $P_{vap}$ of triglycerides. Figure 3.8 shows a prediction map giving the relationship of various methods used to estimate the thermophysical properties of triglycerides in the literature and Appendix B illustrates the methodology of each method. Thus far, there are no reported methods used to predict $C_{P,G}$ of triglycerides.

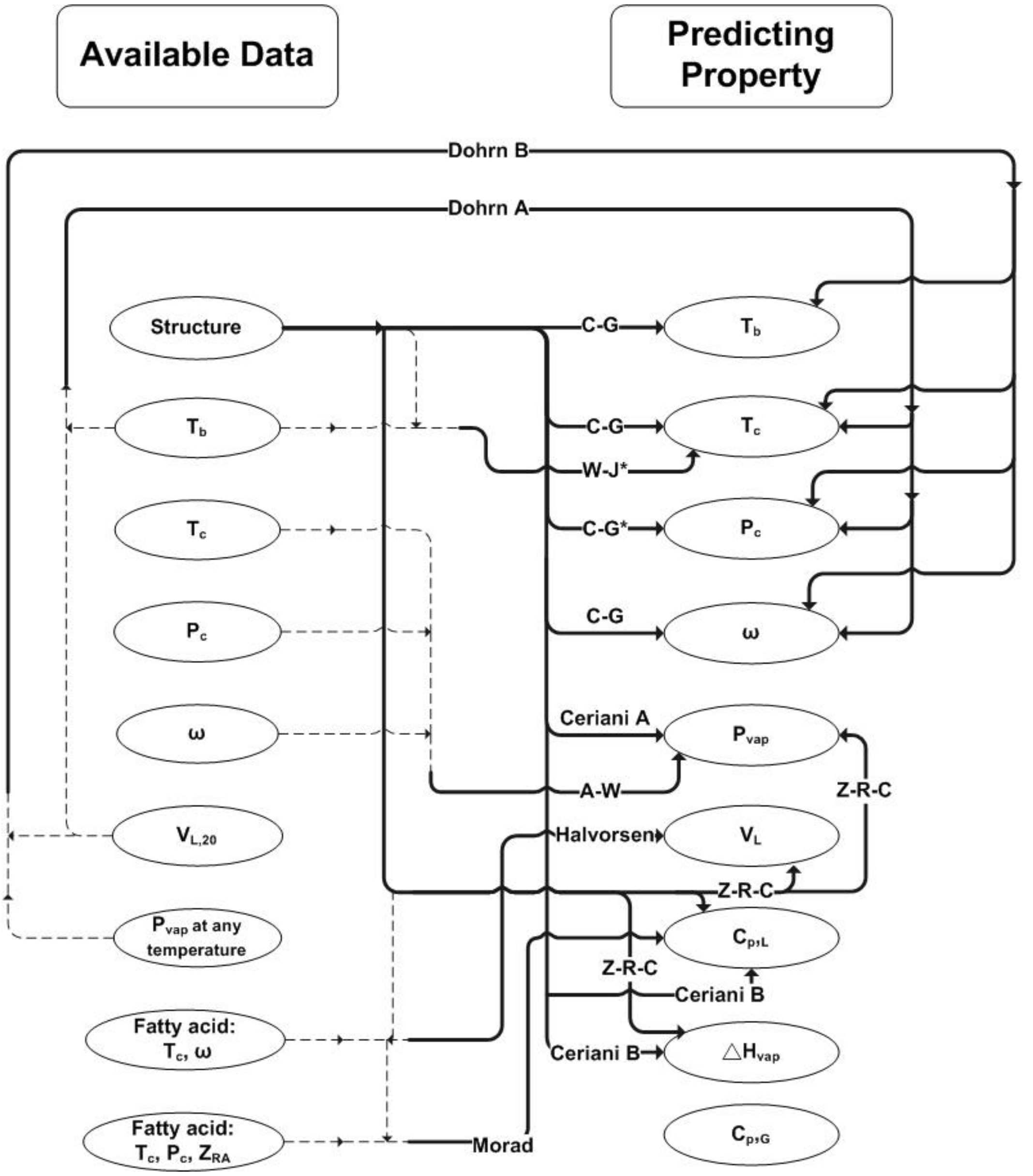

Figure 3.8 Prediction map of thermophysical properties of triglycerides: reference citation-Dohrn A and B [38]; Constantinou and Gani (C-G) [33]; Wilson and Japerson (W-J) [33]; Ceriani A [41]; Ambrose and Walton (A-W)[33]; Halvorsen[39]; Morad[40]; Zong, Ramanathan and Chen(Z-R-C)[42]; Ceriani B[43].”*” in the figure indicates the estimation method suggested by NSIT TDE[32].

Because the values of $T_b$, $P_c$, $T_c$ and ω are not experimentally available, these properties are treated as merely characteristic parameters in thermodynamic modeling[44,45]. Various VLE studies of the triglyceride system with different prediction methods for $T_b$, $P_c$, $T_c$ and $\omega$ seem to give almost equally satisfactory results[13,44,45,46]. However, we note that NIST TDE suggests W-J method[33] and C-G method[33] for $T_c$ and $P_c$ prediction, respectively. Table 3.6 summarizes the suggested values of $T_b$, $P_c$, $T_c$ and $\omega$ by NIST TDE.

Table 3.6 Suggested values of $T_b$, $P_c$, $T_c$ and $\omega$ of TG by NIST TDE

| | C12:0 | C14:0 | C16:0 | C18:0 | C18:1 | C18:2 | C20:0 | C22:0 |
|---|---|---|---|---|---|---|---|---|
| Pc (Pa) | 487709 | 417044.7 | 365772.1 | 327394.2 | 327019.8 | 326646.4 | 297923.6 | 274802.8 |
| Tc (K) | 819 | 828 | 834 | 840 | 841 | 843 | 844 | 847 |
| Tb (K) | 754.9 | 781.3 | 804.6 | 825.6 | 824 | 822.5 | 844.6 | 861.9 |
| ω | 0.15415 | 1.7849 | 2.044 | | | | | |

NIST TDE contains the correlations of $V_L$ and $C_{P,L}$ for only a few triglycerides within narrow temperature ranges. Thus, we use Halvorsen method[39] and Morad method[40] to estimate the $V_L$ and $C_{P,L}$ of triglycerides that are not included in NIST TDE. First, we compare the predictions of both methods with available experimental data. Table 3.7 shows that the two methods accurately predict $V_L$ and $C_{P,L}$, with average relative deviation (ARD) of only 0.65% and 2.72%, respectively. Next, we apply both methods to predict $V_L$ and $C_{P,L}$ of simple triglycerides that are not included in NIST TDE. Lastly, we regress the predicted values to identify the parameters of the NIST TDE Rackett equation and ThermoML equation for $V_L$, which can be incorporated into Aspen Plus or other process simulators. Table 3.8 gives the regressed parameters for $V_L$ and Table 3.9 lists those for $C_{P,L}$. Appendix B shows the NIST TDE Rackett equation and ThermoML equation.

Table 3.7 Comparison of predicted values of $V_L$ and $C_{P,L}$ by Halvorsen method[39] and Morad method[40] with experimental data.

| Property | Triglyceride | Number of Points | Temperature Range (K) | ARD (%) | Exp Data Source | Prediction Method |
|---|---|---|---|---|---|---|
| $V_L$ | C12:0, C14:0, C16:0, C18:1 | 27 | 283 ～ 573 | 0.65 | NIST TDE | Halvorsen[39] |
| $C_{P,L}$ | C12:0,C14:0, C16:0, C18:0, C18:1 | 70 | 314 ～ 453 | 2.72 | NIST TDE; Morad [38] | Morad[40] |

Table 3.8 Regressed parameters for estimating $V_L$ of triglycerides

| NIST TDE Rackett Equation ($m^3$/mol) | C12:0* | C14:0* | C16:0* | NIST TDE ThermoML Equation (kmol/$m^3$) | C18:0 | C18:1 | C18:2 | C20:0 | C22:0 |
|---|---|---|---|---|---|---|---|---|---|
| C1 | 0.2010909 | 0.1978334 | 0.1957933 | C1 | 1.22E+00 | 1.25E+00 | 1.27E+00 | 1.12E+00 | 1.03E+00 |
| C2 | 0.2857143 | 0.2857143 | 0.2857143 | C2 | -7.45E-04 | -7.73E-04 | -7.65E-04 | -6.58E-04 | -5.92E-04 |
| C3 | 819 | 828 | 834 | C3 | 2.79E-07 | 3.30E-07 | 2.95E-07 | 2.09E-07 | 1.65E-07 |
| C4 | 487709 | 417044.7 | 365772.1 | C4 | -5.21E-10 | -5.65E-10 | -5.44E-10 | -4.15E-10 | -3.41E-10 |
| C5 | 110 | 110 | 110 | C5 | 4 | 4 | 4 | 4 | 4 |
| C6 | 819 | 828 | 834 | C6 | 273.15 | 273.15 | 273.15 | 273.15 | 273.15 |
|  |  |  |  | C7 | 573.15 | 573.15 | 573.15 | 573.15 | 573.15 |

Table 3.9 Regressed parameters for estimating $C_{P,L}$ of triglycerides

| NIST TDE ThermoML Equation (J/kmol-K) | C12:0 | C14:0 | C16:0 | C18:0 | C18:1 | C18:2 |
|---|---|---|---|---|---|---|
| C1 | 7.8240E+05 | 9.0710E+05 | 1.0290E+06 | 1.2080E+06 | 1.1040E+06 | 1.0170E+06 |
| C2 | 1.5709E+03 | 1.7778E+03 | 1.9847E+03 | 2.1120E+03 | 2.1503E+03 | 2.1356E+03 |
| C3 | 2 | 2 | 2 | 2 | 2 | 2 |
| C4 | 313.15 | 313.15 | 313.15 | 313.15 | 313.15 | 313.15 |
| C5 | 453.15 | 453.15 | 453.15 | 453.15 | 453.15 | 453.15 |

### 3.4.3 Characterization of Feed Oil.

The complex structure of triglyceride makes it difficult to characterize the feed oil that contains mixed triglycerides. For example, Figure 3.9 shows a possible arrangement of triglyceride molecules of the lard[42] in which each square represents the fatty acid composition of a mixed triglyceride molecule.

| | | | | | | | | | | |
|---|---|---|---|---|---|---|---|---|---|---|
| C16:0<br>C18:0<br>C16:0 | C18:1<br>C18:1<br>C18:1 | C18:1<br>C16:0<br>C18:1 | C18:1<br>C18:1<br>C18:1 | C18:2<br>C18:1<br>C18:0 | C18:1<br>C16:0<br>C18:1 | C16:0<br>C16:0<br>C18:0 | C18:0<br>C18:1<br>C18:1 | C18:0<br>C16:0<br>C18:1 | C16:1<br>C18:1<br>C16:0 | C20:1<br>C18:1<br>C18:0 |
| C18:1<br>C18:0<br>C18:2 | C16:1<br>C16:0<br>C18:1 | C18:2<br>C16:0<br>C18:2 | C16:0<br>C16:0<br>C18:0 | C18:2<br>C18:1<br>C16:0 | C16:1<br>C16:0<br>C18:1 | C18:1<br>C18:2<br>C18:2 | C18:1<br>C14:0<br>C18:0 | C18:1<br>C16:0<br>C18:1 | C18:1<br>C16:0<br>C16:0 | C18:2<br>C18:1<br>C14:0 |
| C18:0<br>C18:0<br>C16:0 | C18:2<br>C16:0<br>C18:1 | C18:1<br>C18:2<br>C18:1 | C18:1<br>C18:0<br>C16:0 | C18:1<br>C18:1<br>C18:1 | C18:1<br>C16:0<br>C18:1 | C18:1<br>C18:1<br>C18:1 | C16:0<br>C16:0<br>C18:1 | C18:0<br>C18:0<br>C16:0 | C18:1<br>C16:0<br>C16:0 | C18:1<br>C18:1<br>C18:1 |

Figure 3.9 Possible profiles of the triglyceride molecules of the lard[42]

In Figure 3.10, we introduce three possible ways to characterize the feed oil, considering it as: (1) a mixture of mixed triglycerides, (2) a mixture of simple triglycerides, or (3) a pseudo-triglyceride. For the first scheme, Zong et al.[42] builds the feed oil by blending together the mixed triglycerides and estimates the thermophysical properties of each mixed triglyceride by a chemical constituent fragment-based method[42]. The fragment-based method divides the mixed triglyceride molecule into four fragments – glycerol fragment and three fatty acid fragments (see Figure 3.11 ) and obtains the contribution of each fragment by correlating the experimental data. The authors develop a property databank of 8 simple and 308 mixed triglycerides formed with 8 common saturated and unsaturated fatty acid fragments (C12:0, C14:0, C16:0, C18:0, C18:1, C18:2, C18:3, C20:0) for use in future versions of Aspen Plus. The properties include vapor pressure, enthalpy of vaporization, liquid heat capacity, enthalpy of formation, liquid molar volume, and liquid viscosity. For example, Zong et al.[42] develop Eq. (9)

to estimate heat of vaporization of mixed triglyceride. They correlate experimental data to obtain the contribution of each fragment, $\Delta H_{vap,i}$ which is linearly increasing with the carbon number of the fatty acid fragment (see Figure 3.12).

$$\Delta H_{vap} = N_{frag} \sum_{i}^{N_{frag}} x_i \times \Delta H_{vap,i} \qquad (9)$$

where $N_{frag}$ is the number of fragments in the mixed triglyceride molecule, $x_i$ is mole fraction of the fragment in the mixed triglyceride molecule, and $\Delta H_{vap,i}$ is the contribution of the fragment i. We note that the fragment-based method is applicable to characterize the feed oil as a mixture of simple triglycerides and as a pseudo-triglyceride molecule.

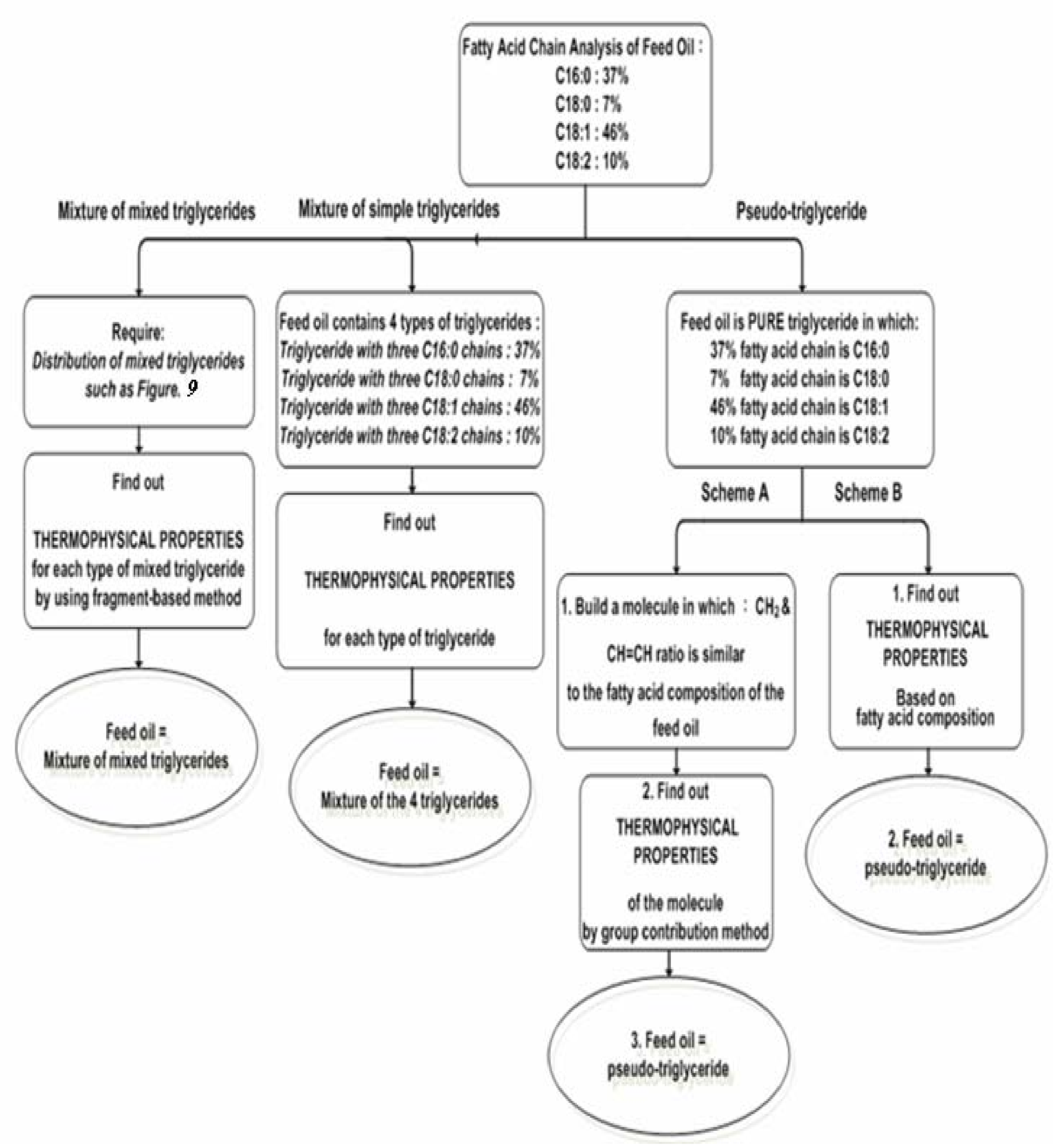

Figure 3.10 Three ways to characterize the feed oil

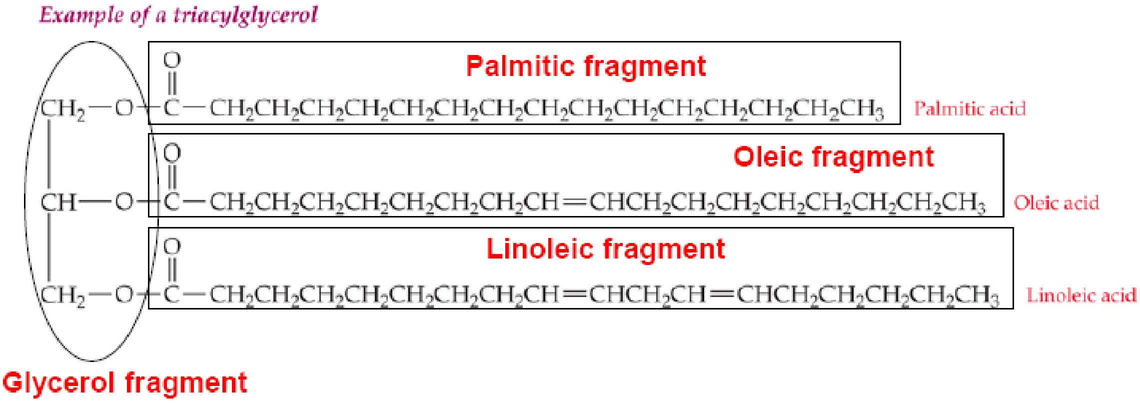

Figure 3.11 Four fragments of mixed triglyceride molecule[42]

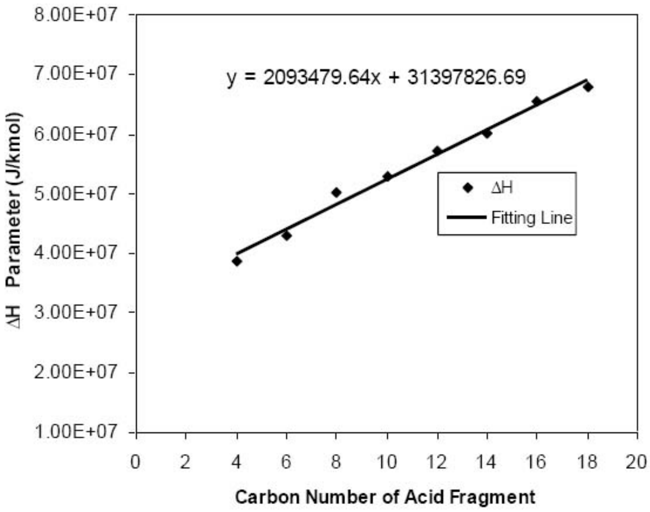

Figure 3.12 $\Delta H_{vap,i}$ vs. carbon number of the fatty acid fragment[42]

Siang et al.[45] model the phase behavior of palm oil by treating the oil as a mixture of simple triglycerides. They use Dohrn method[38] to estimate the critical properties of simple triglycerides and represent the feed oil by mixing the simple triglycerides based on the fatty acid composition. Both Ndiaye et al.[46] and Espinosa et al.[47] apply the pseudo-triglyceride scheme to represent the feed oil in their phase-equilibrium study. They estimate the critical properties by building a molecule that has a similar distribution of the functional groups to the feed oil (i.e. scheme A of pseudo-triglyceride in Figure 3.10). Scheme B of pseudo-triglyceride in Figure 3.10 is identical to the Halvorsen method[39] and Morad method[40] for characterizing the oil molecules. Halvorsen et al.[39] validate the method is good for density predictions of 14 vegetable oils and Morad et al.[40] validate the method is good for liquid heat capacity predictions of 2 vegetable oils and 6 mixed triglycerides. We show an example to demonstrate the scheme A of pseudo-triglyceride in Figure 3.10. Table 3.10 shows the fatty acid composition of a given vegetable oil[47].

Table 3.10 Composition of feed oil as an example for scheme A of pseudo-triglyceride in Figure 3.10

| Fatty acid | $x_i$ mol fraction | $n_i$ number of $CH_2$ group | $m_i$ number of CH= CH group |
|---|---|---|---|
| C16:0 | 0.067 | 42 | 0 |
| C18:0 | 0.0334 | 48 | 0 |
| C18:1 | 0.2583 | 42 | 3 |
| C18:2 | 0.6391 | 36 | 6 |
| C18:3 | 0.0022 | 30 | 9 |

We calculate the average numbers of $CH_2$ (n) and CH=CH (m) groups in the pseudo-triglyceride molecule as follows:

$$\begin{aligned} n &= \sum_i n_i \times x_i = 38.34 \approx 38 \\ m &= \sum_i m_i \times x_i = 4.63 \approx 5 \end{aligned} \tag{10}$$

Hence, we could represent the pseudo-triglyceride molecule with 38 $CH_2$ groups and 5 CH=CH groups in Figure 3.13 .

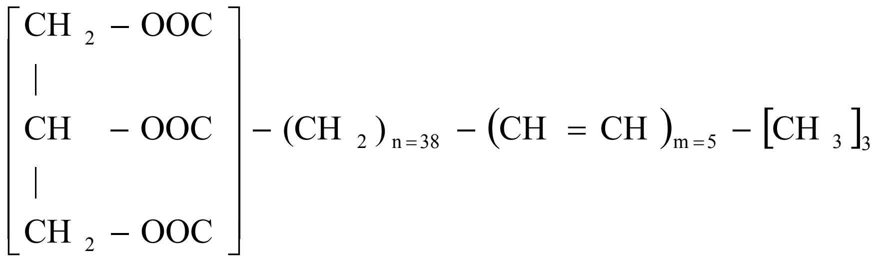

$$\begin{bmatrix} CH_2-OOC \\ | \\ CH\ \ -OOC \\ | \\ CH_2-OOC \end{bmatrix}-(CH_2)_{n=38}-\left(CH=CH\right)_{m=5}-\left[CH_3\right]_3$$

Figure 3.13 Molecular structure of pseudo-triglyceride molecule

The concepts of schemes A and B of pseudo-triglyceride are very similar. Both schemes generate the pseudo-triglyceride based on the fatty acid composition of the feed oil. However, the resulting properties are quite different. This follows because scheme A directly predicts feed oil properties from the high-molecular-weight pseudo-triglyceride, but scheme B estimates feed oil properties by mixing the properties of the pure fatty acids that comprise the feed oil.

### 3.4.4 **FAME**.

Unlike triglycerides, most of the thermophysical properties of the FAMEs are available in the literature and are also incorporated into NIST TDE. Table 3.11 lists the suggested values of $T_b$, $P_c$, $T_c$ and $\omega$ by NIST TDE. Appendix B.2 shows the NIST TDE equations and corresponding parameters for estimating $V_L$, $\triangle H_{vap}$, $P_{vap}$, $C_{P,G}$ and $C_{P,L}$ and Table 3.12 summarize the methods described in Appendix B.

Table 3.11 Suggested values of $T_b$, $P_c$, $T_c$ and $\omega$ of FAME by NIST TDE

| FAME | ω | Pc (Pa) | Tc (K) | $T_b$ (K) |
|---|---|---|---|---|
| C12:0 | 0.69301 | 1731893.8 | 712 | 540.49 |
| C14:0 | 0.9156 | 1412616.6 | 718 | 570.03 |
| C16:0 | 0.89195 | 1205875.1 | 749 | 600.92 |
| C16:1 | 1.0009 | 1279720.6 | 734 | 590.25 |

| | | | | |
|---|---|---|---|---|
| C18:0 | 0.98895 | 1178960.3 | 770 | 624.6 |
| C18:1 | 1.0014 | 1124670.6 | 761 | 618.5 |
| C18:2 | 0.91775 | 1162805.4 | 773 | 621.57 |
| C18:3 | 0.94097 | 1202626 | 774 | 621.8 |
| C20:0 | 1.1468 | 1036965.2 | 767 | 636.91 |
| C20:1 | 1.135 | 990081.9 | 767 | 635.77 |
| C22:0 | 1.3362 | 901920.5 | 785 | 663.99 |
| C22:1 | 1.1856 | 881791 | 784 | 657.94 |
| C24:0 | 1.2315 | 821191.6 | 804 | 680.28 |
| C24:1 | 1.2264 | 822329 | 802 | 678.5 |

Table 3.12 Available methods for $V_L$, $\triangle H_{vap}$, $P_{vap}$, $C_{P,G}$ and $C_{P,L}$ in NIST TDE

| Property | Method | Equation | Parameters |
|---|---|---|---|
| Molar volume | Rackett [33] | Eq. B.46 | Table B.8 |
| Heat of vaporization | Watson [33] | Eq. B.52 | Table B.14 |
| Vapor pressure | Wagner [33] | Eq. B.51 | Table B.13 |
| Gas heat capacity | Aly-Lee [33] | Eq. B.48 | Table B.10 |
| Liquid heat capacity | NIST TDE [32] | Eq.B.50 | Table B.12 |

## 3.5 Thermodynamic Model Selection.

For the alkali-catalyzed transesterification process, selecting the appropriate thermodynamic model plays an important role in modeling separation and purification units. Figure 3.1 shows that the typical separation and purification units include the methanol recovery process, water wash unit, purification of glycerol and biodiesel. The phase behavior between biodiesel fuel and other process components (methanol, water and glycerol) is important when modeling these processes. Because there are only limited experimental data of the biodiesel fuel systems in the literature, many of the alkali-catalyzed transesterification process models[4,5,6,7,8,9,10,11,12] use estimation methods to predict the phase behavior of the separation and purification units. Table 3.13 summarizes the available phase equilibrium data for the biodiesel fuel-methanol-water-glycerol system.

Table 3.13 Available phase equilibrium data of biodiesel fuel (BDF)-methanol-water-glycerol

| LLE | | | | | | |
|---|---|---|---|---|---|---|
| Components | | | | | | Data source |
| Methyl - octanoate | $H_2O$ | | | | | Kuramochi[48] |
| Methyl - palmitate | $H_2O$ | | | | | Kuramochi[48] |
| Methyl - oleate | $H_2O$ | | | | | Kuramochi[48] |
| Methyl - oleate | $H_2O$ | Methanol | Oleic acid | | | Chen[49] |
| Rapeseed Oil BDF | $H_2O$ | Methanol | | | | Stloukal[50] |
| Palm Oil BDF | $H_2O$ | Methanol | | Glycerol | | Di Felice[51] |
| Palm Oil BDF | | | | Glycerol | | Di Felice[51] |
| Methyl - oleate | | Methanol | | Glycerol | | Andreatta[52] |
| Soybean Oil BDF | | Methanol | | Glycerol | | Chiu[53] |
| Methyl - oleate | | Methanol | | Glycerol | | Negi[54] |
| Methyl - oleate | | | | Glycerol | Monoolein | Negi[54] |
| Canola Oil BDF | | Methanol | Oleic acid | | | Batista[55] |
| Soybean Oil BDF | | Methanol | | Glycerol | | Zhou[17] |
| VLE | | | | | | |
| Components | | | | | | Data source |
| Soybean Oil BDF | | Methanol | | | | Chiu[53] |
| | | Methanol | | Glycerol | | Chiu[53] |

Kuramochi et al.[48] review the selection of the predictive thermodynamic model for biodiesel fuel-methanol-water-glycerol system. They recommend both UNIFAC[56] and Dortmund UNIFAC[57] for the methanol recovery process, UNIFAC LLE[58] for the water wash unit, and Dortmund UNIFAC[57] for purification units. They also demonstrate the appropriate way to assign UNIFAC groups to FAME molecules. Table 3.14 lists the suggested assignment of UNIFAC groups by Kuramochi et al.[48].

Table 3.14 UNIFAC group assignment for FAME- methanol-water-glycerol system[48]

| | UNIFAC | Dortmund-UNIFAC | UNIFAC LLE |
|---|---|---|---|
| FAME | $CH_3$, $CH_2$, CH=CH,<br>$CH_2COO$ | $CH_3$, $CH_2$, CH=CH,<br>$CH_2COO$ | $CH_3$, $CH_2$, CH=CH,<br>$CH_2COO$ |
| Glycerol | $CH_3$, $CH_2$, OH | $CH_3$, $CH_2$, OH (P)*, OH (S)* | $CH_3$, $CH_2$, OH |
| Methanol | $CH_3OH$ | $CH_3OH$ | $CH_3$, OH (P)* |

* P and S indicate primary and secondary alcohol, respectively.

## 3.6 Fuel Qualities of FAME and Biodiesel Fuel.

We demonstrate how to estimate crucial biodiesel fuel qualities in this section. Table 3.15 lists the European standards for biodiesel, EN 14214, that specify important biodiesel fuel qualities. We choose the European standards because they are more stringent than the U. S. standards, ASTM 6751. This section focuses on the estimations of density, viscosity, and cetane number, for which experimental data are available for validation purposes. When experimental data for other fuel properties become available, we can develop additional validated property correlations and include them in our model.

Table 3.15 EN 14214 Standard of Biodiesel Fuel

| | EN 14214 |
|---|---|
| Density at 15℃ ($g/cm^3$) | 0.86 - 0.9 |
| Viscosity at 40℃ ($mm^2/s$) | 3.5 - 5 |
| Flash point (℃) | > 101 |
| Water content (ppmwt) | < 500 |
| Cetane number | > 51 |
| Methanol (wt%) | < 0.2 |
| Ester (wt%) | > 96.5 |
| Monoglyceride (wt%) | < 0.8 |
| Diglyceride (wt%) | < 0.2 |
| Triglyceride (wt%) | < 0.4 |

### 3.6.1 Density.

The biodiesel fuel is the mixture of FAMEs. We apply the method of Spencer and Danner[33] which is the default method in Aspen Plus V 7.0 to estimate the density of biodiesel fuel. The equations are listed below.

$$V_L^{mix} = R\frac{T_c}{P_c}\left(Z_{RA,m}\right)^{\left[1+(1-\frac{T}{T_{cm}})^{2/7}\right]} \tag{11}$$

$$\frac{T_c}{P_c} = \sum_i x_i \frac{T_{ci}}{P_{ci}} \tag{12}$$

$$Z_{RA,m} = \sum_i x_i Z_{RA,i} \tag{13}$$

$$T_{cm} = \sum_i \sum_j x_i x_j V_{ci} V_{cj} \left(T_{ci} T_{cj}\right)^{1/2} \left(1 - k_{ij}\right) / V_{cm}^2 \tag{14}$$

$$V_{cm} = \sum_i x_i V_{ci} \tag{15}$$

$$\left(1 - k_{ij}\right) = \frac{8\left(V_{ci} V_{cj}\right)^{1/2}}{\left(V_{ci}^{1/3} + V_{cj}^{1/3}\right)^3} \tag{16}$$

where $T_{ci}$, $P_{ci}$, $V_{ci}$, $Z_{RA,i}$, and $x_i$ are critical temperature, pressure, volume, Rackett parameter, and molar fraction of pure FAME, respectively. Table 3.11 lists the values of $T_c$ and $P_c$ of pure FAME and Table 3.16 shows $V_c$ and $Z_{RA}$ values suggested by NIST TDE. We validate the method with 31 experimental data points and show the results in Figure 3.14. Apparently, the method tends to underestimate the densities, but the predictions are still fairly accurate with an ARD of only 1.01%.

Table 3.16 Suggested values of critical volume and $Z_{RA}$ by NIST TDE

| FAME | $V_c$ ($cm^3/mol$) | $Z_{RA}$ |
|---|---|---|
| C12:0 | 842.02 | 0.2446 |
| C14:0 | 1015.2 | 0.2354 |
| C16:0 | 1129.35 | 0.2228 |
| C16:1 | 949.4 | 0.2072 |
| C18:0 | 1268.1 | 0.2298 |
| C18:1 | 1237.7 | 0.2225 |
| C18:2 | 1208.5 | 0.2226 |
| C18:3 | 1184.7 | 0.2243 |
| C20:0 | 1268.9 | 0.1967 |
| C20:1 | 1195.3 | 0.2138 |
| C22:0 | 1254.7 | 0.1841 |
| C22:1 | 1539.9 | 0.2123 |
| C24:0 | 1398.6 | 0.1833 |
| C24:1 | 1413.1 | 0.2011 |

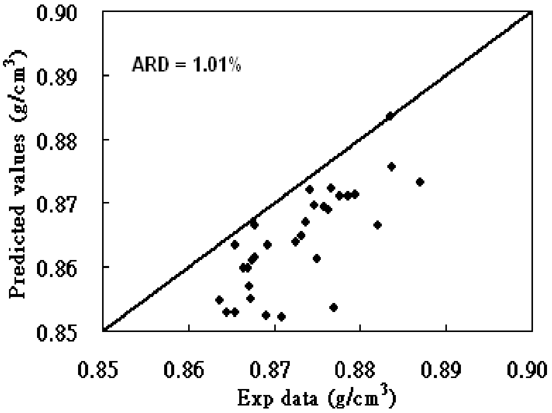

Figure 3.14 Density estimation of biodiesel fuel by using Spencer and Danner[33] method (experimental data from ref. 59,60,61)

### 3.6.2 Viscosity

Viscosity at 40℃ is an important property to evaluate the flow ability of biodiesel fuel. Allen et al.[62] and Krisnangkura et al.[63] apply the following mixing rule to predict the viscosity of biodiesel fuel:

$$\ln\mu_m = \sum_x x_i \ln\mu_i \tag{17}$$

where $\mu_i$ is the viscosity and $x_i$ is mass fraction of pure FAME. Figure 3.15 shows the viscosity at 40℃ of FAMEs from the literature[32, 62]. There are no experimental viscosities of C20:0, C20:1, C22:1, C24:0, and C24:1 FAMEs. Thus, it is not feasible to use Eq. (17) to predict viscosity of biodiesel fuel which is composed of the FAMEs mentioned above.

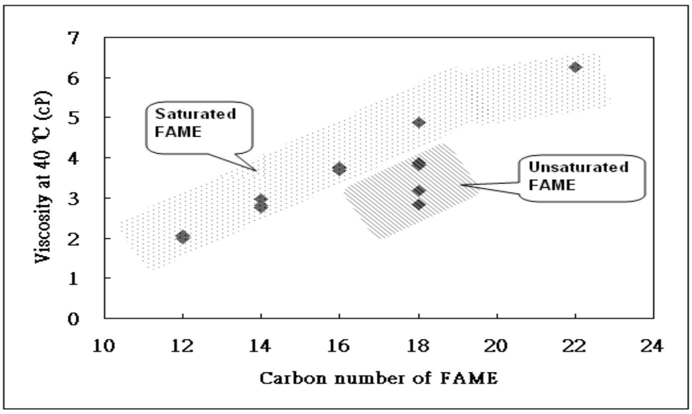

Figure 3.15 Viscosity at 40 ℃ of FAME (data source: ref. 32,62)

In order to obtain a correlation that is independent of viscosity of pure FAME, we first develop Eq. (18), based on the number of carbon atoms ($N_c$) and the number of double bonds ($N_{DB}$) of pure FAME. Figure 3.16 shows the viscosity of pure FAME predicted by Eq. (18) and the ARD is 3.51% for 20 experimental data points.

$$\mu\,(\text{cP})\text{ at }313.15\text{K} = 0.433 \times N_c - 0.699 \times N_{DB} - 3.648 \tag{18}$$

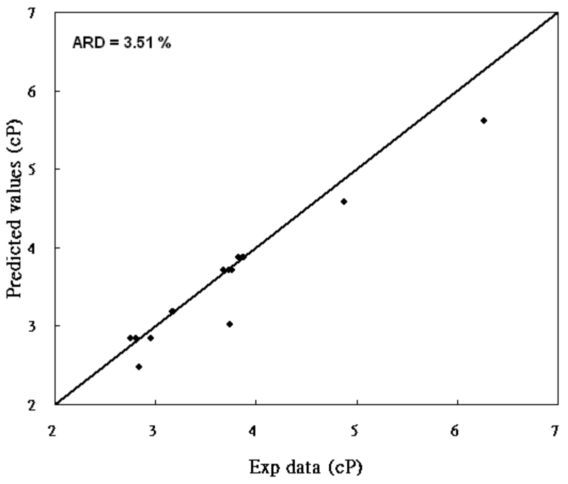

Figure 3.16 Prediction of viscosity at 40℃ of pure FAME by Eq. (18) (data source: ref. 32,62)

We apply Eq. (18) to predict viscosity at 40℃ of biodiesel fuel by its average number of carbon atoms and average number of double bonds. For reported data of kinematic viscosity, we convert them into dynamic viscosity through density estimated by the method mentioned in Section 6.1. Figure 3.17 shows the validated results of viscosity at 40℃ of biodiesel fuel with 60 experimental data points and the ARD is 13.97%. The larger deviation results from the fact that the reported data contain a relatively large variation (see Figure 3.18 ). The reported data do not follow the monotonic trend suggested by Eq. (18). We need more reliable experimental data that contain pure FAMEs and biodiesel fuel to improve the prediction accuracy.

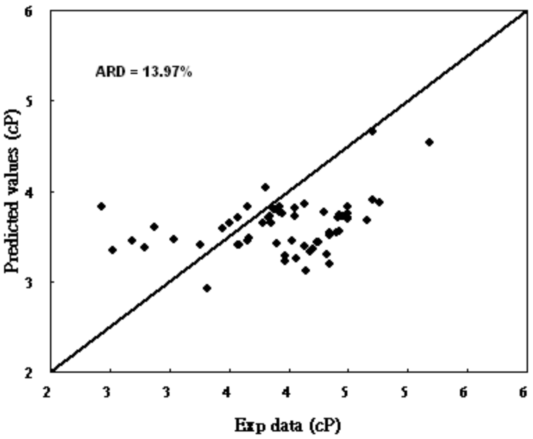

Figure 3.17 Validation of viscosity at 40℃ prediction of biodiesel fuel by Eq. (18)

(data source: ref. 15,59,60,61,62,63,64,65,66,67)

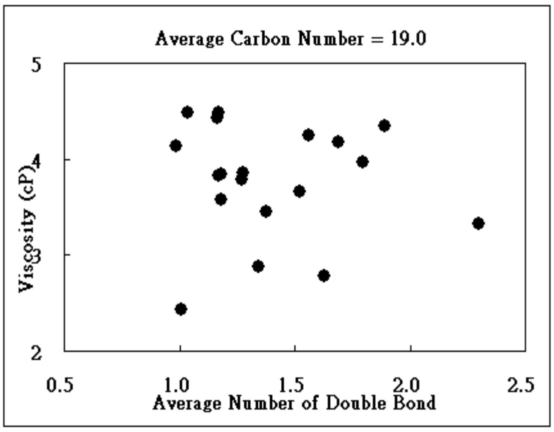

Figure 3.18 Variation of the reported viscosity data

### 3.6.3 Cetane Number.

Cetane number (CN) represents biodiesel's ignition quality under compression ignition conditions. Clements[68] demonstrates that the simple mixing rule, Eq. (19), is able to predict the CN of biodiesel fuel.

$$\text{CN of BDF} = \sum_i x_i \text{CN}_{\text{FAME}} \tag{19}$$

where $x_i$ is weight fraction of FAME and $CN_{FAME}$ is the CN of pure FAME. Figure 3.19 shows the CN of FAMEs in the literature[69,70,71,72,73,74]. There is no experimental CN of C20:0, C20:1, C22:0, C24:0, and C24:1 FAMEs. Thus, it is not possible to use Eq. (19) to predict CN of biodiesel fuel which is composed of the FAMEs mentioned above.

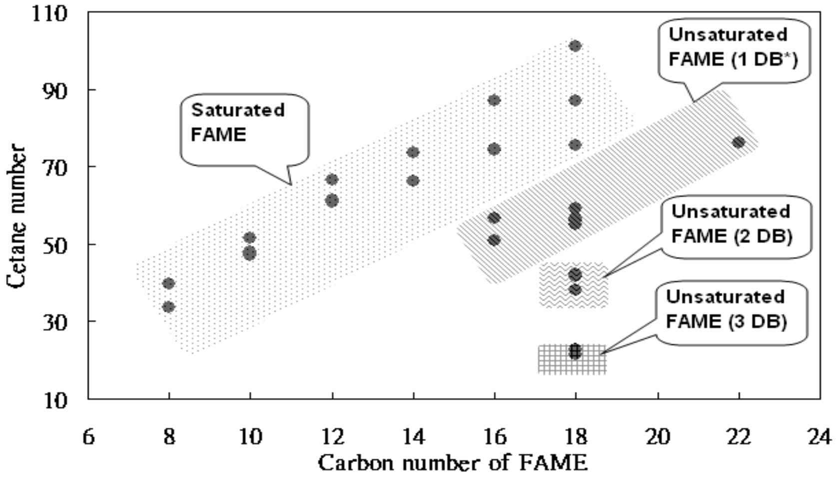

Figure 3.19 Cetane number of FAME (DB = double bond)

In order to obtain a correlation that is independent of CN of pure FAME, we first develop Eq. (20), based on the number of carbon atoms ($N_c$) and the number of double bonds ($N_{DB}$) of pure FAME. Figure 3.20 shows the CN of pure FAME predicted by Eq. (20) and the ARD is 6.78% for 30 experimental data points.

$$CN = 4.201 \times N_c - 20.077 \times N_{DB} + 2.005 \tag{20}$$

We apply Eq. (20) to predict CN of biodiesel fuel by its average number of carbon atoms and average number of double bonds. Figure 3.21 shows the validated results of CN of biodiesel fuel with 31 experimental data points and the ARD is 7.43%.

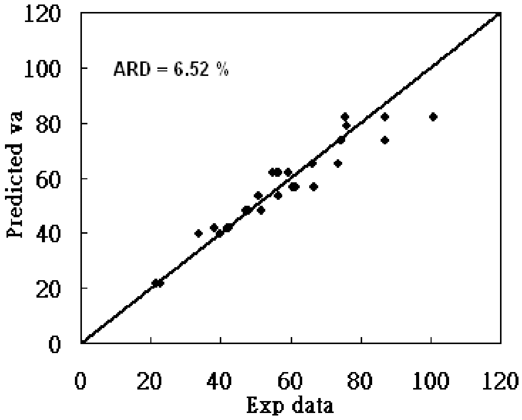

Figure 3.20 Prediction of CN of pure FAME by Eq. (20)

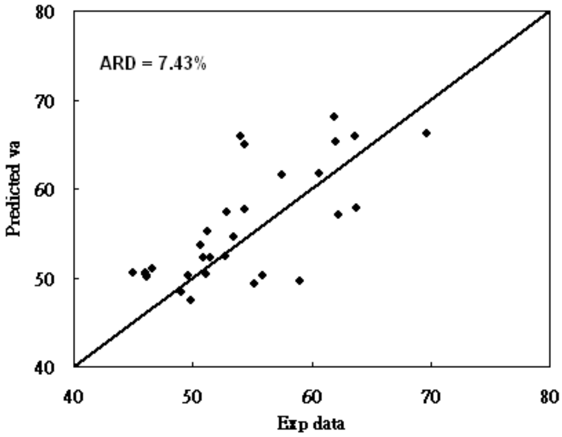

Figure 3.21 Validation of CN prediction of biodiesel fuel by Eq. (20)

(Exp data from ref. 15,66,68,72,74,75,76,77,78,79,80)

### 3.7 Rigorous Model of Alkali-catalyzed Transesterification Process.

This section demonstrates the development of an integrated model that considers feed and product oil characterization, rigorous reaction kinetics, thermophysical property modeling, phase equilibrium, separation and purification, and product quality estimation. We use Aspen Plus V 7.0 and spreadsheet program to develop the rigorous model with the biodiesel production of 25 tons/day.

### 3.7.1 Selection of Feed Oil Characterization Method.

We summarize different characterization methods of feed oil in section 4.3 and it is crucial to select the appropriate characterization method that satisfies two criteria: 1. easy to use. 2. rigorous characterization of feed oil. 3. satisfactory predictions on the required thermophysical properties. Characterizing the feed oil as a pseudo-triglyceride is the easiest one and as a mixture of mixed triglycerides is the most rigorous one. And then, we compare the property predictions of these two extreme methods to justify which one has higher accuracy. There are limited experimental data of critical property, acentric factor, normal boiling point and ideal gas heat capacity of vegetable oils available in the literature. We compare the predictions of vapor pressure, heat of vaporization and density of vegetable oils and Table 3.17 shows the property methods that we apply in both characterization methods.

Table 3.17 Property methods for comparing the two characterization methods

| | Pseudo-triglyceride | Mixture of mixed triglycerides |
|---|---|---|
| $\triangle H_{vap}$ | Zong et al.[42] | |
| Vapor Pressure | Zong et al.[42] | |
| Density | Halvorsen method[39] | Zong et al.[42] |

Figure 3.22 to Figure 3.26 show that the two characterization methods give equally satisfactory property predictions. Therefore, the selection is seeking for the balance between accounting all species/reactions (mixture of mixed triglycerides) and the simplest possible model that provides good engineering approximation (pseudo-triglyceride) rather than the “perfect” solution in every aspect. With established databank, it is convenient to conduct “mixture of mixed triglycerides” approach which rigorously represents feed oil as real mixture of triglycerides. In the other hand,

"pseudo-triglyceride" approach always requires estimation of thermophysical properties. Even for the same feed oil type, the biomass contents vary with growth conditions and geography. Because we are not aware of any established databank and most of the literature report only composition of the feed oil only by its fatty acid distribution (e.g., Table 3.3 ), instead of detail mixed triglyceride compositions; we choose the pseudo-triglyceride scheme to characterize the feed oil in the model. However, "mixture of mixed triglycerides" approach is still recommended when databank or detail mixed triglyceride compositions is available.

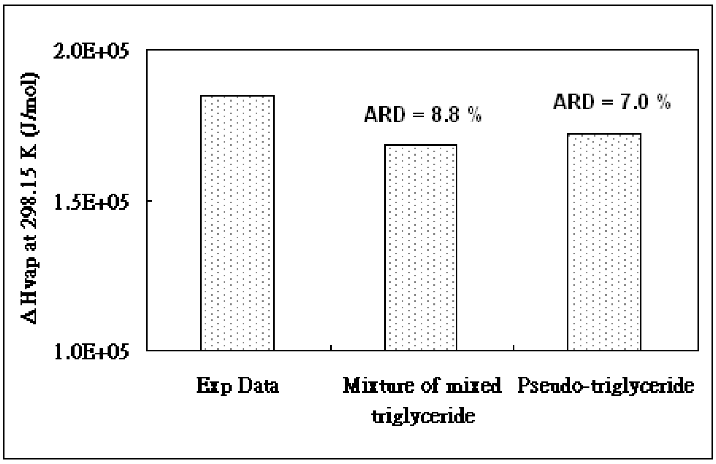

Figure 3.22 Comparison of $\Delta H_{vap}$ prediction by different characterization methods

(data source: ref. 42)

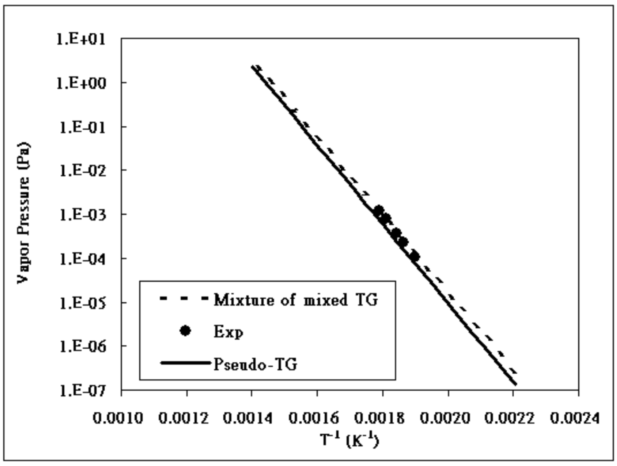

Figure 3.23 Comparison of $P_{vap}$ prediction by different feed oil characterization methods

(data source: ref. 42)

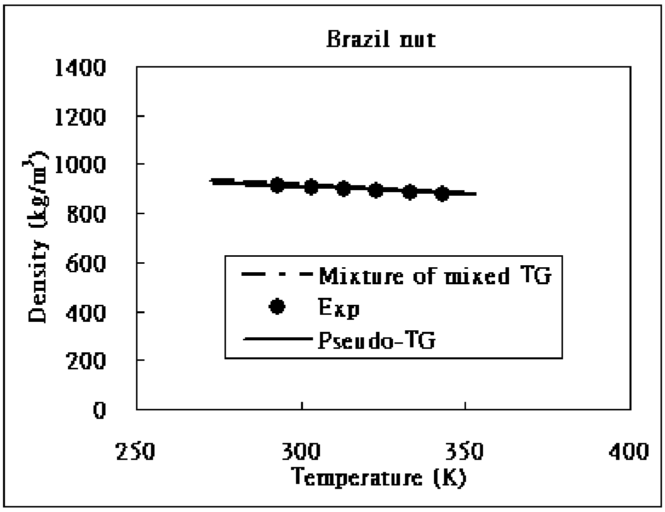

Figure 3.24 Comparison of density prediction by different feed oil characterization methods

(Brazil nut oil, data source: ref.42)

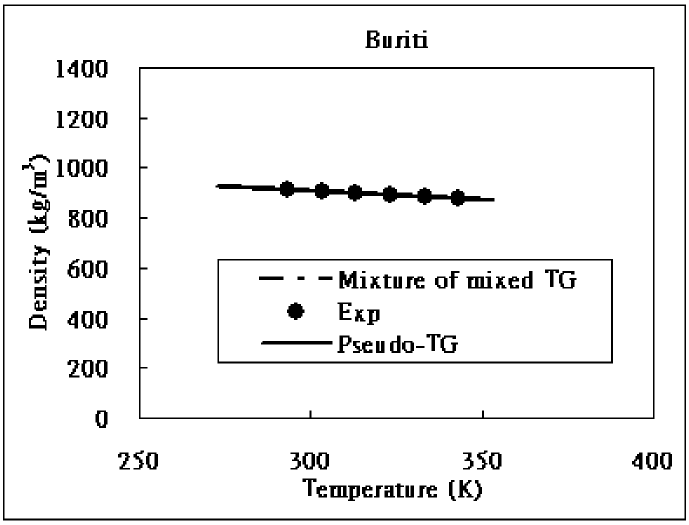

Figure 3.25 Comparison of density prediction by different feed oil characterization methods

(Buriti oil, data source: ref.42)

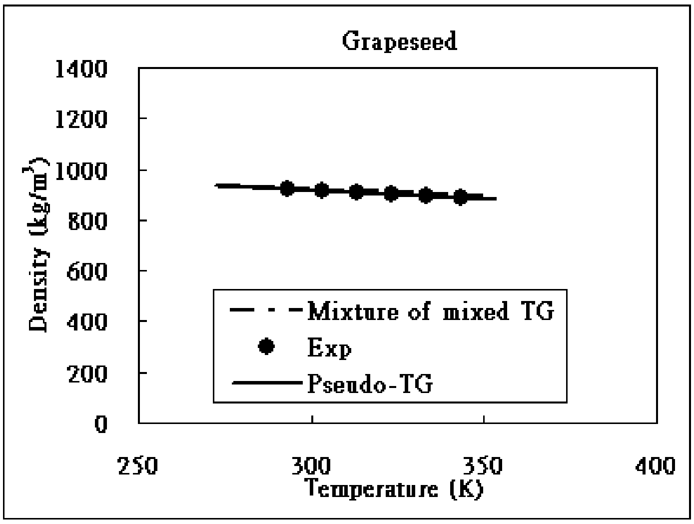

Figure 3.26 Comparison of density prediction by different feed oil characterization methods

(Grape seed oil, data source: ref.42)

### 3.7.2 Modeling Methodology.

Figure 3.27 represents our rigorous modeling methodology. The lumper (a spreadsheet) generates the structure and thermophysical properties of the pseudo-triglyceride molecule according to the fatty acid chain distribution of the feed oil. The reactor model considers rigorous reaction kinetics in which the pseudo-triglyceride reacts with methanol to give the pseudo-FAME, pseudo-DG and pseudo-MG. (refer to Figure 3.4 for the reaction scheme). The delumper (a FORTRAN block) converts the pseudo-FAME molecule into a mixture of FAMEs (biodiesel fuel) by assuming the fatty acid chain distribution of the mixture of FAMEs is the same to feed oil[30,31]. We use Dortmund UNIFAC[57] for methanol recovery and purification units, and UNIFAC LLE[58] for the water wash unit. Based on the composition of the biodiesel fuel, the product quality calculator predicts the crucial qualities of the biodiesel fuel such as specific gravity, cetane number and viscosity. Figure 3.28 shows our rigorous model in Aspen Plus combined with a spreadsheet program and FORTRAN blocks in Aspen Plus.

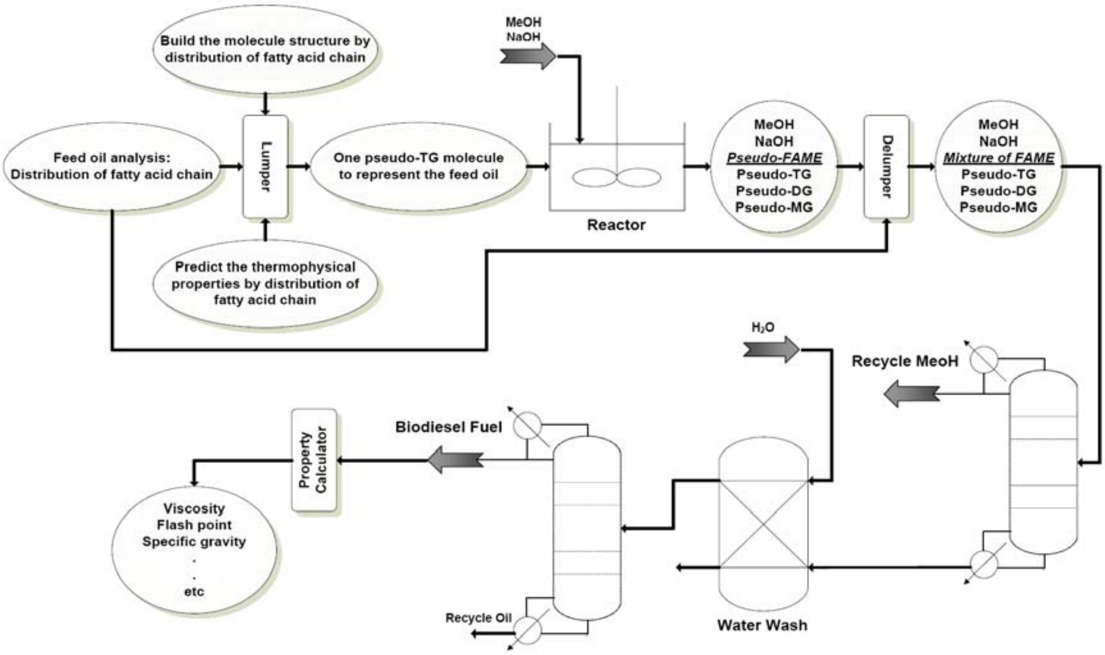

Figure 3.27 Methodology of the rigorous model

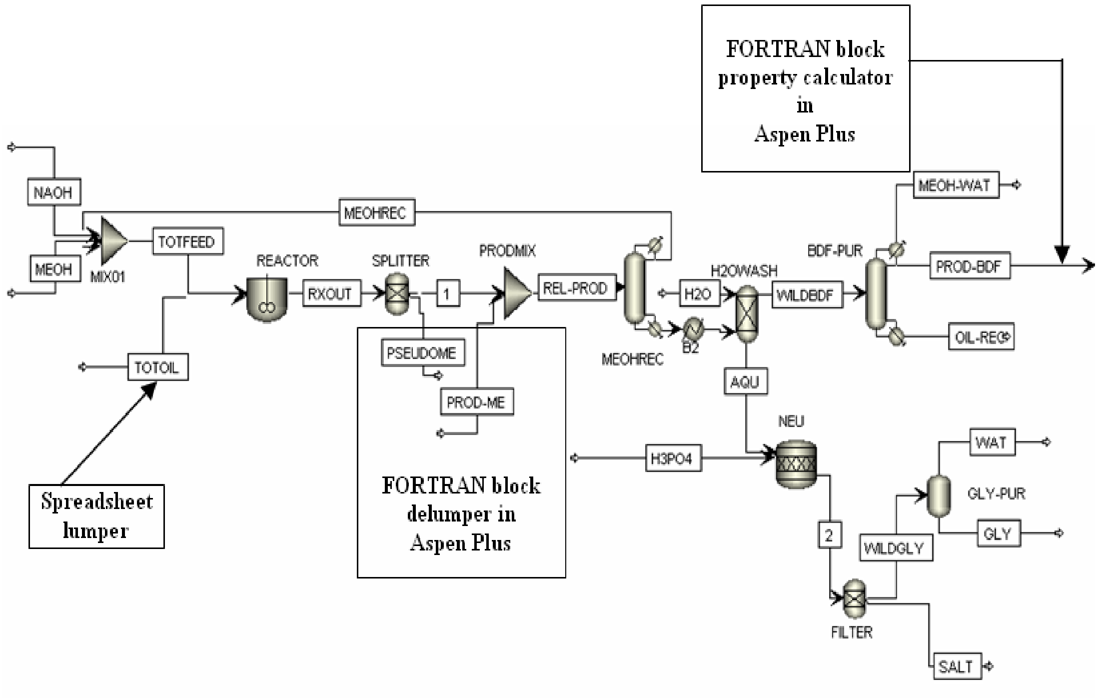

Figure 3.28 The process model of the alkali-catalyzed transesterification process in Aspen Plus

### 3.7.3 Lumper/Delumper.

We apply the lumper and delumper to incorporate the pseudo-components into the simulation model. The lumper generates the pseudo-triglyceride, pseudo-diglyceride, pseudo-monoglyceride and pseudo-FAME molecules that assemble the rigorous reaction kinetics. The delumper converts the pseudo-FAME from the reactor model output into a mixture of FAMEs, the biodiesel fuel. For our example, we assume the feed oil with its composition given in Table 3.10 and Figure 3.13 shows the resulting pseudo-TG. Figure 3.29 to Figure 3.31 represent the corresponding pseudo-DG, pseudo-MG and pseudo-FAME, respectively.

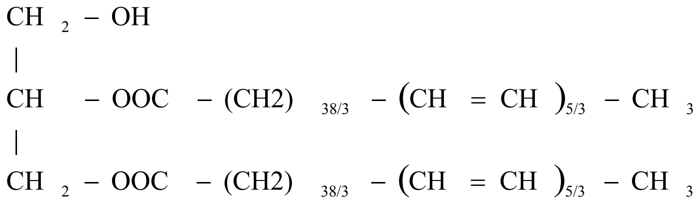

$$\begin{array}{l} CH_2 - OH \\ | \\ CH - OOC - (CH2)_{38/3} - (CH = CH)_{5/3} - CH_3 \\ | \\ CH_2 - OOC - (CH2)_{38/3} - (CH = CH)_{5/3} - CH_3 \end{array}$$

Figure 3.29 The structure of pseudo-DG in our example

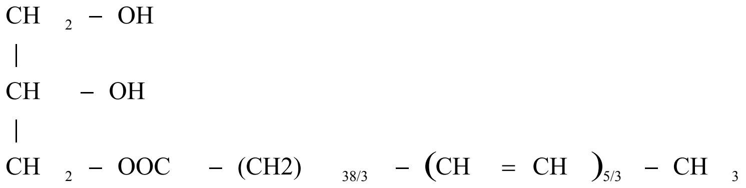

$$\begin{array}{l} CH_2 - OH \\ | \\ CH - OH \\ | \\ CH_2 - OOC - (CH2)_{38/3} - (CH = CH)_{5/3} - CH_3 \end{array}$$

Figure 3.30 The structure of pseudo-MG in our example

$$CH_3 - OOC - (CH2)_{38/3} - (CH = CH)_{5/3} - CH_3$$

Figure 3.31 The structure of pseudo-FAME in our example

Table 3.18 lists the required thermophysical properties and corresponding estimation methods to generate the pseudo-components in the lumper. Sections 3.4.3, 3.6.1 and Appendix B give details of the cited methods. In addition, we assume that the mass densities of the pseudo-DG and pseudo-MG molecules are identical to that of pseudo-TG molecules.

Table 3.18 Required thermophysical properties and corresponding estimation methods for pseudo-components

| | Pseudo-TG | Pseudo-DG | Pseudo-MG | Pseudo-FAME |
|---|---|---|---|---|
| Structure | The method of pseudo-triglyceride A[47] | | | |
| MW | The method of pseudo-triglyceride A[47] | | | |
| $T_b$ | C-G group contribution method based on the built structure[33] | | | |

| | | |
|---|---|---|
| $T_c$ | C-G group contribution method based on the built structure[33] | |
| $P_c$ | C-G group contribution method based on the built structure[33] | |
| $\omega$ | C-G group contribution method based on the built structure[33] | |
| $\triangle H_{vap}$ | Zong et al.[42*] | Vetere method[33**] |
| Density | Halvorsen method[39] | Li's extended Rackett equation[33] |
| $C_{P,G}$ | Rihani group contribution method[81] | |
| Vapor Pressure | Zong et al.[42] | Ambrose method[33] |

* Zong et al.[42] for $\triangle H_{vap}$ at 298.15K and Watson relation for extending to different temperature range. ** Vetere method[33] for $\triangle H_{vap}$ at normal boiling point and Watson relation for extending to different temperature range.

### 3.7.4 **Rigorous Reactor Model**.

We apply the kinetic scheme of Vicente et al.[26] in our rigorous reactor rating model (refer to Table 3.5 for kinetic parameters) and Table 3.19 lists the specification in the model. By the rigorous model, we are able to evaluate how the operating variables affect reactor performances such as catalyst concentration vs. conversion, and residence time vs. reactor volume. For example, Figure 3.32 shows how catalyst concentration affects the conversion. The catalyst is able to accelerate the reaction and increase the conversion under the same residence time. Figure 3.33 represents the relationships among conversion, reactor volume and residence time. As the residence time increases, both of the conversion and reactor volume also increase. These examples show that the rigorous reactor model can help us determine the optimal operating conditions for both existing and new processes.

Table 3.19 Specifications of reactor model

| Specification | Value | Unit |
|---|---|---|
| Reactor temperature | 60 | ℃ |
| Reactor pressure | 4 | Bar |
| Residence time | 60 | Minute |

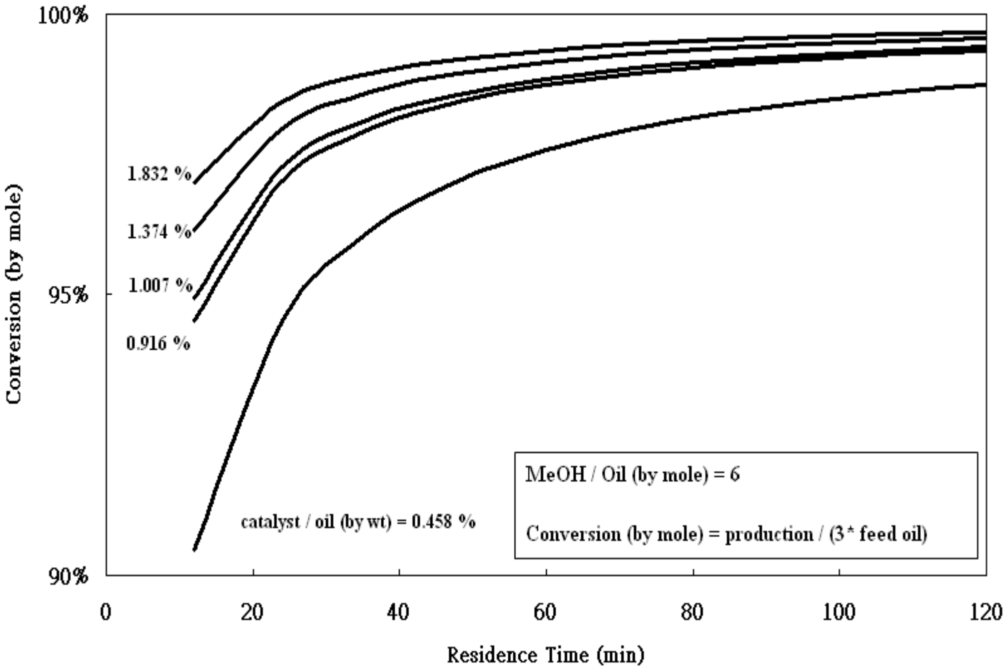

Figure 3.32 The effects of catalyst concentration on conversion

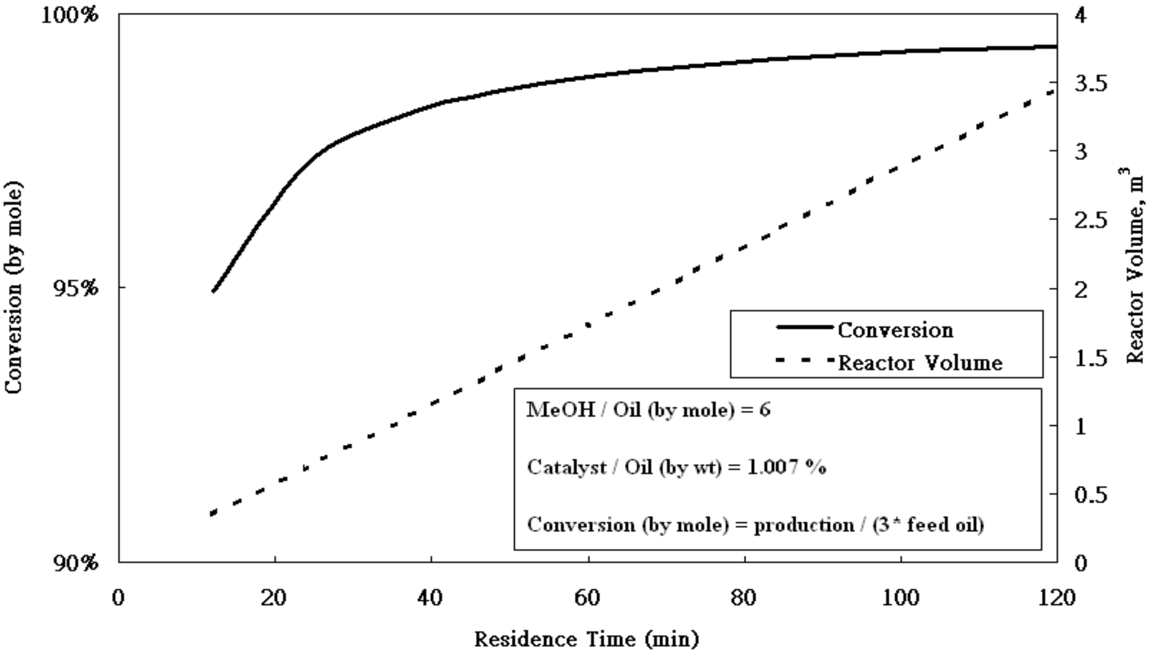

Figure 3.33 The relationships among conversion, reactor volume and residence time

### 3.7.5 Separation and Purification Units.

We apply rigorous thermodynamic models to simulate most of the separation and purification units. As noted in section 5, we use Dortmund UNIFAC[57] to model the methanol recovery column, biodiesel fuel purification column and glycerol purification unit and UNIFAC LLE[58] for water wash unit. Table 3.20 shows the assignments of UNIFAC groups for pseudo-components. For the neutralization unit, we assume that sodium hydroxide is entirely reacted with the phosphoric acid into salt, $Na_3PO_4$, and 100% separation efficiency for the salt filter. Table 3.21 lists the specifications of the separation and purification units in the model.

Table 3.20 Assignments of Dortmund UNIFAC and UNIFAC-LLE groups for pseudo-components

| | Pseudo-TG | Pseudo-DG | Pseudo-MG | Pseudo-FAME |
|---|---|---|---|---|
| CH | 1 | 1 | 1 | 0 |
| $CH_2$ | 37 | 25.33333333 | 13.66666667 | 11.66666667 |
| $CH_3$ | 3 | 2 | 1 | 2 |
| CH=CH | 5 | 3.333333333 | 1.666666667 | 1.666666667 |
| $CH_2COO$ | 3 | 2 | 1 | 1 |
| OH_P | 0 | 1 | 1 | 0 |
| OH_S | 0 | 0 | 1 | 0 |

Table 3.21 Specifications of the separation and purification units

| Methanol recovery column | | |
|---|---|---|
| Specification | Value | Unit |
| Number of theoretical stages | 7 | |
| Feed stage | 4 | |
| Reflux ratio | 2 | By mass |

| | | |
|---|---|---|
| Methanol recovery | 0.94 | By mass |
| Top pressure | 0.2 | Bar |
| Pressure drop | 0 | Bar |
| Water wash column | | |
| Specification | Value | Unit |
| Number of theoretical stages | 6 | |
| Top pressure | 1 | Bar |
| Pressure drop | 0 | Bar |
| Biodiesel fuel purification column | | |
| Number of theoretical stages | 6 | |
| Feed stage | 4 | |
| Bottom rate | 40 | kg/hr |
| Water in BDF | < 400 | ppmwt |
| Top pressure | 0.1 | Bar |
| Bottom pressure | 0.2 | Bar |
| Neutralization reactor | | |
| Specification | Value | Unit |
| Conversion | 100 | % |
| Reactor temperature | 50 | ℃ |
| Reactor pressure | 1.1 | Bar |
| Glycerol purification unit | | |
| Specification | Value | Unit |
| Drum temperature | 130 | ℃ |
| Drum pressure | 0.5 | Bar |

### 3.7.6 Product Quality Calculator.

The model integrates FORTRAN block with Aspen Plus to predict density, viscosity, and cetane number. Section 3.6 demonstrates the estimation methods of product qualities in the model. We normalize the composition of biodiesel fuel by its fatty acid ester distribution. This simplification has little effect on the calculation of product qualities because the purified biodiesel fuel contains at least 96.5 wt% fatty acid ester.

### 3.7.7 Model Results.

Our results show that the product meets most of the biodiesel fuel specifications except for cetane number. This follows because the biodiesel qualities highly depend on the feed oil composition at high conversion and the feed oil contains more triglycerides with unsaturated fatty acid chains (refer to Table 3.10 for feed oil composition). In the following section, we will demonstrate how to apply the model to optimize the qualities of biodiesel fuel. Additionally, purified biodiesel fuel and glycerol are susceptible to thermal decompose above 250℃ and 150℃[4,6], respectively. Our model gives reasonable temperatures of purified PROD-BDF and GLY streams, 118.4 ℃ and 130 ℃. In sum, the model is able to predict reactor and separator performance, stream conditions, product compositions, and product qualities.

Table 3.22 Model results of biodiesel fuel qualities

| | Model results | EN 14214 |
|---|---|---|
| Density at 15℃ (g/cm$^3$) | 0.883 | 0.86 - 0.9 |
| Viscosity at 40℃ (mm$^2$/s) | 3.89 | 3.5 – 5 |
| Water content (ppmwt) | 400 | < 500 |
| Cetane number | 50.28 | > 51 |
| Methanol (wt%) | 0 | < 0.2 |
| Ester (wt%) | 99.96 | > 96.5 |
| Monoglyceride (wt%) | 9.5 ppmwt | < 0.8 |
| Diglyceride (wt%) | 0 | < 0.2 |
| Triglyceride (wt%) | 0 | < 0.4 |

### 3.7.8 Model Application to Product Design: Feed Oil Selection.

The biodiesel quality highly depends on the feed oil composition at high conversion and the operating conditions have only minor effect on process performance and product quality. Thus, we apply seven kinds of vegetable oils in our Aspen Plus simulations (palm, olive, soybean, sunflower, grape, almond and corn whose compositions listed in Table 3.3 ) to illustrate the optimization of biodiesel quality through feed oil selection that has not been reported in the literature. To quanlify the effect of feed oil selection, we define the degree of unsaturation, DB/$N_c$, as the ratio of average number of double bonds (DB) in the feed oil to the average number of carbons ($N_c$) in the feed oil. Figure 3.34 shows the effect of DB/$N_c$ of feed oil on the viscosity and cetane number of biodiesel products, and Table 3.23 gives the structure information of different feed oils. Significantly, both viscosity and cetane number decrease with increasing DB/$N_c$ which is consistent with the trends observed from reported experimental data[15,59] (see Figure 3.35 and Figure 3.36). This implies that more unsaturated bonds of feed oil lead to smaller viscosity and cetane number of biodiesel fuel. The model is able to help engineers choose the appropriate feed oil for biodiesel product design. For example, we narrow the targeted cetane number to 56 or above, and there are four candidates – palm, olive, almond and corn oil. We further restrict the maximum kinematic viscosity to 4.3 mm$^2$/s and the corn oil is the only option to meet our specifications.

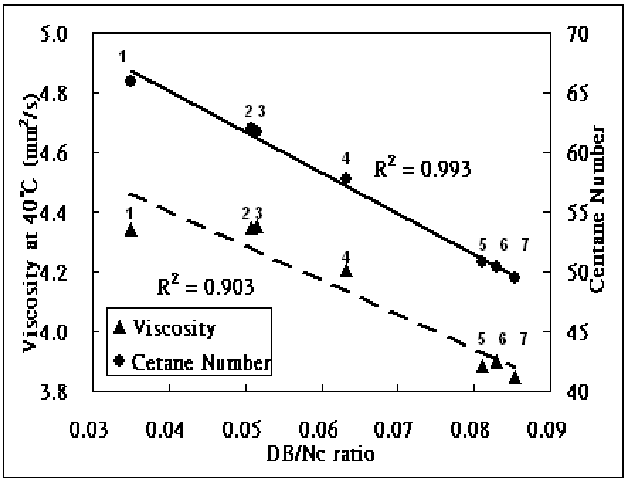

Figure 3.34 The effect of the degree of unsaturation, DB/Nc, of feed oil on product qualities

Table 3.23 Structure information of the seven kinds of feed oil in model applications

| | 1. Palm | 2. Olive | 3. Almond | 4. Corn | 5. Soybean | 6. Sunflower | 7. Grapeseed |
|---|---|---|---|---|---|---|---|
| n | 40.77 | 40.58 | 40.58 | 39.51 | 37.28 | 37.36 | 37.04 |
| m | 1.88 | 2.80 | 2.85 | 3.51 | 4.49 | 4.61 | 4.74 |
| $DB/N_c$ | 0.035 | 0.051 | 0.052 | 0.063 | 0.081 | 0.083 | 0.085 |

* Refer to Figure 3.13 for the definitions of n and m and the structure of pseudo-triglyceride

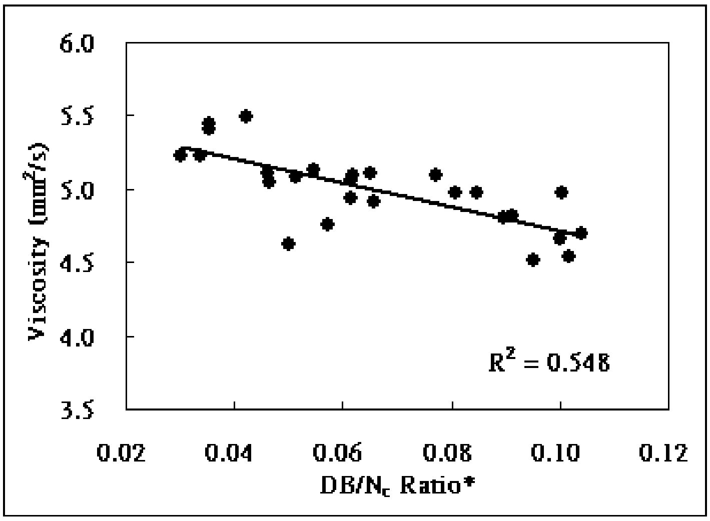

Figure 3.35 Monotonic trend between viscosity and $DB/N_c$ observed from reported data[59] (* $DB/N_c$ of biodiesel)

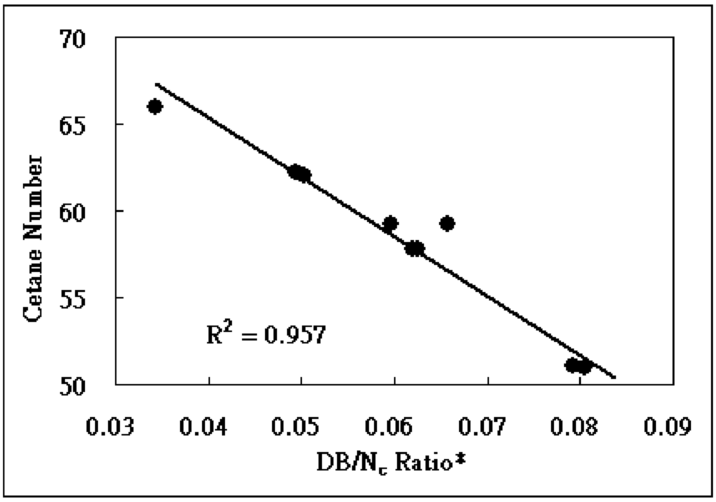

Figure 3.36 Monotonic trend between cetane number and DB/$N_c$ observed from reported data[15]

(* DB/$N_c$ of biodiesel)

### 3.8 Conclusion.

The goal of this paper is to demonstrate a methodology for the integrated process modeling and product design of an entire biodiesel manufacturing train by an alkali-catalyzed transesterification of triglyceride with methanol. To achieve this goal, we first present a comprehensive review of published literature and focus on feed oil characterization, thermophysical property modeling, rigorous reaction kinetics, phase equilibrium for separation and purification units, and prediction of essential biodiesel fuel qualities.

Among these topics, reaction kinetics is the best understood. However, there are significant deficiencies of thermophysical property modeling of triglyceride, diglyceride, and monoglyceride that obstruct the characterization of the feed oil and the development of the reactor model. Thus, we characterize the feed oil and product as a single pseudo-triglyceride through a "lumper" spreadsheet, and generate their essential thermophysical property. We develop the reactor rating model based on rigorous kinetics of reacting the pseudo-triglyceride with methanol to produce pseudo-diglyceride (DG), pseudo-monoglyceride (MG) and pseudo-FAME. We then convert the reactor output of pseudo-FAME molecules into a mixture of FAMEs. i.e., biodiesel, through a FORTRAN block, called a “delumper”. Additionally, there are only limited studies of the phase equilibrium of the biodiesel fuel-methanol-water-glycerol system that is important for the simulation of separation and purification units. We apply Dortmund UNIFAC[57] and UNIFAC LLE[58] to simulate the separation and purification units. In order to make the modeling methodology useful to designing biodiesel product with specified fuel properties, such as density, viscosity, and cetane number, we develop a product fuel property calculator to predict biodiesel qualities. Throughout this development, we validate all the new modeling tools with available experimental data, and quantify the percentage of average relative deviation. The resulting ADR is typically less than 5%.

We then demonstrate a methodology to simulating an integrated process to predict reactor and separator performance, stream conditions, and product qualities with different feedstocks. We demonstrate the ease and accuracy of characterizing the feed oil as a pseudo-triglyceride, instead as a mixture of mixed triglycerides. The results show that the modeling methodology is an efficient tool not only for evaluating and optimizing the performance of an existing biodiesel manufacturing, and but also for optimizing the design of a new process to produce biodiesel with specified fuel properties.

### 3.9 Acknowledgements.

We thank Dr. Chau-Chyun Chen of Aspen Technology and Professor Mahmoud El-Halwagi of Texas A and M University for their valuable review comments. We thank Alliant Techsystems (particularly Mark Matusevich, Vice President; Charles Zisette, Director of Technology), Aspen Technology (particularly Mark Fusco, President and CEO; Chau-Chyun Chen, Vice President of Technology; Larry Evans, Founder; Zhiming Huang, Software Director), China Petroleum and

Chemical Corporation (particularly Wang Tianpu, President; Cao Xianghong, Senior Advisor; Dai Houliang, Senior Vice President), Formosa Petrochemical Corporation (particularly Wilfred Wang, Board Chairman), and Milliken Chemical (particularly John Rakers, President, and Jean Hall, Business Manager) for supporting our educational programs in computer-aided design and process system engineering at Virginia Tech.

## 3.10 Nomenclature

| | |
|---|---|
| A | Pre-exponential term in Arrhenius equation, L/min-mol or $L^2$/min-$mol^2$ in the studies of Vincente et al. |
| ARD | Average relative deviation, % |
| CN | Cetane number |
| $C_{CAT}$ | Catalyst concentration, mol/L |
| $C_{P, G}$ | Ideal gas heat capacity, J/mol-K or J/kmol-K |
| $C_{P, L}$ | Liquid heat capacity, J/mol-K or J/kmol-K |
| Ea | Activation Energy, cal/mol or J/mol |
| $E_i$ | Forward activation Energy of reaction i, cal/mol or J/mol |
| $E_{-i}$ | Backward activation Energy of reaction i, cal/mol or J/mol |
| k | Rate constant, L/mol-min |
| $k_i$ | Forward rate constant of reaction i, L/mol-min |
| $k_{-i}$ | Backward rate constant of reaction i, L/mol-min ($k_i$ / $k_{-I}$ represents the thermodynamic equilibrium constant) |
| $k_o$ | Rate constant at reference temperature, L/mol-min |
| $k_i^{intrinsic}$ | Intrinsic rate constant in the studies of Vincente et al., $L^2$/min-$mol^2$ |
| m | Number of $CH_2$ group |
| $N_c$ | Number of carbon atoms |

| | |
|---|---|
| $N_{DB}$ | Number of double bonds |
| n | Number of CH=CH group |
| $P_c$ | Critical pressure, Bar or Pa |
| $P_{vap}$ | Liquid vapor pressure, Bar or Pa |
| R | Universal gas constant, 1.987 cal/mol-K or 8.314 J/mol-K |
| T | Temperature, K or ℃ |
| $T_o$ | Reference temperature in Arrhenius equation, K or ℃ |
| $T_b$ | Normal boiling temperature, K or ℃ |
| $T_c$ | Critical temperature, K or ℃ |
| $T_r$ | Reduced temperature = $T/T_c$ |
| $V_c$ | Critical molar volume, $m^3$/kmol or $m^3$/mol |
| $V_L$ | Molar volume of pure liquid, $m^3$/kmol or $m^3$/mol |
| $V_{L,}^{mix}$ | Molar volume of liquid mixture, $m^3$/kmol or $m^3$/mol |
| $V_{L,20}$ | Liquid molar volume at 20℃, $m^3$/kmol or $m^3$/mol |
| $x_i$ | Molar fraction or mass fraction |
| $Z_{RA}$ | Rackett parameter in Rackett equation |
| $\Delta H_{vap}$ | Heat of vaporization, J/mol |
| $\omega$ | Acentric factor |
| $\rho_L$ | Liquid mass density, kg/$m^3$ or g/$cm^3$ |
| $\mu$ | Kinetic viscosity, $mm^2$/s or dynamic viscosity, cP |

## 3.11 Literature Cited.

1. http://www.biodiesel.org/resources/definitions/default.shtm, accessed March 20, 2009.
2. Freedman, B.; Butterfield, R. O.; Pryde, E. H. “Transesterification Kinetics of Soybean Oil,” *Journal of the American Oil Chemists’ Society*, **1986**, 63, 1375-1380.

3. Fukuda, H.; Kondo, A.; Noda, H. ”Biodiesel Fuel Production by Transesterification of Oils,” *Journal of Bioscience and Bioengineering*, **2001**, 92, 405-416.
4. Myint, L. L.; El-Halwagi, M. M. “Process Analysis and Optimization of Biodiesel Production from Soybead Oil,” *Clean Technologies and Environmental Policy*, http://www.springerlink.com/content/m673580p1626n12w/fulltext.pdf, accessed May 20, 2009.
5. West, A. H.; Posarac, D.; Ellis, N. “Assessment of Four Biodiesel Production Processes Using HYSYS. Plant,” *Bioresource Technology*, **2008**, 99, 6587-6601.
6. Zhang, Y.; Dube, M. A.; McLean, D. D.; Kates, M. “Biodiesel Production from Waste Cooking Oil: 1. Process Design and Technological Assessment,” *Bioresource Technology*, **2003**, 89, 1-16.
7. Harding, K. G.; Dennis, J. S.; von Blottniz, H.; Harrison, S. T. L. “A Life-cycle Comparison between Inorganic and Biological Catalysis for the Production of Biodiesel,” *Journal of Cleaner Production*, **2007**, 16, 1368-1378.
8. Hass, M. J.; McAloon, A. J.; Yee, W. C.; Foglia, T. A. “A Process Model to Estimate Biodiesel Production Costs,” *Bioresource Technology*, **2006**, 97, 671-678.
9. Tapasvi, D.; Wiesenborn, D.; Gustafson, C. “Process Model for Biodiesel Production from Various Feedstocks,” *Transactions of American Society of Agricultural Engineers*, **2005**, 48, 2215-2221.
10. Kapilakarn, K.; Peugtong, A. “A Comparison of Costs of Biodiesel Production from Transesterification,” *International Energy Journal*, **2007**, 8, 1-6.
11. Stiefel, S.; Dassori, G. “Simulation of Biodiesel Production through Transesterification of Vegetable Oils”, *Industrial and Engineering Chemistry Research*, **2009**, 48, 1068-1071.
12. Apostolakou, A. A.; Kookos, I. K.; Marazioti, C.; Angelopoulos, “Techno-economic

Analysis of a Biodiesel Production Process from Vegetable Oils", *Fuel Processing Technology*, **2009**, 90, 1023-1031.

13. Tang, Z.; Du, Z.; Min, E.; Gao, L.; Jiang, T.; Han, B. "Phase Equilibria of Methanol–Triolein System at Elevated Temperature and Pressure," *Fluid Phase Equilibria*, **2006**, 239, 8-11.
14. Van Gerpen, J.; Shanks, B.; Pruszko, R.; Clements, D.; Knothe, G. "Biodiesel Production Technology," National Renewable Energy Laboratory, Golden, CO., Report No. NREL/SR-510-36244, **2004.**
15. Ramos, M. J.; Fernandez, C. M.; Casas, A.; Rodriguez, L.; Perez, A. "Influence of Fatty Acid Composition of Raw Materials on Biodiesel Properties," *Bioresource Technology*, **2009**, 100, 261-268.
16. Zhou, W.; Boocock, D. G. B. "Phase behavior of the base-catalyzed transesterification of soybean oil," *Journal of the American Oil Chemists' Society*, **2006**, 83, 1041-1045.
17. Zhou, W.; Boocock, D. G. B. "Phase Distribution of Alcohol, Glycerol, and Catalyst in the Transesterification of Soybean Oil," *Journal of the American Oil Chemists' Society*, **2006**, 83, 1047-1052.
18. Stamenkovis, O. S.; Todorovic, Z. B.; Lazic, M. L.; Veljkovic, V. B.; Skala, D. U. "Kinetics of Sunflower Oil Methanolysis at Low Temperature," *Bioresource Technology*, **2008**, 99, 1131-1140.
19. Boocock, D. G. B.; Konar, S. K.; Mao, V.; Lee, C.; Buligan, S. "Fast Formation of High-Purity Methyl Esters from Vegetable Oils," *Journal of the American Oil Chemists' Society*, **1998**, 75, 1167-1172.
20. Freedman, B.; Pryde, E. H.; Mounts, T. L. "Variables Affecting the Yields of Fatty Esters from Transesterified Vegetable Oils," *Journal of the American Oil Chemists' Society*, **1984**,

61, 1638-1643.

21. Vicente, G.; Martinez, M.; Aracil, J.; Esteban, A. “Kinetics of Sunflower Oil Methanolysis,” *Industrial and Engineering Chemistry Research*, **2005**, 44, 5447-5454.
22. Noureddini, H.; Zhu, D. “Kinetics of Transesterification of Soybean Oil,” *Journal of the American Oil Chemists’ Society*, **1997**, 74, 1457-1463.
23. Darnoko, D.; Cheryan, M. “Kinetic of Palm Oil Transesterification in a Batch Reactor,” *Journal of the American Oil Chemists’ Society*, **2000**, 77, 1263-1267.
24. Leevijit, T.; Wisutmethangoon, W.; Prateepchaikul, G.; Tongurai, C.; Allen, M. “A Second Order Kinetics of Palm Oil Transesterification,” *The Joint International Conference on Sustainable Energy and Environment*, Hua Hin, Thailand, **2004**. 277-281.
25. Narvaez, P. C.; Rincon, S. M.; Sanchez, F. J. “Kinetics of Palm Oil Methanolysis,” *Journal of the American Oil Chemists’ Society*, **2007**, 84, 971-977.
26. Vicente, G.; Martinez, M.; Aracil, J. “Kinetics of Brassica Carinata Oil Methanolysis,” *Energy and Fuels*, **2006**, 20, 1772-1726.
27. Bambase Jr., M. E.; Nakamura, N.; Tanaka, J.; Matsumura, M. “Kinetics of Hydroxide-Catalyzed Methanolysis of Crude Sunflower Oil for the Production of Fuel-Grade Methyl Esters,” *Journal of Chemical Technology and Biotechnology*, **2007**, 82, 273-280.
28. Slinn, M.; Kendall, K. “Developing the Reaction Kinetics for a Biodiesel Reactor,” *Bioresource Technology*, 2009, 100, 2324-2327.
29. Schwab, A. W.; Bagby, M. O.; Freedman, B. “Preparation and Properties of Diesel Fuels from Vegetable Oils,” *Fuel*, **1987**, 66, 1372-1378.
30. Wu, M.; Wu, G.; Han, Y.; Zhang, P. “Fatty Acid Composition of Six Edible Vegetable Oils and Their Biodiesel Fuels,” *China Oils and Fats*, **2003**, 28, 65-67.

31. Canakci, M.; Van Gerpen, J. "A Pilot Plant to Produce Biodiesel from High Free Fatty Acid Feedstocks", *Transactions of ASAE*, **2003**, 46, 945-954.

32. National Institute of Science and Technology, ThermoData Engine, NIST TDE (http://trc.nist.gov/tde.html)

33. Poling, B. E.; Prausnitz, J. M.; O'Connell, J. P. The Properties of Gases and Liquids, 5th ed., **2000**, McGraw Hill, New York.

34. National Institute of Science and Technology, NIST Chemistry WebBook (http://webbook.nist.gov/chemistry/)

35. Goodrum, J. W. "Rapid Measurements of Boiling Point and Vapor Pressure of Short-Chain Triglycerides by Thermogravimetric Analysis," *Journal of the American Oil Chemists' Society*, **1997**, 74, 947-950.

36. Goodrum, J. W.; Siesel, E. M. "Thermogravimetric Analysis for Boiling Points and Vapor Pressure," *Journal of Thermal Analysis*, **1996**, 46, 1251-1258.'

37. Goodrum, J. W.; Geller, D. P. "Rapid Thermogravimetric Measurements of Boiling Points and Vapor Pressure of Saturated Medium- and Long-Chain Triglycerides," *Bioresource Technology*, **2002**, 84, 75-80.

38. Dohrn, R.; Brunner, G. "An Estimation Method to Calculate $T_b$, $T_c$, $P_c$, and ω from the Liquid Molar Volume and the Vapor Pressure," *Proceedings of the 3rd International Symposium on Supercritical Fluids, Strasburg, France,* **1994**, 241-248.

39. Halvorsen, J.D.; Mammel, Jr W.C.; Clements , L.D. "Density Estimation for Fatty Acids and Vegetable Oils Based on Their Fatty Acid Composition," *Journal of the American Oil Chemists' Society*, **1993**, 70, 875-880.

40. Morad, N. A.; Mustafa Kamal, M. A. A.; Panau, F.; Yew, T. W. "Liquid Specific Heat Capacity Estimation for Fatty Acids, Triacylglycerols, and Vegetable Oils Based on Their

Fatty Acid Composition," *Journal of the American Oil Chemists' Society*, **2000**, 77, 1001-1005.

41. Ceriani, P.; Meirelles, A. J. A. "Predicting Vapor-Liquid Equilibria of Fatty Systems," *Fluid Phase Equilibria*, **2004**, 215, 227-236.
42. Zong, L.; Ramanathan, S.; Chen, C. C. "Novel Approach for Estimating Thermophysical Properties of Fats & Vegetable Oils for Biodiesel Production Processes", *Industrial and Engineering Chemistry Research* (In Pressed)
43. Ceriani. R.; Gani, R.; Meirelles, A. J. A. "Prediction of Heat Capacities and Heats of Vaporization of Organic Liquids by Group Contribution Methods" *Fluid Phase Equilibria*, **2009**, 283, 49-55.
44. de la Fuente B, J. C.; Fornari, T.; Brignole, E.; Bottini, S. "Phase Equilibria in Mixtures of Triglycerides with Low-Molecular weight alkanes," *Fluid Phase Equilibria*, **1997**, 128, 221-227.
45. Siang, L. C.; Manan, Z. A.; Sarmidi, M. R. "Simulation Modeling of the Phase Behaviour of Palm Oil with Supercritical Carbon Dioxide," *Proceeding of International Conference On Chemical and Bioprocess Engineering, 27th – 29th August 2003, Universiti Malaysia Sabah, Kota Kinabatu*, 427-434.
46. Ndiaye, P. M.; Franceschi, E.; Oliveira, D.; Dariva, C.; Tavares, F. W.; Oliveira, J. V. "Phase Behavior of Soybean Oil, Castor Oil and Their Fatty Acid Ethyl Esters in Carbon Dioxide at High Pressures," *Journal of Supercritical Fluids*, **2006**, 37, 29-37.
47. Espinosa, S.; Fornari, T.; Bottini, S. B.; Brignole, E. A. "Phase Equilibria in Mixtures of Fatty Oils and Derivatives with Near Critical Fluids Using the GC-EOS Model," *Journal of Supercritical Fluids*, **2002**, 23, 91-102.
48. Kuramochi, H.; Maeda, K.; Kato, S.; Osako, M.; Nakamura, K.; Sakai, S. "Application of

UNIFAC Models for Prediction of Vapor-Liquid Equilibria and Liquid-Liquid Equilibria Relevant to Separation and Purification Processes of Crude Biodiesel Fuel," *Fuel*, **2009**, 88, 1472-1477.

49. Chen, F.; Sun, H.; Naka, Y.; Kawasaki, J. "Reaction and Liquid-Liquid Distribution Equilibria in Oleic Acid/Methanol/Methyl Oleate/Water System at 73℃," *Journal of Chemical Engineering of Japan*, **2001**, 34, 1479-1485.
50. Stloukal, R.; Komers, K.; Machek, J. "Ternary Phase Diagram Biodiesel Fuel-Methanol-Water," *Journal für praktische Chemie Chemiker-Zeitung,* **1997**, 339, 485-487.
51. De Felice, R.; De Faveri, D.; De Andreis, P.; Ottonello, P. "Component Distribution between Light and Heavy Phases in Biodiesel manufacturinges," *Industrial and Engineering Chemistry Research*, **2008**, 47, 7862-7867.
52. Andreatta, A. E.; Casas, L. M.; Hegel, P.; Bottini, S. b.; Brignole, E. A. "Phase Equilibria in Ternary Mixtures of Methyl Oleate, Glycerol, and Methanol," *Industrial and Engineering Chemistry Research*, **2008**, 47, 5157-5164.
53. Chiu, C.; Goff, M. J.; Suppes, G. J. "Distribution of Methanol and Catalysts between Biodiesel and Glycerin Phases," *AIChE Journal*, **2005**, 51, 1274-1278.
54. Negi, D. S.; Sobotka, F.; Kimmel, T.; Wozny, G.; Schomacker, R. "Liquid-Liquid Phase Equilibrium in Glycerol-Methanol-Methyl Oleate and Glycerol- Monoolein-Methyl Oleate Ternary Systems," *Industrial and Engineering Chemistry Research*, **2006**, 45, 3693-3696.
55. Batista, E.; Monnerat, S.; Kato, K.; Stragevitch, L.; Meirelles, A. J. A. "Liquid-Liquid Equilibrium for Systems of Canola Oil Oleic Acid and Short-Chain Alcohols," *Journal of Chemical Engineering Data*, **1999**, 44, 1360-1364.
56. Hansen, H. K.; Rasmussen, P.; Fredenslund, A.; Schiller, M.; Gmehling, J. "Vapor-Liquid

Equilibria by UNIFAC Group Contribution. 5. Revision and Extension," *Industrial and Engineering Chemistry Research*, **1991**, 30, 2352-2355.

57. Gmehling, J.; Li, J.; Schiller, M. "A Modified UNIFAC model. 2. Present Parameter Matrix and Results for Different Thermodynamic Properties," *Industrial and Engineering Chemistry Research*, **1993**, 32, 178-193.
58. Magnussen, T.; Rasmussen, P.; Fredenslund, A. "UNIFAC Parameter Table for Prediction of Liquid-Liquid Equilibriums," *Industrial and Engineering Chemistry Research*, **1981**, 20, 331-339.
59. Chuck, C. J.; Bannister, C. D.; Hawley, J. G.; Davidson, M. G.; Bruna, I. L.; Paine, A. "Predictive Model to Assess the Molecular Structure of Biodiesel Fuel," *Energy and Fuels*, **2009**, 23, 2290-2294.
60. Lang, X.; Dalai, A. K.; Bakhshi, N. N.; Reaney, M. J.; Hertz, P. B. "Preparation and Characterization of Bio-diesel from Various Bio-oils," *Bioresource Technology*, **2001**, 80, 53-62.
61. Benjumea, P.; Aqudelo, J.; Agudelo, A. "Basic Properties of Palm Oil Bio-diesel Blends," *Fuel*, **2008**, 87, 2069-2075.
62. Allen, C. A. W.; Watts, K. C.; Ackman, R. G.; Pegg, M. J. "Predicting the viscosity of biodiesel fuels from their fatty acid ester composition," *Fuel*, **1999**, 78, 1319-1326.
63. Krisnangkure, K.; Yimsuwan, T.; Pairintra, R. "An Empirical Approach in Predicting Biodiesel Viscosity at Various Temperature," *Fuel*, **2006**, 85, 107-113.
64. Moser, B. R. "Influence of Blending Canola, Palm, Soybean, and Sunflower Oil Methyl Esters on Fuel Properties of Biodiesel," *Energy and Fuels*, **2008**, 22, 4301-4306.
65. Demirbas, A. "Chemical and Fuel Properties of Seventeen Vegetable Oils," *Energy Sources*, **2003**, 25, 721-728.

66. Tat, M. E.; Van Gerpen, J. H. “The Specific Gravity of Biodiesel and Its Blends with Diesel Fuel,” *Journal of the American Oil Chemists' Society*, **2000**, 77, 115-119.

67. Leung, D. Y. C.; Guo, Y. "Transesterification of Neat and Used Frying Oil: Optimization for Biodiesel Production", *Fuel Processing Technology*, **2006**, 87, 883–890.

68. Clements, L. D. “Blending Rules for Formulating Biodiesel Fuel,” *Proceeding of the Third Liquid Fuel Conference*, American Society of Agricultural Engineers, Nashville, Sep. 15-17, **1996**, 44053.

69. Knothe, G. “Dependence of Biodiesel Fuel Properties on the Structure of Fatty Acid Alkyl Esters,” *Fuel Processing Technology*, **2005**, 86, 1059-1070.

70. Freedman, B.; Bagby, M. O. “Predicting Cetane Numbers of n-Alcohols and Methyl Esters from Their Physical Properties,” *Journal of the American Oil Chemists' Society*, **1990**, 67, 565-571.

71. Mccormick, R. L.; Graboski, M. S.; Alleman, T. L.; Herring, A. M.; Tyson, K. S. “Impact of Biodiesel Source Material and Chemical Structure on Emissions of Criteria Pollutants from a Heavy-Duty Engine,” *Environmental Science and Technology*, **2001**, 35, 1742-1747.

72. Bamgboye, A. I.; Hansen, A. C. “Prediction of Cetane Number of Biodiesel Fuel from the Fatty Acid Methyl Ester (FAME) Composition,” *International Agrophysics*, **2008**, 22, 21-29.

73. Knothe, G. “Designer Biodiesel: Optimizing Fatty Ester Composition to Improve Fuel Properties,” *Energy and Fuels*, **2008**, 22, 1358-1364.

74. Knothe, G.; Dunn, R. O.; Bagby, M. O. “Biodiesel: The Use of Vegetable Oils and Their Derivatives as Alternative Diesel Fuels,” *ACS Symposium Series*, **1997**, 666, 172-208.

75. Chen, X.; Yuan, Y.; Sun, P. “Effects of Structural Features of the Fatty Acid Methyl Esters upon the Cetane Number of Biodiesel,” *Chemical Engineering of Oil and Gas*, **2007**, 36,

481-484 (in Chinese).

76. Peterson, C. L.; Taberski, J. S.; Thompson, J. C.; Chase, C. L. “The Effect of Biodiesel Feedstock on Regulated Emissions in Chassis Dynamometer Tests of a Pickup Truck,” *Transactions of ASAE*, **2000**, 43, 1371-1381.

77. Yahya, A.; Marley, S. J. “Physical and Chemical Characterization of Methyl Soyoil and Methyl Tallow Esters as CI Engine Fuels,” *Biomass and Bioenergy*, **1994**, 6, 321-328.

78. Sinha, S.; Agarwal, A. K.; Garg, S. “Biodiesel Development from Rice Bran Oil: Transesterification Process Optimization and Fuel Characterization,” *Energy Conversion and Management*, **49**, 1248-1257.

79. Chang, D. Y. Z.; Van Gerpen, J. H.; Lee, I.; Johnson, L. A.; Hammond, E. G.; Marley, S. J. “Fuel Properties and Emissions of Soybean Oil Esters as Diesel Fuel,” *Journal of the American Oil Chemists’ Society*, **1996**, 73, 1549-1555.

80. Dunn, R. O.; Bagby, M. O. “Low-Temperature Properties of Triglyceride-Based Diesel Fuels: Transesterified Methyl Esters and Petroleum Middle Distillate/Ester Blends,” *Journal of the American Oil Chemists’ Society*, **1995**, 72, 895-904.

81. Rihani, D. N.; Doraiswany. L. K. “Estimation of Heat Capacity of Organic Compounds from Group Contributions,” *Industrial and Engineering Chemistry Fundamentals*, **1965**, 4, 17-21.

82. Glisic, S.; Skala, D. “The Problems in Design and Detailed Analyses of Energy Consumption for Biodiesel Synthesis at Supercritical Conditions”, *Journal of Supercritical Fluids*, **2009**, 49, 293-301.

83. Kiwjaroun, C.; Tubtimdee, C.; Piumsomboon, P. “LCA studies Comparing Biodiesel Synthesized by Conventional and Supercritical Methanol Methods” *Journal of Cleaner Production*, **2009**, 17, 143-15.

## 3.12. Appendix A – An Illustration of How to Access NIST TDE When Applying Aspen Plus to Develop a Biodiesel Process Model.

To access NIST TDE Data Engine in Aspen Plus version 2006.5 or V7.0

Step 1. Enter the FAME in the component list

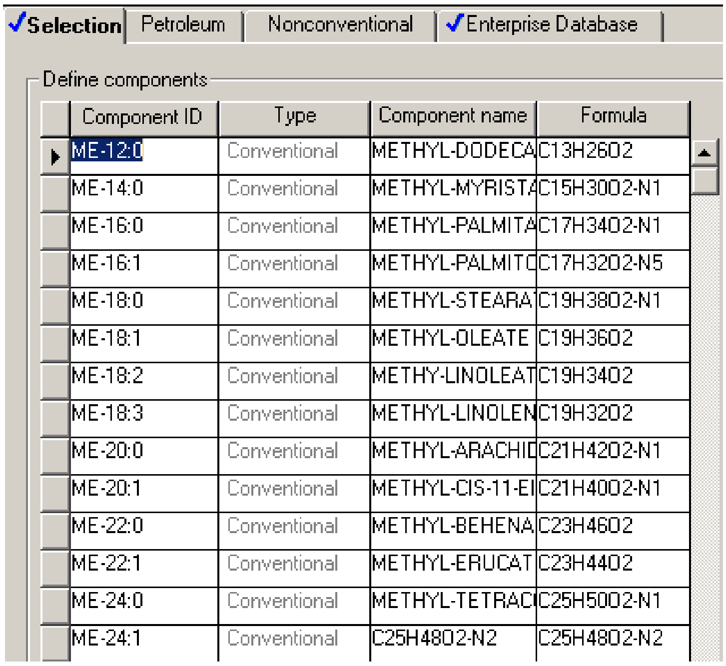

| Component ID | Type | Component name | Formula |
|---|---|---|---|
| ME-12:0 | Conventional | METHYL-DODECA | C13H26O2 |
| ME-14:0 | Conventional | METHYL-MYRISTA | C15H30O2-N1 |
| ME-16:0 | Conventional | METHYL-PALMITA | C17H34O2-N1 |
| ME-16:1 | Conventional | METHYL-PALMITO | C17H32O2-N5 |
| ME-18:0 | Conventional | METHYL-STEARA | C19H38O2-N1 |
| ME-18:1 | Conventional | METHYL-OLEATE | C19H36O2 |
| ME-18:2 | Conventional | METHY-LINOLEAT | C19H34O2 |
| ME-18:3 | Conventional | METHYL-LINOLEN | C19H32O2 |
| ME-20:0 | Conventional | METHYL-ARACHID | C21H42O2-N1 |
| ME-20:1 | Conventional | METHYL-CIS-11-EI | C21H40O2-N1 |
| ME-22:0 | Conventional | METHYL-BEHENA | C23H46O2 |
| ME-22:1 | Conventional | METHYL-ERUCAT | C23H44O2 |
| ME-24:0 | Conventional | METHYL-TETRACI | C25H50O2-N1 |
| ME-24:1 | Conventional | C25H48O2-N2 | C25H48O2-N2 |

Step 2. Go to “Tools” -> “NIST Thermo Data Engine (TDE)”

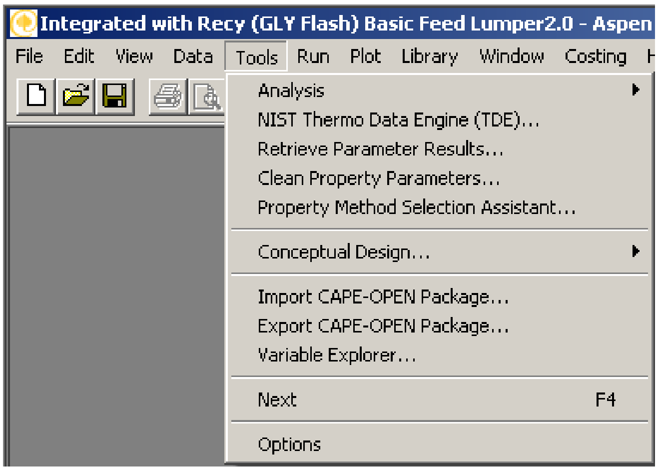

Step 3. Select the component

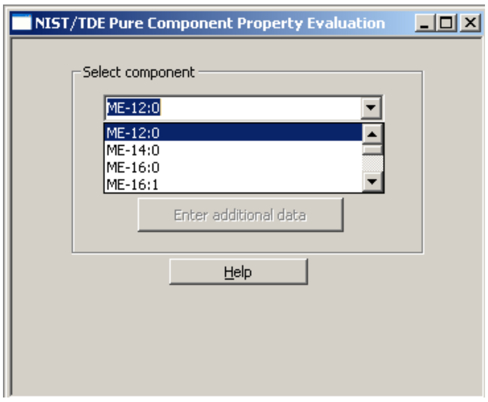

Select component: ME-12:0

- ME-12:0
- ME-14:0
- ME-16:0
- ME-16:1

Step 4. Click “Evaluate now”

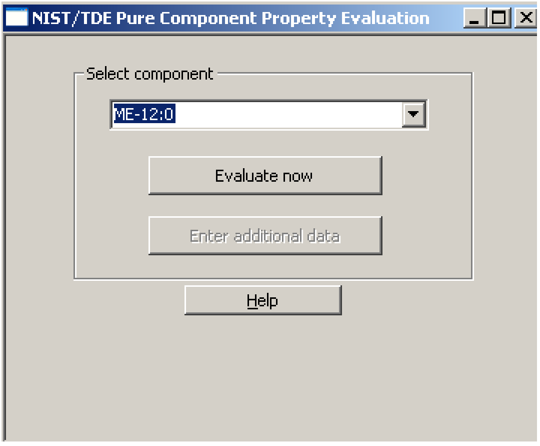

Select component: ME-12:0

Step 5. The user can access the value of a specific property, eq. Liquid Density

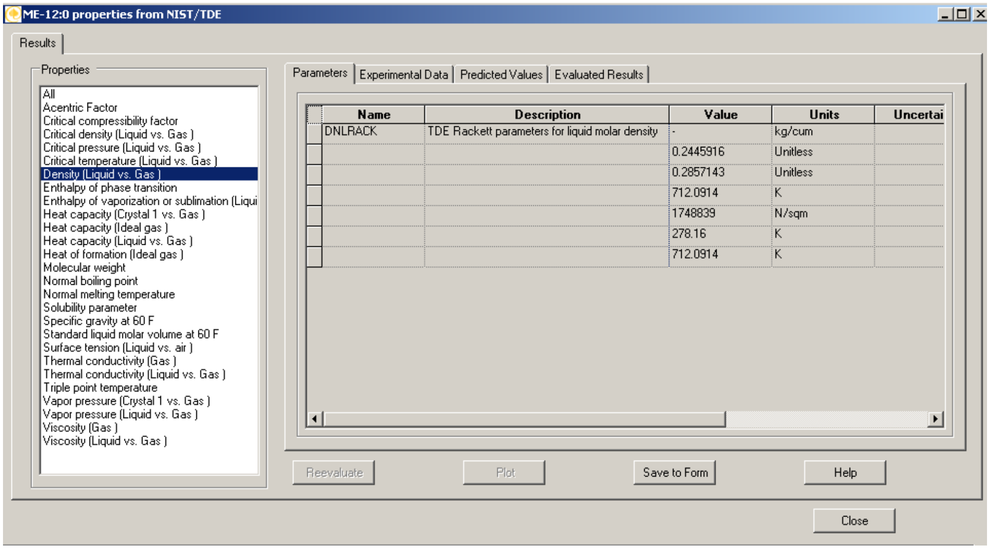

All
Acentric Factor
Critical compressibility factor
Critical density (Liquid vs. Gas )
Critical pressure (Liquid vs. Gas )
Critical temperature (Liquid vs. Gas )
Density (Liquid vs. Gas )
Enthalpy of phase transition
Enthalpy of vaporization or sublimation (Liqui
Heat capacity (Crystal 1 vs. Gas )
Heat capacity (Ideal gas )
Heat capacity (Liquid vs. Gas )
Heat of formation (Ideal gas )
Molecular weight
Normal boiling point
Normal melting temperature
Solubility parameter
Specific gravity at 60 F
Standard liquid molar volume at 60 F
Surface tension (Liquid vs. air )
Thermal conductivity (Gas )
Thermal conductivity (Liquid vs. Gas )
Triple point temperature
Vapor pressure (Crystal 1 vs. Gas )
Vapor pressure (Liquid vs. Gas )
Viscosity (Gas )
Viscosity (Liquid vs. Gas )

| Name | Description | Value | Units | Uncertai |
|---|---|---|---|---|
| DNLRACK | TDE Rackett parameters for liquid molar density | - | kg/cum | |
| | | 0.2445916 | Unitless | |
| | | 0.2857143 | Unitless | |
| | | 712.0914 | K | |
| | | 1748839 | N/sqm | |
| | | 278.16 | K | |
| | | 712.0914 | K | |

## 3.13. Appendix B – Prediction Methods for Thermophysical Properties.

### *$T_b$, $T_c$, $P_c$, $\omega$: Constantinou and Gani Method* [29]

Required data: structure

$$T_b\ (\mathrm{K}) = 204.359 \times \ln[\sum_k N_k \times \mathrm{tb1k} + W \times \sum_j M_j \times \mathrm{tb2j}] \qquad (B.1)$$

$$T_c\ (\mathrm{K}) = 181.128 \times \ln[\sum_k N_k \times \mathrm{tc1k} + W \times \sum_j M_j \times \mathrm{tc2j}] \qquad (B.2)$$

$$P_c\ (\mathrm{bar}) = [\sum_k N_k \times \mathrm{pc1k} + W \times \sum_j M_j \times \mathrm{pc2j} + 0.10022]^{-2} + 1.3705 \qquad (B.3)$$

$$\omega = 0.4085 \times \left\{ \ln \left[ \sum_k N_k \times \omega 1\mathrm{k} + W \times \sum_j M_j \times \omega 2\mathrm{j} + 0.10022 + 1.1507 \right] \right\}^{(1/0.505)} \qquad (B.4)$$

where W = 0 when only applying first-order and W = 1 when applying first-order and second-order.

Table B.1. Constantinou and Gani Contributions of $T_b$, $T_c$, $P_c$ for Triglyceride

| C-G | tb1k | tc1k | pc1k | ω |
|---|---|---|---|---|
| $CH_3$ | 0.8849 | 1.6781 | 0.0199 | 0.296 |
| $CH_2$ | 0.9225 | 3.492 | 0.0106 | 0.147 |
| CH | 0.6033 | 4.033 | 0.0013 | -0.071 |
| CH2COO | 3.3953 | 13.8116 | 0.0218 | 0.765 |
| CH=CH | 1.8433 | 7.3691 | 0.0179 | 0.252 |
| CH3COO | 3.636 | 12.5965 | 0.02902 | 0 |
| OH | 3.2152 | 9.7292 | 0.005148 | 0.737 |
|  | tb2j | tc2j | pc2j | ω |
| $CH_z$-$CH_m$=CH m = 0, 1; n = | -0.1406 | -0.5231 | 0.003538 | -0.0115 |
| CHOH | -0.5385 | -2.8035 | -0.00439 | 0.03654 |

### *$T_c$: Wilson and Jasperson Method* [29]

Required data: $T_b$ and structure

$$T_c\ (\mathrm{K}) = \frac{T_b}{[0.048271 + \sum_k N_k \times \Delta\mathrm{tck} + \sum_j M_j \times \Delta\mathrm{tcj}]^{0.2}} \qquad (B.5)$$

Table B.2. Wilson and Jasperson Contributions of $T_c$ for Triglyceride

| | Δtck |
|---|---|
| C | 0.008532 |
| H | 0.002793 |
| O | 0.020341 |
| | Δtcj |
| -COO- | -0.015 |

### $T_b$, $T_c$, $P_c$: Dohrn and Brunner Method A [34]

Required data: $T_b$ and $V_{L,20}$

$$a_c = \Omega_a \times a^{(1)} \times \left(\frac{b_c}{\Omega_b} \times T_b\right)^{a^{(2)}} \tag{B.6}$$

$$b_c = \Omega_b \times \left(b^{(1)} \times V_{L,20} \times T_b + b^{(2)}\right) \tag{B.7}$$

$$T_c(\mathrm{K}) = \frac{\Omega_b \times a_c}{\Omega_a \times b_c} \frac{1}{R} \tag{B.8}$$

$$P_c(\mathrm{kPa}) = \frac{a_c}{\Omega_a} \left(\frac{\Omega_b}{b_c}\right)^2 \tag{B.9}$$

$$\omega = -\frac{3}{7} \frac{\mathrm{Log}(101.3\,\mathrm{kPa}/P_c)}{(T_c / T_b - 1)} - 1 \tag{B.10}$$

where $\Omega_a = 0.45724$, $\Omega_b = 0.0778$, $a^{(1)} = 21.26924$ kJ/kmol-K, $a^{(2)} = 0.913049$, $b^{(1)} = 0.02556188$ $\mathrm{K}^{-1}$, $b^{(2)} = 0.168721\ \mathrm{m}^3\,\mathrm{kmol}^{-1}$, $R = 8.314$ kJ/kmol-K, $V_{L,20}$ is liquid density at 20℃

### $T_b$, $T_c$, $P_c$, $\omega$: Dohrn and Brunner Method B [34]

Required data: vapor pressure at any temperature ($P^{sat}$ at $T_1$) and $V_{L,20}$

$$a_c = \Omega_a \times a^{(1)} \times \left(\frac{b_c}{\Omega_b} \times T_b\right)^{a^{(2)}} \tag{B.11}$$

$$b_c = \Omega_b \times \left(b^{(1)} \times V_{L,20} \times T_b + b^{(2)}\right) \tag{B.12}$$

$$T_c(K) = \frac{\Omega_b \times a_c}{\Omega_a \times b_c}\frac{1}{R} \tag{B.13}$$

$$P_c(kPa) = \frac{a_c}{\Omega_a}(\frac{\Omega_b}{b_c})^2 \tag{B.14}$$

$$\omega = -\frac{3}{7}\frac{Log(P^{sat}\text{ at }T_1/P_c)}{(T_c/T_1 - 1)} - 1 \tag{B.15}$$

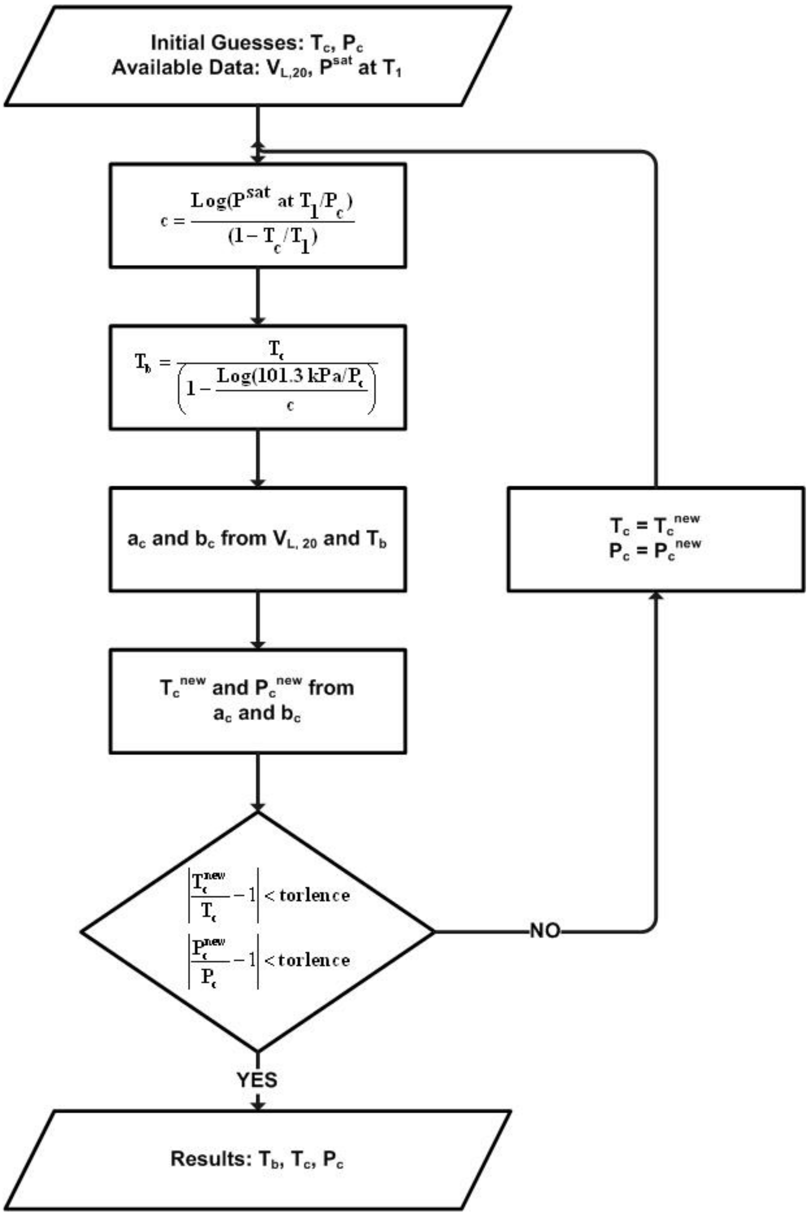

Figure B.1. Iteration step of Dohrn and Brunner Method to predict $T_b$, $T_c$, $P_c$ and$\omega$

Dohrn and Brunner[34] use Joback[29] method to obtain the initial guesses of $T_c$ and $P_c$. Joback method for $T_c$ and $P_c$:

$$\mathbf{T_b\ (K) = 198 + \sum_k N_k \times tbk} \tag{B.16}$$

$$\mathbf{T_c\ (K) = T_b \times \left[ 0.584 + 0.965 \times \left( \sum_k N_k \times tck \right) - \left( \sum_k N_k \times tck \right)^2 \right]^{-1}} \tag{B.17}$$

$$\mathbf{P_c\ (Bar) = \left[ 0.113 + 0.0032 \times N_{total\ atoms} - \left( \sum_k N_k \times pck \right) \right]^{-2}} \tag{B.18}$$

Table B.3. Joback Group Contributions of $T_c$ and $P_c$ for Triglyceride

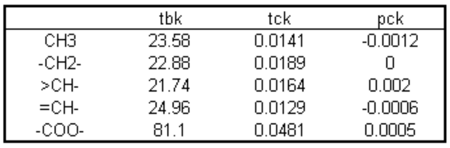

| | tbk | tck | pck |
|---|---|---|---|
| CH3 | 23.58 | 0.0141 | -0.0012 |
| -CH2- | 22.88 | 0.0189 | 0 |
| >CH- | 21.74 | 0.0164 | 0.002 |
| =CH- | 24.96 | 0.0129 | -0.0006 |
| -COO- | 81.1 | 0.0481 | 0.0005 |

***$P_{vap}$: Ambrowse and Walton Method*** [29]

Required data: $T_c$, $P_c$, ω

$$\mathbf{\ln(\frac{P_{vap}}{P_c}) = f^{(0)}(T_r) + \omega f^{(1)}(T_r) + \omega^2 f^{(2)}(T_r)} \tag{B.19}$$

$$\mathbf{f^{(0)}(T_r)} = \frac{-5.97616 \times \tau + 1.29874 \times \tau^{\mathbf{1.5}} - 0.60394 \times \tau^{\mathbf{2.5}} - 1.06841 \times \tau^{\mathbf{5}}}{\mathbf{T_r}} \tag{B.20}$$

$$\mathbf{f^{(1)}(T_r)} = \frac{-5.03365 \times \tau + 1.11505 \times \tau^{\mathbf{1.5}} - 5.41217 \times \tau^{\mathbf{2.5}} - 7.44628 \times \tau^{\mathbf{5}}}{\mathbf{T_r}} \tag{B.21}$$

$$\mathbf{f^{(2)}(T_r)} = \frac{-0.64771 \times \tau + 2.41539 \times \tau^{\mathbf{1.5}} - 4.26979 \times \tau^{\mathbf{2.5}} + 3.25259 \times \tau^{\mathbf{5}}}{\mathbf{T_r}} \tag{B.22}$$

$$\tau = \mathbf{1 - T_r} \tag{B.23}$$

where $T_r$ is reduced temperature.

***$P_{vap}$: Ceriani and Meirelles Method*** [37]

Required data: Structure

$$\mathbf{\ln(P_{i,\,vap}, Pa) = \sum_k N_k \times \left( A_{1k} + \frac{B_{1k}}{T^{1.5}} - C_{1k} \times \ln(T) - D_{1k} \times T \right) + \left[ M_i \times \sum_k N_k \times \left( A_{2k} + \frac{B_{2k}}{T^{1.5}} - C_{2k} \times \ln(T) - D_{2k} \times T \right) \right] + Q} \tag{B.24}$$

$$\mathbf{Q = \xi_1 \times q + \xi_2} \tag{B.25}$$

$$\mathbf{q = \alpha + \frac{\beta}{T^{1.5}} - \gamma \times \ln(T) - \delta \times T} \tag{B.26}$$

$$\mathbf{\xi_1 = f_0 + N_c \times f_1} \tag{B.27}$$

$$\mathbf{\xi_2 = s_0 + N_{cs} \times s_1} \tag{B.28}$$

where T is temperature in Kevin, $M_i$ is molecular weight and $A_{1k}$, $B_{1k}$, $C_{1k}$, $D_{1k}$, $A_{2k}$, $B_{2k}$, $C_{2k}$, $D_{2k}$ are group contribution terms. $N_c$ is the total number of carbon atoms in the molecule and $N_{cs}$ is the number of carbons of the substitute fraction. For example, $N_{cs}$ of lauric acid chain, $-OOC-(CH_2)_{10}-CH_3$, is 11.

Table B.4. Ceriani and Meirelles Contributions of Vapor Pressure

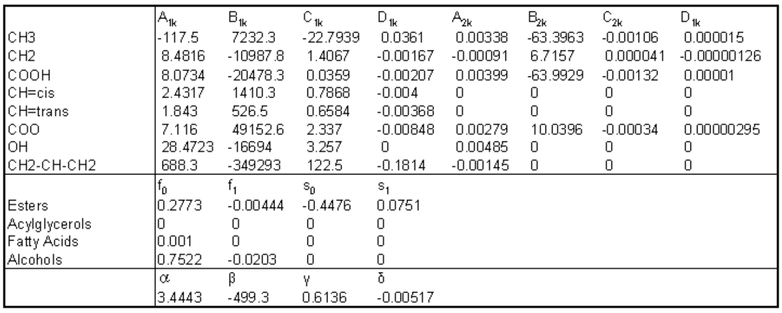

| | $A_{1k}$ | $B_{1k}$ | $C_{1k}$ | $D_{1k}$ | $A_{2k}$ | $B_{2k}$ | $C_{2k}$ | $D_{1k}$ |
|---|---|---|---|---|---|---|---|---|
| CH3 | -117.5 | 7232.3 | -22.7939 | 0.0361 | 0.00338 | -63.3963 | -0.00106 | 0.000015 |
| CH2 | 8.4816 | -10987.8 | 1.4067 | -0.00167 | -0.00091 | 6.7157 | 0.000041 | -0.00000126 |
| COOH | 8.0734 | -20478.3 | 0.0359 | -0.00207 | 0.00399 | -63.9929 | -0.00132 | 0.00001 |
| CH=cis | 2.4317 | 1410.3 | 0.7868 | -0.004 | 0 | 0 | 0 | 0 |
| CH=trans | 1.843 | 526.5 | 0.6584 | -0.00368 | 0 | 0 | 0 | 0 |
| COO | 7.116 | 49152.6 | 2.337 | -0.00848 | 0.00279 | 10.0396 | -0.00034 | 0.00000295 |
| OH | 28.4723 | -16694 | 3.257 | 0 | 0.00485 | 0 | 0 | 0 |
| CH2-CH-CH2 | 688.3 | -349293 | 122.5 | -0.1814 | -0.00145 | 0 | 0 | 0 |
| | $f_0$ | $f_1$ | $s_0$ | $s_1$ | | | | |
| Esters | 0.2773 | -0.00444 | -0.4476 | 0.0751 | | | | |
| Acylglycerols | 0 | 0 | 0 | 0 | | | | |
| Fatty Acids | 0.001 | 0 | 0 | 0 | | | | |
| Alcohols | 0.7522 | -0.0203 | 0 | 0 | | | | |
| | $\alpha$ | $\beta$ | $\gamma$ | $\delta$ | | | | |
| | 3.4443 | -499.3 | 0.6136 | -0.00517 | | | | |

***$\rho_L$*: *Halvorsen Method***[35] for triglycerides

Required data: $T_c$, $P_c$, $Z_{RA}$ of the fatty acids

$$\rho^{TG} = \frac{\left(\sum \mathbf{x}_{\mathbf{i}}^{\mathbf{FA}} \times \mathbf{MW}_{\mathbf{i}}^{\mathbf{FA}}\right)}{\mathbf{R} \times \left(\sum \frac{\mathbf{x}_{\mathbf{i}}^{\mathbf{FA}} \times \mathbf{T}_{\mathbf{c,i}}^{\mathbf{FA}}}{\mathbf{P}_{\mathbf{c,i}}^{\mathbf{FA}}}\right) \times \left(\sum \mathbf{x}_{\mathbf{i}}^{\mathbf{FA}} \times \mathbf{Z}_{\mathbf{RA,i}}^{\mathbf{FA}}\right)^{[1+(1-\mathbf{T_r})^{2/7}]}} + \mathbf{F_c} \tag{B.29}$$

$$\mathbf{T_r} = \frac{\mathbf{T}}{\sum \mathbf{x}_{\mathbf{i}}^{\mathbf{FA}} \times \mathbf{T}_{\mathbf{c,i}}^{\mathbf{FA}}} \tag{B.30}$$

$$\mathbf{MW^{TG}} = 3 \times \sum \mathbf{x}_{\mathbf{i}}^{\mathbf{FA}} \times \mathbf{MW}_{\mathbf{i}}^{\mathbf{FA}} + 38.0488 \tag{B.31}$$

$$\mathbf{F_c} = \mathbf{0.0236} + \mathbf{0.000082} \times \left|\mathbf{875} - \mathbf{MW^{TG}}\right| \quad \textbf{when } \mathbf{MW^{TG}} \geq \mathbf{875} \tag{B.32}$$

$$\mathbf{F_c} = \mathbf{0.0236} + \mathbf{0.000098} \times \left|\mathbf{875} - \mathbf{MW^{TG}}\right| \quad \textbf{when } \mathbf{MW^{TG}} \leq \mathbf{875} \tag{B.33}$$

where $x_i^{FA}$ is molar fraction of the i$^{th}$ fatty acid chain in the triglyceride molecule, $MW_i^{FA}$ is the molecular weight of the i$^{th}$ fatty acid, $T_{c,i}^{FA}$ is the critical temperature of the i$^{th}$ fatty acid, $P_{c,i}^{FA}$ is the critical pressure of the i$^{th}$ fatty acid and $Z_{RA,i}$ is the Rackett parameter of the i$^{th}$ fatty acid.

Table B.5. Required Parameters for Halvorsen Method of $\rho_L$ Prediction

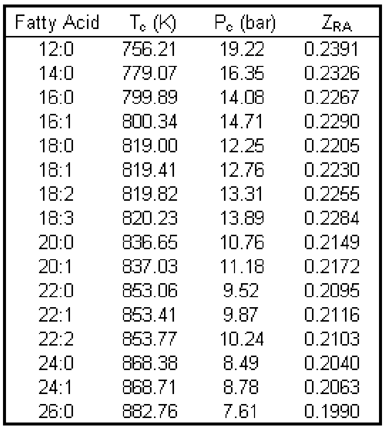

| Fatty Acid | $T_c$ (K) | $P_c$ (bar) | $Z_{RA}$ |
|---|---|---|---|
| 12:0 | 756.21 | 19.22 | 0.2391 |
| 14:0 | 779.07 | 16.35 | 0.2326 |
| 16:0 | 799.89 | 14.08 | 0.2267 |
| 16:1 | 800.34 | 14.71 | 0.2290 |
| 18:0 | 819.00 | 12.25 | 0.2205 |
| 18:1 | 819.41 | 12.76 | 0.2230 |
| 18:2 | 819.82 | 13.31 | 0.2255 |
| 18:3 | 820.23 | 13.89 | 0.2284 |
| 20:0 | 836.65 | 10.76 | 0.2149 |
| 20:1 | 837.03 | 11.18 | 0.2172 |
| 22:0 | 853.06 | 9.52 | 0.2095 |
| 22:1 | 853.41 | 9.87 | 0.2116 |
| 22:2 | 853.77 | 10.24 | 0.2103 |
| 24:0 | 868.38 | 8.49 | 0.2040 |
| 24:1 | 868.71 | 8.78 | 0.2063 |
| 26:0 | 882.76 | 7.61 | 0.1990 |

Example: find the density of triolein (18:1) at 20℃

Procedure:

1. Triolein is pure triglyceride which is composed of three oleic acid chains (18:1).

2. $$\sum x_i^{FA} \times MW_i^{FA} = 1 \times MW_{18:1}^{FA} = 282.46\,(kg / kmol) = 0.28246\,(kg/mol)$$

3. $$\sum \frac{x_i^{FA} \times T_{c,i}^{FA}}{P_{c,i}^{FA}} = \frac{1 \times T_{18:1}^{FA}}{P_{18:1}^{FA}} = 6.4217\,E - 04\,(K / Pa)$$

4. $$\sum x_i^{FA} \times Z_{RA,i}^{FA} = 1 \times Z_{18:1}^{FA} = 0.223 \quad \text{and}$$

$$T_r = \frac{T}{\sum x_i^{FA} \times T_{c,i}^{FA}} = \frac{T}{1 \times T_{c,18:1}^{FA}} = \frac{293.15}{819.41} = 3.5776E - 01$$

5. $$\left(\sum x_i^{FA} \times Z_{RA,i}^{FA}\right)^{[1+(1-T_r)^{2/7}]} = \left(1 \times Z_{18:1}^{FA}\right)^{[1+(1-T_r)^{2/7}]} = 5.9437E - 02$$

6. $$\begin{aligned} MW^{TG} &= 3 \times \sum x_i^{FA} \times MW_i^{FA} + 38.0488 = 3 \times (1 \times 282.46) + 38.0488 \\ &= 885.4288\,(kg/kmol) \end{aligned}$$

7 $$F_c = 0.0236 + 0.000082 \times \left|875 - MW^{TG}\right| = 2.4455E - 02\,(g/cm^3) = 2.4455E01\,(kg/m^3)$$

$$\rho^{TG}\,(\frac{kg}{m^3}) = \frac{\left(\sum x_i^{FA} \times MW_i^{FA}\right)}{R \times \left(\sum \frac{x_i^{FA} \times T_{c,i}^{FA}}{P_{c,i}^{FA}}\right) \times \left(\sum x_i^{FA} \times Z_{RA,i}^{FA}\right)^{[1+(1-T_r)^{2/7}]}} + F_c$$

8. $$\begin{aligned} &= \frac{0.28246\,(\frac{kg}{mol})}{8.314\,(\frac{Pa - m^3}{K - mol}) \times 6.4217E - 04\,(\frac{K}{Pa}) \times 5.9437E - 02} + 2.455E01\,(\frac{kg}{m^3}) \\ &= 914.66\,\frac{kg}{m^3} \end{aligned}$$

9. The experimental value is 912.6 kg/m$^3$ and the ARD is 0.23%.

***$C_{P,\,L}$*: Morad Method**[36] for triglycerides

Required data: $T_c$, ω of the fatty acids

$$\mathbf{C^{TG}_{P,L} = C^{IG}_{p,mix} + R \times \left( \begin{array}{l} 1.45 + 0.45 \times (1 - T_r)^{-1} + \\ 0.25 \times \omega_{mix} \times \left[ \left( 17.11 + 25.2 \times \dfrac{(1-T_r)^{1/3}}{T_r} + \dfrac{1.742}{(1-T_r)} \right) \right] \end{array} \right)} \tag{B.34}$$

$$\mathbf{T_r = \frac{T}{\sum x_i^{FA} \times T_{c,i}^{FA}}} \tag{B.35}$$

$$\mathbf{C^{IG}_{p,mix} = \sum x_i^{FA} \times C^{IG,FA}_{p,i}} \tag{B.36}$$

$$\mathbf{\omega_{mix} = \sum x_i^{FA} \times \omega_i^{FA}} \tag{B.37}$$

$$\mathbf{MW_{mix} = \sum x_i^{FA} \times MW_i^{FA}} \tag{B.38}$$

$$\mathbf{MW^{TG}} = 3 \times \sum \mathbf{x_i^{FA} \times MW_i^{FA}} + 38 \tag{B.39}$$

$$\mathbf{F_c = -0.2386 - 0.0005 \times \left| 850 - MW^{TG} \right| \quad when\ MW^{TG} \geq 850} \tag{B.40}$$

$$\mathbf{F_c = -0.3328 + 0.0001 \times \left| 850 - MW^{TG} \right| \quad when\ MW^{TG} \leq 850} \tag{B.41}$$

where R=1.987 Cal/K-mol and the unit of heat capacity is Cal/K-mol. Table B. 6 lists the required parameters of fatty acids.

Table B.6. Required Parameters for Morad Method of $C_{P,L}$ Prediction

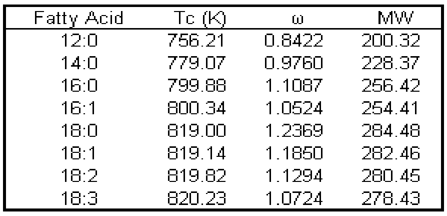

| Fatty Acid | Tc (K) | ω | MW |
|---|---|---|---|
| 12:0 | 756.21 | 0.8422 | 200.32 |
| 14:0 | 779.07 | 0.9760 | 228.37 |
| 16:0 | 799.88 | 1.1087 | 256.42 |
| 16:1 | 800.34 | 1.0524 | 254.41 |
| 18:0 | 819.00 | 1.2369 | 284.48 |
| 18:1 | 819.14 | 1.1850 | 282.46 |
| 18:2 | 819.82 | 1.1294 | 280.45 |
| 18:3 | 820.23 | 1.0724 | 278.43 |

$\mathbf{C_{p,i}^{IG,FA}}$ is idea gas heat capacity of fatty acid. Morad et al.[36] use Rihani method[76] to estimate $\mathbf{C_{p,i}^{IG,FA}}$ :

$$\mathbf{C_{p}^{IG,FA}} = \sum \mathbf{N_k} \times \mathbf{a_k} + \sum \mathbf{N_k} \times \mathbf{b_k} \times \mathbf{T} + \sum \mathbf{N_k} \times \mathbf{c_k} \times \mathbf{T^2} + \sum \mathbf{N_k} \times \mathbf{d_k} \times \mathbf{T^3} \tag{B.42}$$

where $N_k$ is the number of the given functional groups. The unit of $\mathbf{C_{p}^{IG,FA}}$ is Cal/K-mol.

Table B.7. Rihani Contributions of Ideal Gas Heat Capacity for Fatty Acid

|  | $a_k$ | $b_k$ | $c_k$ | $d_k$ |
|---|---|---|---|---|
| CH3 | 6.0870E-01 | 2.1433E-02 | -8.5200E-06 | 1.1350E-09 |
| CH2 | 3.9450E-01 | 2.1363E-02 | -1.1970E-05 | 2.5960E-09 |
| CH | -3.5232E+00 | 3.4158E-02 | -2.8160E-05 | 8.0150E-09 |
| -CH=CH- cis | -3.1210E+00 | 3.8060E-02 | -2.3590E-05 | 5.5040E-09 |
| -CH=CH- trans | 9.3770E-01 | 2.9904E-02 | -1.7490E-05 | 3.9180E-09 |
| -COOH | 1.4055E+00 | 3.4632E-02 | -2.5570E-05 | 6.8860E-09 |
| -COO- | 2.7350E+00 | 1.0751E-02 | 6.6700E-06 | -9.2300E-09 |

### ***$\triangle H_{vap}$ : Vetere method combined with Watson relation***[29]

Required data: $T_b$, $T_c$, $P_c$

$$\Delta H_{vap,b} = R \times T_b \frac{\left(1 - T_{br}\right)^{0.38}\left(\ln P_c - 0.513 + \dfrac{0.5066}{P_c T_{br}^{\ 2}}\right)}{1 - T_{br} + \ln T_{br}\left(1 - \left(1 - T_{br}\right)^{0.38}\right)} \tag{B.43}$$

$$\Delta H_{vap} = \Delta H_{vap,b}\left(\frac{1 - T_r}{1 - T_{br}}\right)^{0.38} \tag{B.44}$$

where $\Delta H_{vap,b}$ is heat of vaporization at normal boiling point, $T_r$ is reduced temperature, and $T_{br}$ is reduced temperature at normal boiling point

## NIST TDE Equations for Thermophysical Property

$V_L$: NIST Rackett Equation [28]

$$V_L = \frac{R \times T_c}{P_c \times Z_{RA}^{-\left[1+\left(1-\frac{T}{T_c}\right)^{C2}\right]}} \tag{B.45}$$

Table B.8. The Parameters of NIST Rackett Equation

| NIST TDE Rackett Equation ($m^3$/mol) | C1 ($Z_{RA}$) | C2 | C3 ($T_c$, K) | C4 ($P_c$, Pa) | C5 | C6 |
|---|---|---|---|---|---|---|
| C12:0 | 0.2445916 | 0.2857143 | 712 | 1748839 | 278 | 712 |
| C14:0 | 0.2353773 | 0.2857143 | 718 | 1448599 | 292 | 718 |
| C16:0 | 0.2227887 | 0.2857143 | 749 | 1205875 | 303 | 749 |
| C16:1 | 0.2071558 | 0.2857143 | 734 | 1279721 | 240 | 734 |
| C18:0 | 0.2298488 | 0.2857143 | 770 | 1178960 | 312 | 770 |
| C18:1 | 0.2225078 | 0.2857143 | 751 | 1124671 | 253 | 751 |
| C18:2 | 0.2226222 | 0.2857143 | 773 | 1162805 | 234 | 773 |
| C18:3 | 0.224261 | 0.2857143 | 774 | 1202626 | 110 | 774 |
| C20:0 | 0.1967211 | 0.2857143 | 767 | 1036965 | 319 | 767 |
| C20:1 | 0.2138194 | 0.2857143 | 767 | 990082 | 636 | 767 |
| C22:0 | 0.1841152 | 0.2857143 | 785 | 901921 | 326 | 785 |
| C22:1 | 0.2122916 | 0.2857143 | 784 | 881791 | 110 | 784 |
| C24:0 | 0.183291 | 0.2857143 | 804 | 821192 | 332 | 804 |
| C24:1 | 0.2010567 | 0.2857143 | 802 | 822329 | 678 | 802 |
| Parameter | C1 | C2 | C3 | C4 | C5 | C6 |
| Description | $Z_{RA}$ | - | $T_c$ | $P_c$ | $T_{lower}$ | $T_{upper}$ |
| Unit | N/A | N/A | K | Pa | K | K |

$V_L$: NIST ThermoML Equation [28]

$$\mathbf{V_L = \sum_{i=1}^{C_5} C_i \times T^{n-1}} \tag{B.46}$$

Table B.9. The Parameters of NIST ThermoML Equation for $V_L$

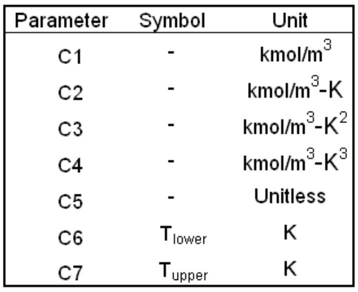

| Parameter | Symbol | Unit |
|---|---|---|
| C1 | - | kmol/$m^3$ |
| C2 | - | kmol/$m^3$-K |
| C3 | - | kmol/$m^3$-$K^2$ |
| C4 | - | kmol/$m^3$-$K^3$ |
| C5 | - | Unitless |
| C6 | $T_{lower}$ | K |
| C7 | $T_{upper}$ | K |

$C_{P,\,IG}$: NIST Aly-Lee Equation [28]

$$\mathbf{C_{P,IG}=C_1+C_2\times\left(\frac{C_3/T}{Sinh(C_3/T)}\right)^2+C_4\times\left(\frac{C_5/T}{Cosh(C_5/T)}\right)^2} \tag{B.47}$$

Table B.10. The Parameters of NIST Aly-Lee Equation for $C_{P,\,IG}$ for FAME

| NIST Aly-Lee Equation (J / kmol-K) | C1 | C2 | C3 | C4 | C5 | C6 | C7 |
|---|---|---|---|---|---|---|---|
| C12:0 | 240063.9 | 542541.1 | -819 | 121697.8 | 0 | 200 | 980 |
| C14:0 | 205454.4 | 805594.2 | -574 | -442429.9 | 650 | 200 | 980 |
| C16:0 | 230137.9 | 910125.1 | -574 | -497826.1 | -650 | 200 | 980 |
| C16:1 | 234231.9 | 895310.9 | -588 | -512600 | -664 | 200 | 980 |
| C18:0 | 267382.2 | 563286.7 | -569 | 596005.8 | -1600 | 200 | 980 |
| C18:1 | 269559.9 | 532189.6 | -577 | 616279.7 | -1617 | 200 | 980 |
| C18:2 | 261554.1 | 984480.8 | -1271 | 490798 | -556 | 200 | 980 |
| C18:3 | 265702.7 | 972734.7 | -614 | -599483.1 | -687 | 200 | 980 |
| C20:0 | 278834.7 | 1117297 | -1214 | 609431 | -536 | 200 | 980 |
| C20:1 | 282797.7 | 1102514 | -1240 | 579972.5 | -545 | 200 | 980 |
| C22:0 | 299203.3 | 1224641 | 564 | -674861.1 | -641 | 200 | 980 |
| C22:1 | 307461.3 | 1206798 | 1237 | 638488.9 | -544 | 200 | 980 |
| C24:0 | 345378.1 | 741693.7 | 568 | 774619.4 | -1600 | 200 | 980 |
| C24:1 | 347594 | 710543.1 | 574 | 794868.1 | -1613 | 200 | 980 |
| Parameter | C1 | C2 | C3 | C4 | C5 | C6 | C7 |
| Description | - | - | - | - | - | $T_{lower}$ | $T_{upper}$ |
| Unit | J/kmol-K | J/kmol-K | K | J/kmol-K | K | K | K |

$C_{P,\,L}$: NIST ThermoML Equation [28]

$$\mathbf{C_{P,L}=\sum_{i=1}^{C_3}C_i\times T^{n-1}} \tag{B.48}$$

Table B.11. The Parameters of NIST ThermoML Equation for $C_{P,\,L}$

| Parameter | Symbol | Unit |
|---|---|---|
| C1 | - | J/kmol-K |
| C2 | - | J/kmol-K$^2$ |
| C3 | - | Unitless |
| C4 | $T_{lower}$ | K |
| C5 | $T_{upper}$ | K |

$C_{P,L}$: NIST TDE Equation [28]

$$C_{P,L} = \frac{C_5}{1-\dfrac{T}{C_6}} + \sum_{i=1}^{C_7} C_i \times \left(1-\frac{T}{C_6}\right)^{n-1} \tag{B.49}$$

Table B.12. The Parameters of NIST TDE Equation for $C_{P,L}$ for FAME

| NIST TDE Equation (J/kmol-K) | C1 | C2 | C3 | C4 | C5 | C6 | C7 | C8 | C9 |
|---|---|---|---|---|---|---|---|---|---|
| C12:0 | 508414.7 | -1413.503 | 4.966722 | -0.004025 | 8804.63 | 712 | 4 | 278 | 698 |
| C14:0 | 974844.7 | -4513.728 | 12.42177 | -0.009581 | 11780.11 | 718 | 4 | 292 | 704 |
| C16:0 | 767706.7 | -2508.638 | 7.655214 | -0.005827 | 10693.47 | 749 | 4 | 303 | 734 |
| C16:1 | 472441.6 | -168.3002 | 1.95041 | -0.001492 | 7765.68 | 734 | 4 | 240 | 719 |
| C18:0 | 689451.7 | -1677.292 | 6.066038 | -0.004698 | 10924.92 | 770 | 4 | 312 | 755 |
| C18:1 | 466346.9 | 120.4442 | 1.566388 | -0.00124 | 7728.59 | 761 | 4 | 253 | 746 |
| C18:2 | 471973.1 | -38.21093 | 1.788936 | -0.001336 | 7519.56 | 773 | 4 | 234 | 758 |
| C18:3 | 498535.9 | -209.9461 | 1.964523 | -0.001379 | 7539.46 | 774 | 4 | 250 | 759 |
| C20:0 | 910960 | -2927.919 | 9.154863 | -0.007013 | 13838.95 | 767 | 4 | 319 | 750 |
| C20:1 | 526862.5 | 76.54091 | 1.84262 | -0.001448 | 8310.67 | 767 | 4 | 250 | 750 |
| Parameter | C1 | C2 | C3 | C4 | C5 | C6 | C7 | C8 | C9 |
| Description | - | - | - | - | - | $T_c$ |  | $T_{lower}$ | $T_{upper}$ |
| Unit | J/kmol-K | J/kmol-K | J/kmol-K | J/kmol-K | J/kmol-K | K | N/A | K | K |

$P_{vap}$: NIST Wagner Equation [28]

$$\mathbf{\ln(P_{vap}) = \ln(P_c) + \left( \begin{array}{l} C_1 \times \left(1-\dfrac{T}{C_6}\right) + C_2 \times \left(1-\dfrac{T}{C_6}\right)^{1.5} \\ + C_3 \times \left(1-\dfrac{T}{C_6}\right)^{2.5} + C_4 \times \left(1-\dfrac{T}{C_6}\right)^{5} \end{array} \right) \Big/ \left(\dfrac{T}{C_6}\right)} \tag{B.50}$$

Table B.13. The Parameters of NIST Wagner Equation for $P_{vap}$ for FAME

| NIST Wagner Equation (Bar) | C1 | C2 | C3 | C4 | C5 | C6 | C7 | C8 |
|---|---|---|---|---|---|---|---|---|
| C12:0 | -9.694324 | 2.509544 | -4.402982 | -9.230351 | 14.3745 | 712 | 278 | 712 |
| C14:0 | -10.32312 | 0.2486618 | -0.272116 | -15.16169 | 14.1861 | 718 | 292 | 718 |
| C16:0 | -10.98844 | 4.20676 | -8.735103 | -5.583598 | 14.0027 | 749 | 303 | 749 |
| C16:1 | -11.50495 | 4.414073 | -9.852489 | -5.443423 | 14.0622 | 734 | 240 | 734 |
| C18:0 | -11.01778 | 3.60513 | -9.883088 | -2.333603 | 13.9801 | 770 | 312 | 770 |
| C18:1 | -11.90171 | 5.368385 | -10.61564 | -5.806015 | 13.933 | 761 | 253 | 761 |
| C18:2 | -11.17148 | 4.445311 | -9.284593 | -5.08707 | 13.9664 | 773 | 234 | 773 |

| | | | | | | | | |
|---|---|---|---|---|---|---|---|---|
| C18:3 | -10.5887 | 2.436575 | -6.783611 | -7.340778 | 14 | 774 | 200 | 774 |
| C20:0 | -12.79261 | 6.579309 | -14.06263 | -4.254656 | 13.8518 | 767 | 319 | 767 |
| C20:1 | -12.46868 | 5.523578 | -12.0696 | -5.475907 | 13.8055 | 767 | 200 | 767 |
| C22:0 | -13.41457 | 5.666122 | -13.2316 | -8.207159 | 13.7123 | 785 | 326 | 785 |
| C22:1 | -12.9095 | 6.159538 | -13.16899 | -5.268222 | 13.6897 | 784 | 200 | 784 |
| C24:0 | -13.15767 | 6.335366 | -13.74519 | -5.33026 | 13.6185 | 804 | 332 | 804 |
| C24:1 | -13.28506 | 6.719306 | -14.09176 | -5.100378 | 13.6199 | 802 | 200 | 802 |
| Parameter | C1 | C2 | C3 | C4 | C5 | C6 | C7 | C8 |
| Description | - | - | - | - | ln ($P_c$) | $T_c$ | $T_{lower}$ | $T_{upper}$ |
| Unit | N/A | N/A | N/A | N/A | ln (Bar) | K | K | K |

$\triangle H_{vap}$: NIST Watson Equation [28]

$$\ln(\Delta H_{vap}) = C_1 + \sum_{i=2}^{C_6} C_i \times \left(\frac{T}{C_5}\right)^{i-2} \times \ln(1-\frac{T}{C_5}) \tag{B.51}$$

Table B.14. The Parameters of NIST Watson Equation for $\triangle H_{vap}$ for FAME

| NIST Watson Equation (J / kmol) | C1 | C2 | C3 | C4 | C5 | C6 | C7 | C8 |
|---|---|---|---|---|---|---|---|---|
| C12:0 | 18.71476 | 1.562579 | -1.321583 | 0.2647786 | 712 | 4 | 278 | 712 |
| C14:0 | 19.11147 | 2.941289 | -3.70431 | 1.327995 | 718 | 4 | 292 | 718 |
| C16:0 | 18.36144 | -0.701121 | 2.342368 | -1.24532 | 749 | 4 | 303 | 749 |
| C16:1 | 19.10368 | 2.33551 | -2.86149 | 1.05891 | 734 | 4 | 240 | 734 |
| C18:0 | 18.34189 | -0.918448 | 2.425747 | -1.143153 | 770 | 4 | 312 | 770 |
| C18:1 | 18.67553 | 0.0416939 | 1.315343 | -0.907716 | 761 | 4 | 253 | 761 |
| C18:2 | 19.07527 | 2.26599 | -2.78663 | 1.03997 | 773 | 4 | 234 | 773 |
| C18:3 | 18.49942 | -0.978716 | 3.4717 | 2.2344 | 753 | 4 | 255 | 753 |
| Parameter | C1 | C2 | C3 | C4 | C5 | C6 | C7 | C8 |
| Description | - | - | - | - | $T_c$ | - | $T_{lower}$ | $T_{upper}$ |
| Unit | N/A | N/A | N/A | N/A | K | N/A | K | K |

# Chapter 4 Conclusions and Recommendations.

This dissertation investigates the issues noted in Chapter 1 and provides new methodologies to properly simulate the two liquid fuel processes – hydrocracking process and biodiesel process. This section summarizes the achievements and the suggestion to implement our methodologies.

**Hydrocracking process:**

1. We develop two integrated HCR process models which include reactors, fractionators and hydrogen recycle systems.
2. We provide the step-by-step guideline of model development that has not been reported in the literature.
3. We apply the Gauss-Legendre Quadrature to convert kinetic lumps into pseudo-components based on boiling point ranges (delumping) for rigorous fractionator simulation.
4. Our delumping method gives a continuous response to changes in fractionator specification such as distillate rate.
5. We update API correlations of flash point and freezing point to plant operation and production.
6. The integrated HCR process models are able to predict accurately the product yields, distillation curves of liquid products, and temperature profiles of reactors and fractionators.
7. The integrated HCR process models also gives good estimations on liquid product qualities – density, flash point and freezing point of diesel fuel (MP HCR) and jet fuel (HP HCR) – by using updated API correlations.
8. We apply the integrated MP HCR process model to conduct simulation experiment to quantify the effects of operating variables on product yields.
9. We apply the integrated HP HCR process model to generate delta-base vector for LP based production planning.

Currently, the methodology only requires daily measurements in the refinery to build an integrated HCR process model. To better implement this model into process integration and production planning, we suggest a to-do list:

1. Calibrate the model every two to three weeks to ensure that the model always reflects the latest production and operation scenario.
2. Re-calibrate the model when feedstock is significantly changed from base case
3. Apply SimDist analysis whenever it is available.

To further improve our models, we may include Apply SimDist analysis for feed characterization, and to incorporate detailed molecular information for feed characterization and customize our feed lump distribution if these measurements are available regularly. We can also to customize the calibration environment to include product property and product composition as objective functions if detailed molecular information of product is available.

**Biodiesel process:**

1. We present a comprehensive review of published literature and focus on feed oil characterization, thermophysical property modeling, rigorous reaction kinetics, phase equilibrium for separation and purification units, and prediction of essential biodiesel fuel qualities.
2. We characterize the feed oil and product as a single pseudo-triglyceride through a “lumper” spreadsheet, and generate their essential thermophysical property.
3. We develop the reactor rating model based on rigorous kinetics of reacting the pseudo-triglyceride with methanol to produce pseudo-diglyceride (DG), pseudo-monoglyceride (MG) and pseudo-FAME
4. We convert the reactor output of pseudo-FAME molecules into a mixture of FAMEs. i.e., biodiesel, through a FORTRAN block, called a “delumper”.

5. We develop a product fuel property calculator to predict biodiesel qualities namely density, viscosity, and cetane number.
6. Our modeling methodology is an efficient tool not only for evaluating and optimizing the performance of an existing biodiesel manufacturing, and but also for optimizing the design of a new process to produce biodiesel with specified fuel properties

We use the experimental observation in the literature to develop the methodology. The following list shows the way to improve the methodology:

1. Current methodology utilizes alkali-catalyzed reaction kinetics with NaOH to model the reactor. In practice, $NaOCH_3$ is better than NaOH as catalyst because NaOH will react with free fatty acid into soap and water. With the existence of water, trigleceride will be hydrolyzed which not only reduce biodiesel yield but also increase the difficulty to purify the produced biodiesel. Thus, we suggest using the alkali-catalyzed reaction kinetics with $NaOCH_3$ when it is available.
2. There is a lack of physical property data of triglyceride molecules in the literature. Current methodology is utilizing predictive methods to estimate required physical properties. Su et al.[1] present a comprehensive review and comparison of different prediction methods based on all of the available experimental data in the literature. We suggest following their recommendations if there is no experimental data are available.
3. There are little phase equilibrium data of triglyceride-glycerol-methanol-biodiesel system. We suggest updating the thermodynamics model to ensure that the phase equilibrium calculation of separation and purification units match real physics when the data are available.
4. Currently, biodiesel is sold as biodiesel blend which is blended with petro-diesel in market. Therefore, predicting fuel properties of biodiesel blend is another interesting issue. There

are two ways to address this issue

a. Use pure property data of both biodiesel and petro-diesel to estimate the properties of biodiesel blend. This approach requires property measurement of both biodiesel and petro-diesel.

b. Build a databank including property data and compositional analysis of both biodiesel and petro-diesel. And then, figure out a simple way to predict the fuel property of biodiesel blend. We could do this by predicting pure property of both biodiesel and petro-diesel followed by the property estimation of biodiesel blend or predicting property of biodiesel blend according to its molecular information. Both strategies require a huge databank which is not available in the literature.

## Literature Cited

1. Su, Y.C.; Liu, Y. A.; Diaz Tovar, C. A. and Gani, R, "Selection of Prediction Methods for Thermophysical Properties for Process Modeling and Product Design of Biodiesel Manufacturing", *Industrial and Engineering Chemistry Research*, **2011**, 50, 6809-6836.